Phosphorylation by distinct kinases regulates cardiovirus Leader protein function at the nuclear pore complex

By

Holly A. Basta

A dissertation submitted in partial fulfillment of

the requirements for the degree of

Doctor of Philosophy

(Cellular and Molecular Biology)

at the

UNIVERSITY OF WISCONSIN-MADISON

201I

Date of final oral exam: 12/18/13

The dissertation is approved by the following members of the Final Oral Committee:

    Ann Palmenberg, Professor, Biochemistry
    Paul Ahlquist, Professor, Plant Pathology
    Daniel Loeb, Professor, Oncology
    Nathan Sherer, Assistant Professor, Oncology
    Robert Striker, Associate Professor, Medicine

Acknowledgements

Dr. Ann Palmenberg

For showing me what a mentor should be.

Dr. Paul Ahlquist, Dr. Daniel Loeb, Dr. Robert Striker, Dr. Paul Bertics, Dr. Julie Olson and Dr. Nathan Sherer

For constructive comments, support and guidance through my graduate career.

Dr. Jean-Yves Sgro, Dr. Shamaila Ashraf, Dr. Yury Bochkov and Dr. James Gern

For a productive collaboration on the modelling of rhinovirus C.

The Palmenberg Lab

Dr. Bradley Brown, Kelly Watters, Jessica Ciomperlik, Valjean Bacot-Davis, Ryan Petty and Marchel Hill.

For encouragement, guidance and friendship.

CMB

For joy and adventures.

My husband, Tyler

For putting it all in perspective and always making me laugh.

My family

For getting me here and helping me through it.

For Arya Cynthia Peterson

You actually didn't help at all, but I love you anyway.

Table of Contents

Abstract

Phosphorylation by distinct kinases regulates cardiovirus Leader protein functions at the nuclear pore complex

Holly A. Basta

Under the supervision of Ann C. Palmenberg

At the University of Wisconsin, Madison

Active nucleocytoplasmic transport is inhibited by the cardiovirus encephalomyocarditis virus (EMCV). EMCV's Leader (L) protein is necessary and sufficient for this inhibition, through its functions at the nuclear pore complex (NPC). Before now, those functions were known to include binding of RanGTPase, the energy source behind active transport, and phosphorylation of nucleoporins (nups), the proteins that compose the NPC. L has no kinase activity, but rather, causes the activation of mitogen activating kinases (MAPKs) that target phenylalanine-glycine containing nups (62, 98, 153, 214 and 358).

The aim of this work is to determine whether other cardioviruses, specifically Saffold virus (SafV) 2 and Theiler's murine encephalitis virus (TMEV, BeAn strain) L proteins fulfill the same roles at the NPC that EMCV L does. While EMCV infection causes devastating encephalitis and myocarditis followed by death of the rodent hosts, SafV causes mild or asymptomatic infection in humans and TMEV(BeAn) causes persistent demyelination in rodents. As L is responsible for much of EMCV's anti-host functions (repressing the interferon response, IRF-3, etc.), it is logical that differences in disease etiology may be caused by the L protein. Furthermore, this protein varies the

most between EMCV, SafV and TMEV, with the SafV and TMEV L containing additional, functionally uncharacterized domains.

Herein we use recombinant protein assays to show that all three cardiovirus Ls inhibit nucleocytoplasmic trafficking and induce the phosphorylation of nups. All three L proteins can bind RanGTPase and the viral protein 2A. Additionally, exportins (Crm1 and CAS) are bound directly by all three Ls, and MAPKs are activated and bound indirectly.

Differences in these L proteins are identified, however, in their phosphorylation state. EMCV L is phosphorylated (at Thr_{47}) by casein kinase (CK2). *In vitro* phosphorylation assays identified a second kinase, spleen tyrosine kinase (Syk) that phosphorylated EMCV L (at Tyr_{41}) only after CK2. Interestingly, CK2 does not act upon SafV or TMEV L proteins, despite Ls being phosphorylated in multiple cytosol types. We identify AMP-activated protein kinase (AMPK) as a kinase that targets SafV and TMEV L proteins (at Thr_{58} and Ser_{57}, respectively). AMPK also acts upon the CK2 site in EMCV.

Prior to this work, it was known that mutations to EMCV L's phosphorylation site slowed its ability to inhibit nucleocytoplasmic trafficking. This work shows that this attenuation of L function is a result of reduced nup phosphorylation. Furthermore, mutation of phosphorylation sites in all three Ls reduce their ability to bind exportins and MAPKs.

This work suggests a model in which cardiovirus L protein binds the viral protein 2A (which contains a nuclear localization signal), trafficks to the NPC where it

dissociates from 2A, becomes phosphorylated (which increases its affinity for exportins), and binds a complex of RanGTPase, exportin, and one or more MAPK. This complex phosphorylates nups, thereby inhibiting nucleocytoplasmic transport. Abundance and activity of L-targeting kinases may therefore be the limiting factor in L activity, manifesting a difference in cardiovirus L function.

List of Figures

List of Tables

Appendices

List of Abbreviations

ALI	Air-liquid interface
AMPK	AMP-activated protein kinase
Apaf1	Apoptotic protease activating factor 1
BHK	Baby hamster kidney
CamKKβ	Ca^{2+}/calmodulin-dependent protein kinase kinase β
CAS	Cellular apoptosis susceptibility protein (aka Exportin-2)
CC	Compound C (AMPK inhibitor)
CK2	Casein kinase 2
CNS	Central nervous system
CPE	Cytopathic effect
CRE	Cis-responsive element
Crm1	Chromosome region maintenance 1 protein homolog
CSF	Cerebral spinal fluid
EBV	Epstein barr virus
eIF	Eukaryotic initiation factor
EMCV	Encephalomyocarditis virus
ER	Endoplasmic reticulum
ERK	Extracellular-signal-regulated kinases
EV	Enterovirus
FMDV	Foot and mouth disease virus
G3BP	RasGAP-SH3-binding protein
GCN2	General control nonrepressed 2
GEF	Guanine nucleotide exchange factor
GSK3	Glycogen synthase kinase 3
HBE	Human bronchial epithelial
HCMV	Human cytomegalovirus
HEAT	Huntingtin, elongation factor 3, protein phosphatase 2A and TOR1
HIF-1	Hypoxia-inducible factor 1
HIV-1	Human immunodeficiency virus 1
HRI	Heme-regulated eIF2α kinase
HSE	Human sinus epithelial
HSV	Herpes simplex virus
IFN	Interferon
IPMX	Human inositol phosphate multikinase
IRES	Internal ribosome entry site
IRF-3	Interferon regulatory factor 3
ITAM	Immunoreceptor tyrosine-based activation motifs
JNK	c-Jun amino-terminal kinase
Kap	Karyopherin
K_d	Dissociation constant
L	Leader
LKB1	Liver kinase B1
MAPK	Mitogen-activated protein kinase
MAPKK	Mitogen-activated protein kinase kinase
MAPKKK	Mitogen-activated protein kinase kinase kinase
MAV	Antiviral signaling adaptor proteins
Mcl-1	Myeloid leukemia cell differentiation protein
MDA5	Melanoma-differentiated-associated gene 5
MK	MAPK-activated protein kinases

MNK	MAPK-interacting kinases
MS	Multiple sclerosis
MSK	Mitogen- and stress-activated kinases
Nap1	Nucleosome assembly protein 1
NCT	Nucleocytoplasmic trafficking
NES	Nuclear export signal
NFκB	Nuclear factor κB
Nim	Neutralizing immunogen
NLS	Nuclear localization signal
NPC	Nuclear pore complex
Nups	Nucleoporins
NMR	Nuclear magnetic resonance
ORF	Open reading frame
P bodies	Processing bodies
PCBP	Poly r(C) binding protein
PERK	Protein kinase RNA-like endoplasmic reticulum kinase
Pfu	Plaque forming units
pI	Isoelectric point
PKR	Protein kinase R
PPARγ	Peroxisome proliferator-activated receptor γ
PTB	Polypyrimidine tract binding protein
RCC1	Regulator of chromosome condensation 1
RdRp	RNA-dependent RNA-polymerase
RF	Replicative form
RHO	Ras homolog
RIG-1	Retinoic acid-inducible gene 1
ROS	Reactive oxygen species
RSK	90 kDa ribosomal S6 kinases
RV	Rhinovirus
S6K1	Ribosomal S6 kinase 1
SafV	Saffold virus
SF	Splicing factor
SG	Stress granules
SH2	Src homology 2
Src	Src tyrosine kinase
STAT-1	Signal transducer and activator of transcription 1
SYK	Spleen tyrosine kinase
TIA-1	T-cell-restricted intracellular antigen-1
TMEV	Theiler's murine encephalitis virus
TMEV-IDD	TMEV-induced demyelinating disease
TLR	Toll-like receptor
TO	Theiler's original
TRAF-3	TNF-receptor-associated factor 3
UTR	Untranslated region
VCAM-1	Vascular cell adhesion molecule 1
VE	Vilyuisk encephalitis
VHEV	Vilyuisk human encephalomyelitis virus
VP	Viral protein
VSV	Vesicular stomatitis virus

CHAPTER 1.

Introduction

Picornaviruses

Taxonomy. The *Picornaviridae* family harbors 28 species grouped into 12 genera (Table 1-1). Genus designations are made by gene cassette, internal ribosomal entry site (IRES) type and sequence identity over structural (P1) or enzymatic (P2/3) regions of the genome (>40% P1, >40% P2 and >50% P3 amino acid identity). Species designation takes into account host range, cellular receptors, compatibility in proteolytic processing, replication, encapsidation and genetic recombination, gene cassettes and sequence identity (typically >70% P1 amino acid identity) (ICTVIX report).

The *Picornaviridae* family contains many medically and agriculturally relevant viruses (Table 1-1), most notably within the *enterovirus, cardiovirus* and *apthovirus* genera. The enteroviruses target humans (*Human enterovirus A-D, rhinovirus A-C*), other primates (*Simian enterovirus*) and some domestic animals (*Bovine enterovirus*). Poliovirus is historically the most highly studied enterovirus, and represents a devastating human pathogen as well as a (mostly) successful vaccination program. The *cardiovirus* genus (the subject of this thesis) consists of only two known species: the *encephalomyocarditis virus* (EMCV) and the *Theilovirus*. The single known serotype of EMCV has been isolated from over 30 species, including mammals, birds and invertebrates (144). EMCV infection causes encephalitis and myocarditis. The *Theilovirus* species contains the human pathogens Saffold virus (SafV) and Vilyuisk human encephalomyelitis virus (VHEV), and the rodent pathogens Theiler's murine encephalitis (TMEV) and Thera virus. The agriculturally ruinous *Foot-and-mouth*

Genus	Species	# of types	Leader type
Enterovirus	*Human enterovirus A*	21	None
	Human enterovirus B	59	
	Human enterovirus C	19	
	Human enterovirus D	3	
	Simian enterovirus A	1	
	Bovine enterovirus	2	
	Porcine enterovirus B	2	
	Human rhinovirus A	75	
	Human rhinovirus B	25	
	Human rhinovirus C	10	
	Unassigned: simian enteroviruses	3	
Cardiovirus	*Encephalomyocarditis virus*	1	Non-enzymatic
	Theilovirus	12	
Aphthovirus	*Foot-and-mouth disease virus*	7	Protease
	Equine rhinitis A virus	1	
	Bovine rhinitis B virus	1	
	Unassigned: bovine rhinoviruses	2	
Hepatovirus	*Hepatitis A virus*	1	None
Parechovirus	*Human parechovirus*	14	None
	Ljungan virus	4	
Erbovirus	*Equine rhinitis B virus*	3	Protease
Kobuvirus	*Aichi virus*	1	Function unknown
	Bovine kobuvirus	1	
	Unassigned: porcine kobuvirus	1	
Teschovirus	*Porcine teschovirus*	11	Function unknown
Sapelovirus	*Porcine sapelovirus*	1	Function unknown
	Simian Sapelovirus	3	
	Avian sapelovirus	1	
Senecavirus	*Seneca Valley virus*	1	Function unknown
Tremovirus	*Avian encephalomyelitis virus*	1	None
Avihepatovirus	*Duck hepatitis A virus*	3	None
Unassigned	Seal picornavirus 1	1	None
Unassigned	Human cosavirus A	4	None
	Human cosavirus B	?	
	Human cosavirus C	?	
	Human cosavirus D	?	
	Human cosavirus E	1	
Unassigned	Human klassevirus or salivirus	1	Function unknown

Table 1-1. Picornavirus genera and L protein presence/type. Adapted from "Picornaviruses" 2013. Chapter 2, pg 21.

disease virus (FMDV) (*Aphtovirus* genus) has resulted in culling of millions of domestic animals and has led to trade bans with affected countries. FMDV is highly contagious and can infect over 70 species, causing vesicular disease. There are also a number of candidate new species (see Table 1-1), and more are constantly being discovered.

Hallmarks of Picornaviruses. Picornaviruses are small ("pico") RNA viruses with monopartite, positive-sense, single-stranded genomes. Genomes range from 7032 (Tremovirus) to 8828 bases (Erbovirus). In general, Picornaviruses replicate by first binding to a cellular receptor, then undergoing receptor-mediated endocytosis and uncoating. Translation occurs in a cap-independent manner using the IRES and the resulting polyprotein is processed by virally-encoded protease(s). Membrane associated replication complexes form, where negative-strand RNA is synthesized and used as templates for the production of more positive-strand genomes. The positive-sense RNA is then either used to prime more translation, or is encapsidated. The virions mature and are released through cell lysis (Fig 1-1).

The Picornaviral RNA genome alone is infectious and highly structured (~60-65% of the total sequence). The 5' and 3' untranslated regions (UTRs) contain most of the defined structural features (Fig 1-2). The 5' UTR is composed of three distinct structures: the 5' terminal domain, the IRES, and the 5' spacer. The 5' terminal domain has unbranched terminal stems that are thought to interact with viral and/or cellular proteins to initiate negative-strand synthesis and to facilitate the switch from replication to translation. The Picornavirus IRES can be one of four known types based on secondary/tertiary structures. Cardioviruses have a type II IRES that allows for highly efficient cap-independent translation, even when isolated from the viral genome, making
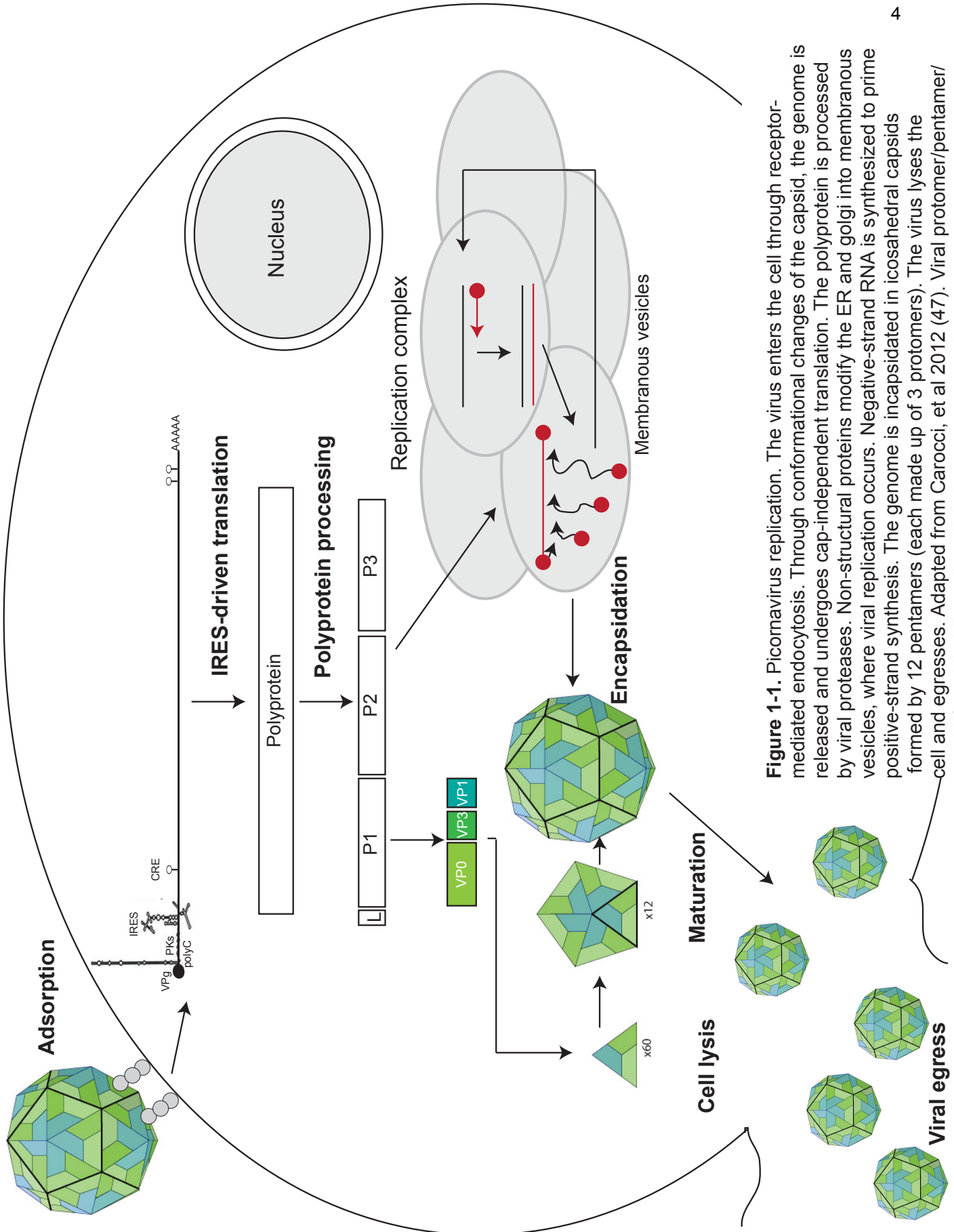
Figure 1-1. Picornavirus replication. The virus enters the cell through receptor-mediated endocytosis. Through conformational changes of the capsid, the genome is released and undergoes cap-independent translation. The polyprotein is processed by viral proteases. Non-structural proteins modify the ER and golgi into membranous vesicles, where viral replication occurs. Negative-strand RNA is synthesized to prime positive-strand synthesis. The genome is incapsidated in icosahedral capsids formed by 12 pentamers (each made up of 3 protomers). The virus lyses the cell and egresses. Adapted from Carocci, et al 2012 (47). Viral protomer/pentamer/capsid from Viral Zone (http://viralzone.expasy.org/).

it a valuable tool in biotechnology (39). The 5' spacer is highly variable, even within a given species, but it often contains pseudoknots (e.g. a single type I pseudoknot in EMCV) (200). The biological role of the spacer is unclear, but there is evidence it is important for replication (200). The 3'UTR is characterized by two or more sequential stem loops, thought to contribute to initiation of negative strand synthesis. The 3' UTR terminates in a poly(A) tail, which binds poly(A) binding protein that is thought to bridge the 5' and 3' UTR activities during translation and replication (349). A final RNA structural element found in all Picornaviruses is the cis-responsive element (CRE), a 40-60 base loosely paired unbranched stem. The CRE can be located at different sites in the viral RNA (ex. 5'UTR for FMDV and in the P1 region of EMCV), and is essential for postive-strand RNA synthesis (241).

In addition to RNA structure conservation, the Picornaviruses share a cassette of hallmark proteins encoded by a single long polyprotein (Fig 1-2). The P1 region is proteolytically cleaved into VP0 (precursor to VP2 and 4), VP1 and VP3 capsid proteins. Each icosahedral capsid is composed of 60 copies each of VP1-3. To form the capsid, the single proteins arrange into a protomer, then a pentamer, and finally 12 pentamers encase the RNA genome to create an immature virion (121). VP0 is then cleaved into VP2 and VP4 by an unknown mechanism to create the mature virion (128). VP1-3 contain β-barrel jelly roll motifs, whose loops, along with the arrangment of these proteins in the capsid, determine receptor preference and antigenic properties.

Next in the polyprotein, all Picornaviruses encode 2B, which likely functions in the production of membranous vesicular replication structures (60) (Fig 1-2). For enteroviruses, 2B has been shown to interact with membranes through an N-terminal
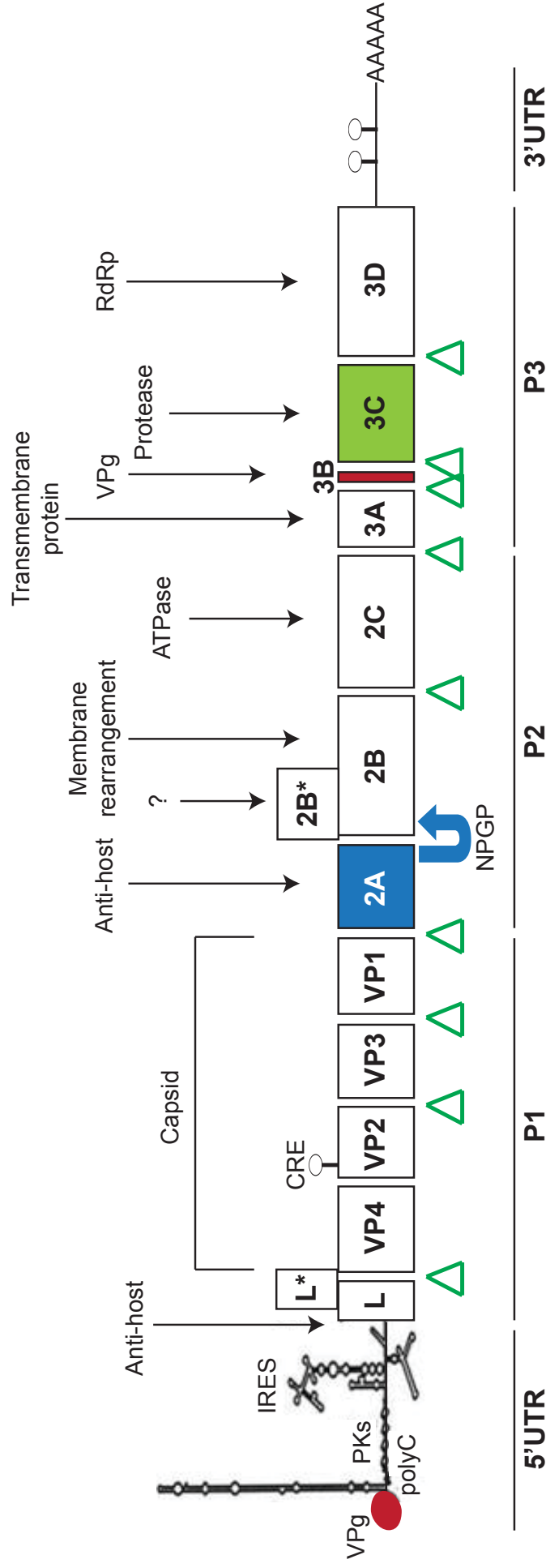
Figure 1-2. Cardiovirus polyprotein. The Cardioviruses encode a single polyprotein that is processed by 3C^{pro} (green arrows) and ribosomal skipping (blue arrow). Replication is undergone by the virally encoded RNA-dependent RNA-polymerase (RdRp) 3D. Translation is cap-independent; the ribosome binds the 5' internal ribosome entry site (IRES). The capsid is composed of viral proteins VP1-4. L and 2A perform antihost functions. Certain Cardioviruses encode alternate reading frames L* and/or 2B*. CRE=cis replicating element, PKs=pseudoknots. Adapted from Carocci, et al. 2012.

6

amphipathic helix and localizes to the endoplasmic reticulum (ER) and Golgi (314), but this structure is not conserved in all Picornaviruses. The $2C^{ATPase}$ is also implicated in membranous vesicular replication structures, and though the specific biological role is also unclear, Picornavirus 2Cs have conserved ATPase and RNA-binding motifs (212, 269).

The exact role of the conserved 3A protein is also under debate; the enterovirus 3AB precursor is anchored within membrane-associated replication complexes (311), potentially orienting VPg in the correct position to initiate viral replication (244). Coxsackie and poliovirus 3As can inhibit protein transport from the ER to the Golgi (219). It is also thought that 3A could be a cofactor in $3D^{pol}$ function, and/or binding of 3CD to template stem-loops (173, 214).

3B encodes the VPg protein that covalently links the 5' end of the genome at a conserved UU (223). The VPg has no known role in translation, but can be detached from the RNA by a cellular enzyme (6, 316).

$3C^{pro}$ is well defined and responsible for the proteolytic cleavage of the polyprotein. It is a Cys-reactive proteinase with chymotrypsin-like folds that, in addition to viral protein processing, targets specific cellular proteins, disrupting processes like mRNA transcription and cap-dependent translation. Interestingly, all $3C^{pros}$ have a conserved RNA-binding site (205).

Finally, $3D^{pol}$ is the viral RNA-dependent RNA-polymerase (RdRp), the key subunit in replication complexes that activates the synthesis of both positive- and negative-strand RNA.

Many Picornaviral genera encode additional proteins, for example, 2A and leader (L) of the *cardiovirus* genus (see below).

Cardioviruses

Taxonomy. There are two species of cardiovirus: the EMCVs and the Theiloviruses. The Theiloviruses are further subdivided into SafV and TMEV clades (Fig 1-3).

EMCV was discovered in attempts to adapt poliovirus to mice; researchers at Columbia University mistakenly reported sucessful adaptation as the virus caused flaccid paralysis in the hind limbs of mice followed by death. However, it is likely EMCV was endemic in laboratory mice, and the effects were enhanced by direct intercerebral transfer (290). EMCV is now known to be a common and widespread animal pathogen infecting avian, mammalian and even invertebrate hosts (144). EMCV is most commonly isolated in suckling pigs, where it causes sudden death. Rodents are thought to be the natural host, in which EMCV causes myocarditis and fatal encephalitis. Certain strains also cause diabetes in mice by specifically destroying pancreatic β cells (339). EMCV (often the mengo strain) is considered the prototypical member of the cardioviruses. The mengo strain was used to create a live attenuated vaccine (84) that is safe and efficacious for a variety of domestic and zoo animals.

SafV was discovered in 2007, isolated from a stool sample collected in 1981 from a child with a fever of unknown origin (147). Since then, research has shown that nearly 90% of adults in the US have seroconverted to SafV (58), and this number is even higher in other countries (350). No clear association has yet been made to a particular set of disease symptoms.
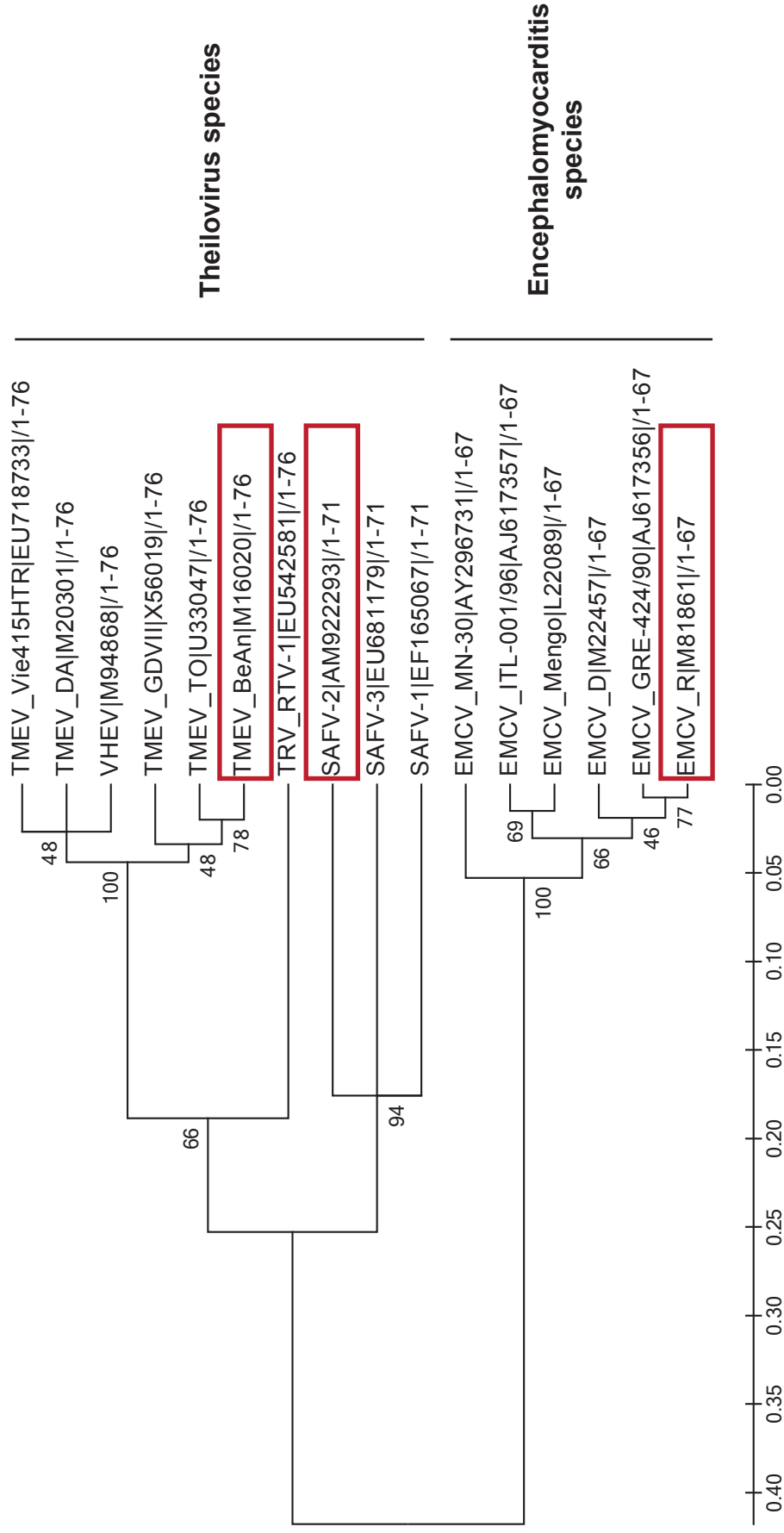
Figure 1-3. Phylogenetic tree of Cardiovirus Genus representatives. Phylogenetic tree created from a ClustalX (172) alignment of the polyprotein (in amino acids) with the UPGMA method in MEGA4 (www.megasoftware.net). Viruses focused on in this thesis are boxed in red. Bootstrap values are indicated at branch points. Branch length scale denoted below.

9

There are a number of theories regarding Saffold's disease etiology:

1. *Multiple sclerosis.* The closest relative of SafV is TMEV. Certain strains of TMEV cause persistent demyelination in mice and are often used to simulate multiple sclerosis (MS)-like symptoms (94). TMEV produces a chronic inflammatory central nervous system (CNS) demyelinating disease and recent work has shown that the Leader (L) protein alone causes dysfunction and death in oligodendrocytes (98). Although a link between SafV and MS in humans has yet to be found, a recent genomics study implicated the apoptotic factor Bcl-2 (see Leader section for TMEV L's role in Bcl-2-mediated apoptosis (296)) in MS susceptibility (352). Furthermore, abnormalities in translation are often found in MS patients (ER stress or inherited demyelinating disease) (286). This is interesting because some cardioviruses have been shown to disrupt translation (7). Some studies have analyzed cerebrospinal fluid (CSF) samples (59) and found no viral genomes; however, one group found SafV in CSF samples from a child with ataxia caused by cerebellitis and another child who died suddenly with no history of illness (221). Furthermore, SafV can persist in HeLa cells (126). SafV causes paralysis and neuropathological changes when injected into mice, similar to TMEV infection (124), further suggesting a potential role for SafV in demyelinating disease in humans.

2. *Respiratory illness.* SafV was isolated in 0.4% of nasopharyngeal samples and 0.6% of throat swabs in patients with lower respiratory track infections in China (263). Multiple other studies have isolated SafV in respiratory track samples, with similarly low frequency (2, 59, 140, 141, 312, 320).

3. *Flaccid paralysis.* SafV has been found via RT-PCR in stool samples from South Asian children suffering from polio-negative acute flaccid paralysis (35). Like poliovirus, Saffold virus is acquired in early childhood (350) and is associated with gastroenteritis (35, 58, 59, 82, 263, 333). Perhaps, like polio, an infection later in life may cause more severe disease. Sampling thus far has focused on single samples or short time spans, preventing discovery of persistent infections, adulthood infections, or the presence of "lifetime shedders" as seen in polio (157).

4. *Asymptomatic.* A number of studies have isolated SafV from asymptomatic patients, suggesting perhaps the virus may not cause clinical disease (2, 35, 82).

TMEVs are the rodent-infecting members of the Theilovirus species. TMEV was isolated by Max Theiler in 1934 (307) and is a common infection in both laboratory and wild rodents. In nature, infection is thought to be feco-oral, resulting in asymptomatic gastrointestinal infection. In susceptible hosts, however, TMEV can occasionally invade the CNS (308), causing either an acute lethal encephalitis or a persistent demyelinating infection, depending on the virus strain. Neurovirulent (GDVII and FA) strains infect neurons, are highly lytic, but do not persist. Alternately, persistent or "Theiler's original" (TO) strains (including DA and BeAn) establish a lifelong infection typified by inflammation and demyelination. The TO strains first infect and replicate in neurons, macrophages and glial cells, causing mild encephalitis. After 2-3 weeks, the virus is cleared from the brain by the host immune response, and infection shifts to the spinal cord white matter where it persists in macrophages and oligodendrocytes for the lifetime of the host (15, 187, 268, 273). The TO strains therefore are often used to model MS-like symptoms in mice (for review, see (230)). In cell culture (baby hamster kidney

(BHK-21) cells), GDVII (neurovirulent) strains grow to a 10-fold higher titer than TO (persistent demyelinating) strains, with larger plaque sizes (2.5 mm vs. 0.5 mm diameter) (186).

VHEV is the only non-rodent virus that groups with the TMEVs rather than the SafVs (Fig 1-3). This virus has been implicated in encephalomyelitis of the indigenous people of the Sakha Republic in the Vilyui River Valley. Vilyuisk encephalitis (VE) is a progressive neurological disorder, beginning with acute encephalitis with fever, chills, headaches, vomiting and meningeal involvment. This progresses to confusion, quadraparesis and death within a few months. VE has a mortality rate of approximately 15%. VE can also manifest as subacute or chronic infection, lasting 3.5 years or more (185). Despite its name, VHEV is not universally accepted as the causitive agent of VE. In the original studies (1954-1957), mice were inoculated with human specimens (284). Of the 11 viruses identified, one cross-reacted with both TMEV and EMCV (weakly) and was called VHEV. Later sequencing of this isolate showed VHEV to be a divergent relative of TMEV (66% nucleotide identity in P1, compared to 50% between TMEV and EMCV species and 90% within TMEV isolates) (259). It is yet to be determined if VHEV represents a contaminating rodent virus or the genuine causitive agent of VE. Other suggested causative agents include *Acanthamoeba castellani* (62) and herpes simplex viruses (HSV) 1 and 2 (103).

Cardiovirus replication. Like all Picornaviruses, cardioviruses share a general 5'UTR-P1-P2-P3-3'UTR polyprotein layout, with the P1 region containing capsid proteins VP1-4 processed by virally encoded protease 3C^{pro}. Cardioviruses range in size from 7-8 kb, beginning with a highly structured 5' UTR (Fig 1-2).

EMCV enters the cell employing sialoglycoproteins, specificially the vascular cell adhesion molecule 1 (VCAM-1) (133). The receptors for SafV and TMEV have not yet been determined. Once in the cell, EMCV uncoating does not require an acidic pH, as is needed for FMDV. Likely, the interaction of EMCV's capsid with the receptor induces the confomational changes required for the release of RNA into the cytoplasm (130, 196). Like all Picornaviruses, the cardioviruses have an icosahedral capsid composed of VP1-4 proteins. The VP1 of cardioviruses forms a star-shaped plateau, the branches of which are separated from VP3 by ~22 angstrom deep "pits" that are thought to serve as receptor binding sites (289).

Once the RNA is released into the cytoplasm, it immediately undergoes translation using host machinery (Fig 1-1). Instead of a 5' cap, the viral genome (messenger sense RNA) has a covalently linked VPg (3B), the role of which in translation has yet to be determined. Unlike enteroviruses, the cardioviruses do not have a 5' cloverleaf after the VPg; instead their 5' UTRs form a stable stem-loop structure required for replication. After these stem-loops, EMCV has a string of 200+ cytidine bases, known as the poly(C) tract (76). Though the function of the poly(C) tract is unknown, truncation attenutes EMCV and mengo virulence in mice (83, 199). Interestingly, neither the SafVs nor the TMEVs have a poly(C) tract.

Cardiovirus translation is cap-independent, driven by a type II IRES (Fig 1-1). Compared to the type I IRES of enteroviruses, type II IRESs can function in a wide range of tissues and conditions (e.g., cell free translation systems like rabbit reticulocytes) (143). Though the exact cellular factors for type II IRES-driven translation are not known, the EMCV IRES requires binding of eukaryotic initiation factors (eIFs)

(excluding eIF4E) and the polypyrimidine tract binding protein (PTB) (21, 149). TMEV neurovirulence was found to depend on the expression of TMEV IRES-binding proteins and PTB (252). Binding of cellular proteins to the IRES allows the recuitment of the 40S ribosomal subunit and other translation initiation factors, to initiate translation at the adjacent start codon.

To free up translation equipment for IRES-driven translation, many Picornaviruses inhibit cellular cap-dependent translation. EMCV's 2A protein plays an essential role in this process (7). The cardiovirus 2A protein, unlike the enterovirus 2A, does not have protease activity, but is instead released from the polyprotein by a sequence-mediated ribosome peptidyl transferase failure called a ribosome skip at the NPGP motif (79). Interestingly, this utilization of ribosome skipping is fairly common in viruses, but quite rare in eukaryotes (192). Cardiovirus 2A (130-140aa) has a very basic isoelectric point (pI) (~9.5) and a nuclear localization signal (NLS). 2A localizes to nucleoli (7), where it is thought to bind to RNA (B. Brown, unpublished) and eIF4E (104). 2A is believed to mediate polyribosome disassembly, associating with the small ribosome subunit and facilitating IRES-mediated translation at the expense of cellular mRNA translation (105). Interestingly, 2A has been found to bind the viral L protein *in vitro*, albeit with a high dissociation constant (K_d) (1.5μM) (Appendix 3). Cardiovirus 2A and L proteins are considered "viral security proteins" (270), because they are responsible for the anti-host functions of the virus and vary the most in sequence conservation among the *cardiovirus* genus.

Recent studies have identified two potential alternate open reading frames (ORFs) in cardioviruses (Fig 1-2). First, L* is found in TMEVs but not EMCVs or SafVs.

It is expressed at very low levels during infection and is thought to be an important determinant of TMEV persistence and resulting demyelination (55, 95, 313). A second alternate ORF, 2B* (128-129 aa), is produced by ribosomal frameshifting at a conserved motif (GGUUUUY) shortly before the start of EMCV 2B. Mutation of this site was found to produce a small plaque phenotype in BHK-21 cells. The Theiloviruses have a much shorter ORF at this locations, but maintain the ribosomal frameshift motif (190).

Co- and post-translational processing of the polyprotein is mediated mainly by EMCV's protease: 3C^{pro}. 3C^{pro} is a highly specific cysteine protease that cleaves between Gln or Glu and Gly, Ser or Ala residues (37, 239). Even the precursors to 3C^{pro} (P3, 3ABC and 3CD) can cleave as efficiently as 3C^{pro} alone (239). 3C^{pro} is highly labile and encodes a "LLVRGRTLVV" ubiquitination motif that targets it to the proteasome (177, 287). Later in infection, mature 3C^{pro} can act in trans, processing newly synthesized polyproteins. Unlike poliovirus and FMDV, EMCV 3C^{pro} has only one identified cellular substrate: retinoic acid-inducible gene 1 (RIG-1), an immune response factor responsible for sensing RNA (237).

Once released from the polyprotein, 2B and 3A are thought to induce the formation of the membranous vesicles in the ER and Golgi where viral replication occurs (288) (Fig 1-1). The mechanism for this membrane rearrangment is unknown. The 2B protein of enteroviruses localizes to the ER and Golgi and reduces Ca^{2+} levels in organelles, as well as inhibiting protein trafficking through the Golgi (72-74, 78). EMCV 2B, however, shares little sequence similarity with enterovirus 2Bs and is much larger. It does not localize to the ER, nor does it inhibit trafficking, but it can reduce Ca^{2+} levels in the ER (but not the Golgi) (61, 73, 325). An alternate theory is that EMCV

hijacks the natural autophagic pathway to create membrane vesicles (159). However these membranous vesicles are formed, EMCV replication occurs on the surface of the vesicles, via a replication complex that includes 3D^{pol}, 3C^{pro}, 2C and 3AB.

Negative-strand synthesis occurs first, to form templates for positive-strand genomes (Fig 1-1). The shift from translation to replication has not been elucidated for cardioviruses, but in poliovirus it is thought that 3CD interacts with the cellular protein poly r(C) binding protein (PCBP) as it is bound to the 5' cloverleaf (123). This binding likely forms a bridge that allows the uridylylation of 3B (VPg) by 3D^{pol} using the AAACA motif of the CRE as a template for 3D^{pol}-mediated VPg uridylation (243) that primes viral replication. The CRE is found in the VP2 region of all cardioviruses; the CREs of cardioviruses are functionally interchangeable, but cannot be swapped for enterovirus CREs (189).

Negative-strand synthesis leads to the formation of a double-stranded RNA structure called the replicative form (RF) (215) (Fig 1-1). The RF structure is unwound for positive-strand synthesis, presumably by the predicted helicase activity of 2C (251). From the RF, the mechanism by which positive-strand synthesis occurs is unclear; it is suggested that initiation of positive-strand synthesis may use pre-uridylylated VPgs left over from negative-strand synthesis (242). Alternatively, uridylylated VPg may be produced at the poly(A) tail of the positive-strand for the synthesis of the negative-strand, while uridylylation at the CRE is used for positive-strand synthesis alone (217).

Newly sythesized RNA is then encapsidated. Viral particles are formed when P1 is cleaved into VP0 (VP2+4), Vp1 and VP3 by 3C^{pro}, which autoassemble into

protomers and then pentamers. Twelve pentamers make up the icosahedral capsid (Fig 1-1). It is not known whether protomers assemble around the viral genome or if the genome is injected into pre-formed capsids, but experimental evidence has revealed the presence of empty capsids, suggesting that capsids do not form around the genome. Only newly synthesized, positive-sense, VPg-linked genomes are packaged (224, 225). Viral RNA must be present in the capsid for the final capsid maturation step: VP0 cleavage into VP2 and VP4.

EMCV egresses through cell lysis, either by sheer viral overload or by possible cell permeabilization by a virally encoded protein (Fig 1-1).

Leader (L) protein

L is the N' terminal protein of the cardiovirus polyprotein and plays an essential role in viral replication during the first 1-2 hours of infection. L (like 2A) is considered a "viral security protein" as it is not involved in replication, but serves to thwart the immune response and promote viral spread (3). The cardiovirus L shares no homologs in either structure or function among other Picornaviruses (Table 1-2), nor anywhere else in nature. The L protein varies more than any other part of the cardiovirus genome, sharing only 35% amino acid identity between the EMCV and Theilovirus species (245). Though L structure and function are well-studied for EMCV, SafV and TMEV Ls bring up many unanswered questions (Table 1-2).

L function or feature	EMCV	TMEV	Saffold
Required for viral persistence	NA	+	ND
Dispensable for viral genome replication	+	+	ND
Inhibition of type I IFN production	+	+	ND
Inhibition of IRF3 dimerization	+	+	ND
Inhibition of chemokine gene transcription	+	+	ND
Disruption of stress granules	+	+	+
Perturbation of nucleocytoplasmic trafficking	+	+	ND
Alteration of nuclear pore architecture	+	ND	ND
Hyperphosphorylation of nucleoporins	+	+	ND
Interaction with RanGTPase	+	ND	ND
Is phosphorylated	+	ND	ND
Binds Exportins	+	ND	ND
Binds MAPKs	+	ND	ND
Activates MAPKs	+	ND	ND

Table 1-2. Known L functions prior to this study. Modified from "Picornaviruses" 2013 Chapter 26 pg 412. NA=not applicable. ND=not determined.

Structure of L. The EMCV L protein is 67 aa long, while the SafV (71 aa) and TMEV (76 aa) are slightly longer. The nuclear magnetic resonance (NMR) structure has been solved for EMCV (mengo) L ((64), Palmenberg, unpublished), revealing two domains: the zinc finger and the acidic domain (Fig 1-4). The flexible region between these two domains is called the "hinge" region. The novel CHCC zinc finger motif is conserved in the cardioviruses, as is the acidic domain. Compared to EMCV, the Theiloviruses have an additional C-terminal "Theilo domain" of unknown function, and the TMEV strains all have a serine/threonine (S/T) rich domain between the acidic and Theilo domains (Fig 1-4).

L Localization. EMCV L localizes to the nuclear rim in HeLa cells during infection (256), though whether it resides just within or just outside the nucleus is unknown. When L is transfected in BHK-21 cells in the absence of viral infection, TMEV (GDVII strain) L localizes to the cytoplasm, while TMEV (DA) L localizes throughout the cell. This difference in localization was attributed to the S/T rich domain (306). Localization of SafV L protein has yet to be determined.

Role of L in apoptosis. General caspase-mediated apoptosis (programmed cell death) can be mounted in one of two general pathways: the intrinsic or the extrinsic pathway. In the extrinsic pathway, ligands bind to death receptors to activate caspase-8, which activates the "executioner caspase", caspase-3 (295). When damage occurs within the cell (as in viral infection), the intrinsic pathway is activated. In the intrinsic pathway, the mitochondrial membrane is disrupted and cytochrome C is released into the cytosol, where it binds apoptotic protease activating factor 1 (Apaf1) to activate caspase-9 and thereby caspase-3 (266).
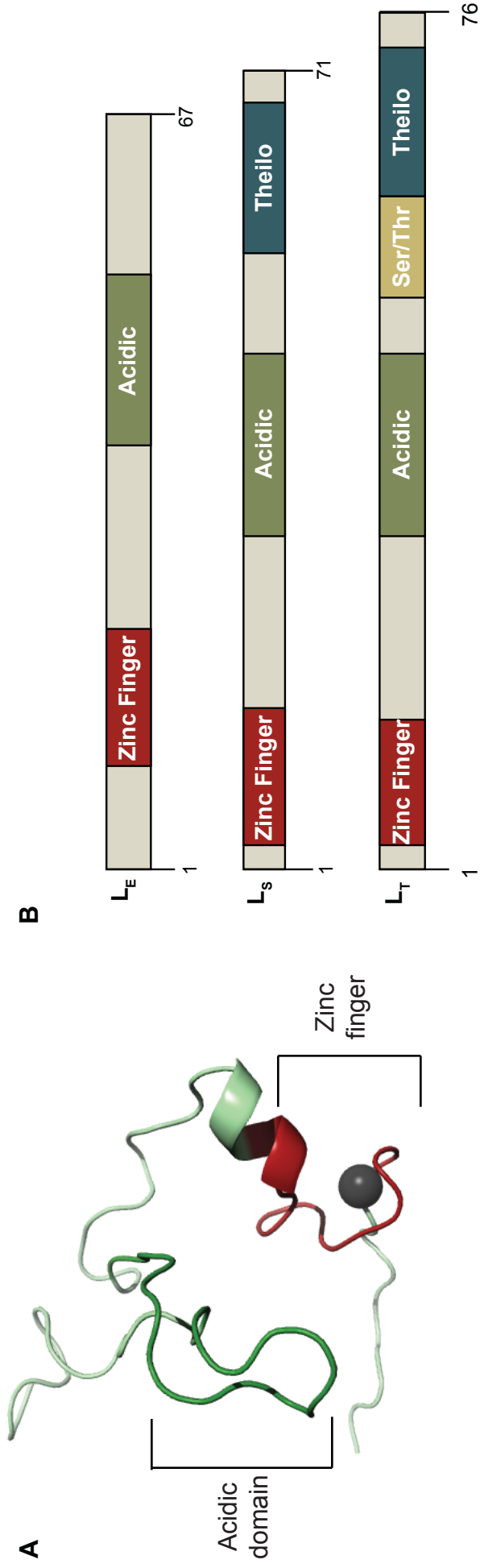
Figure 1-4. Cardiovirus L structure. A. EMCV (mengo) L NMR structure (Palmenberg, unpublished) with zinc finger (red) and acidic domain (green). Image rendered in MacPyMol (1). B. Organization of EMCV (L_E), Saffold (L_S) and TMEV (L_T) L domains. Lengths shown represent amino acids.

In mouse macrophages (the cell in which the TO strains of TMEV persist), TMEV DA L activates the intrinsic apoptosis pathway (145, 296) (Fig 1-5), activating p38 mitogen activating kinase (MAPK) (2-4 hours post infection), followed by the activation of tumor suppressor protein p53 (3-6 hours post infection). p53 stimulates the transcription of pro-apoptotic genes *puma* and *noxa*. At 4-10 hours post infection, myeloid leukemia cell differentiation protein (Mcl-1) and A1 pro-survival proteins are undetectable (296, 297). This leads to a release of Bax (a Bcl-2 pro-apoptotic protein), which forms homo-oligomers and translocates into and permeabilizes the mitochondrial outer membrane, releasing cytochrome and initiating the caspase cascade, causing apoptosis (296, 297) (Fig 1-5A). Apoptosis restricts viral yield and increases particle to plaque forming units (pfu) ratio (145, 296).

Cardiovirus L proteins have been dubbed "pro-apoptotic" and "anti-apoptotic" in various studies and cell lines. In BHK-21 cells, however, only 20% of cells undergo apoptosis, either when infected with TMEV (DA) or transfected with L alone (13). Another group found TMEV (DA) L to be apoptotic in HeLa cells, while the GDVII strain is anti-apoptotic in HeLa cells. Both caused cleavage of caspase-3 in BHK-21 cells, but failed to initiate a full apoptotic response (300). EMCV (mengo) L was also found to be anti-apoptotic in HeLa cells, interfering downstream of caspase activation (270). To further complicate the issue, TMEV (DA) L was found to be pro-apoptotic, but L* (the alternate reading frame found only in TMEV TO strains) to be anti-apoptotic in BHK-21 cells (97, 127, 229). Furthermore, Carocci et al. found that EMCV 2A was required for the inhibition of apoptosis in BHK-21 cells (51).
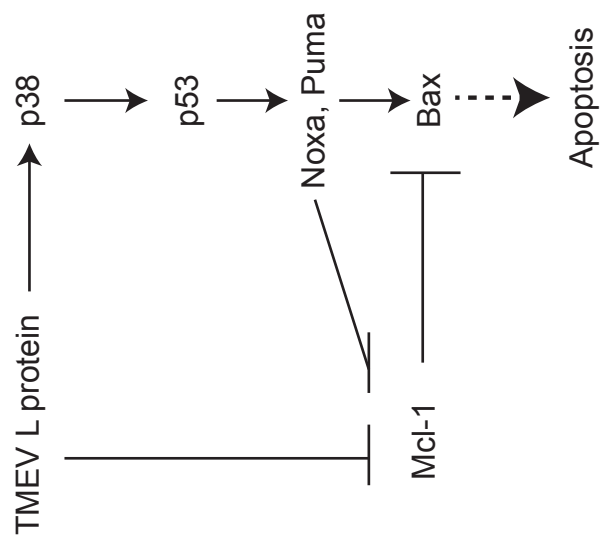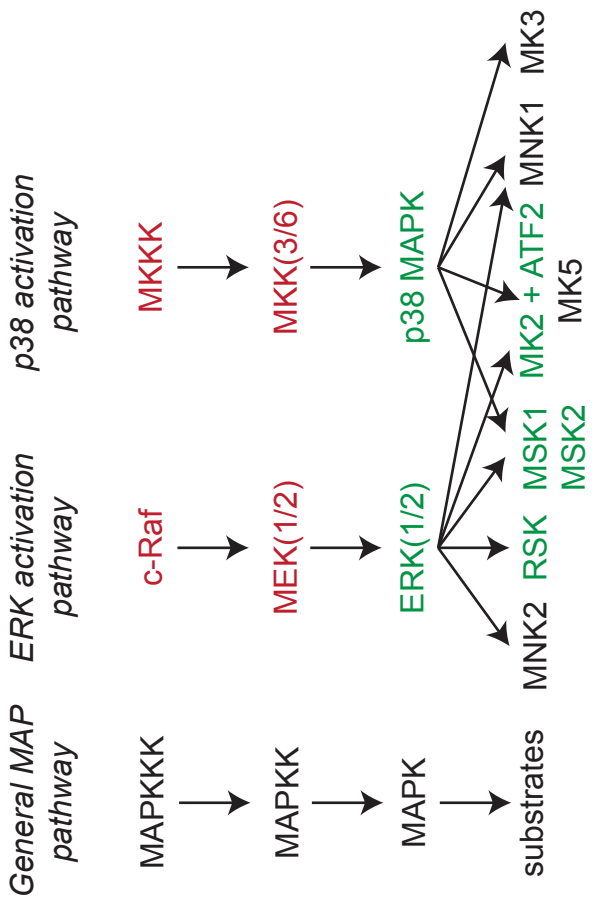
Figure 1-5. Cellular pathways activated by Cardiovirus L proteins. A. TMEV L-induced apoptosis pathway. Adapted from "Picornaviruses" 2013. Chapter 20, pg 328. B. EMCV L activates members of two MAPK pathways (p38 and ERK). MAPK family members activated by EMCV L are shown in green, while those not activated are shown in red. Those not tested are shown in black. Adapted from Roux and Blenis 2004 (274) and Porter et al. 2010 (254).

The differences in apoptotic response may be related to the differences in cardioviral L's varying interferon (IFN)-response disruption. Specifically TMEV DA and GDVII Ls disrupt different steps in the interferon regulatory factor 3 (IRF-3) pathway (299). Alternatively, differences in cell lines may account for the differences in apoptotic response: HeLa cells are responsive to IFN, while BHK-21 cells have a defect in the IFN-response pathway (57).

L inhibits stress granule formation. Stress granules (SGs) are aggregates of stalled replication complexes that form in response to environmental stress (UV radiation, oxidative stress, hypoxia, heat shock, etc.). More specifically, phosphorylation of eIF2α leads to translational arrest, triggering aggregation and SG formation. A number of different kinases phosphorylate eIF2α: protein kinase R (PKR) (activated by cytosolic double-stranded RNA), protein kinase RNA-like ER kinase (PERK) (activated by ER-stress), general control nonrepressed 2 (GCN2) kinase (triggered by amino acid starvation) and heme-regulated eIF2α kinase (HRI) (stimulated by oxidative stress or heme depletion) (for review see (77)). When cells recover from stress, SGs disperse and mRNA goes back to being translated or is degraded in processing (P) bodies (9).

Viral infection can also trigger SG formation, which has a negative impact on the replication of some viruses, likely due to the sequestration of cellular translation factors. Many viruses have mechanisms to combat the formation of SGs, including West Nile, Dengue, Semliki Forest Virus and poliovirus (87, 207, 326). Poliovirus has the best studied mechanism of SG combat: first, the virus triggers the formation of unique SG that contain Sam68, cellular mRNA (but not viral RNA) and T-Cell-Restricted Intracellular Antigen-1 (TIA-1) (253). The SGs are then disrupted by poliovirus 3C^{pro}

cleavage of RasGAP-SH3-binding protein (G3BP) (326), a key factor in the nucleation of SGs (310).

TMEV L protein is necessary and sufficient to prevent the formation of SGs, both those triggered by viral infection and those chemically induced by sodium arsenite (which triggers heat shock proteins) or thapsigargin (which causes ER stress) (43). When the L portion of the polyprotein is deleted or mutated (either a zinc finger or Theilo domain mutation), SGs form and contain PTB (an IRES-interacting protein) and G3BP (which is not degraded by TMEV like it is in polio infection), but not viral RNA. SGs could form in signal transducer and activator of transcription 1 (STAT-1) deficient cells, suggesting that their inhibition is not linked to L's ability to disrupt the type I IFN response (43). As shuttling proteins are abundant in SGs, perhaps L's ability to disrupt nucleocytoplasmic trafficking prevents SG formation.

L inhibits trafficking. Trafficking in and out of the nuclear pore complex (NPC) is a collaboration between nucleoporins (nups), RanGTPase and karyopherins (kaps) (importins, exportins and transportins) (Fig 1-6). Nups make up the NPC; some serve as scaffolding while about 10 nups contain phenylalanine-glycine (FG) repeats. These FG-repeat nups are natively unfolded and form a web-like mesh in the central channel of the NPC (240). The FG repeats are surrounded by hydrophilic spacer sequences that are thought to interact with the hydrophobic regions of kaps (29). The energy source for active nucleocytoplasmic trafficking is provided by the small GTPase Ran. Ran exists in either GDP- (primarily in the cytoplasm) or GTP- (primarily in the nucleus) bound forms. Regulator of chromosome condensation 1 (RCC1) is Ran's guanine nucleotide exchange factor (GEF), which facilitates Ran's conversion from the GDP to GTP-bound
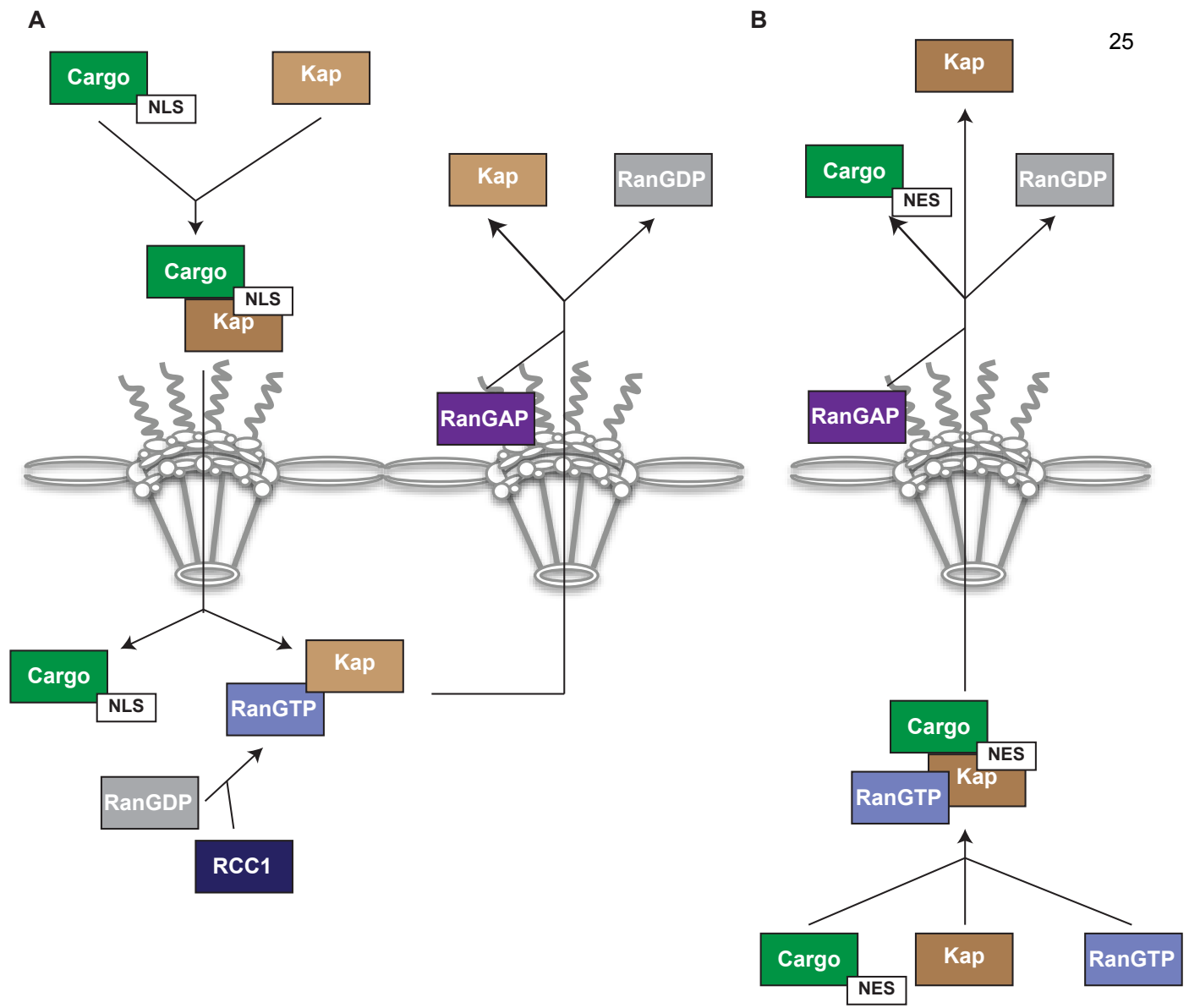
Figure 1-6. Nucleocytoplasmic transport. A. Nuclear import. Karyopherins (kap), specifically importins, bind cargoes with nuclear localization signals (NLSs) and traverse the nuclear pore complex (NPC) by interact with phenylalanine-glycine (F/G) repeat nucleoporins (nups). RanGTP then disassociates cargo from kap, and kap is recycled back to the cytoplasm. B. Nuclear export. Cargoes with nuclear export signals (NESs) are bound by kaps (exportins) bound to RanGTP. Exportins associate with FG repeat nups to move through the NPC to the cytosol, where RanGTP is hydrolyzed to RanGDP by RanGAP and the export complex disassociates. C. Structure of Crm1 exportin (brown) bound to RanGTP (blue) and cargo (snuportin) (green) (PDB:3GJX).
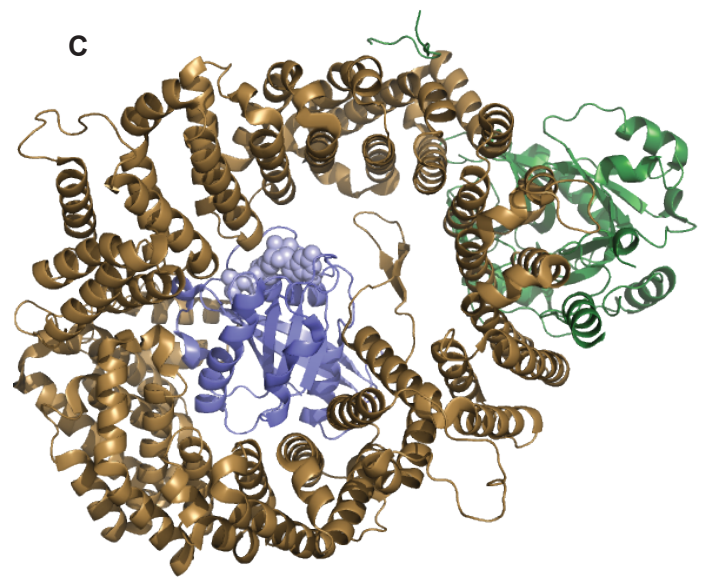
state in the nucleus. For nucleocytoplasmic trafficking, Ran interacts with kaps, binding them inside the nucleus to release import cargo, or forming an export complex with cargo that dissociates when Ran cycles to the GDP bound form in the cytoplasm (Fig 1-6). Kaps bind cargoes that contain either nuclear localization signals (NLSs) or nuclear export signals (NESs) of cargoes greater than 40kDa (smaller molecules can passively diffuse).

The preference of kaps for an NLS or NES (as in many cases proteins contain both) can be enhanced by phosphorylation at or near the NLS/NES. For example, the nucleocytoplasmic shuttling protein nucleosome assembly protein 1 (Nap1) is a cofactor for the nuclear import of histones, which is phosphorylated by casein kinase 2 (CK2) at three serines. This phosphorylation promotes the import of Nap1 into the nucleus (48). Likewise, the phosphorylation of extracellular signal-regulated kinase 1/2 (ERK1/2) MAPK by CK2 promotes its binding to importin 7 and translocation to the nucleus (254). Export can also be regulated by phosphorylation: ribosomal S6 kinase 1 (S6K1), peroxisome proliferator-activated receptor γ (PPARγ) and human inositol phosphate multikinase (IPMX) can all be phosphorylated by CK2, which enhances their chromosome region maintenance 1 protein homolog (Crm1)-dependent export (211, 236, 318). CK2 is not the only kinase that is responsible for NLS/NES modulation; hypoxia-inducible factor 1 (HIF-1) is phosphorylated by ERK1/2, enhancing its Crm1-dependent export (218).

Trafficking can also be inhibited by phosphorylation. EMCV L protein was shown to inhibit nucleocytoplasmic trafficking, bind RanGTPase and trigger the phosphorylation of specific FG repeat nups (Nups62, 98, 153 and 214) through MAPK

activation (p38 and ERK) (256-258). A number of studies have found that nups can be

phosphorylated in virus-independent scenarios, including oxidative stress (68) and

mitosis (195). Furthermore, phosphoproteomic screens identified FG nups as targets of

the ERK MAPK (166). ERK phosphorylation of Nup50 was shown to reduce its affinity

for importin β family proteins (specifically importin β and transportin) (165). ERK was

also found to target Nup153 and Nup214 and inhibit their binding to importin β *in vitro*

(166). The exact mechanism by which phosphoryation regulates trafficking is not

known, but it has been hypothesized that phosphorylation may reduce the hydrophilic

character of regions between the FG repeats, weakening their interaction with

hydrophobic karyopherins (166).

The cardioviruses inhibit nucleocytoplasmic trafficking likely for two reasons: first,

to block the IFN response that would normally be mounted upon detection of infection,

and second, to free up nuclear factors the virus needs for cytoplasmic replication. These

goals are also important for many other viruses. Enteroviruses, including poliovirus and

all three rhinovirus (RV) species (A, B and C), use the 2A protease (2A^{pro}) to cleave

specific nups, thereby inhibiting their interactions with kaps and preventing trafficking

(238, 324). Interestingly, each RV species' 2A^{pro} has unique nup cleavage site

preferences, as well as different rates of cleavage (324). These distinct cleavage events

translate to differences in how fast certain trafficking pathways are inhibited (Watters, in

preparation). Non-picorna viruses also inhibit trafficking: vesicular stomatitis virus (VSV)

matrix protein specifically targets the Rae1 mRNA export pathway, presumably by

interacting with Rae1 and Nup98 to form incompetent export complexes (89).

L causes MAPK activation. Members of the MAPK family (p38 and ERK) were identified as the culprits of EMCV L-induced nup phosphorylation (257). EMCV L causes activation of these kinases (257), and ERK activation has been shown to inhibit importin α/β-mediated nuclear import (71).

All eukaryotic cells possess multiple MAPK pathways that are involved in a plethora of biological functions including gene expression, mitosis, metabolism, motility, etc. Five groups of MAPKs have been characterized in mammals: ERK1/2, c-Jun amino-terminal kinases (JNKs) 1, 2, and 3, p38 isoforms α, β, γ, and δ, and ERKs 3, 4, and 5 (for review see (51)). MAPKs are activated by various stimuli; in general, ERK1/2 are activated by growth factors and phorbol esters, while p38 and JNK kinases respond to stress stimuli (osmotic shock, ionizing radiation, cytokines, etc.) (for review see (246)). These stimuli are sensed by a MAPK kinase kinase (MAPKKK), which activates a MAPK kinase (MAPKK), which activates a MAPK, which in turn can phosphorylate a number of substrates at a Ser/Thr-Pro motif (Fig 1-5B). MAPK substrates include phospholipases, transcription factors, cytoskeletal proteins, and other kinases (MAPK-activated protein kinases, or MKs). MKs include 90 kDa ribosomal S6 kinases (RSKs), mitogen- and stress-activated kinases (MSKs), MAPK-interacting kinases (MNKs), MAPK-activated protein kinases 2, 3 and 5 (MK2, 3 and 5) (277).

EMCV L causes activation of ERK1/2 and p38 and their substrates RSK and MK2, respectively (257). The precise point at which these MAPK pathways are activated by L is currently under investigation.

Inhibition of the interferon response. Cardiovirus L proteins block IFN β transcription (114, 265, 299). Type I IFNs are produced in response to viral antigen recognition by cellular receptors, including Toll-like receptors (TLRs), RIG-I and melanoma-differentiated-associated gene 5 (MDA5). Binding of picornaviral RNA by MDA5 causes association of antiviral signaling adaptor proteins (MAVs) on the outer mitochondrial membrane. MAVs associate with TNF-receptor-associated factor 3 (TRAF-3), which activates IKK-related kinases, leading to phosphorylation of IRF-3. IRF-3 phosphorylation triggers its dimerization and translocation to the nucleus, where it activates the transcription of IFN-β. A variety of viruses disrupt the type I IFN response: hepatitis A virus cleaves MAVs (338) and poliovirus cleaves MDA-5 (25). Cardioviruses disrupt the type I IFN response at multiple steps: at the transcription level (114, 265), inhibiting activation of activator of nuclear factor κB (NFκB) (351) and inhibiting IRF-3 dimerization (299), and at the translation level by blocking mRNA trafficking (22, 75, 183, 257, 258). The type I IFN response activates cytokines, which are also repressed by cardiovirus Ls (164, 245, 265, 315).

L plays a role in viral persistence. TMEV TO strains can cause persistent demyelination in susceptible mice, causing an MS-like disease termed TMEV-induced demyelinating disease (TMEV-IDD). TMEV-IDD is generally thought to be immune response-mediated, however, there is some evidence of direct virus involvement. The TMEV (DA) virus and antigens were found in oligodendrocytes (the CNS cells that make myelin), which showed a "dying back" pathology (267, 268). Furthermore, the DA virus was found to cause demyelination in nude mice (271).

Intial work with transgenic mice found that a subgenomic segment of TMEV including the 5'UTR, L, L* and P1 could cause demyelination (18). Using a transgenic mouse with tamoxifen-inducible expression of TMEV (DA strain) L coding-region alone in oligodendrocytes, Ghadge et al found that, in young mice, L expression caused acute progressive fatal paralysis with abnormalities in oligodendrocytes and demyelination. In older mice, L expression caused transient weakness with demyelination. High levels of L expression caused death of myelin-synthesizing cells, while lower expression caused cellular disfunction with cell survival. Oligodendrocyte death and apoptosis occurred without T-cell infiltration, suggesting that the immune system was not involved (98). Interestingly, this also occurs in the early stages of MS in humans (122). Furthermore, a genomic screen of MS patients identified Bcl-2 (a pro-apoptotic protein activated in response to TMEV L (296)) as important to susceptibility (352).

Kinases that target the cardiovirus L protein

EMCV L's ability to inhibit nucleocytoplasmic trafficking is disrupted by mutations to its phosphorylation sites (114, 183, 351). EMCV L was found to be phosphorylated on a Tyr (86), later identified as Tyr_{41} (Chapter 2), and on Thr_{47} (351).

Casein kinase 2 (CK2). CK2 was identified in recombinant protein assays to target EMCV L at Thr_{47} (351). Inhibitors to CK2 reduce EMCV L's phosphorylation as well as L-induced nup phosphorylation (Chapter 2).

CK2 is a constitutively active Ser/Thr kinase that is implicated in a wide range of biological processes, including cellular proliferation and apotosis (188). CK2 is a tetrameric complex composed of two regulatory subunits (2β) and two catalytic subunits

(α/α'). CK2 is predicted by phosphoproteomics studies to act upon as many as 20% of all cellular substrates (282). CK2 is of particular interest because it is frequently upregulated in cancer and contributes to tumorogenesis (85, 298). In fact, it is thought that CK2 can promote cell survival; conversely inhibition of CK2 causes apoptosis in cancer cells (298).

CK2 has a number of viral protein substrates and is important for the replication of epstein barr virus (EBV), HSV, hepatitis B virus, human cytomegalovirus (HCMV) , human immunodeficiency virus (HIV), and human papillomavirus (209).

Spleen tyrosine kinase (SYK). SYK is a cytoplasmic kinase that phosphorylates EMCV L protein at Tyr_{41} (Chapter 2). SYK is a 72 kDa non-receptor tyrosine kinase that contains two SRC homology 2 (SH2) domains and a C-terminal kinase domain. SYK is an evolutionary ancient kinase, conserved even in invertebrates (for review, see (213)). Though initially thought to be specific to hematopoetic cells, SYK has been found in many cell types, including fibroblasts, epithelial cells, breast tissue, hepatocytes, neuronal cells, and vascular endothelial cells (337). SYK is involved in the phosphorylation cascades of a number of pathways, notably p38, ERK, Ras homolog (RHO) family and NFκB. SYK plays a pivitol role in cytoskeletal changes, reactive oxygen species (ROS) production, differentiation, proliferation, survival and cytokine release (for review, see (213)).

Interestingly, SYK is associated with pattern recognition receptors responsible for sensing certain viruses (for review, see (213)). Additionally, some viruses that contain immunoreceptor tyrosine-based activation motifs (ITAMs) require SYK for their

oncogenic activity, including EBV, mouse mammary tumor virus and Kaposi's sarcoma-associated herpesvirus (153, 170, 180, 191, 213, 272).

We believe that CK2 primes EMCV L to be recognized and phosphorylated by SYK. This sort of priming has been observed for other kinase pairs as well: glycogen synthase kinase 3 (GSK3) requires priming by CK2 (303), while CK1 requires a phosphate to be added at position P-3 in order to recognize its substrate (91). Furthermore, other viruses also have a step-wise phosphorylation event; VSV phosphoprotein requires phosphorylation by two distinct kinases for its activity (30), one of which is CK2 (23).

AMP-activated protein kinase (AMPK). AMPK phosphorylates all three cardiovirus Ls tested *in vitro* (Chapter 3). AMPK plays a pivotal role in maintaining cellular homeostasis by responding to intracellular AMP levels, targeting catabolic pathways (to generate more ATP) and repressing anabolic pathways (that consume ATP) (112, 113) (Fig 1-7). The AMPK structure is a heterotrimer composed of α, β and γ subunits: The α subunit (two isoforms that differ in tissue-specific expression and activation) is the catalytic subunit (Fig 1-7). AMPK is activated by phosphorylation of Thr_{172} (AMP binding prevents the dephosphorylation of this site (283)); located at the N-terminus along with the catalytic domain (304). AMPK contains an autoinhibitory domain from aa 312-335, so a truncation from aa 1-312 is constitutively active even without the β and γ subunits (70). The β subunit (two isoforms) and the γ subunit (3 isoforms) are regulatory subunits. β contributes to the interaction between AMPK and glycogen, likely through the N-terminal carbohydrate-binding module (255), as well as an adaptor between the α and γ subunits (which don't bind on their own) (327). The γ subunit has four

33
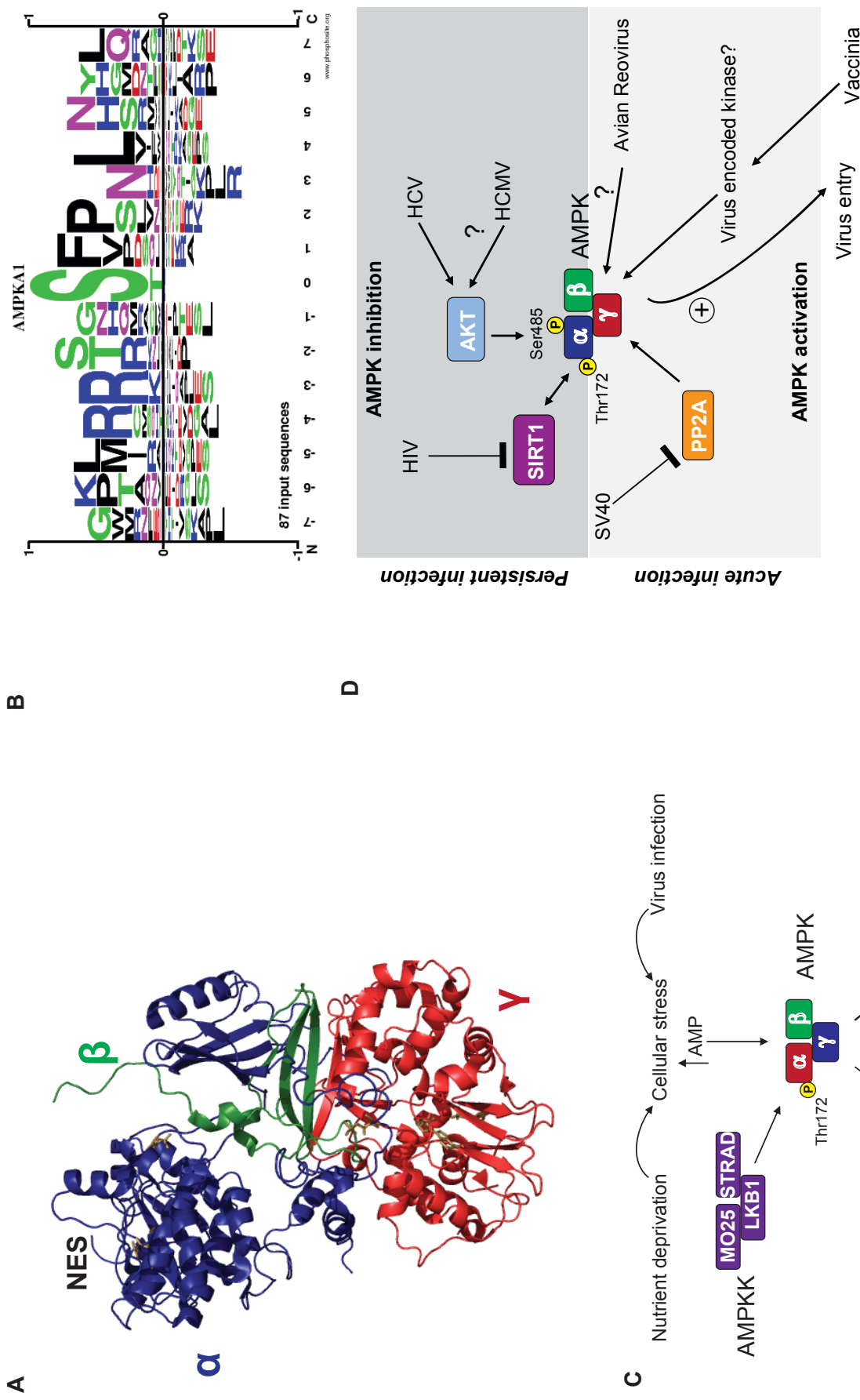
Figure 1-7. AMP-activated protein kinase (AMPK). A. Structure of AMPK (PDB: 2Y94); α subunit (containing the NES) is in blue, β is in green and γ is red. B. Weblogo of AMPK substrate preference (www.phosphosite.org). C. AMPK activation. In cellular stress conditions, cellular AMP levels increase, binding the γ subunit and locking AMPK in the activated (phosphorylated) conformation. Active AMPK stimulates catabolism and represses anabolism pathways to regain the energy balance in the cell. Adapted from Mankouri and Harris 2011 (194). D. Viruses often repress AMPK during persistent infection, and activate it during acute infection. Adapted from Mankouri and Harris 2011(194).

cystathionine β-synthase domains that can bind AMP, ADP or ATP to regulate activation of the α subunit through allosteric structural changes that modulate phosphorylation and dephosphorylation of Thr_{172} (226, 283, 331). There are a number of AMPK isoforms, all of which are encoded by distinct genes distributed across five chromosomes in humans (301). AMPK is highly conserved in eukaryotes (down to yeast and plants) (113).

In addition to sensing the energy balance of the cell, AMPK also regulates ROS/redox balance, autophagy, cell proliferation, apoptosis, polarity, mitochondrial function and genotoxic response (for review see (321)).

AMPK can be activated by hypoxia, physical exercise or hormones (specificially leptin and adiponectin). There are also known chemical activators to AMPK: AICAR (mimics ADP in activating AMPK) (65), glucose analogue 2-deoxy-D-glucose (mimics caloric restriction) (56, 322), and metaformin (used to treat Type 2 diabetes) (346). Others include thiazolidinediones (PPARγ activators) and A-769662 (direct AMPK activator).

AMPK can be inhibited by high glucose and glucogen, lipid overload, and amino acids, all of which are related to obesity and Type 2 diabetes. There is one chemical inhibitor to AMPK: compound C (CC). Unfortunately, CC also affects a number of kinases that are also intimately involved in L function, including ERK1/2, p38 and CK2 (19).

AMPK has two upstream activating kinases: liver kinase B1 (LKB1) (115, 328) and Ca^{2+}/calmodulin-dependent protein kinase kinase β (CaMKKβ) (116, 134). AMPK can be repressed by phosphatases PP2Cα or PP2A (330).

AMPK is ensconced in a number of viruses' replication cycles (for review, see (197)) (Fig 1-7). Some viruses inhibit AMPK, usually during persistent infection, including HIV (via inhibition of an AMPK-activating kinase) (341), hepatitis C virus and HCMV latent infection (via activation of an AMPK-inhibiting kinase) (198). Other viruses activate AMPK, often during acute infection: activation of AMPK is important for HCMV acute infection (206), SV40 blocks a phosphatase that dephosphorylates/inactivates AMPK (168), while avian reovirus and vaccinia activate AMPK through unknown mechanisms (146). In avian reovirus infection, AMPK activation also leads to increased activation of p38 MAPK kinase (146), while in porcine circovirus infection AMPK activation leads to ERK activation (347) (Fig 1-7). AMPK may therefore be involved with L function at both the L phosphorylation event as well as the nup phosphorylation cascade.

AMPK shuttles between the nucleus and the cytoplasm via Crm1-mediated export and a Ran-dependent import pathway (154). Under stress conditions or during MAPK inhibition (specifically the inhibition of ERK1/2), this shuttling is impaired and AMPK accumulates in the nucleus (161), impairing AMPK function (154). L has been shown to bind Ran ((256), Chapter 4), Crm1 (J. Ciomperlik unpublished, Chapter 4) and ERK1/2 (J. Ciomperlik unpublished, Chapter 4), likely placing L and AMPK in the same cellular location.

Leader binding partners

EMCV L's best-defined binding partner is RanGTPase (256). L amino acids 35-40 have been implicated in Ran-binding (16) and the NMR structure of L-Ran bound is underway. L-Ran binding is facilitated by RCC1, Ran's GEF, and the K_d of L and Ran is ~3 nM (249). The L-Ran interaction is necessary for L's ability to induce nup phosphorylation (16).

Cardiovirus Ls bind the viral 2A protein *in vitro*; EMCV L and 2A bind with a K_d of 1.5 µM, presumably as a way to traverse to the nuclear rim (exploiting 2A's NLS) (Appendix 3).

L binds kap β family proteins. The exportins Crm1 and CAS were identified in a mass spectrometry analysis of EMCV L binding partners pulled out of HeLa cytosol (J. Ciomperlik unpublished). Though it was initially assumed these kaps were associated with L via a RanGTPase mediator, studies with recombinant proteins showed that EMCV L and Crm1 can bind in the absence of RanGTPase (J. Ciomperlik unpublished). CAS has also been shown to interact with EMCV L (J. Ciomperlik unpublished) as well as SafV and TMEV L (Chapter 4), as has Kapβ (to low levels) (J. Ciomperlik unpublished), but it is unknown at present whether these interactions are Ran-dependent.

Crm1 (aka exportin 1, Xpo1) is a member of the kap β superfamily that binds leucine-rich NESs. Crm1 binds a wide array of proteins (169) and specific RNAs (including rRNAs, U-sn-RNAs, SRP-RNAs and many viral RNAs). Crm1 has a helicoidal structure composed of 19 HEAT (huntingtin, elongation factor 3, protein phosphatase

2A and TOR1) repeats (63). The cargo binds to the outer surface of Crm1, while Ran binds an acidic loop within HEAT repeat 8 (see Fig 1-6C). The potent inhibitor leptomycin B binds the NES binding region in HEAT repeat 10 at a conserved Cys (135). Affinity for Crm1 can be modified by cargo phosphorylation, but NES affinity for Crm1 tends to be low and is thought to be the rate-limiting step of transport (156). A quaternary complex containing Crm1, RanGTP, RanBP3 and NES cargo interacts with nups (184). This complex is thought to bind to the Nup214-Nup88 complex and disassemble following interaction with soluble RanBP1 and/or RanGAP. Reimport may involve Nup358 (135).

Exportin-2 (CAS) binds an acidic patch on importin α in the presence of RanGTP to recycle importin α back into the cytoplasm. CAS is phosphorylated and highly expressed in proliferating tissues. It is implicated in cell proliferation, apoptosis and control of p53-mediated gene expression. In stress conditions, CAS localizes to the nucleus. Inhibition of MEK and pI3 kinases increase the concentration of CAS (162). Unlike Crm1, CAS has few defined cargoes. Besides importin α, ERK3 is the only other well-characterized CAS cargo. ERK3 shares 50% identity with ERK1/2, and is unstable in the cell, degraded by the proteosome within 30 min (66).

Through pulldown assays of L, MAPKs were also found to associate with L in cytosol (J. Ciomperlik unpublished, Chapter 4). These MAPKs include MEK2, MSK2, p38 and ERK1/2. Interestingly, recombinant ERK1/2 and L alone did not associate (J. Ciomperlik unpublished), suggesting a complex in which L associates with MAPKs through Ran and/or an exportin.

Model of L function

We propose that L first binds 2A, either in the context of the polyprotein or shortly after release, hitching a ride to the nuclear rim through the use of its NLS. There, L is displaced by Ran (to which it binds with a higher K_d) and forms a complex with an exportin (Crm1, CAS, etc.) (phosphorylation enhances this L-exportin interaction) and an activated MAPK or MAPK complex (likely ERK1/2 and/or p38). The MAPKs are thereby localized to the NPC where they phosphorylate nups, inhibiting kap-nup interaction and disrupting nucleocytoplasmic trafficking (Fig 1-8).

A.

B.
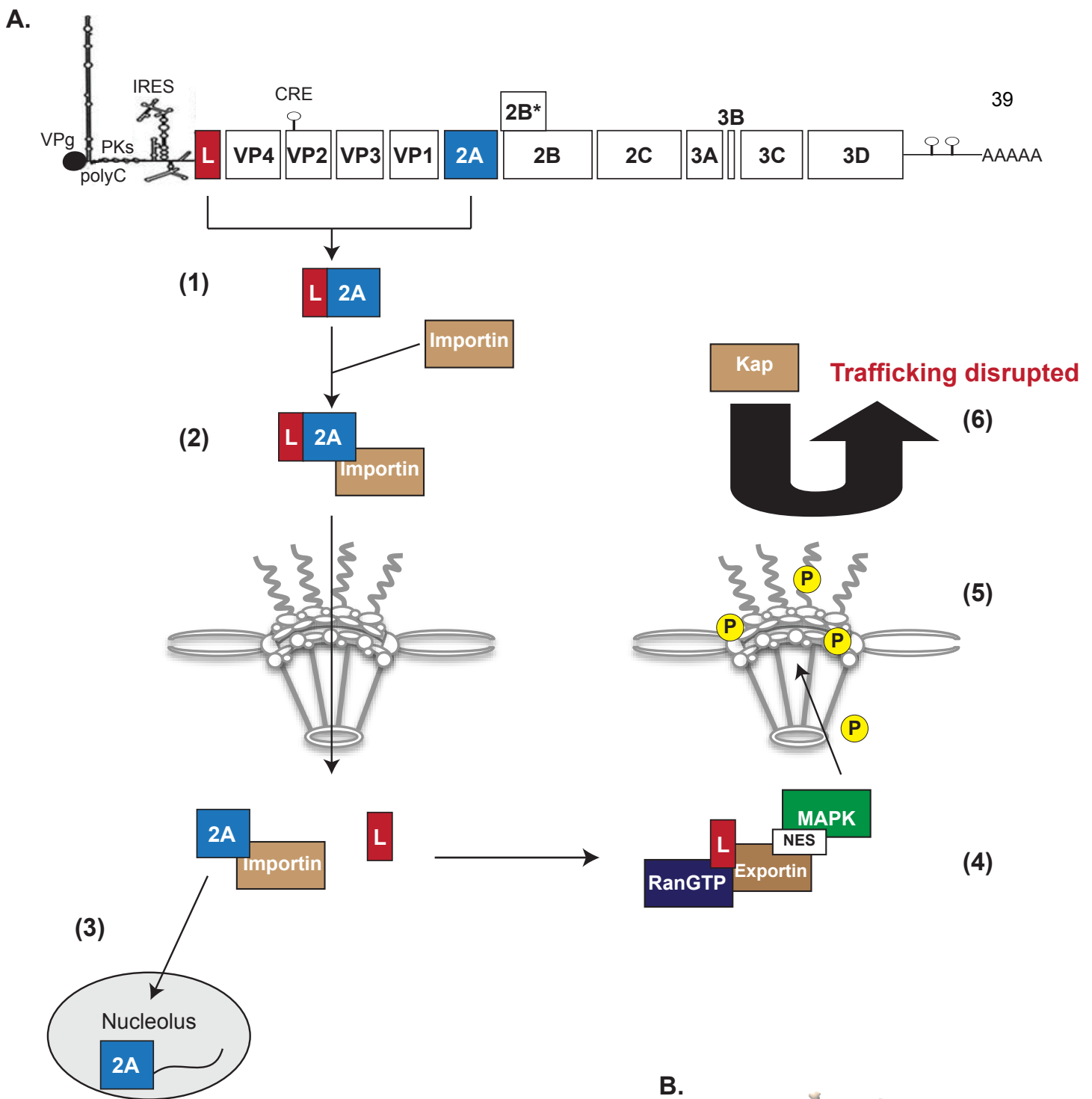
Figure 1-8. Model of EMCV L function. A. (1) L binds 2A, which contains an NLS. (2) L-2A traffics to the nucleus. (3) L and 2A dissociate and 2A traffics to the nucleolus, where it binds RNA. (4) L binds RanGTPase, an exportin (ex. Crm1), and MAP kinases, localizing ERK1/2 and/or p38 to the nuclear pore, where it (5) phosphorylates nups. Nup phosphorylation impedes association of karyopherins, (6) disrupting active nucleocytoplasmic trafficking (Chapter 4). B. Model of complex of EMCV L (red) (Palmenberg unpublished) with Ran (blue), Crm1 (tan) and cargo (snuportin) (green) (PDB:3GJX).

39
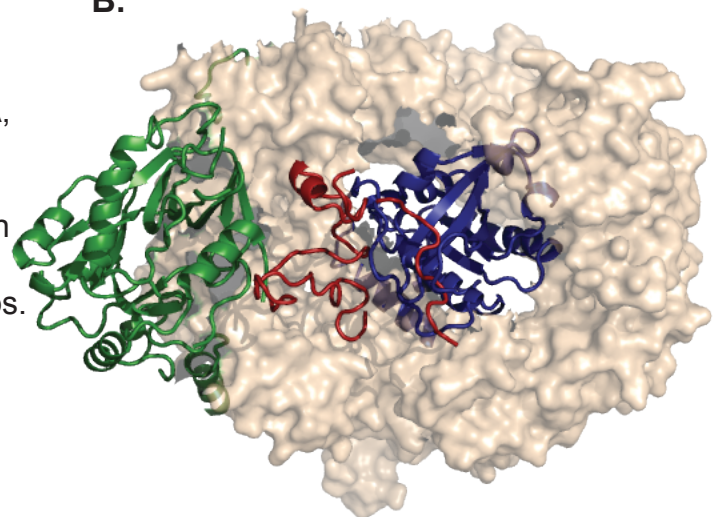
Thesis preview

The aim of this work was to define and compare the functions of the cardiovirus L protein of EMC, Saf and TME (BeAn) viruses at the nuclear pore. Cell transfections, infections and *in vitro* assays with recombinant proteins were used to dissect L's role in inhibition of nucleocytoplasmic trafficking, and the binding partners and cellular cascades involved in this inhibition. In **Chapter 2**, we define EMCV L's phosphorylation sites and identify the kinases involved. These phosphorylation events are found to be important for L-directed nup phosphorylation, but not Ran-binding. In **Chapter 3**, we define the Theiloviruses SafV and TMEV (BeAn) L phosphorylation sites, distinct from both each other and EMCV's, and identify AMPK as a kinase that acts upon these proteins. For **Chapter 4**, we define the binding partners of SafV and TMEV(BeAn) Ls, and find that, like EMCV L, the Theilo Ls bind Ran, exportins CAS and Crm1, and (indirectly) members of the MAPK family. Furthermore, the Theilo Ls were necessary and sufficient to disrupt nucleocytoplasmic trafficking through multiple pathways, and induce the phosphorylation of nucleoporins. Finally, we find that phosphorylation of L proteins increases their affinity for exportins, and therefore MAPKs, thereby localizing MAPKs to the NPC where they can phosphorylate nups causing disruption of nucleocytoplasmic trafficking.

CHAPTER 2.

Encephalomyocarditis Virus Leader is Sequentially Phosphorylated by CK2 and Syk as a Requirement for Subsequent Phosphorylation of Cellular Nucleoporins

Holly A. Basta, Valjean R. Bacot-Davis, Jessica J. Ciomperlik and Ann C. Palmenberg

Author contributions: HAB performed *in vitro* phosphorylation reactions in Fig 2-1 and 2-2E, and transfections in Fig 2-5. VRBD performed *in vitro* phosphorylation assays for Fig 2-2A-E and the Ran-binding experiment for Fig 2-3. JJC performed the *in vitro* and *in vivo* CK2 inhibitor studies in Fig 2-4 and 2-6.

ABSTRACT

Encephalomyocarditis virus and *Theilovirus* are species in the *Cardiovirus* genus of the *Picornaviridae* family. For all cardioviruses, the viral polyprotein is initiated with a short Leader (L) protein unique to this genus. The NMR structure of L_E from encephalomyocarditis virus (EMC) has been determined. The protein has an NH_2-proximal CHCC zinc-finger, central linker and a contiguous, highly acidic motif. The *Theiloviruses* encode the same domains, with one or two additional, COOH-proximal domains, characteristic of the human Saffold viruses (SafV), and Theiler's murine encephalomyelitis viruses (TME), respectively. The expression of a cardiovirus L, in recombinant form, or during infection/transfection, triggers an extensive, cell-dependent, anti-host phosphorylation cascade, targeting nucleoporins (Nups) that form the hydrophobic core of nuclear pore complexes (NPC). The consequent inhibition of nucleocytoplasmic trafficking is potent, and prevents the host from mounting an effective anti-viral response. For this inhibition, the L proteins themselves must be phosphorylated. In cells, extracts or recombinant form, L_E was shown to be phosphorylated at Thr_{47} and $Tyr_{41.}$ The first reaction (Thr_{47}), by casein kinase 2 (CK2) is an obligatory, sequential precedent to the second event (Tyr_{41}), catalyzed by spleen tyrosine kinase (Syk). Site mutations in L_E, or kinase-specific inhibitors, prevented L_E phosphorylation and subsequent Nup phosphorylation. Parallel experiments with L_S (SafV-2) and L_T (TME BeAn) proteins confirmed the general cardiovirus requirement for L phosphorylation, but CK2 was not the culpable kinase. It is likely L_S and L_T are both

activated by alternative kinases in different cell types, probably reactive within the Theilo-specific domains.

INTRODUCTION

Cardioviruses in the *Picornaviridae* family are subdivided into two species, the *Encephalomyocarditis viruses* (EMCV) and *Theiloviruses* (TMEV). EMC-R is the prototype isolate for this genus. Although various EMCV have been isolated from diverse mammalian hosts, predominantly these are rodent viruses. Most are fairly homogeneous in sequence, host-range and pathogenicity (for review see (49)), in that they cause myocarditis, encephalitis or diabetes-like symptoms (340). The TMEV in contrast, include variants like Vilyuisk human encephalomyelitis virus, Theiler's-like rat virus, Theiler's murine encephalitis virus (TME) and the Saffold viruses (SafV) 1-8. Strains of TME are subdivided into those which are neurovirulent (e.g. GDVII and FA) and those that cause persistent demyelination (e.g. DA and BeAn). The demyelinating strains are frequently used to model multiple sclerosis etiologies in mice (for review, see (230)). The SafV are human viruses, first isolated from a stool sample of a feverish child (148). They are yet to be linked to any particular human disease, although recent work suggests they can stubbornly persist in their hosts (126) and SafV-2 has the potential to become neurotropic when inoculated intracerebrally into mice (124).

A hallmark of all cardioviruses is the short Leader (L) protein translated at the NH_2-terminus of the viral polyprotein (Supplemental Fig 2-1). While other picornaviruses can encode alternative proteins at this location (e.g. *Aphtho-* and *Erbovirus* L^{pro}), the

cardiovirus Ls always display an unusual CHCC zinc-binding domain, a central linker, a short, concentrated acidic region, and additional Ser/Thr-rich motifs, characteristic of their species (54, 64, 86, 245, 264). After translation, these highly charged (pI of ~ 3.7) proteins are released from an L-P1-2A precursor by the activities of the downstream 3C protease. Post-release from the polyprotein during infection, or as a recombinant protein, the L from EMC-R (L_E, 67 amino acids), triggers a lethal cellular phosphorylation cascade, aimed at the nucleoporins (Nups), which form the hydrophobic core of nuclear pore complexes (NPC). The degree of Nup hyper-phosphorylation is so extensive, and so unlike anything that happens during the normal cell cycle, that it completely disrupts all tested active host nucleocytoplasmic trafficking pathways (22, 183, 258) (J. Ciomperlik unpublished results). The altered NPC become open to widespread passive diffusion, allowing essential components to leak from the nucleus and become available for cytoplasmic viral replication. At the same time, active trafficking of signaling proteins (e.g. for interferon induction) or transport of transcribed cellular mRNAs, ceases abruptly. This potent, unique anti-host response presumably prevents the cell from mounting an effective retaliation against the virus, and is probably the reason most EMCV, and certainly EMC-R, are highly pathogenic to mice (LD_{50} = <100 pfu) (109).

The L_E-dependent Nup phosphorylation cascade requires an early obligate binding between L_E and the NPC transport regulatory protein, Ran-GTPase (16, 256). Stoichiometric interaction requires catalytic facilitation by RCC1, a nuclear-localized guanidine-nucleotide exchange factor, which helps Ran morph into the appropriate (GDP or empty) conformer (160). Once bound however, L_E:Ran complexes are virtually

non-dissociable. They have a K_D of ~3 nM and cannot be disrupted by exogeneous nucleotides, implying that Ran becomes locked into some virus-preferred format (249). L_E:Ran is the foundation complex through which host kinases are subsequently recruited in poorly understood secondary steps, to carry out the actual Nup hyper-phosphorylation events within the NPC. Inhibition of ERK1/2 or p38 pathways prevents L_E activities during EMC-R infection, identifying these kinases as participants, if not the actual phosphate contributors (257).

Complicating this picture are observations (86, 351), or in some cases predictions (264, 305), that L_E as well as L_T (from TME), are themselves phosphorylated during infection. L_E (recombinant or during infection) exposed to eukaryotic cells or cytosol, reacts with antibodies specific to phospho-tyrosine, predicted as Tyr_{41} (86), but other studies have suggested Thr_{47} as the target site (351). Mutation here ($Thr_{47}Ala$) disrupts L_E functions during infection, such that NPC trafficking inhibition is delayed (183), Nup phosphorylation is abrogated (22) and IFN-α/β transcription is no longer blocked (114). The L_E functions can be restored by substituting a phosphomimetic glutamate ($Thr_{47}Glu$) at this key position (22, 114, 183). However, *in vitro* Nup phosphorylation assays with digitonin-treated cells and recombinant L_E, are not responsive to mutation at Tyr_{41} or Thr_{47} (86, 258). Casein kinase II (CK2) can phosphorylate recombinant L_E at Thr_{47} in cell-free assays (351), but there is no evidence this is the kinase that acts upon L_E *in vivo*. Nor is there evidence in cells, or any recombinant reconstructions, that currently discriminate L_E, L_T, or L_S (SafV) phosphorylation as a consequence or antecedent to the Nup phosphorylation cascades.

The L_T and L_S proteins share many properties with L_E, including the NH_2 zinc-binding domain, central linker, acidic domain and COOH terminal 8 amino acids (see Sup Fig 2-1). They are shorter by 7 residues at the immediate NH_2 terminus, but instead have insertions of 10 (Saf) or 15 (TME) extra residues just upstream of the conserved COOH motif. The extra common residues ("Theilo domain"), and the extra TME-specific residues ("Ser/Thr domain"), make the L_S (71 aa) and L_T (76 aa) a bit longer than the L_E although they all are expected to have reasonably similar biological functions (245). The L_T (DA strain) has been linked to disruption in NPC trafficking (75), induction of Nup phosphorylation (specifically Nup98) (265) and inhibition of interferon responses (315). The L_E from EMC-R can actually replace L_T (DA) in infectious virus, albeit with somewhat reduced viral replication efficiency (245). Neither L_T nor L_S from any strain has ever been tested directly as a phosphorylation substrate. Thr_{63} of L_T (DA) was suggested as such, because Thr_{63}Ala substitution reduced Nup98 phosphorylation in L929 cells. Virus with this mutation had reduced toxicity to BALB/3T3 cells, while an analogous phosphomimetic, Thr_{63}Asp, retained the wild-type phenotype (264). The L_T Ser_{57} (DA, BeAn) locale, was also proposed as a putative phosphorylation site, because as one of the few known sequence discontinuities in the Ser/Thr rich domain, this amino acid (Pro_{57}, GDVII), correlates with virus growth kinetics in BHK cells (305).

Now, with recombinant proteins, infections, transfections and cell-free assays, we have identified 2 obligate, sequential L_E phosphorylation steps. Neither influences the initial L_E binding to Ran (16), and yet both are both required for subsequent activation of the L-dependent Nup hyper-phosphorylation pathways. The primary event at Thr_{47} is catalyzed to completion by cellular CK2. The secondary event at Tyr_{41} is by cellular

spleen tyrosine kinase (Syk). In parallel, recombinant L_T (BeAn) and L_S (SafV-2) are shown to be directly phosphorylated by various cell extracts, including HeLa, but CK2 is not the primary agent, and the sites are not orthologous to L_E.

MATERIALS AND METHODS

Plasmids. Bacterial plasmids encoding active N-terminal GST-tagged EMC-R L protein (GST-L_E) have been described (64, 256). Pilot studies indicated analogous GST-fusions were not active for L_T and L_S proteins (not shown), so a new panel was engineered to place equivalent GST tags at the COOH termini, using multi-step PCR and a common backbone vector (pTriEx1.1, Novagen). A GST amplicon from pDEST24 (Invitrogen) converted the normal initiation AUG into a Leu codon (Supplemental Table 1, primers 1437 and 1390). Ligation into the backbone vector (pTriEx1.1) preceded ligation with a second amplicon (primers 1426 and 1345) encoding L_E from pFluc/L (256). Then, the vector sequence upstream of the L_E AUG codon was altered to provide stronger translation activity during eukaryotic transfection (primers 1433 and 1434). Plasmids pL_T-GST and pL_S-GST were constructed in parallel. A SafV-2 L amplicon was generously provided by Dr. Howard Lipton, after PCR from a full-length cDNA, (primers 1238 and 1239). After subcloning, the L_S gene was reamplified (primers 1393 and 1394) then ligated into the backbone vector (pL_S-GST). Plasmid pL_T-GST was similar, except the starting cDNA was from TME (BeAn), using primers 1120 and 1121 (into pGEX-6p-2, Amersham Biosciences). Two more steps into pT1.1 (primers 1244 and 1245) and then into pT1.1-GST (primers 1391 and 1392) completed the process. The final plasmid

set (pL$_E$-GST, pL$_S$-GST, pL$_T$-GST) differ only in the sequence of the L genes. Site-directed mutagenesis used 2-step PCR on these templates (129) with the indicated inside (mutagenic) and flanking primers (Supp Table 1) to create single or double-mutant sequences. Sequencing and restriction digests confirmed all constructs. The panel encodes T7 and CMV promoters and readily expressed the respective L$_X$-GST proteins as COOH-terminal GST fusions in *E.coli* (after IPTG induction) or HeLa cells (after plasmid transfection).

Protein Expression and Isolation. Protein samples for GST-L$_E$, L$_E$-GST, L$_T$-GST, L$_S$-GST and mutated derivatives were prepared as described (16, 64). Briefly, after IPTG induction of plasmid-transformed *E.coli* (Rosetta Competent Cells, Novagen), the lysates were fractionated with Glutathione Sepharose High Performance columns (GE Healthcare Life Sciences). Retained protein was exchanged into buffer (10 mM Bis Tris propane, 50 mM NaCl, 2mM DTT, pH 7.4) via spin column concentration (Millipore), and then subjected to anion exchange chromatography using a Bio-Scale Mini Ion Exchange cartridge (Bio-Rad). The L$_X$-GST peaks were concentrated (into 25 mM HEPES, 150 mM KCl, 2 mM DTT, pH 7.3) and stored at -80°C. Protein samples prepared this way typically contain 10-20% GST truncation products from premature termination within ORF, in addition to the full-length Lx-GST. In contrast, GST-L$_E$ preparations, especially those which undergo an additional Sephacryl S-100 fractionation (16) don't have such fragments. His-Ran was expressed and purified as described (16). Recombinant kinases CK2 (New England Biolabs), Syk (SignalChem) and Src (Cell Sciences) were obtained commercially.

Cell Procedures. HeLa cells (ATCC CRL-1958) were grown in suspension (37°C, 10% calf serum, 5% CO_2) in modified Eagle's medium. At 24 h pre-infection or transfection, they were plated into dishes. Infection (MOI=30) with vEC_9 (109) used an attachment period (30 min, 20°) before the cells were transferred to 37°C (4-5 h). In kinase inhibition studies, the cells were pretreated with (E)-3-(2,3,4,5-tetrabromophenyl) acrylic acid (TBCA, 10μM, Calbiochem) or 4,5,6,7-tetrabromo-2-azabenzimidazole (TBB, 50μM, Calbiochem) for 1 h pre-infection. The samples were maintained in the dark before, during and after (4-5 h) infection. Transfections with pL_X-GST cDNAs (1μg) used lipofectamine (1μM, Invitrogen) techniques (37°C, 5% CO_2, overnight) in 24-well plates with OptiMem media (Invitrogen). BHK-21 cells were a generous gift from Dr. John Yin. At harvest, all cells were washed with PBS, lysed in gel loading buffer (SDS), boiled and then fractionated by Laemmli SDS-PAGE.

Western Analyses. Proteins fractionated by SDS-PAGE were electro-transferred onto polyvinylidene difluororide membranes (Immobilon-P, Millipore), then blocked (10% nonfat dry milk) in Tris-buffer saline (TBST: 20 mM Tris, pH 7.6, 150 mM NaCl, 0.5% Tween-20, 20°C, 1 h). The membranes were washed (3x) with TBST before incubation (4°C, overnight) with an appropriate primary antibody (1% milk, TBST). These included αNup (mAb414, Covance) against Phe/Gly-containing Nups, αGST (mAb, 71087, Novagen) and αtubulin (mAb, T4026, Sigma-Aldrich). After further washes (3x, TBST), a secondary antibody (αmouse A2554, Sigma-Aldrich) was added (1% milk, TBST), incubated (20°C, 1 h) then removed (3x, TBST) before the membranes were reacted with enhanced chemiluminescence substrate (GE Healthcare) and exposed to film.

Phosphorylation Reactions. HeLa or BHK-21 cytosol from uninfected cells was prepared via dounce homogenization (324). Rabbit reticulocytes lysates were commercial (Promega). For inhibitor testing, TBCA (10μM) or TBB (50μM) in DMSO pretreated the HeLa cytosol (30 min, 37°C, in the dark) before use, and then were maintained in the reactions at the same concentrations. Phosphoryation reactions (80 μl, with 30 μl cytosol, 2 μl 10 mM ATP, 2 μg Lx-GST, 0.75 μl [γ-^{32}P]-ATP, ~12μCi/μl) were in GST binding buffer (50 mM HEPES, 150 mM NaCl, 0.5% NP40, pH 7.4) for 45 min (37°C). Glutathione Sepharose 4B beads (10 μl per sample, GE Healthcare Life Sciences) were then added, followed by agitation (room temp, 2 h). The beads were collected by centrifugation (500xg), washed with GST buffer (4x) then boiled with SDS gel loading buffer. Protein fractionation was by SDS-PAGE (8-10%), with band visualization by phosphoimaging (Typhoon 9200 Variable Mode Imager, GE Healthcare), silver stain or Western analysis.

Reactions with recombinant kinases were similar, except CK2 (10 units, New England Biolabs), Syk (10.3 units, SignalChem) and/or Src (10 units Cell Sciences) replaced the cytosol, and the commercial buffers recommended for these enzymes were used. Phosphorylation reactions with GST-L$_E$:Ran complexes were initiated with GST or GST-L$_E$ bound-Ran complexes on Glutathione Sepharose 4B beads, as described (16). The beads were collected by centrifugation (500xg) and then resuspended in reaction buffer (commercial for each kinase, 25 μl), containing 0.5 μl [γ-^{32}P] ATP (12.16μCi/μl), CK2 (10 U), Syk (10.3 U), or both enzymes (10 U each). Incubation was at 37°C for up to 60 min. The bead-bound complexes were washed, boiled with SDS and fractionated by SDS-PAGE.

Phosphorylation Quantitation. After Western assays or phosphoimigaging the gel-fractionated proteins bands were scanned by densitometry (Total Lab-TL 100, Sigma-Aldrich). Observed pixels were normalized to GST or tubulin loading controls in the wild type (L_E) or untreated (inhibitor) control samples. Stoichiometry measurements required the excision of (^{32}P) gel bands after autoradiography (4 independent lanes per sample type), followed by scintillation counting, using a method similar to Hollinger and Hepler 2004 (131). Controls and calibrated standards measured the degree of quench (4-8%). The dpm of recovered ionizing radiation was divided by the [γ-^{32}P]-ATP specific activity (304 μCi/μM) to determine the recovered phosphate. The protein content of analogous samples was assayed with BCA protein assay reagent kits (Thermo Scientific). Typically, this averaged ~78 pM of GST or GST-L_E per isolated gel slice. Stoichiometry, expressed as percent, recorded recovered phosphate (pM) per recovered protein (pM). Values >100% indicate multiple phosphorylation events (131).

Sequence Analysis. A dataset of unique Cardiovirus L sequences (Supplemental Figure 2-1) was compiled from GenBank and aligned by ClustalX (175). Post-translational modification predictions were performed with NetPhos2.0 (36), Phosphomotif Finder (5) and Phosida (100). Alignments were displayed with Weblogo (69).

RESULTS

L_E Mutagenesis. Recombinant EMC (Mengo strain) Leader protein (L_M) can be phosphorylated *in vitro* with CK2 at Thr$_{47}$ (351). Deletion analysis and ^{32}P-labeling

experiments by Dvorak et al 2001 (86) showed the closely-related EMC-R L protein (L_E) is phosphorylated during infection at a Tyr residue, presumed to be Tyr_{41}. Motif identification alogrithms, NetPhos 2.0 (36), Phosida (100) and PhosphoMotif Finder (5) concurred that both sites could be kinase targets (Sup Fig 2-1), but it was unknown whether these sites were alternatives, or additive. Accordingly, single and double substitution mutations ($Tyr_{41}Phe$, $Thr_{47}Ala$) were engineered into recombinant L_E-GST cDNA and the isolated proteins were tested for ^{32}P-incorporation (γ-ATP) after incubation with HeLa cell extracts (Fig 2-1A). GST tags were included because the small, highly charged L_E proteins by themselves are captured inefficiently by membranes during blotting steps (86, 256, 258). Relative to the wild-type protein, $Thr_{47}Ala$ and $Tyr_{41}Phe$ reduced label incorporation by 82% and 40% respectively. It required both mutations to eliminate all detectable phosphorylation. Parallel, single-proton NMR determinations confirmed these L_E sequences were properly folded (16). Therefore, both sites are phosphorylation targets and they contribute additively.

Phosphorylation by CK2 and Syk. Kinase identification by motif prediction is an uncertain process because many enzymes accept numerous related substrates and there is often functional redundancy. Of the multiple algorithms queried in this study, all concurred that L_E Thr_{47} fit the general consensus, [S/T]XX[D,E], for CK2. The Tyr_{41} site was anticipated less frequently, but when identified, spleen tyrosine kinase (Syk), and the related Src tyrosine kinase (Src) were the most commonly suggested enzymes. Syk and Src both phosphorylate a family of overlapping substrates, but neither has a precisely-defined target consensus with which they are guaranteed to react.
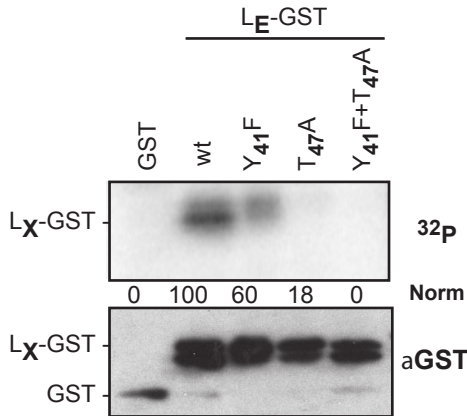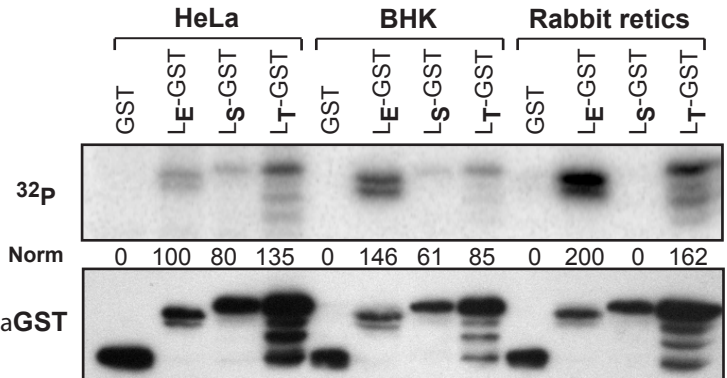
Figure 2-1. LX-GST phosphorylation in cytosol. (A) Recombinant L_E-GST and its phosphorylation site mutants were reacted with HeLa cytosol and [γ-^{32}P]-ATP. After SDS-PAGE, bands were detected by phosphorimaging (^{32}P) or Western analyses (αGST). Captured pixels were normalized relative to "wt" for ^{32}P and GST signals ("Norm"). (B) Similar to A, the panel of recombinant L_x-GST proteins were reacted with cytosol from HeLa cells, BHK cells or rabbit reticulocytes. Normalization was to L_E-GST.

Generically, both will accept Tyr in a regional acidic environment (+3, -3), with a preference for nearby aliphatics (120, 334).

When (commercial) recombinant CK2 was added to GST-L_E the reactions reached completion within 10-15 min (Fig 2-2B). Samples (4x) from each time-point were measured for both protein content and ^{32}P incorporation allowing an approximation of the stoichiometry. Although there is always variation in such measurements (Sup Table 2), in this case, the values fluctuated around a median of ~96% (StDev ±37%), or close to saturation. Surprisingly, parallel reactions with Syk had virtually undetectable incorporation when the enzyme was tested alone (Fig 2-2A). But when both enzymes were added together (Fig 2-2C), the ^{32}P counts more than doubled over that of CK2 alone, to a median of ~195% (StDev ±57%). In this case, completion required 15-30 min of reaction. These results are consistent with a secondary, Syk-dependent phosphorylation of GST-L_E at Tyr_{41}, sequential to that of CK2 at Thr_{47}. Reactions with Src, instead of Syk were not equivalent (Fig 2-2D). This enzyme did not react with GST-L_E even when added in combination with CK2.

During infection, L_E undergoes a tight 1:1 binding interaction with Ran-GTPase as an obligate step in NPC trafficking inhibition (249, 256). The complexes form between GST-L_E and Ran recombinant proteins (16) in the complete absence of L_E phosphorylation. The primary hinge-linker contact points for L_E (Lys_{35}-Trp_{40}) lie immediately adjacent to the Tyr_{41} and Thr_{47} phosphorylation sites, and although neither mutation inhibits complex formation (16), it was unknown whether Ran binding subsequently masked these sites, or if L_E phosphorylation needed to occur before Ran binding. Pre-formed recombinant GST-L_E:Ran complexes for the panel of L_E
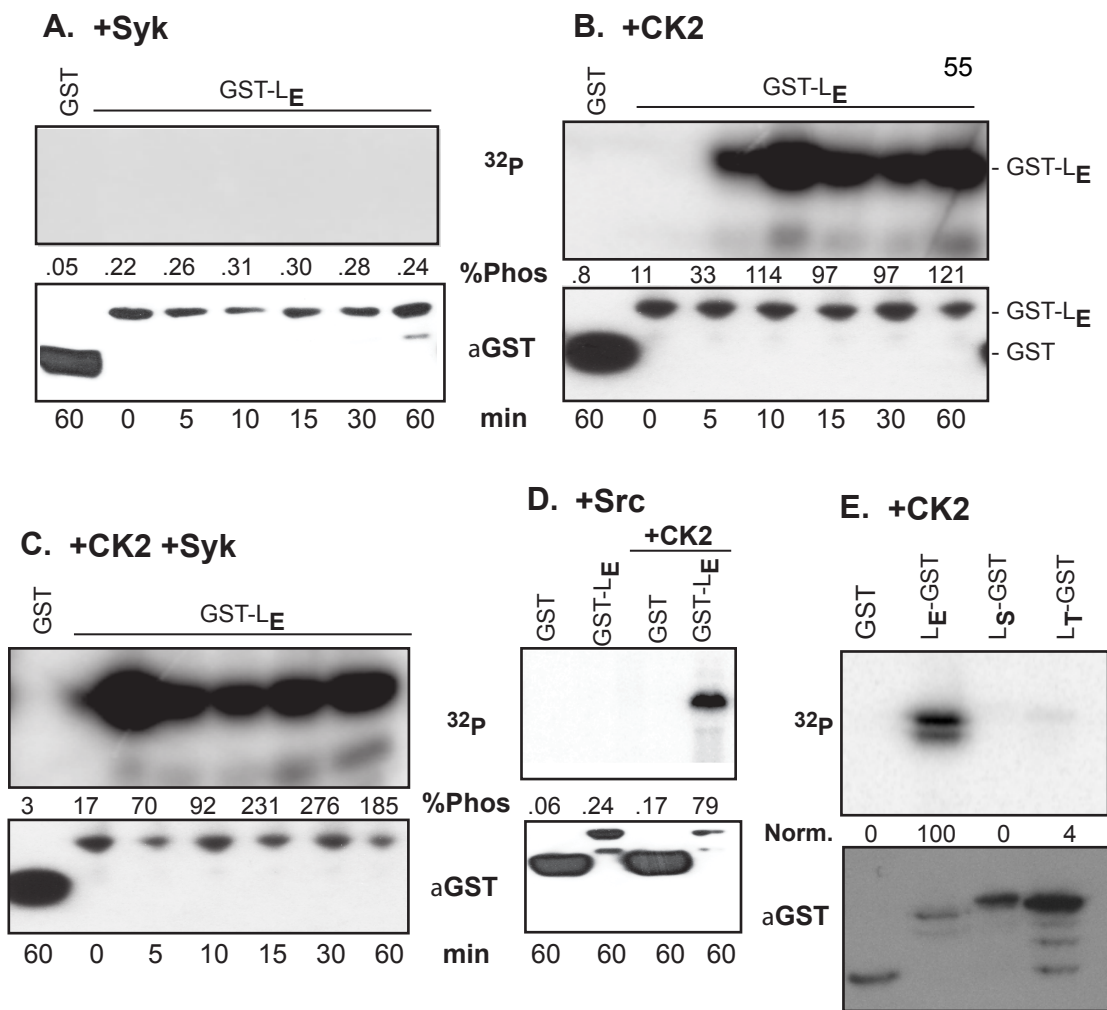
Figure 2-2. Phosphorylation quantitation. GST-L$_E$ was reacted with recombinant Syk (A), CK2 (B), or Syk + CK2 (C) for the indicated times (min). After SDS-PAGE, samples were cut from the gel(s) and analyzed for protein and ^{32}P content (Methods). Averaged values for 4 replicates (Suppl Table 2-2) are shown as "%Phos". (D) Similar to B and C, GST-L$_E$ was reacted with recombinant Src, or Src +CK2. (E) Similar to B, the panel of L$_X$-GST proteins was reacted with CK2. In this case, captured pixels were normalized relative to L$_E$-GST for ^{32}P and GST signals ("Norm").

phosphorylation mutants were reacted with CK2, Syk or a combination of these kinases. The phosphomimetic (Thr$_{47}$Asp) was included as a structural mimic for pseudo-phosphorylation at this site. As with the isolated GST-L$_E$ samples, CK2 readily labeled the wild-type protein as well as the Tyr$_{41}$Phe mutant, the only other sequence with an intact Thr$_{47}$ (Fig 2-3A). When similar complexes were pre-reacted with CK2 (cold ATP) and then labeled in the presence of Syk, the wild-type and the phosphomimetic were the only active substrates (Fig 2-3B). Simultaneous addition of CK2 and Syk again allowed Tyr$_{41}$Phe, to be actively labeled (Fig 2-3C). Clearly, neither kinase was inhibited by the Ran binding status of GST-L$_E$. With or without Ran, CK2 reactions at Thr$_{47}$, or a phosphomimetic at this position, were obligatory precursors to subsequent Syk reactions at Tyr$_{41}$.

CK2 Inhibition. HeLa cell extracts contain endogeneous CK2, and presumably this enzyme is responsible for initial L$_E$-GST reactions in that context (e.g. Fig 2-1A). The addition of CK2 inhibitors, TBCA and TBB, reduced HeLa cytosol-mediated incorporation significantly (Fig 2-3A). However, neither drug was completely effective, with 57% and 61% inhibition respectively. Parallel reactions with recombinant CK2 in buffer gave similar results (Fig 2-3B), indicating these particular inhibitors do not prevent all activity by this enzyme. The experimental "normalized" values in cytosol, were determined by relative densitometry and cannot distinguish L$_E$-GST samples with 1 or 2 added phosphates. Even partial phosphorylation by the primary kinase could (putatively) have still allowed reactions with the secondary enzyme. Collectively, though, the data demonstrate that CK2 is present in HeLa extracts, and logically it acts as the
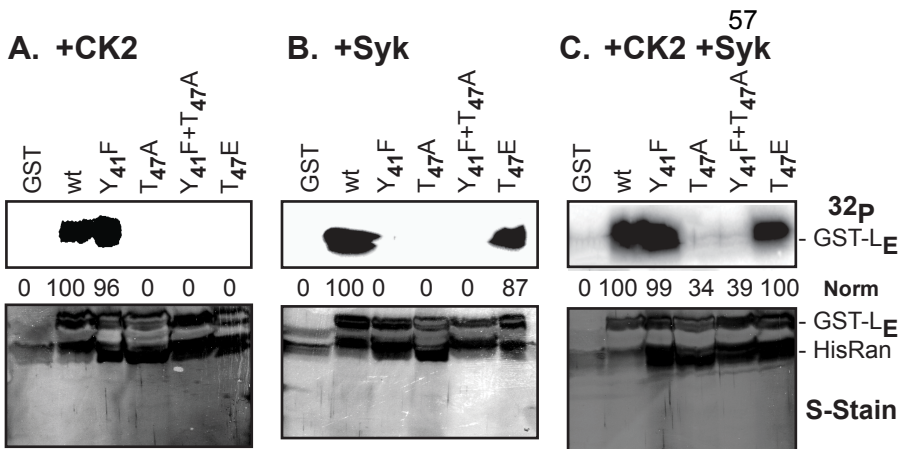
Figure 2-3. Phosphorylation of GST-L_E:Ran complexes. GST-L_E and the indicated mutant derivatives were reacted with recombinant His-Ran and the stoichiometric (1:1) complexes were isolated as described (Bacot-Davis et al 2013). Equivalent fractions were reacted with CK2 (A), Syk (B) or CK2 +Syk as in Fig 2 (60 min). After SDSPAGE, bands were detected by phosphorimaging (^{32}P) or silverstain ("S-stain"). Captured pixels were averaged (n=4) and normalized relative to "wt" for ^{32}P signals ("Norm"). For panels A&B, "100" denotes the maximum signal for one phosphorylation event. For panel C, "100" denotes the maximum signal for up to two events.

natural, dominant phosphorylation agent for the first L_E event (at Thr_{47}), just like the purified enzyme.

L_E-GST and Nup Phosphorylation. Digitonin-treated HeLa cells in the presence of *Xenopus* or HeLa extracts undergo GST-L_E dependent hyper-phosphorylation of Nups (258). The activity can be assayed by upward mobility shifts, particularly for Nup_{62}, when samples are labeled with ^{32}P or reacted with Nup-specific antibodies. GST-L_E with large deletions (e.g. removal of the acidic domain), or gross structural rearrangements (e.g. $C_{19}A$), do not induce this activity. Surprisingly, recombinant L_E with single point mutations at Tyr_{41} and Thr_{47} are functional in this assay, although mutation to Thr_{47} in Mengovirus is debilitating to virus growth (86, 258, 351). The primary difference in these approaches is the dose of Leader protein. Digitonin assays expose nuclei to high levels of GST-L_E. Infections provide significantly lower concentrations of translated L_E. To test the Leader phosphorylation mutations independent of infection, the panel of matched L_X-GST cDNAs was transfected into HeLa cells. As expected, the conformational mutation, $C_{19}A$, prevented Nup_{62} phosphorylation (Fig 2-4A). The $Thr_{47}Ala$ mutation and the phosphomimetic, $Thr_{47}Asp$, both reduced the Nup_{62} phosphorylation signal to 33-34%. The observed values at this primary site were lower than for the secondary $Tyr_{41}Phe$ mutation (by itself). However, when both GST-L_E phosphorylation sites were changed ($Tyr_{41}Phe + Thr_{47}Ala$), there was no observable shift in the Nup_{62} band. Therefore, at least one and preferably both L_E phosphorylation events must be prerequisites for this activity.

The Leader phosphorylation requirement is also manifest during virus infection. When vEC_9 is infected into HeLa cells, Nups become phosphorylated in a L_E-dependent
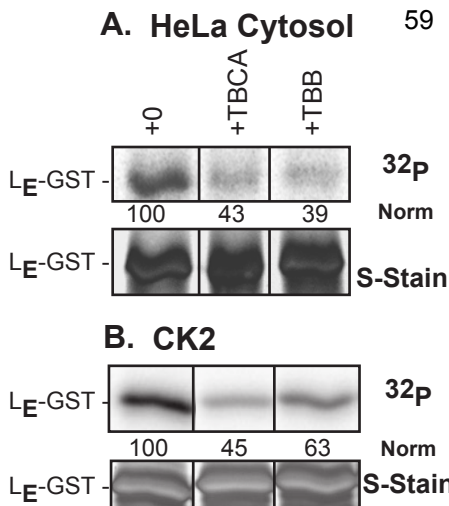
Figure 2-4. CK2 inhibitors. (A) HeLa cytosol was pretreated with TBCA or TBB, before L_E-GST was added with [γ-^{32}P]-ATP, as in Fig 1A. (B) GST-L_E was reacted with recombinant CK2 in the presence of TBCA or TBB and [γ-^{32}P]-ATP as in Fig 2B (45 min). After SDS-PAGE, bands were detected by phosphorimaging (^{32}P) or silver stain ("S-stain"). Captured pixels were normalized relative to "wt" for ^{32}P signals ("Norm").

manner (258). But, exposure of the cells with TBCA or TBB reduced the Nup_{62} phosphor-shifts to 62% and 16% respectively (Fig 2-5). For intact cells, TBCA is specific for CK2 at this concentration (Calbiochem screen of 28 common kinases) as is TBB (Calbiochem screen of 33 common kinases, *www.emdmillipore.com*). CK2 itself is not responsible for Nup phosphorylation (data not shown and (257)). The process only occurs when there is properly folded L_E that can act as a phosphorylation-competent substrate for CK2 and Syk.

Other Cardioviruses. The TME and Saf Leader proteins are orthologs and presumed functional analogs to L_E with regard to Nup phosphorylation triggers. Well-characterized cDNAs for SafV-2 and TMEV (BeAn) were chosen to represent this species. Ls and L_T share 43% and 39% amino acid identity relative to L_E, respectively (Sup Fig 2-1). Matched L_S-GST and L_T-GST genes were cloned into the same eukaryotic/prokaryotic expression vector as L_E-GST. Upon transfection of HeLa cells, both Theilovirus proteins induced Nup_{62} phosphorylation, but neither was as effective as GST-L_E, where the band shift was nearly twice as pronounced (Fig 2-5B). All the shifts were L_X-dependent activities though, because disruption of each Leader conformation with a debilitating zinc-finger mutation (i.e. $Cys_{11}Ala$) significantly reduced Nup_{62} phosphorylation.

Among the known set of Saf and TME viruses, none conserve the identical context of Thr_{47} required for primary kinase recognition of L_E (Sup Fig 2-1). That Theilovirus Leader proteins are themselves phosphorylated *in vitro* or *in vivo*, or whether such activity is dependent on cell type, has never been demonstrated. Transfections (e.g. L_X-GST) and infections rarely produce enough Leader from any cardiovirus for a thorough study of native phosphorylation status. Instead, as a first test

A. L_E-GST

	wt	$C_{19}A$	$Y_{41}F$	$T_{47}D$	$T_{47}A$	$Y_{41}F+T_{47}A$
Norm	100	5	80	34	33	0

Nup$_{62}$-   αNup

αTubulin

B. L_E- L_S- L_T-GST

	GST	wt	$C_{19}A$	wt	$C_{11}A$	wt	$C_{11}A$
Norm	1	100	22	47	3	39	1

Nup$_{62}$-   αNup
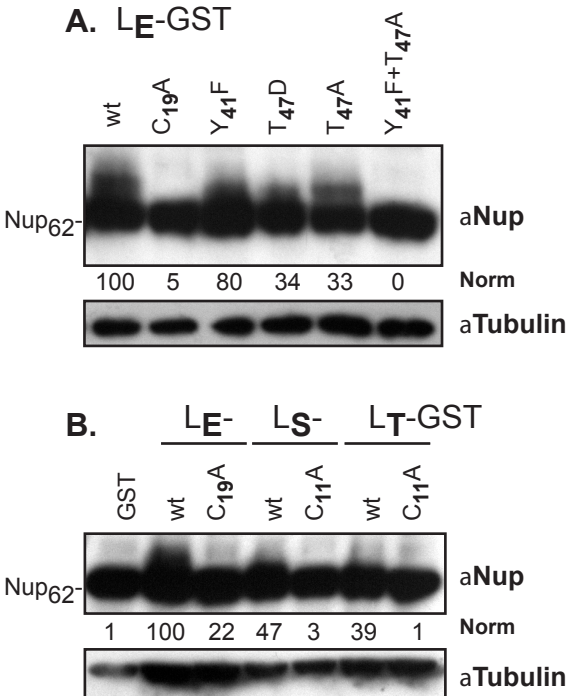
αTubulin

Figure 2-5. Nup phosphorylation after transfection. HeLa cells were transfected with the panel of L_E-GST cDNAs (Methods). After 24 h, the cells were collected, lysed then fractionated by SDS-PAGE. Western analyses were with αNup and αTubulin. Phosphoshift was quantified using Total-Lab Quant. Normalization was relative to tubulin and the "wt" signal. Upwards mobility shift was quantified as in Porter et al 2010 (20). (B) Similar to A, cDNAs for L_x-GST and inactive (C_xA) mutant derivatives were transfected into HeLa cells them monitored for Nup62 phosphorylation activity.

F

62
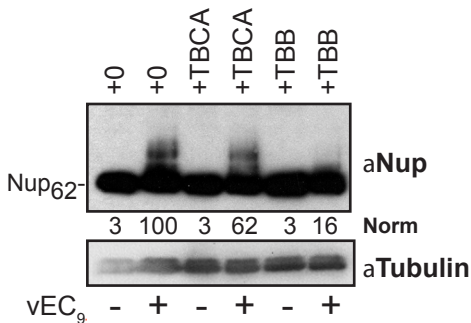
Figure 2-6. Nup phosphorylation during infection. HeLa cells were pretreated with TBCA or TBB, then infected with vEC_9 (MOI=30). The inhibitors were maintained during infection. Harvested cells (5 h) were fractionated by SDS-PAGE and subject to Western analyses as in Fig 2-5.

of such activity, the matched set of recombinant L_X-GST proteins were reacted with cytosol from HeLa cells, BHK cells or rabbit reticulocytes (Fig 2-1B). All 3 extracts labeled L_E-GST and L_T-GST with ^{32}P, albeit with quite different efficiencies. For L_E-GST, the preferred efficiency, normalized to the amount of protein, was reticylocytes> BHK > HeLa, with a nearly 4-fold difference over spectrum of cell types. For L_T-GST, it was reticulocytes > HeLa> BHK. Equivalent amounts of L_S-GST were only weakly labeled in HeLa and BHK by comparison, and not phosphorylated at all in reticulocyte extracts.

The varied reactivity of these proteins in multiple cell types is expected if each Leader sequence relied on different kinases for self-phosphorylation. Indeed, when recombinant CK2 was added directly to these proteins, it was unable to label L_S-GST or L_T-GST (Fig 2-2E). Therefore, while phosphorylation is obviously part of the Leader activity profile for all cardioviruses, each species (or clade?) seems to take advantage of its unique sequences to present preferred sites to different endogeneous kinases, perhaps in a cell-specific manner.

DISCUSSION

Many viral proteins are phosphorylated by cellular kinases for a variety of functional reasons. The dengue virus NS5 RNA-dependent-RNA-polymerase, for example, has a bipartite nuclear localization signal (NLS) that is turned on and off by phosphorylation with CK2 (93). In fact, CK2 is one of the most commonly identified kinases utilized by viruses to phosphorylate their proteins (155). Before the current report, it was known that the EMCV Leader protein was phosphorylated during infection,

presumably by CK2 at Thr_{47}. The significance of that modification, or of dual modification at Thr_{47} and Tyr_{41}, was unclear.

The data presented here show that L_E phosphorylation, first at Thr_{47} and then at Tyr_{41}, are both required to optimize the ability of EMCV to trigger Nup phosphorylation and the consequent inhibition of cellular nucleocytoplasmic trafficking. Logically, such an important, initial reactive step should be performed by a constitutively active, ubiquitous kinase like CK2 (102). L_E mutations and CK2 inhibitors identified this enzyme in cells or recombinant form, as reactive with Thr_{47}. This event was an obligate precursor to subsequent phosphorylation with Syk at Tyr_{41}. Although several other kinases are known to require CK2 activity before they can act, for example, glycogen synthase kinase (90, 323), to our knowledge this is the first example of CK2 priming a Syk event. Syk, another ubiquitous kinase, usually selects tyrosine sites surrounded by negative charges (132). Yet Tyr_{41} within the highly acidic domain of L_E (pI 3.7) was completely unreactive, unless CK2 was added beforehand. Cooperation between Syk and CK2 has been reported before. Luz et al 2011 found that CK2 and Syk will co-phosphorylate CFTR, the protein responsible for cystic fibrosis. Those data attributed the primary phosphorylation event to Syk, with the consequence as altered CFTR trafficking (194).

The exact cellular mechanistic steps enabled by L_E phosphorylation, remain to be determined, although intracellular localization, trans-nuclear trafficking, or changes in binding partner preference are certainly possibilities. Syk reactions at Tyr_{41} were able to bypass the requirement for prior phosphorylation by CK2 at Thr_{47} when a phosphomimetic aspartate was encoded at this position (Fig 2-3). However, both sites

needed to be wild-type and properly phosphorylated for maximum Nup phosphorylation

(Fig 2-5). Surprisingly, the L_E phosphorylation status does not inhibit tight Ran binding

(249) and the protein could be readily phosphorylated after complex formation (Fig 2-3).

If simple L_E trafficking were affected by phosphorylation, one might not expect this

result. Rather, we favor the idea these L_E modifications play a role subsequent to Ran

binding, perhaps in the selection, tethering or retention of the actual Nup

phosphorylation agents, like ERK1/2 and p38 ((257), J. Ciomperlik unpublished results).

Now that sequential, defined self-phosphorylation by CK2 and Syk are acknowledged

precursors to L_E trafficking inhibition, the next steps in reconstruction the full reaction

cascade can be approached.

The Theilovirus Leaders, L_T and L_S are presumed to have analogous functions to

L_E, and yet they differ in their display of 1-2 added short peptide insertions that are

exceptionally rich in putative cellular phosphorylation motifs. Neither the L_T with

$[C_{40}]$XDLD, or the L_S with $[T_{40}]$XXL[D,E], from any described virus in this species has

the required CK2 consensus sequence (Sup Fig 2-1). Furthermore, only the L_S but not

the L_T sequences maintain the potential secondary site (Tyr_{34}) equivalent to L_E Tyr_{41}.

CK2 does not react with either protein in recombinant form, although both proteins do

become phosphorylated when treated with extracts from HeLa or BHK cells (Fig 2-1). It

will require extensive mutagenesis, NMR folding studies, and kinase "guesses" to

establish where and how L_T and L_S encode their alternative sites. That they behave

different from each other in reticulocyte extracts, suggests the individual Theilo-domains

may be targeted independently. It is clear however, that each of these Leader proteins

participates directly in the pathways causing Nup phosphorylation. Transfection of L_X-

GST cDNA into cells directly triggered this activity. Parallel L_X zinc-finger mutations were inhibitory in all cases (Fig 2-5). These functional differences are conceivably clade-specific adaptations to particular cell types, and most probably, the respective differential phosphorylation patterns are the key to these proteins' variability.

ACKNOWLEDGMENTS

Supplemental Table 2-1: Primer sequences

Primer	Use[1]	Sequence[2]
1120	L_T (1)	TGTCACCATGGCCTGCAAACATGGATACCCAG
1121	L_T (1)	CCCCGGCCGTTATTACTGGGGTTCCATGACAATATCGCGT
1149	L_S outside R	TGTTTCCCCGGGTCCAATAACCTAGTATAGGGGACAT
1214	L_E outside F	GATGCATGCTCGAGTCACTACTGT
1237	L_E outside R	TCGATCTCAGTGGTATTTGTG
1238	L_S (1)	GTTGACTGGCCCATGGCGTGCAAACACGGATATCC
1239	L_S (1)	CTTTCACTCGAGTTCTCCTTCCATTCAATGTCTTG
1244	L_T (2)	GCCCCTGAGCTCTATGGCCTGCAAACATGGATA
1245	L_T (2)	GGCCGCTCGAGCTGGGGTTCCATGACAAT
1345	GST (2)	GGAAGCCCGCTCGAGCTGTAACTCGAAAAC
1390	GST (1)	CCTTTCGGCTCGAGTTAGCAG
1391	L_T (3)	GAGAGAATTCATGGCCACAACC
1392	L_T (3)	GGTGGTGAAGCTTCTGTAACTC
1393	L_S (2)	CAAAGGAGAGAATTCATGGCGTGCAAAC
1394	L_S (2)	GGTGAAGCTTTTGTGGTTCCATTTC
1396	L_T outside R	GGTGAAGCTTCTGGGGTTCCATG
1426	GST (2)	CACGATGATACCATGGCCACAACAATG
1433	GST (3)	GATATCCCGGGTTAATTAAGGAGCGCCGCCATGGCCACAACCATGGAA
1434	GST (3)	ATCCTCTCCATCAGTCAATAACTCCTCTGGGTACCATTCTTCATCATACTTTAGCA
1437	GST (1)	CAAAGTGAAGCTTCTGTCCCCTATAC
1514	$L_{S,T}$ outside F	TTCGGCTTCTGGCGTGTGA
1610	L_E $Y_{41}F$	GTATGATGAAGAATGGTTCCCAGAGGAGTTATTG
1611	L_E $Y_{41}F$	CAATAACTCCTCTGGGAACCATTCTTCATCATAC
1616	L_E $T_{47}A$	CCCAGAGGAGTTATTGGCTGATGGAGAGGATGATG
1617	L_E $T_{47}A$	CATCATCCTCTCCATCAGCCAATAACTCCTCTGGG
1638	L_E $C_{19}A$	CTTTTGAGGAAGCCCCAAAATGCTC
1639	L_E $C_{19}A$	GAGCATTTTGGGGCTTCCTCAAAAG
1640	L_S $C_{11}A$	GATATCCGCTTATGGCCCCTCTTTGCACTG
1641	L_S $C_{11}A$	CAGTGCAAAGAGGGGCCATAAGCGGATATC
1642	L_T $C_{11}A$	GATACCCAGATGTGGCCCCTATTTGCACAG
1643	L_T $C_{11}A$	CTGTGCAAATAGGGGCCACATCTGGGTATC

[1] Primer pairs were used in various cloning steps for these genes. The separate steps (Methods) are indicated in parentheses. "Outside" primers refer to those flanking L used in combination with mutagenic primers in 2-step PCR methods.

[2] Primer sequences are 5'-3'.

Supplemental Table 2-2: Phosphorylation Quantitation

Kinase[1]	Substrate[1]	Rxn time (min)[1]	Sample1[2]	Sample2[2]	Sample3[2]	Sample4[2]
CK2	GST	60	1	1	0.09	1
CK2	GST-L_E	0	33	9.4	9.4	13
CK2	GST-L_E	5	33	32	33	32
CK2	GST-L_E	10	60	65	70	260
CK2	GST-L_E	15	96	96	99	96
CK2	GST-L_E	30	97	96	99	96
CK2	GST-L_E	60	182	80	40	180
Syk	GST	60	0.07	0.04	0.04	0.04
Syk	GST-L_E	0	0.22	0.26	0.22	0.23
Syk	GST-L_E	5	0.24	0.26	0.26	0.26
Syk	GST-L_E	10	0.31	0.33	0.31	0.31
Syk	GST-L_E	15	0.31	0.30	0.30	0.30
Syk	GST-L_E	30	0.28	0.29	0.28	0.28
Syk	GST-L_E	60	0.24	0.24	0.26	0.24
CK2 + Syk	GST	60	3	3	3	3
CK2 + Syk	GST-L_E	0	5	7	7	8
CK2 + Syk	GST-L_E	5	67	67	67	77
CK2 + Syk	GST-L_E	10	91	94	91	92
CK2 + Syk	GST-L_E	15	260	205	200	260
CK2 + Syk	GST-L_E	30	374	370	180	180
CK2 + Syk	GST-L_E	60	370	370	190	190
Src	GST	60	0.06	0.06	0.06	0.06
Src	GST-L_E	60	0.24	0.23	0.24	0.23
CK2 + Src	GST	60	0.14	0.14	0.14	0.24
CK2 + Src	GST-L_E	60	80	78	118	80

[1] Phosphorylation reactions between the indicated substrate(s) and recombinant kinases were as in Fig 2-2 ABCD.

[2] For each enzyme/substrate combination, 4 separate samples were analyzed for protein content and ^{32}P incorporation as described in Methods (Fig 2-2). The results from each determination are shown as percent incorporation (saturation) per unit of substrate. The mean values label the lanes in Fig 2-2 ABCD.

A.

B.
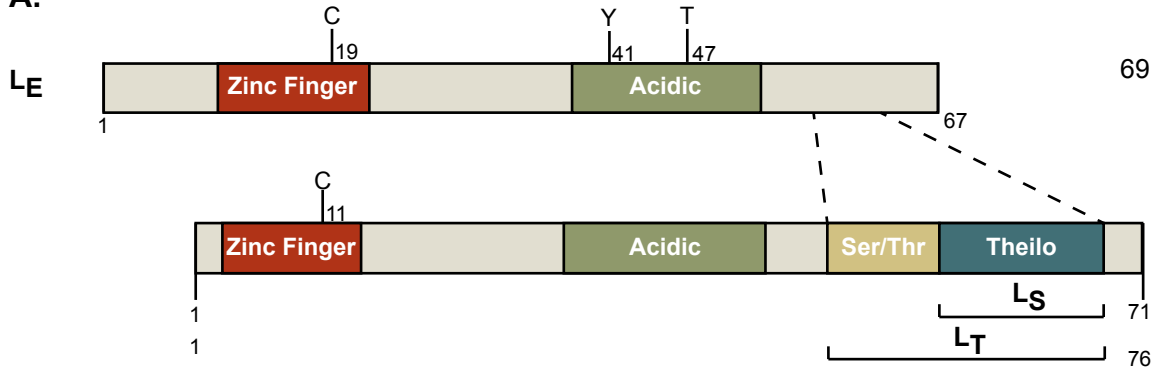
Syk, Src: **Y** in an acidic environment with nearby aliphatics

CK2: [S/**T**]xx[D,E]
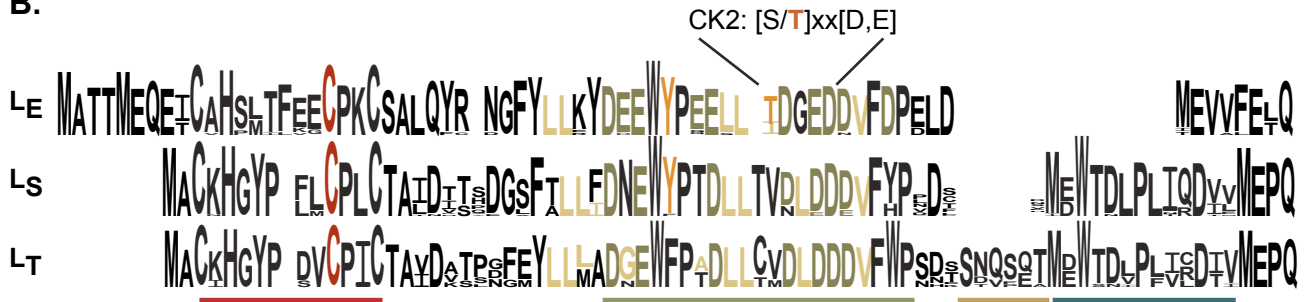
C.
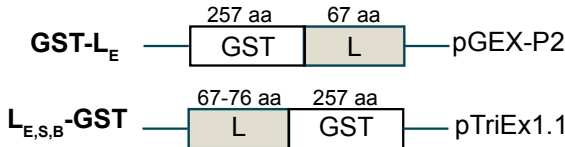
Supplementary figure 2-1. Cardiovirus Leader proteins. (A) Domain maps for L_E, L_S and L_T show the cited mutations and named sequence motifs (B). ClustalX (30) was used to create an alignment of unique cardiovirus Leader sequences (46 sequences) which are summarized by Weblogo depictions. Zinc finger mutations ($C_{11/19}$) are highlighted in red. Mapped L_E phosphorylation sites are in orange. Consensus Syk and CK2 phosphorylation motifs are indicated.

CHAPTER 3.

Cardiovirus Infection Causes Activation of AMP-activated Protein Kinase,

which Phosphorylates the Leader Protein at Discrete Sites.

Holly A. Basta and Ann C. Palmenberg

Author contributions: HAB performed all experiments.

ABSTRACT

Cardioviruses, including the *encephalomyocarditis virus* (EMCV) and *Theilovirus* species, encode a small, unique protein named Leader (L). This protein modulates the cell to enhance viral infection by inhibiting active nucleocytoplasmic transport and suppressing the interferon response. L localizes to the nuclear rim, binds the cellular protein RanGTPase and causes activation of mitogen activating kinases (MAPKs). These MAPKs phosphorylate nuclear pore proteins (nucleoporins, or nups), presumably causing the observed inhibition of active transport. Phosphorylation of the EMCV L protein itself at two distinct sites has been shown to be important for nup phosphorylation and trafficking inhibition. These phosphorylation events are sequential, with the primary kinase being casein kinase 2 (CK2). While other cardioviruses, Saffold virus (SafV) 2 and Theiler's murine encephalitis virus (TMEV), BeAn strain (both Theilo-species viruses) are phosphorylated, the responsible kinase is not CK2. We show here that these Theilovirus L proteins (L_S and L_T), along with EMCV's L (L_E), can be phosphorylated by AMP-activated protein kinase (AMPK) at distinct sites (Thr_{47} for EMCV, Thr_{58} for SafV and Ser_{57} for TMEV). Viral infection (vEC_9 or vBeAn) causes activation of AMPK. Mutation of the AMPK phosphorylation site in each L attenuates AMPK activation during infection, as well as L-directed MAPK activation and nucleoporin phosphorylation.

INTRODUCTION

Picornaviruses are small, positive-sense, single-stranded RNA viruses. The *cardiovirus* genus, divided into *encephalomyocarditis* (EMCV) and *Theilovirus* species,

encompasses a group of viruses that is diverse in both host range and disease etiology. The EMCV species primarily infects rodents, but has been isolated from a menagerie of mammalian hosts (50), causing severe encephalitis and myocarditis. The *Theilovirus* species is further divided into Theiler's murine encephalitis viruses (TMEV) and Saffold viruses (SafV). The TMEVs infect rodents and cause either acute neurovirulence (GDVII and FA strains) or persistent demyelination (DA and BeAn) akin to multiple sclerosis (MS) in humans. The SafV are human viruses, and have been linked to a range of symptoms (gasteroenteritis, respiratory illness, flaccid paralysis, etc.). There is also speculation that SafV may play a role in MS, as SafV can become persistent in cell culture (126) and shows neurotropic symptoms in mice when inoculated intracerebrally (124).

The cardioviruses encode a unique protein, Leader (L), not found elsewhere in nature. This small (~7kDa) protein is responsible for much of the virus' anti-host functions. TMEV (DA) L can inhibit stress granule formation (43), EMCV and TMEV Ls can inhibit nucleocytoplasmic trafficking (22, 75, 183, 257, 258), and SafV, TMEV and EMCV Ls can all induce phosphorylation of nucleoporins (nups) ((258, 264), (26)), likely by causing the activation of mitogen activating kinases (MAPKs) (257). During EMCV infection, MAPKs ERK1/2 and p38 and their downstream substrates MAPKAP-2 (MK2) and RSK are activated in an L-dependent manner (257). Chemical inhibition of ERK1/2 and p38 abolishes L-directed nup phosphorylation (257). TMEV and EMCV Ls can be either pro- or anti-apoptotic, depending on the viral strain and cell culture system (13, 51, 97, 127, 229, 270, 300). EMCV L can bind RanGTPase (K_d=~3nM), localizing to the

nuclear rim (249, 256), and the viral protein 2A (R. Petty in preparation), which contains a nuclear localization signal (NLS) (104).

The cardiovirus L proteins vary more than the rest of the genome; EMCV and TMEV(BeAn) Ls share less than 40% amino acid identity. EMCV (mengo strain) L's NMR structure has been solved (Palmenberg, unpublished) (Fig 3-1) and contains a zinc finger and an acidic domain, which are conserved in all cardioviruses. The Theiloviruses have additional C-terminal domains: the Ser/Thr rich domain (found in TMEVs) and the Theilo domain (found in SafVs and TMEVs) (Fig 3-1). The function of these domains has only been partially elucidated. Mutations to the Theilo domain in TMEV (DA) L cause reduced apoptotic activity, decreased ability to inhibit nucleocytoplasmic trafficking, reduced Nup98 phosphorylation ability, decreased ability to inhibit IFN-β and RANTES, decreased ability to inhibit IRF-3 dimerization, and decreased persistence in FVB/N mice (264). Furthermore, mutations to the Theilo domain prevent TMEV (DA) L's ability to inhibit stress granule formation (43). These Theilo domain mutations show similar etiology to the zinc finger mutation, which creates a misfolded L protein (16), suggesting that the Theilo domain contains important structural features. Mutations to the Ser/Thr rich domain (3S-3A, mutating Ser 51, 53 and 54), however, had little or no effect on TMEV (DA) L functionality (264). Other studies posit that the Ser/Thr domain is responsible for differences between TMEV GDVII and DA L's abilities to cause apoptosis (300) and L's intracellular localization (306). Residues in both the Theilo domain (Thr_{63}) (264) and the Ser/Thr domain (Ser_{57}) of TMEV (DA strain) (306) have been suggested to contain a phosphorylation site.

Indeed, TMEV L is phosphorylated (26), but prior to this study the sites of phosphorylation had not been determined.

Phosphorylation plays an important role in EMCV L functionality, as mutations to phosphorylation sites delay L's nucleocytoplasmic shutdown ability (183), allow increased IFN-β production during infection (351) and attenuate L-directed nup phosphorylation (26). EMCV L is phosphorylated sequentially by casein kinase 2 (CK2) and spleen tyrosine kinase (Syk) on Thr_{47} and Tyr_{41}, respectively (26). The kinases involved in Theilovirus L phosphorylation have not been characterized before now, but CK2 was previously found *not* to be the responsible kinase (26).

Here we define the phosphorylation sites of SafV-2 (L_S) and TMEV (BeAn) (L_T) L proteins (Ser_{57} and Thr_{63}, respectively), and identify AMP-activated protein kinase (AMPK) as a kinase that acts upon these sites. Additionally, AMPK can phosphorylate EMCV L (L_E) at Thr_{47} (the previously defined CK2 phosphorylation site). AMPK is activated during Cardiovirus infection (vEC_9) and mutation of the AMPK phosphorylation sites in L attenuates this activation. Finally, the L phosphorylation site-mutated proteins cause attenuation of MAPK activation in infection, as well as L-directed nup phosphorylation.

MATERIALS AND METHODS

Plasmids. pL_E-GST, pL_S-GST and pL_T-GST and select mutations (L_E-C_{19}A, -Y_{41}F, -T_{47}A, L_S-C_{11}A and L_B-C_{11}A) were prepared as described in (26). Additional mutations were created using site-directed mutagenesis by overlap extension (129). Briefly, the forward flanking primer (1514) and the reverse mutagenic primer (ex. 1627) amplified

the N- terminal half of L, while the reverse flanking primer (1149 or 1237) and the forward mutagenic primer (ex. 1626) amplified the C-terminal half of L. These PCR fragments contained overlapping sequence, and a third PCR reaction amplified the full L with single amino acid mutation from the two halves using the flanking primers (Table S1). Insert and vector (pT1.1-GST) were digested with XbaI and HindIII (NEB), ligated with T4 DNA ligase (NEB) and transformed into competent MV1190 *E. coli*. Restriction digests and Sanger sequencing confirmed all sequences.

EMCV-R cDNA pEC9 is as described (109). pEC9-$T_{47}A$ (a generous gift from F. Porter) was created with a two-step site directed mutagenesis procedure as above, with primers 972+1033 and 975+1034. The insert and vector (pEC9) were digested with AvrII and NheI (NEB), ligated and *E. coli* transformed as above.

pGEM^R-3 TMEV(BeAn) cDNA (47, 167) was a generous gift from Dr. Howard Lipton. pGEM^R-3 TMEV (BeAn) L $S_{57}A$ cDNA was created using the procedure above, with primers 1761+1637 and 1763+1636. The insert and vector were digested with SacII and AgeI and ligated as above. STBL4 competent *E. coli* were transformed, and the sequence confirmed as above.

Recombinant proteins. Protein samples for L_E-GST, L_S-GST, L_T-GST, and phosphorylation site mutated L_X-GSTs were prepared as described (64). Briefly, plasmid-transformed Rosetta Competent *E. coli* (Novagen) were induced with IPTG, sonicated and lysates were fractionated with a Glutathione Sepharose High Performance column (GE Healthcare Life Sciences). Protein was eluted with free

glutathione, exchanged into buffer (25 mM HEPES, 150 mM KCl, 2 mM DTT, pH 7.3) and stored at -80°C. AMPK (α1,β1,γ1) was obtained commercially (SignalChem).

Cells and viruses. HeLa cells (ATCC CRL-1958) adapted for suspension (37°C, 10% calf serum, 5% CO_2) were grown in modified Eagle's medium. Cells were plated 24 hrs before transfection or infection. HeLa cytosol from was prepared via dounce homogenization as in (324).

Viral stocks were derived from HeLa cell transfection of cDNA-derived RNA transcripts, which were titered by plaque assay. Transfections were performed with Lipofectamine 2000 (Invitrogen) according to the manufacturer's instructions. For infection (MOI=50) with vEC_9 and vEC_9-T_{47}A in HeLa cells, virus was allowed to attach for 30 min, room temperature before being aspirated and replaced with liquid overlay (50% P5, 1% 100x GOP, 1% 20% dextrose) and incubated at 37°C for 6 hours.

***In vitro* phosphorylation assays.** Phosphoryation reactions (80 μl total, with 30 μl cytosol, 2 μl 10 mM ATP, 2 μg L_x-GST, 0.75 μl [γ-^{32}P]-ATP) were performed in GST binding buffer (50 mM HEPES, 150 mM NaCl, 0.5% NP40, pH 7.4) for 45 min (37°C). Glutathione sepharose 4B beads (10 μl per sample, GE Healthcare Life Sciences) were then added, followed by agitation (4°C, 2h). The beads were collected by centrifugation (500 g), washed with GST buffer (4x) then boiled in SDS gel loading buffer. Protein fractionation was by SDS-PAGE (8 or 10%), with band visualization by phosphorimaging (Typhoon 9200 Variable Mode Imager, GE Healthcare), silverstain, or western blot analysis.

AMPK reactions (10 μl, 2 μl 0.5 mM AMP, 1 μl 50 ng/ul AMPK, 2 μg L_x-GST) in AMPK assay buffer (25 mM MOPS pH 7.2, 25 mM MgCl$_2$, 5 mM EGTA, 2 mM EDTA, 0.25 mM DTT) were activated with 2 μl AMPK assay cocktail (0.25 mM ATP, 0.167 µCi/µl [γ-^{32}P]-ATP in AMPK assay buffer) for 15 min, 30°C. L_x-GST protein was then pulled down with glutathione beads, washed and analyzed as above.

Ran pulldown. To ensure L phosphorylation, reactions (240 μl total, with 90 μl cytosol, 6 μl 10 mM ATP, 6 μg L_x-GST) were performed in GST binding buffer as above. Glutathione sepharose 4B beads were added, agitated (4°C, overnight), collected by centrifugation (500 g), washed with GST buffer (4x) then boiled in SDS gel loading buffer. Protein fractionation was by SDS-PAGE (10%), with band visualization by western blot.

Western blot analysis. After SDS-PAGE gel fractionation, proteins were electrotransferred to polyvinylidene difluoride membranes (Immobilon-P, Millipore), blocked in 10% nonfat dry milk in Tris-buffer saline (TBST: 20 mM Tris, pH 7.6, 150 mM NaCl, 0.5% Tween-20) (room temperature, 1 h). After washing (TBST, 3x), membranes were incubated (1% milk, TBST, 4°C, overnight) with one of the following primary antibodies: αGST (mouse mAb, 71087, Novagen), αP-AMPKα (Thr$_{172}$, 40H9) (rabbit mAb, 2535, Cell Signaling), αCK2 (rabbit pAb, 06-873, Millipore), αtubulin (mouse mAb, T4026, Sigma-Aldrich), αRan (N-19) (goat pAb, sc1155, Santa Cruz), αNup (mouse mAb, mAb414, Covance), αP-p38 (Thr180/Tyr182) (rabbit, pAb, 9211, Cell Signalling), αp38α (rabbit pAb, 9218, Cell Signalling), αP-ERK1/2 (D13.14.4E) (rabbit mAb, 4370, Cell Signalling), αERK1/2 (rabbit pAb, 06-182, Millipore), αP-MAPKAP-2 (Thr334,

27B7) (rabbit mAb, 3007, Cell Signalling), αMAPKAP-2 (rabbit pAb, 3042, Cell

Signalling), AMPKα (23A3) (rabbit mAb, 2603, Cell Signaling), or mengovirus 3Dpol

(described previously (8)). After washing (TBST, 3x), membranes were incubated with

αmouse secondary antibody (A2554, Sigma-Aldrich) or αrabbit IgG (H+L) HRP

conjugate (W4011, Promega) (1% milk in TBST, room temperature, 1 h). Membranes

were washed a final time (TBST, 3x), reacted with enhanced chemiluminescence

substrate (GE Healthcare) and exposed to film.

Quantification. Phosphorylation signal was quantified by densitometry using TotalLab

Quant (Nonlinear Dynamics Ltd, Newcastle, UK), normalizing to input protein (from

western blot or silverstain).

To calculate phosphates:mol of protein, *in vitro* phosphorylation reactions in

HeLa cytosol or with rAMPK were performed as described above, pulldowns were

performed, and proteins were analyzed by SDS-PAGE gel (phosphorscreen or

silverstain). L protein bands were then excised from the silver stained gel, and soaked

in scintillation fluid overnight. Vials were then analyzed by scintillation counting, and

stoichiometry was calculated as in Hollinger and Hepler (131). Numbers near 1 indicate

a single phosphate per mol protein.

Sequence analysis. A dataset of unique cardiovirus L proteins was compiled from

GenBank, aligned by ClustalX (175) and displayed as Weblogos (69). Post-translational

modification prediction was performed by PPSP (set to "high sensitivity" for "all

kinases") (335), NetPhosK1.0 (set to "prediction without filtering" (fast), threshold=0.5)

(38), NetPhos2.0 (36), Phosida (100), DiPHOS (specified predict for viruses) (138),

Phosphomotif Finder (5) and ScanSite (set to "low stringency") (227). Secondary

structure prediction was performed using the Protean program in the Lasergene suite

(DNASTAR, Madison, WI).

RESULTS

Phosphorylation site prediction. We previously reported that $L_{S,T}$-GST proteins are

phosphorylated, though not by CK2 as with L_E-GST, due to a lack of conservation of the

CK2 motif (26). To narrow the potential phosphorylation sites, we used phosphorylation

site prediction servers PPSP (335), NetPhosK 1.0 (38), NetPhos 2.0 (36), Phosida

(100), DIPHOS (138), PhosphoMotif Finder (5) and Scan Site (227) (Table 3-1). Kinases

predicted by these programs are listed in Supplemental Tables S2 and S3. Using these

predicted sites, we narrowed further by those sites that were conserved within SafV or

TMEV groups, or found to be important in other studies. The final dataset consisted of 6

L_S-GST and 8 L_T-GST potential phosphorylation sites (Fig 3-1). These sites were

mutated individually using a site-directed mutagenesis by overlap extension technique

in pT1.1 L_X-GST vectors and proteins were expressed and purified.

Phosphorylation site determination. We performed *in vitro* phosphorylation assays in

HeLa cytosol to determine the phosphorylation site(s) in L_S-GST and L_T-GST. We found

that the unstructured zinc finger-mutated L protein ($C_{11}A$) had reduced phosphorylation

for both L_S-GST and L_T-GST (40 and 28%, respectively) (Fig 3-2). Mutation of Tyr_7 in

both proteins also drastically reduced phosphorylation signal, though it is not yet known

whether this is due to misfolding, as this residue is within the zinc finger domain. For L_S-

GST, residues Thr_{36} and Tyr_{49} were identified as likely phosphorylation sites (Fig 3-2A),

Position[1]	PPSP	NetPhosK 1.0	NetPhos 2.0	Phosida	DIPHOS	Phospho Motif Finder	Scan Site
SafV							
7	✓		✓	✓	✓		
15	✓		✓		✓	✓	
20	✓		✓	✓	✓		
21	✓		✓		✓		
26	✓	✓	✓		✓		
34	✓		✓	✓	✓	✓	✓
36	✓	✓	✓		✓	✓	
40	✓	✓	✓		✓	✓	✓
49	✓		✓	✓	✓	✓	
58	✓		✓		✓	✓	
BeAn							
7	✓		✓	✓	✓	✓	
15	✓		✓		✓	✓	
20	✓	✓	✓		✓	✓	
25	✓		✓	✓	✓	✓	✓
34	✓		✓	✓	✓	✓	
36	✓	✓	✓		✓	✓	
51	✓		✓		✓	✓	
53	✓		✓		✓	✓	
54	✓		✓	✓	✓		
57	✓	✓	✓	✓	✓		✓
59	✓		✓		✓	✓	
63	✓		✓		✓		

Table 3-1. Predicted phosphorylation sites. [1]Red positions indicate those for which L-GST mutations were made.
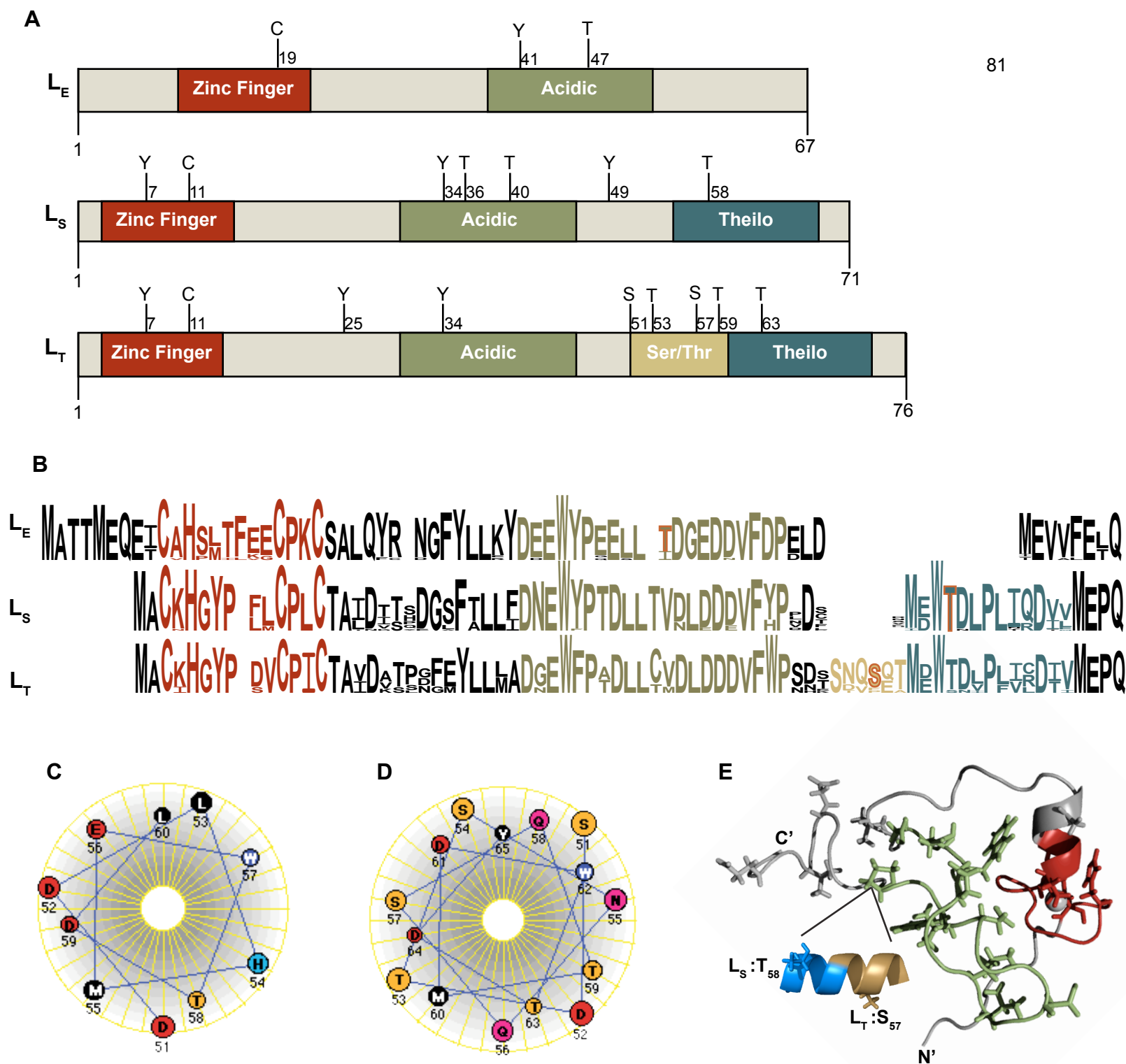
Figure 3-1. A. Protein map of $L_{E,S,T}$ domains (zinc finger = red, acidic = green, Ser/Thr = yellow, Theilo = blue) with mutated sites and positions denoted above. B. Weblogo of unique Cardiovirus L sequence alignment, divided into EMCV, Saffold and TMEV groups. Colors as in A. AMPK phosphorylation sites are outlined in orange. C. Helical wheel created with Lasergene Suite (DNASTAR, Madison, WI) of L_S Theilo domain. Colors scheme is M,I,L,V in black, F,Y,W in dark blue, G,A,P in green, D,E in red, N,Q in pink, K,H,R in light blue, S,T in orange, and C is yellow. D. Helical wheel of L_T Ser/Thr domain and Theilo domain. Colors as in C. E. Structure of L_E(mengo) (Palmenberg unpublished) with residues conserved within the Cardiovirus genus shown as sticks. The Ser/Thr and Theilo domains modeled below as a helix. L_S and L_T phosphorylation sites (Thr$_{58}$ and Ser$_{57}$, respectively) are shown as sticks on the helix. Colors are as in A. Structure rendered and helix modeled in MacPyMol.

with more moderate phosphorylation signal reduction seen for Thr_{40} and Thr_{58} mutated

proteins. Tyr_{34} and Ser_{57} were identified as phosphorylation sites for L_T-GST.

Interestingly, when certain sites were mutated to phosphomimetic Asp residues in L_T-

GST (S_{51}, T_{53} and T_{59}), phosphorylation signal increased (Fig 3-2B).

L_X-GST phosphorylation by rAMPK. AMPK was selected as a potential L-

phosphorylating kinase because it was predicted to act upon all three cardioviruses

(albeit at different sites) (Table S2,3), and is involved in the replication cycles of many

other viruses (for review, see (197)). $L_{E,S,B}$-GST proteins were reacted with rAMPK in *in*

vitro phosphorylation reactions, and found to be efficiently phosphorylated (50ng AMPK,

15 minute incubation), while the GST tag alone did not collect any phosphates (Fig 3-3).

L_E-GST was phosphorylated to the highest level, followed by L_S-GST and L_B-GST (Fig

3-3).

Stoichiometry of AMPK phosphorylation. To determine the number of phosphates

added by AMPK, increasing amounts of AMPK were incubated with L_S-GST protein in

an *in vitro* phosphorylation assay. We found that with the addition of only 5ng of AMPK,

there was detectable phosphorylation signal (quantified by densitometry) (Fig 3-4A).

Furthermore, the phosphorylation signal continued to increase with the addition of more

AMPK (Fig 3-4A). To determine the number of phosphates the densitometry signal

represented, we reacted L_S-GST with either HeLa cytosol or AMPK in *in vitro*

phosphorylation reactions, and quantified phosphorylation signal by scintillation

counting. Using the method of Hollinger and Hepler (131), we found that with the

addition of 50ng of AMPK, there is approximately one phosphate per molecule of L_S-

GST protein (Fig 3-4B). This number is much higher than the phosphorylation signal of
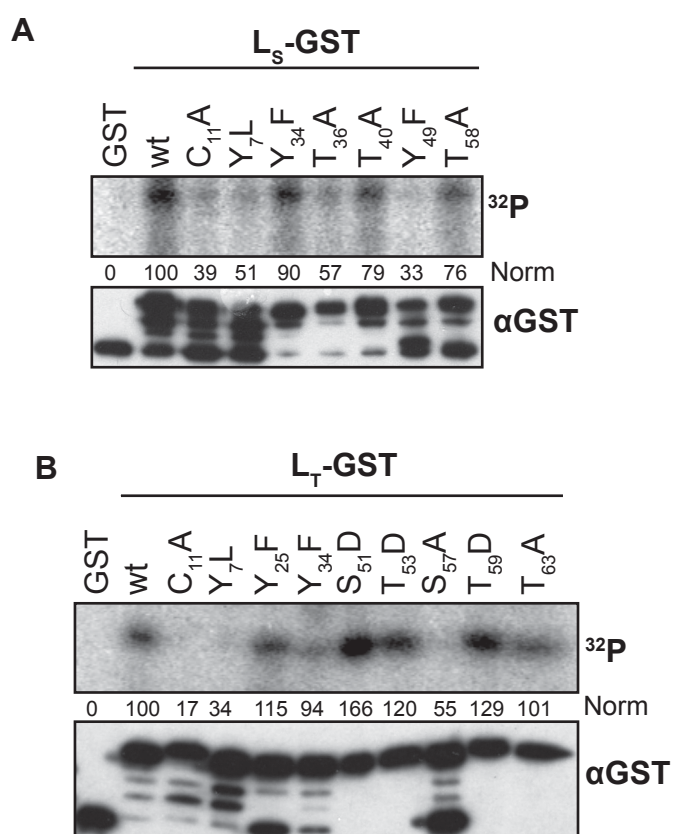
Figure 3-2. *In vitro* phosphorylation of Theilo L proteins in HeLa cytosol. A. L$_S$-GST mutant panel, B. L$_T$-GST mutant panel. L-GST phosphorylation site-mutated proteins were reacted with HeLa cytosol and [γ-^{32}P]-ATP, pulled down with glutathione beads, fractionated on SDS-PAGE gels, and exposed to a phosphorscreen (^{32}P) or subjected to western blot for GST. Phosphorylation signal (measured by densitometry, TotalLabQuant) normalized to amount of GST signal, with GST set to 0 and wt set to 100.
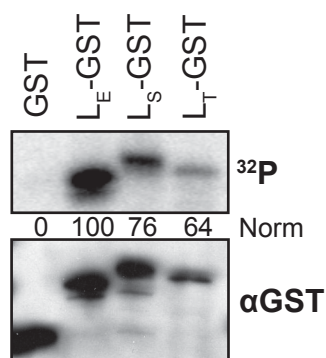
Figure 3-3. *In vitro* phosphorylation of Cardiovirus L proteins by rAMPK. A. $L_{E,S,T}$ wt-GST proteins were reacted with rAMPK and $[\gamma\text{-}^{32}P]$-ATP (15 minutes, 30°C) and L-GST was pulled down with glutathione beads. Proteins were fractionated on SDS-PAGE gels and exposed to phosphorscreen (^{32}P) or analyzed via western blot to GST. The GST tag alone serves as a negative control. Phosphorylation signal was measured by densitometry (TotalLabQuant) and normalized to GST signal.

A

B

0.12   0.14   0.13   1.04   Phosphates:mol protein

C
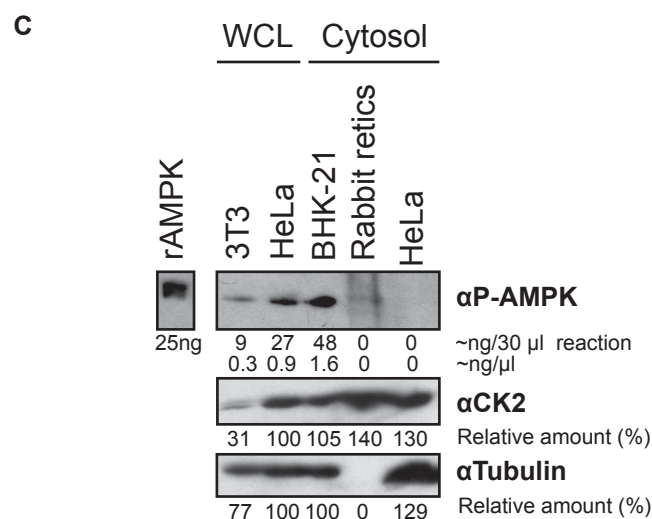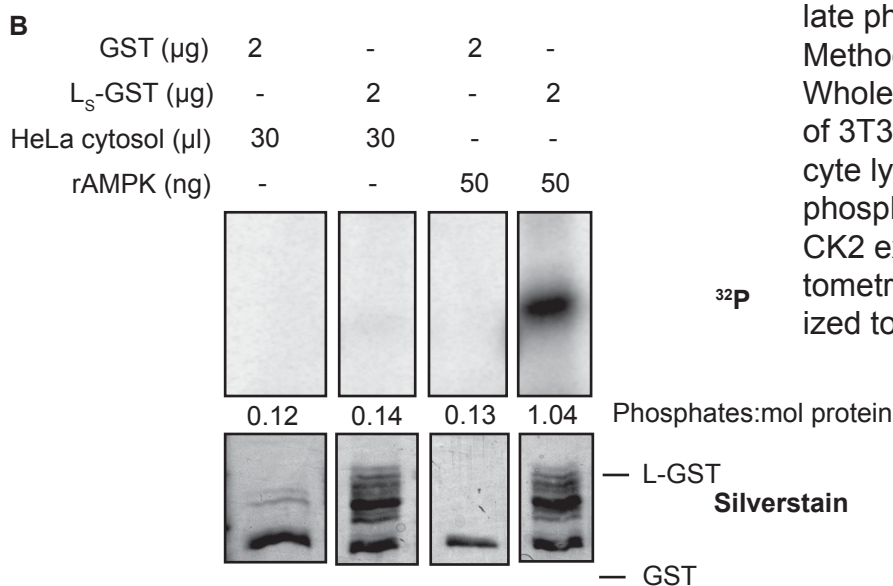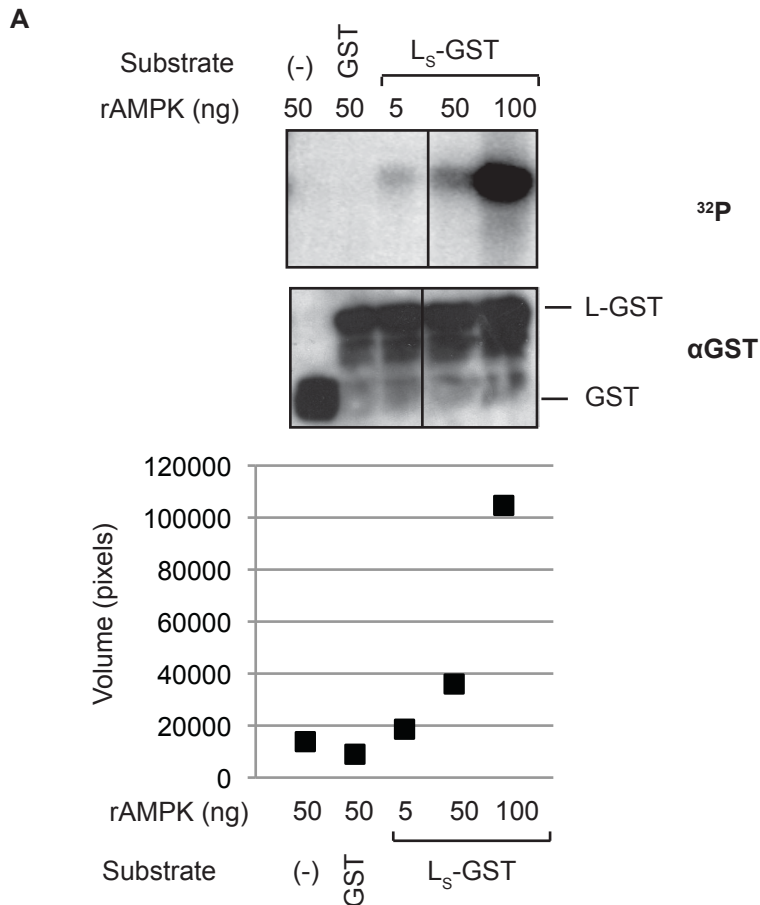
Figure 3-4. Stoichiometry of L_S-GST phosphorylation. A. L_S-GST protein was reacted with different concentrations of rAMPK (5, 50 or 100ng) and [γ-^{32}P]-ATP for 15 minutes, 30°C. Reactions with no substrate or the GST tag alone serve as controls. GST and LS-GST were pulled down with glutathione beads, and analyzed via phosphorscreen (^{32}P) or western blot probed for GST. Phosphorylation was quantified via densitometry with TotalLabQuant. Total pixels from ^{32}P signal are plotted. B. L_S-GST protein was reacted with either HeLa cytosol (45 minutes, 37°C) or rAMPK (15 minutes, 30°C) and [γ-^{32}P]-ATP. GST protein serves as a control. Proteins were pulled down and analyzed via phosphorscreen as in A. and silver total protein stain. Silverstained bands were then excised, soaked in scintillation fluid, and analyzed by scintillation counting to calculate phosphates per mol (see Materials and Methods). **C.** Expression of AMPK and CK2. Whole cell lysates (WCL) or cytosolic fractions of 3T3, HeLa, BHK-21 cells and rabbit reticulocyte lysates were analyzed via western blot for phosphorylated (active) AMPK (P-AMPK) and CK2 expression. Blots were quantified by densitometry (TotalLabQuant) and AMPK was normalized to a known input 25ng of rAMPK protein.

L_S-GST reacted with HeLa cytosol, suggesting that only a portion of the input L_S-GST

protein is phosphorylated (Fig 3-4B). Additionally, as phosphorylation signal continues

to rise with the addition of >50ng AMPK, L_S-GST can likely be phosphorylated on more

than one site.

As $L_{E,S,T}$-GST are phosphorylated to differing levels in various cytosol types (26),

so we then determined the levels of AMPK and CK2 in the cytosol types tested (Fig 3-

4C). We found abundant CK2 in all cytosol types, which coincides with the finding that

L_E-GST was effectively phosphorylated in HeLa, BHK-21 and rabbit reticulocyte lysates

(26). Active (phosphorylated) AMPK levels were lowest in rabbit reticulocyte lysates and

HeLa cytosol (Fig 3-4C), consistent with the undetectable phosphorylation signal of L_S-

GST when reacted with retics (26). Interestingly, L_T-GST was thoroughly

phosphorylated in rabbit reticulocytes (26), despite their diminution of active AMPK (Fig

3-4C). Compared to rAMPK levels used in *in vitro* phosphorylation assays, BHK-21

cytosol (48ng for typical 30 µl reactions) was the only cytosol type tested to contain

levels of active (phosphorylated) AMPK on the same order of magnitude as rAMPK

assays that add approximately one phosphate to L_S-GST (50ng) (Fig 3-4). The alpha

subunit of AMPK is conserved in mouse, rat and rabbit, so the observed differences are

not likely due to antibody sensitivity.

AMPK phosphorylation sites. To determine if the potential phosphorylation sites

identified (Fig 3-2) were authentic AMPK phosphorylation sites, we reacted the

predicted Ser/Thr phosphorylation site mutated proteins with rAMPK in *in vitro*

phosphorylation reactions. We included the $L_{S,T}$-GST Ser or Thr mutated proteins with

the highest decrease in phosphorylation signal (Fig 3-2), as well as L_S-GST T_{58}A as it

was predicted to be a AMPK site (Table S2) and the equivalent site in L_T-GST, because it was predicted to be a phosphorylation site by others (264). We found that L_S-GST Thr_{58} and L_T-GST Ser_{57} were phosphorylated by AMPK (Fig 3-5). Furthermore, AMPK targets the same L_E-GST residue previously found to be phosphorylated by CK2 (Thr_{47}) ((351), (26)).

L phosphorylation effects on Ran binding. L_E binds RanGTPase at a very tight K_d (~3nM) (249, 256). Ran binding has no effect on L_E's phosphorylation state (26). Conversly, mutations to L_E phosphorylation sites do not disrupt Ran binding (16). Using glutathione pulldown assays with recombinant L_X-GST protein and HeLa cytosol, we show that the Theilovirus Ls can also bind Ran, and that phosphorylation site mutations have no effect on L affinity for either Ran (Fig 3-6).

Kinase activation during infection. Inhibition of certain MAPK family members can abrogate L-directed nup phosphorylation during infection (257). We show here that mutation of the primary L phosphorylation site (L_E-T_{47}A) attenuates L-directed Nup62 phosphorylation in HeLa infections (MOI=50, 6hr PI) (Fig 3-7). This nup phosphorylation deficit associates with decreased activation of MAPKs p38, ERK1/2 and the downstream kinase MK2 (41%, 49/89% and 31%, respectively) by L phosphorylation site-mutated viruses vEC_9 L-T_{47}A and (infection in HeLa cells). Amount of $3D^{pol}$ indicates equivalent viral loads at this time point (6 h PI). At later timepoints (ex. 27 h post-RNA transfection), however, vEC_9 L-T_{47}A exhibits a small plaque phenotype (Fig 3-S1).
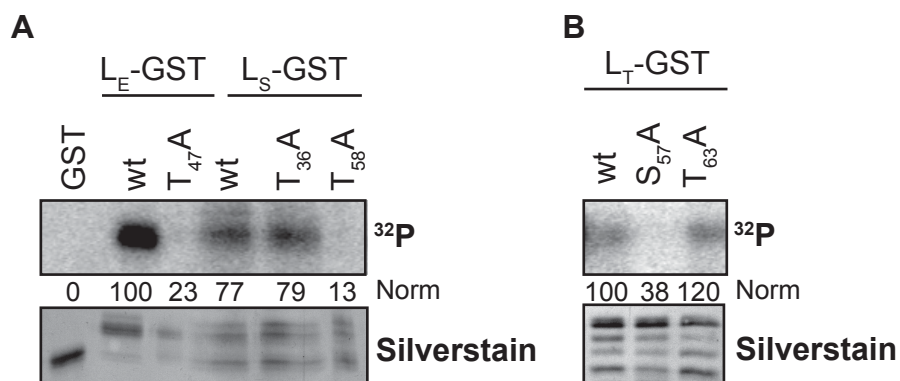
Figure 3-5. Sites of AMPK phosphorylation. Phosphorylation site mutated L-GST proteins were reacted with rAMPK and [γ-^{32}P]-ATP (15 minutes, 30°C) (A. L_E-GST and L_S-GST phosphorylation site mutations, B. L_T-GST phosphorylation site mutations). L-GST proteins were pulled down with glutathione beads and fractionated on SDS-PAGE gels and analyzed by phosphorscreen (^{32}P) and silverstain. Phosphorylation signal was quantified by densitometry (TotalLabQuant) and normalized to silverstain.
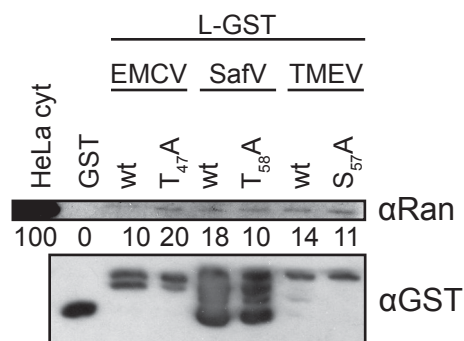
Figure 3-6. Ran binding by L phosphorylation site-mutated proteins. LX-GST proteins were reacted with HeLa cytosol and ATP (45 minutes, 37°C) and pulled down with glutathione beads (overnight, 4°C), fractionated on SDS-PAGE gels, and analyzed via western blots for Rand and GST. Blots were quantified by desitometry (TotalLabQuant) normalized to GST signal.
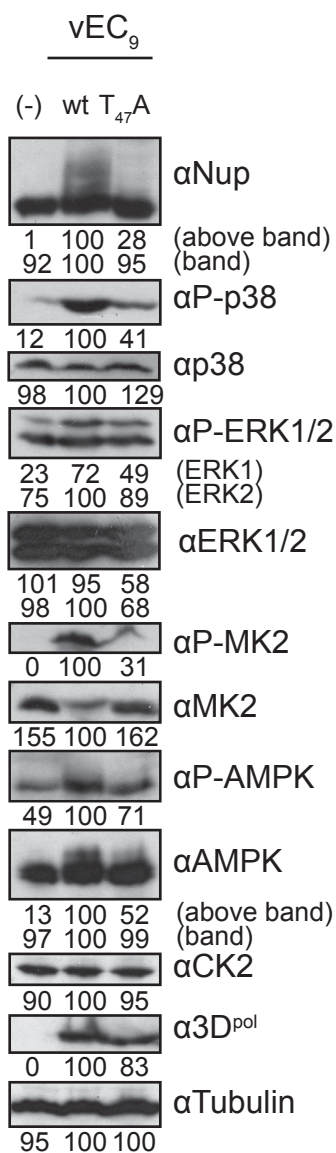
Figure 3-7. Effects of viral infection on cellular kinases and nup phosphorylation. HeLa cells were infected with EMCV wt (vEC$_9$) and phosphorylation site mutated (T$_{47}$A) viruses (6 hours, 37°C), fractionated on SDS-PAGE gels and analyzed via western blot for nups (mAb414), phosphorylated p38 (P-p38), total p38 (p38), phosphorylated ERK1/2 (P-ERK1/2), total ERK1/2 (ERK1/2), phosphorylated MAPKAP2 (P-MK2), total MK2 (MK2), phosphorylated (Thr172) AMPK (P-AMPK), total AMPK (AMPK), CK2, 3D^{pol} (indicates viral infection) and tubulin (loading control). TotalLabQuant was used to quantitate bands.

While CK2 and AMPK levels remained constant during infection (vEC9 in HeLa cells), AMPK phosphorylation increased, as evidenced by an upwards mobility shift. This phosphorylation shift appears to be conferred by addition of phosphates to Thr_{172}; there is approximately twice as much activated (Thr_{172}-phosphorylated) AMPK in vEC_9 infected vs. uninfected samples (Fig 3-7). As with MAPK activation, AMPK is intermediately activated during infection with vEC_9 L-T_{47}A.

Secondary structure prediction. The additional domains found in the Theilo viruses form two distinct cassettes, the Ser/Thr domain and the Theilo domain. We noticed that each domain is about two turns of a helix in length (8 and 7 residues respectively), and the two domains are flanked by Pro residues (Fig 3-1B). When these two domains are modeled as a helix, residues fall into a clear acidic side that includes the BeAn phosphorylation site (Ser_{57}) (Fig 3-1C, D). The non-AMPK SafV phosphorylation site (Thr_{36}) aligns with an acidic residue conserved in the EMCV species (Fig 3-1B), suggesting that the variance seen in phosphorylation sites is an alternative mechanism to achieve the same acidic patches.

DISCUSSION

Post-translational modifications are a creative way for small proteins to modulate functionality without sacrificing sequence space. Cardioviruses have adapted to take advantage of multiple cellular kinase pathways in their replication cycle. The cardiovirus L protein in particular can cause activation of specific members of the MAPK pathway, which are thought to phosphorylate nuclear pore proteins to shutdown active cellular transport (257, 258). The L_E protein itself is also phosphorylated by kinases

independent of the MAPK pathway, CK2 (351) and Syk (26). Other cardiovirus L

proteins ($L_{S,T}$) are phosphorylated as well (26), but it was previously unknown at which

sites and by which kinases this phosphorylation occurred. We characterize herein the

phosphorylation sites of L_S and L_T, and implicate AMPK as a kinase that acts upon

these sites.

To guide our investigation to phosphorylation sites and kinase discovery, we

initially relied upon computational phosphorylation site predictors. As each site predicted

a different set of sites and kinases, we used the consensus of 7 programs to select our

mutation panel. Though no single site was selected by all programs, the experimentally

determined phosphorylation sites were selected by the majority of programs (L_S: Thr_{36}

5/7, Tyr_{49} 5/7 and Thr_{58} 4/7; L_T: Ser_{57} 6/7) (Table 1). They differed considerably,

however, in which kinases they predicted to phosphorylate these sites (Tables S2,3).

PPSP correctly predicted AMPK for L_T Ser_{57}, but not L_S Thr_{58}, while Phosphomotif

Finder predicted correctly for L_S but not L_T (Tables S2,3). We gleaned the correct

answer from the program consensus, but no one program correctly identified both

phosphorylation site and kinase.

While important major domains are generally conserved (zinc finger and acidic

domain) (Fig 3-1B) the phosphorylation sites of cardiovirus Ls are not conserved,

despite their importance to L function (26). Interestingly, phosphorylation in L_S appears

to be a mechanism to compensate for sequence changes that have decreased the

proteins acidic nature: Thr_{36} aligns to a conserved Glu in the EMCV species, while Tyr_{49}

aligns to a conserved EMCV Asp. The AMPK site, Thr_{58}, lies in the Theilo domain,

which is not found in the EMCV species. Despite the conservation of the Theilo domain

within the Theiloviruses, the equivalent Thr_{63} of L_T, which was predicted to be a phosphorylation site by Ricour et al 2009 (264), is not the AMPK site. Rather, Ser_{57} was identified as the AMPK phosphorylation site. When phosphomimetic Asp substitutions were made at potential phosphorylation sites in L_T, phosphorylation signal increased over wt. Whether these phosphomimetic mutations enhanced a phosphorylation site (for example, Syk prefers acidic regions) or enhanced binding to a partner that facilitated phosphorylation is yet to be determined.

Why do cardiovirus Ls have different phosphorylation sites, when the end goal of nucleocytoplasmic trafficking inhibition is the same? This phosphorylation site variability may indicate cell-type preference, i.e. they have adapted to use a kinase abundant in their cell type of choice, or binding to a specific partner that varies by species. Alternatively, phosphorylation could represent a regulation method. For instance, EMCV L can be phosphorylated by the highly expressed and constitutively active CK2 and also by AMPK, both of which are found in many cell types. With AMPK being less abundant and active, the activity of Theilovirus Ls may be delayed, allowing some antiviral signaling and the establishment of persistence.

Interestingly, AMPK is involved in the switch between latent and lytic replication for some viruses. HIV-1 Tat protein inhibits SIRT1, resulting in AMPK inhibition during lytic infection (341). Though AMPK activation inhibits replication, it is involved in the reactivation of latent HIV genomes (210). HCMV represses AMPK during latency (via activation of an AMPK-inhibiting kinase) (198), but activates it during acute infection (206). Though AMPK's role in the switch between latent and lytic replication is not fully characterized, these findings are particularly interesting when applied to L_T

phosphorylation, as the AMPK phosphorylation site, L_T Ser_{57}, is thought to be a major determinant in the differences between persistent demyelinating strains of TMEV (DA, BeAn) and neurovirulent strains (GDVII). This residue is a Ser in all persistent demyelinating strains, and a Pro in the neurovirulent strains. Mutation of this residue in GDVII to a Ser results in a DA phenotype (low titer, small plaques) in BHK-21 cells, while mutating DA Ser_{57} to a Pro results in a GDVII phenotype (high titer, big plaques) (305). Furthermore, DA L is highly apoptotic to HeLa cells while GDVII L is not, and the DA Ser_{57}Pro mutation attenuates L apoptotic ability in HeLa cells (300). Based on secondary structure predictions, we hypothesize that a Pro at this site would disrupt the Ser/Thr domain helix, potentially disrupting the entire domain. Further investigation will show whether GDVII can be phosphorylated by AMPK at a different site (PSSP predicts AMPK sites at GDVII residues 51, 54 and 63), and whether or not AMPK plays any role in L Ser_{57}-containing viruses becoming persistent.

This study unveils the possibility that multiple kinases can act upon a single cardiovirus L phosphorylation site. Though we believe that most L_E phosphorylation can be attributed to the more abundant and constitutively active CK2, there is evidence that AMPK may also contribute to L_E phosphorylation. CK2 inhibitors TBCA and TBB decrease L-induced Nup62 phosphorylation to 62 and 16% respectively (26). Though these inhibitors are considered highly specific, they have been found to have off-target effects on AMPK activity. TBCA (10μM) has an IC_{50} of 101 ± 2 for AMPK (vs. 3 ± 1 for CK2) and TBB (10μM) has an IC_{50} of 73 ± 2 for AMPK (vs. 28 ± 1 for CK2) (233). Interestingly, we see a larger effect by the TBB inhibitor only in the presence of both CK2 and AMPK (in HeLa cytosol), where it inhibits L_E phosphorylation and L-induced

nup phosphorylation more effectively. TBCA, however, more effectively at inhibits CK2 alone (26), suggesting that perhaps the enhanced effect of TBB is due to its inhibition of both CK2 and AMPK.

AMPK is not necessarily the only kinase to act upon the Theilovirus Ls. While L_S was not detectibly phosphorylated in rabbit reticulocyte lysates (26), which contain very little active AMPK (Fig 3-4C), L_T is still thoroughly phosphorylated in these lysates, suggesting an alternate kinase. Further definition of SafV's preferred cell type and characterization of kinases in primary cells will be needed to determine the most biologically significant kinase for Theilovirus phosphorylation.

How does phosphorylation modulate L's function? We propose a model in which L localizes to the nuclear rim (249, 256) via interaction with the NLS-containing viral 2A protein, then binds RanGTPase with a tight K_d (~3nM), displacing 2A ((249), Appendix 3). The Ran-binding site for L_E has been localized between residues 35-40 (16), preceding the phosphorylation sites. In fact, phosphorylation at both sites can occur when Ran is pre-bound to L_E (26). Phosphorylation state of L does not affect L-Ran binding; phosphorylation site-mutated L proteins bind just as well to Ran as wt L (Fig 3-6). Phosphorylation state does, however, appears to play a role in L-directed kinase activation during infection (Fig 3-7). Phosphorylation site-mutated virus vEC_9 L-T_{47}A activates a less robust MAPK (ERK1/2 and p38) response during infection than wt vEC_9 (Fig 3-7). Furthermore, MK2, a downstream substrate of both ERK1/2 and p38, is also phosphorylated to a lower level in wt infection than in vEC_9 L-T_{47}A infection. This inability of phosphorylation site-mutated viruses to sufficiently activate MAPKs translates to a decrease in L-directed nup phosphorylation ability (Fig 3-7).

Like MAPKs p38 and ERK, AMPK is also activated during vEC_9 infection, and phosphorylation site mutation vEC_9 L-T_{47}A reduces this phosphorylation. In addition to directly phosphorylating L, AMPK may also be involved in L-induced MAPK activation. In avian reovirus infection, AMPK activation leads to increased activation of p38 (146), while in porcine circovirus infection AMPK activation leads to ERK activation (347). Furthermore, the same phosphatase that regulates AMPK dephosphorylation (PP2A) (329) also regulates that of ERK1/2 (4). Furthermore, okadaic acid, a PP2A inhibitor, enhances L-directed nup phosphorylation (J. Ciomperlik, unpublished). AMPK may therefore be involved with L function at both the L phosphorylation event as well as the nup phosphorylation cascade.

ACKNOWLEDGEMENTS

We thank Adam Swick and John Yin for BHK-21 cells and Howard Lipton for the generous gift of SafV-2 and TMEV (BeAn) cDNAs. Frederick Porter created the EC_9-T_{47}A cDNA.
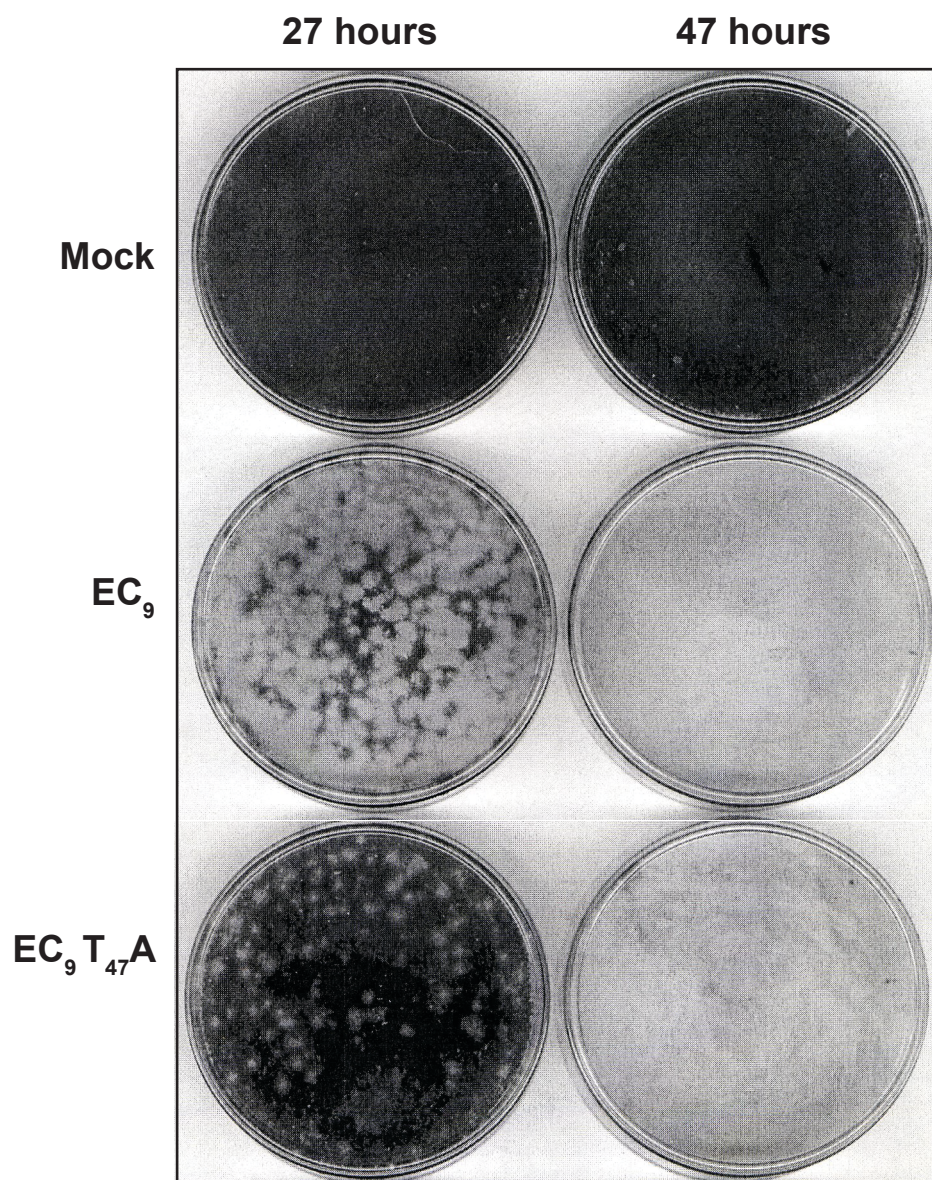
Supplemental Figure 3-1. Plaque assay of cDNA-expressed RNA transcript transfection of EMCV EC_9 and phosphorylation site mutated EC_9 $T_{47}A$. Plaque assays analyzed at 27 and 47 hours post transfection.

Supplemental Table 3-1. Primer sequences.

Primer	Sequence	Mutation
1514	5'-TTCGGCTTCTGGCGTGTGA-3'	Flanking FWD
1149	5'-TGTTTCCCCGGGTCCAATAACCTAGTATAGGGGACAT-3'	Flanking REV L_S
1237	5'-TCGATCTCAGTGGTATTTGTG-3'	Flanking REV L_B
1626	5'-GCAAACACGGAGATCCGCTTATGTG-3'	L_S-Y_7D
1627	5'-CACATAAGCGGATCTCCGTGTTTGC-3'	
1656	5'-GCAAACACGGAGTTCCGCTTATGTG-3'	L_S-Y_7L
1657	5'-CACATAAGCGGAACTCCGTGTTTGC-3'	
1589	5'-GCAAACACGGAGCTCCGCTTATGTG-3'	L_S-Y_7A
1590	5'-CACATAAGCGGAGCTCCGTGTTTGC-3'	
1519	5'-GATAATGAATGGGACCCAACTGACC-3'	L_S-Y_{34}D
1520	5'-GGTCAGTTGGGTCCCATTCATTATC-3'	
1612	5'-GATAATGAATGGTTCCCAACTGACC-3'	L_S-Y_{34}F
1613	5'-GGTCAGTTGGGAACCATTCATTATC-3'	
1778	5'-GATAATGAATGGGCCCCAACTGACC-3'	L_S-Y_{34}A
1779	5'-GGTCAGTTGGGGCCCATTCATTATC-3'	
1620	5'-GAATGGTACCCAGCTGACCTATTG-3'	L_S-T_{36}A
1621	5'-CAATAGGTCAGCTGGGTACCATTC-3'	
1622	5'-CAACTGACCTATTGGCTGTAGACCTAGAG-3'	L_S-T_{40}A
1623	5'-CTCTAGGTCTACAGCCAATAGGTCAGTTG-3'	
1669	5'-CTAGAGGATGAAGTGTTTTTTCCTGATGACCTCCATATG-3'	L_S-Y_{49}F
1670	5'-CATATGGAGGTCATCAGGAAAAAACACTTCATCCTCTAG-3'	
1523	5'-CATATGGAATGGGATGATCTACCACTG-3'	L_S-T_{58}D
1524	5'-CAGTGGTAGATCATCCCATTCCATATG-3'	
1624	5'-CATATGGAATGGGCTGATCTACCACTG-3'	L_S-T_{58}A
1625	5'-CAGTGGTAGATCAGCCCATTCCATATG-3'	
1628	5'-GCAAACATGGAGACCCAGATGTGTG-3'	L_B-Y_7D
1629	5'-CACACATCTGGGTCTCCATGTTTGC-3'	
1686	5'-GCAAACATGGACTCCCAGATGTGTG-3'	L_B-Y_7L
1687	5'-CACACATCTGGGAGTCCATGTTTGC-3'	
1591	5'-GCAAACATGGAGCCCCAGATGTGTG-3'	L_B-Y_7A
1592	5'-CACACATCTGGGGCTCCATGTTTGC-3'	
1671	5'-CGGCTTTGAATTTTTGCTCATGG-3'	L_B-Y_{25}F
1672	5'-CCATGAGCAAAAATTCAAAGCCG-3'	
1525	5'-CAGACGGAGAATGGGACCCTACGGACCTTC-3'	L_B-Y_{34}D
1526	5'-GAAGGTCCGTAGGGTCCCATTCTCCGTCTG-3'	
1614	5'-CAGACGGAGAATGGTTCCCTACGGACCTTC-3'	L_B-Y_{34}F
1615	5'-GAAGGTCCGTAGGGAACCATTCTCCGTCTG-3'	
1780	5'-CAGACGGAGAATGGGCCCCTACGGACCTTC-3'	L_B-Y_{34}A
1781	5'-GAAGGTCCGTAGGGGCCCATTCTCCGTCTG-3'	
1527	5'-GTCTTCTGGCCTGACGACACGAGCAATC-3'	L_B-S_{51}D
1528	5'-GATTGCTCGTGTCGTCAGGCCAGAAGAC-3'	
1529	5'-GGCCTTCGGACGACAGCAATCAATC-3'	L_B-T_{53}D
1530	5'-GATTGATTGCTGTCGTCCGAAGGCC-3'	
1618	5'-CGAGCAATCAACCTCAAACAATG-3'	L_B-S_{57}P
1619	5'-CATTGTTTGAGGTTGATTGCTCG-3'	
1636	5'-CGAGCAATCAAGCTCAAACAATG-3'	L_B-S_{57}A
1637	5'-CATTGTTTGAGCTTGATTGCTCG-3'	
1533	5'-CAATCAATCTCAAGATATGGACTGGACTG-3'	L_B-T_{59}D
1534	5'-CAGTCCAGTCCATATCTTGAGATTGATTG-3'	
1634	5'-CTCAAACAATGGACTGGGCTGACGTACCGCTCATAC-3'	L_B-T_{63}A
1635	5'-GTATGAGCGGTACGTCAGCCCAGTCCATTGTTTGAG-3'	
1761	5'-ATCTCCCCCGCGGTAACTGGTGACAGTT-3'	Flanking Fwd cDNA BeAn
1763	5'-TGAAGAACCGGTGGCGTACTGGAG-3'	Flanking Rev cDNA BeAn

972	5'-CGAGCATTCCTAGGGGTCTTTCCC-3'	Flanking Fwd pEC$_9$
975	5'-ACACTGATCAGACAGATTCTCCA-3'	Flanking Rev pEC$_9$
1033	5'-TTATTGGCTGATGGAGAGGATGATGTC-3'	pEC$_9$-T$_{47}$A
1034	5'-CTCTCCATCAGCCAATAACTCCTCTGG-3'	

Supplemental Table 3-2. Kinases predicted to target SafV L.

POS	PPSP	NetPhosK 1.0	NetPhos 2.0	Phosida	DIPHOS	Phospho Motif Finder	Scan Site
7	ABL, ALK, EGFR, FYN, IGFR, IR, JAK, MET, SRC, SYK, ZAP70		*Y	ALK	*Y		
15	CHK1/2, CK2, GSK3, MAPK, MAPKK, MAPKKK, NIMA, P34CDC2, PDK, PKG, PKR, PLK, SGK		*T		*T	CK2	
20	AMPK, ATM, CaM-I-IV, CHK1/2, CK1, CK2, DNA-PK, GRK, MAPKK, MAPKKK, MLCK, NIMA, P34CDC2, PDK, PKA, PKR, PLK, ROCK, SGK		*T	NEK6	*T		
21	AMPK, ATM, CAK, CaM-I/IV, CHK1/2, CK1, CK2, DNA-PK, GRK, IPL1, KIS, MAPK, MAPKAPK2, MAPKK, MLCK, P34CDC2, PKA, PKB, PKG, PLK		*S		*S		
26	CAK, CHK1/2, CK1, GSK3, ILK, IPL1, MAPK, MAPKK, MAPKK, MAPKKK, P34CDC2, PAK, PDK, PKG, PKR, PLK, ROCK	CK2	*T		*T		
34	ABL, ALK, BTK, EGFR, EPHA, FAK, FGR, FYN, HCK, IGFR, IR, JAK, LCK, LYN, MET, RET, SRC, SYK, TRK, VEGFR, ZAP70		*Y	EGFR	*Y	SHP1	SHC PTB
36	CAK, CDKS, CHK1/2, DAPK, GRK, GSK3, MAPK, MAPKK, MAPKKK, P34CDC2, PDK, PKR, PLK, ROCK	CK2	*T		*T	DNA-PK, GRK1, CK1	
40	CAK, CHK1/2, CK1, CK2, GSK3, ILK, IPL1, MAPK, MAPKK, P34CDC2, PKB, PKG, PKR, PLK, SGK	CK2	*T		*T	CK1	CDK2, ATM, CK2
49	ABL, ALK, BTK, EGFR, EPHA, FAK, FES, FGR, FYN, HCK, IR, LYN, MET, PDGFR, RET, RLK, SRC, SYK, TRK, VEGFR, ZAP70		*Y	SRC	*Y	ALK	
58	AURORA-A, CAK, CAM-I/IV, CDKS, CHK1/2, CK1, CK2, GRK, GSK3, MAPK, MAPKKK, MPCK, NIMA, P34CDC2, PDK, PKA, PKG, PKR, PLK, ROCK		*T		*T	AMPK	

Supplemental Table 3-3. Kinases predicted to target TMEV (BeAn) L.

POS	PPSP	NetPhosK 1.0	NetPhos 2.0	Phosida	DIPHOS	Phospho Motif Finder	Scan Site
7	ABL, ALK, BTK, EGFR, EPHA, FAK, FGR, FYN, IGFR, IR, JAK, LCK, LYN, PDGFR, MET, RLK, SYK, SRC, TIE2, TRK, VEGFR, ZAP70		*Y	ALK	*Y	JAK2	
15	CDKS, CHK1/2, CK1, CK2, GSK3, ILP1, MAPK, MAPKK, MAPKKK, NIMA, P34CDC2, PDK, PKG, PLK, SGK		*T		*T	CK2, GRK1	
20	ATM, CAK, CDKS, CHK1/2, CK1, CK2, DAPK, DNA-PK, GRK, GSK3, ILK, KIS, MAPK, MAPKK, MTOR, P34CDC2, PKR, PLK	P38 MAPK, CDK5	*T		*T	GSK3, ERK1, ERK2, CDK5	
25	ABL, EGFR, FGFR, FGR, FMS, FYN, HCK, IGFR, IR, JAK, MET, RET, SRC, SYK, VEGFR, ZAP70		*Y	ALK	*Y	EGFR, TC-PTP	PDGFR, FGR, IRK, P85 SH2, PLCg N-term SH2, PLCg C-term SH2
34	ABL, ALK, BTK, EGFR, EPHA, FYN, HCK, IGFR, IR, JAK, LYN, MET, RET, SRC, SYK, TRK, VEGFR, ZAP70		*Y	EGFR	*Y	SHP1	
36	CAK, CDKS, CHK1/2, DAPK, GRK, GSK3, MAPK, MAPKK, MAPKKK, MLCK, P34CDC2, PKR, PLK	CK2	*T		*T	DNA-PK	
51	AMPK, ATM, CAM-I/IV, CDKS, CHK1/2, CK1, CK2, DNA-PK, GRK, GSK3, IKK, MAPK, MAPKK, MLCK, NIMA, P34CDC2, PHK, PKA, PKR, PLK, SGK		*S		*S	CK2, DNA-PK	
53	GRK, NIMA, CDKS, CHK1/2, CK1, CK2, DNA-PK, GRK, GSK3, ILK, MAPK, MAPKK, MAPKKK, NIMA, P34CDC2, PDK, PKR, PLK		*T		*T	GRK2	
54	AMPK, ATM, CAK, CAM-II, CDKS, CK1, CK2, DNA-PK, GRK, GSK3, IKK, KIS, PHK, MAPK, MLCK, NIMA, P34CDC2, PHK, PKA, PKB, PKC, PKG, PKR, PLK, SGK		*S	CK1	*S		
57	AMPK, ATM, AURORA-A, CAK, CAM-II, CDKS, CHK1/2, CK1, CK2, DNA-PK, GRK, GSK3, IKK, ILP1, KIS, MAPK, MAPKK, MLCK, NIMA, P34CDC2, PAK, PLK, PKA, PKB, PKC, PKG, PKR, PLK	CK1, DNAPK, ATM	*S	CK1, DDR	*S		CDK2, DNA PK
59	AMPK, ATM, CAK, CAM-II, CHK1/2, CK1, CK2, DAPK, DNA-PK, GRK, IKK, ILK, ILP1, MAPK, MAPKAPK2, MAPKK, MAPKKK, NIMA, P34CDC2, PAK, PDK, PKA, PKB, PKC, PKG, PKR, PLK, ROCK, SGK		*T		*T	GRK1	
63	AMPK, ATM, AURORA-A, CAK, CDKS, CHK1/2, CK1, CK2, MAPK, MAPKK, MAPKKK, NIMA, P34CDC2, PDK, PKG, PRK, PLK, ROCK		*T		*T		

CHAPTER 4.

Cardiovirus Leaders activate and complex with mitogen-activating kinases (MAPKs) and exportins to inhibit nucleocytoplasmic trafficking

Holly A. Basta and Ann C. Palmenberg

Plans for publication: Fig 4-1, 4-2 to be included in "Nucleocytoplasmic trafficking inhibition of multiple trafficking pathways by Cardiovirus Leaders." Jessica J. Ciomperlik, Holly A. Basta, Kelly E. Watters and Ann C. Palmenberg.

Fig 4-3, 4-4 to be included in "EMCV L directs MAPK ERK2 to inhibit nucleocytoplasmic trafficking via nucleoporin hyperphosphorylation." Jessica J. Ciomperlik, Holly A. Basta, and Ann C. Palmenberg (in preparation).

Fig 4-6 and 4-8 to be included in "EMCV L requires binding to transportins for nucleocytoplasmic trafficking inhibition." Jessica J. Ciomperlik, Holly A. Basta, and Ann C. Palmenberg (in preparation).

Author contributions: HAB performed all experiments (Fig 4-1 through 4-8).

ABSTRACT

Picornaviruses disrupt nucleocytoplasmic trafficking during infection, but different genera accomplish this inhibition using diverse proteins and mechanisms. Encephalomyocarditis virus (EMCV), the prototypical member of the *cardiovirus* genus, inhibits trafficking through the actions of its Leader (L) protein, a small (67 amino acid), highly acidic protein, which binds RanGTPase (16, 249, 256), causes activation of mitogen-activating kinases (257), and induces phosphorylation of nuclear pore complex (NPC) proteins called nucleoporins (nups) (258). Before now, little was known about the functionality of other cardiovirus L proteins, which vary in sequence and contain additional domains not found in the EMCV L. Here, using *in vitro* assays with recombinant proteins and cell transfections, we found that representatives from the rest of the *cardiovirus* genus, Saffold virus 2 (SafV) and Theiler's murine encephalitis virus (TMEV) (BeAn strain) can disrupt nucleocytoplasmic trafficking through the classical, M9 and SR import pathways. Furthermore, SafV and TMEV (BeAn) Ls can activate the MAPK pathway, as previously shown for EMCV L (257). We define conserved binding partners Crm1 and CAS and (indirect) partners, MAPKs. In addition, the Theilo virus Ls have unique, undefined binding partners. L phosphorylation has been shown to affect L-directed trafficking inhibition (351) (183) and nup phosphorylation (Chapter 2). Here we show that mutation of L phosphorylation sites leads to decreased exportin binding, and thereby decreased MAPK binding. We propose this decreased binding as a mechanism by which L phophorylation site mutation disrupts nup phosphorylation and trafficking.

INTRODUCTION

Picornaviruses are small (around 7kB) single-stranded RNA viruses. With limited genetic space, Picornaviruses modify host processes rather than carry all the genes needed to execute their replication process. Modulation of the host cell triggers immune system involvement, so Picornaviruses devote some of their precious coding capacity to combating the host immune response. The *cardiovirus* genus encodes the Leader (L) protein, which prevents interferon (IFN) α/β signalling (114, 265, 299). This antihost protein can also modulate apoptosis pathways (13, 51, 97, 127, 229, 270, 300), inhibit stress granule formation (43), and disrupt nucleocytoplasmic trafficking (22, 75, 183, 257, 258). This trafficking inhibition is thought to be achieved by L's ability to bind RanGTPase and induce the phosphorylation of nuclear pore proteins (nucleoporins, or nups) through activation of the mitogen activating kinase (MAPK) pathway (257, 258, 264). The multifunctional L protein is small (~7kDa) and highly acidic (pI=~3.7), with a novel zinc finger and an acidic domain (64) (Palmenberg unpublished).

The L protein is unique to the *cardiovirus* genus, with no homologs among other Picornaviruses or elsewhere in nature. These L proteins also vary considerably within the *cardiovirus* genus (3). Encephalomyocarditis virus (EMCV), the prototypical cardiovirus, is a rodent virus that can infect many other organisms (144) causing encephalitis and myocarditis. EMCV's L protein contains only a zinc finger and acidic domain. Saffold virus (SafV), a recently discovered human virus of disputed pathogenicity (350) encodes an L protein with a zinc finger, acidic domain, and an additional "Theilo" domain (264). Theiler's murine encephalomyelitis virus' (TMEV) (represented here by the BeAn strain) L protein shares the three domains of SafV, with one additional "serine-threonine" (Ser/Thr) domain. TMEV (BeAn) causes persistent

demyelinating disease, similar to multiple sclerosis (MS) in humans (for review, see

(230)).

Active nucleocytoplasmic trafficking is required for proteins larger than 40kDa,

which cannot passively diffuse. The major players in active nucleocytoplasmic trafficking

are RanGTPase, which, by cycling between the GDP- and GTP-bound forms, provides

the energy source for trafficking. Cargoes are bound by karyopherins (importins,

exportins or transportins). RanGDP binds to importins to stimulate the release of their

cargo, while RanGTP binds, exports and traverses through the nucleus with the

exportin-cargo complex. Hydrolysis to GDP triggers cargo release (Fig 1-6).

Phenylalanine-glycine (F/G) repeat nucleoporins (nups) reside in the NPC and

transiently bind karyopherins, passing them through the NPC (240). Specific

karyopherins have been shown to interact with a subset of phenylalanine-glycine (F/G)

repeat nucleoporins (nups). F/G-repeat nups are localized throughout the NPC and are

engaged in active nucleocytoplasmic transport, while other nups serve as scaffolding.

Major F/G repeat nups include Nup358 (aka RanBP2) and 214, found in the cytoplasmic

filaments, Nup153 and Nup53, components of the nuclear basket, and Nup98 and

Nup62, found in the central channel.

A number of different trafficking pathways have been identified, utilizing specific

karyopherins that interact with select cargoes and traverse the NPC via a unique path.

The major trafficking pathways that have been identified are the import pathways

importin α/β, SR and M9 import pathways and the export pathways Crm1 and CAS.

These pathways are characterized by the nuclear localization signals (NLSs) or nuclear

export signals (NESs) their karyopherins recognize.

The best characterized transport pathway is the classical (importin α/β) import pathway. Up to 45% of proteins are thought to utilize this import pathway (174); importin α recognizes and binds cargo with basic mono- or bi-partite NLSs in the cytoplasm. Importin β then associates and mediates movement through the NPC. Nup50 and CAS exportin then intervene to help deliver the cargo to the nucleus (99, 203, 204). Other nups involved in classical import include Nups 358, 153, 62 (53, 137, 247). Cargoes of the classical pathway incude U snRNPs, ribosomal proteins, cyclin B and many viral proteins (for review see (216)).

The M9 pathway utilizes transportin-1 that binds the M9 NLS, which has been defined as a 19 residue sequence that is necessary and sufficient for shuttling (SNFGPMKGGNFGGRSSGPY) (139). Nups 358 and 98 are involved in the M9 import, while Nup153 trafficks in an M9-dependent manner (20, 92, 137). Cargoes include poly(A)-binding protein 2 and hnRNP A1 (45, 261). Transportin-1 can also mediate nuclear import of HIV Rev (12).

Transportin-3 is the major karyopherin in the SR import pathway, which trafficks cargos with arginine-serine (RS) NLSs (152). Cargoes include pre-mRNA splicing factors (SFs). No nups have yet been associated with the SR pathway, but Nup153 and transportin-3 were both found to be important for HIV infection (202).

Crm1 is a member of the karyopherin β superfamily that exports cargoes with leucine-rich NESs. These cargoes include many transcription factors, many translation factors, and most cellular RNA, including rRNA (for review, see (135)). During transport, a complex containing Crm1, RanGTP, RanBP3 and the NES cargo can interact with

nups (184). Nups358, 214, 153 and 98 are all implicated in the Crm1 pathway (32, 53, 136, 228).

Another exportin pathway, CAS (exportin-2) binds an acidic patch on importin α in the presence of RanGTP to recycle importin α back into the cytoplasm. Like Crm1, CAS is a member of the karyopherin β superfamily. Unlike Crm1, CAS has a modest number of identified cargoes. Besides importin α, ERK3 MAPK is the only other well-characterized CAS cargo (66). The CAS pathway is not yet well characterized, and the nups involved in CAS-dependent transport are unknown.

Phosphorylation plays a major role in active transport: phosphates can enhance karyopherin preference for a cargo (48, 254)(117, 132, 195)(171, 172, 218), or decrease karyopherin affinity for nups (as is believed occurs in L-induced nucleocytoplasmic trafficking inhibition) (165, 166). Its thought that phosphorylation may reduce the hydrophilic character of the FG repeat regions, weakening their interaction with hydrophobic karyopherins (166).

Cardioviruses have been shown to inhibit nucleocytoplasmic trafficking through the classical import pathway (22, 75, 183, 257, 258), and this inhibition can be carried out by the Leader (L) protein alone (75, 257, 258). EMCV L binds RanGTPase (256) and induces phosphorylation of specific F/G-repeat nups (358, 214, 153 and 62) (258). Furthermore, TMEV L has been previously shown to trigger phosphorylation of Nup98 (264). Both Ran binding and nup phosphorylation are thought to be involved in the inhibition of nucleocytoplasmic trafficking. Before this study it was unknown whether

these nup phosphorylation events affected other trafficking pathways, or if this mode of trafficking inhibition was undergone by all cardioviruses or just EMCV.

Mitogen-activated protein kinases (MAPKs) have been implicated in EMCV L-induced nup phosphorylation; specifically ERK1/2 and p38 and their downstream substrates RSK and MK2, respectively (257). EMCV L causes activation of these kinases (257) and ERK activation has been shown to inhibit importin α/β-mediated nuclear import (71). MAPK pathways are involved in diverse biological functions, including gene expression, mitosis, metabolism, motility, etc. MAPKs can be activated by various stimuli; in general, the ERK1/2 pathway is activated by growth factors and phorbol esters, while the p38 pathway respond to stress stimuli (osmotic shock, ionizing radiation, cytokines, etc.) (for review see (246)). Functional MAPK complexes have been shown to form between p38 isoforms and MEK3/6 (88), p38 and MK2 (31), and RSK1, ERK1/2, MSK1 and MSK2 (277).

Mass spectrometry of EMCV L binding partners in HeLa cells identified karyopherins Crm1 and CAS (J. Ciomperlik unpublished). As EMCV L has been shown to bind Ran (256), we initially thought L bound karyopherins through a Ran adaptor. Using recombinant proteins, however, we found EMCV L could bind Crm1 in the absence of Ran (J. Ciomperlik unpublished). Furthermore, EMCV L can also pulldown members of the MAPK family, including p38 and ERK1/2 (J. Ciomperlik unpublished). The EMCV L-ERK1/2 interaction, however, *is* indirect, as recombinant L cannot pulldown recombinant ERK1/2 alone in the absense of cytosol (J. Ciomperlik unpublished).

Before this study, it was unknown whether these karyopherins, Ran and MAPK interactions with L were specific to EMCV's L or if they were general to all cardioviruses. Additionally, it was unknown which import/export pathways other than the classical pathway were disrupted by cardioviruses.

We show here that EMCV, SafV and TMEV(BeAn) Ls are necessary and sufficient to disrupt nucleocytoplasmic trafficking via the classical, M9 and SR pathways. MAPKs are activated in the presense of each of the three Ls. Binding partners are conserved: all three Ls bind Ran, Crm1, CAS and MAPK family members ERK1/2, p38 and MSK2. In addition to this conservation of known binding partners, the cardiovirus Ls each have a unique cohort of binding partners, though the identity of these partners currently remains unknown. Taken together, these results provide a model in which cardiovirus Ls localize MAPKs to the NPC by binding karyopherins and Ran. These MAPKs phosphorylate specific F/G-repeat nups, disrupting active trafficking via the classical, M9 and SR pathways. Crm1-mediated export is also disrupted by EMCV L (J. Ciomperlik unpublished), though this pathway was not tested in this study. Binding to karyopherins and thereby MAPKs is reduced by mutations to phosphorylation sites, suggesting that phosphorylation enhances these interactions.

MATERIALS AND METHODS

Plasmids. pIRES-GFP was a generous gift from Kelly Watters (see Watters et al 2013, in preparation). pIRES-GFP L_E was created by amplifying EMCV L from pTriEx1.1 L_E-GST vector (see Chapter 2) with primers 1399 (5'-AACACGATCCCGGGGATGGCCACAA-3') and 1400 (5'-

TGGTGATGGGCGGCCGCTTACTGTAAC-3'). Insert and vector were digested with XmaI and NotI and ligated together with T4 DNA ligase (NEB). MV1190 cells were transformed, colonies were screened and then confirmed by restriction digest and Sanger sequencing. L_E-GST, L_S-GST and L_T-GST are as in Chapter 2. Phosphorylation site mutations (L_E-GST: $Y_{41}F$, $T_{47}A$, $Y_{41}F/T_{47}A$; L_S-GST: $T_{58}A$; L_T-GST: $S_{57}A$) are as in Chapters 2 and 3.

Recombinant proteins. Protein samples for L_E-GST, L_S-GST, L_T-GST, and phophorylation site mutated L_x-GSTs were prepared as described (64). Briefly, plasmid-transformed *E. coli* (Rosetta Competent Cells, Novagen) were induced with IPTG, sonicated and lysates were fractionated with a Glutathione Sepharose High Performance column (GE Healthcare Life Sciences). Protein was eluted with free glutathione, exchanged into buffer (25 mM HEPES, 150 mM KCl, 2 mM DTT, pH 7.3) and stored at -80^oC. His-Ran was expressed and purified as described (16).

Cells and viruses. HeLa cells (ATCC CRL-1958) adapted for suspension (37°C, 10% calf serum, 5% CO_2) were grown in modified Eagle's medium. Cells were plated 24 hrs before transfection. Transfections of pL_x-GST (1µg) were performed with Lipofectamine 2000 (Invitrogen) (1µg) according to the manufacturer's instructions.

NLS/NES cell lines are as in Watters et al 2013 (in preparation). Briefly, retroviral vectors were generated by transfection of pCMS28-mCherry-reporter plasmid, Gag-Pol packaging plasmid, and VSV-G envelope plasmid into 29T3 cells. HeLa cells were then transduced with retroviral vectors. Single clones of transduced HeLa cells were selected to generate a HeLa cell line stably expressing mCherry-reporters. These cell lines were

maintained in suspension culture (37°C; Eagle's medium, 10% NBCS, 2% fetal bovine serum FBS 400 mg/mL G418, under 5% CO$_2$). Reporter NLS/NES sequences are listed in Table 4-1.

Pulldown assays. Protein binding reactions (80 μl total, with 30 μl cytosol, 2 μl 10 mM ATP, 2 μg L$_x$-GST) were performed in GST binding buffer (50 mM HEPES, 150 mM NaCl, 0.5% NP40, pH 7.4) for 45 min (37°C). Glutathione sepharose 4B beads (10 μl per sample, GE Healthcare Life Sciences) were then added, followed by agitation (room temperature, 2 h). The beads were collected by centrifugation (500 g), washed with GST buffer (4x) then boiled in SDS gel loading buffer. Protein fractionation was by SDS-PAGE (8 or 10%) followed by western analysis.

Western blots. After SDS-PAGE gel fractionation, proteins were electrotransferred to polyvinylidene difluororide membranes (Immobilon-P, Millipore), blocked in 10% nonfat dry milk in Tris-buffer saline (TBST: 20 mM Tris, pH 7.6, 150 mM NaCl, 0.5% Tween-20) (room temperature, 1 h). After washing (TBST, 3x), membranes were incubated (1% milk, TBST, 4°C, overnight) with primary antibody. After washing (TBST, 3x), membranes were incubated with secondary antibody (1% milk in TBST, room temperature, 1 h). Membranes were washed a final time (TBST, 3x), reacted with enhanced chemiluminescence substrate (GE Healthcare) and exposed to film.

Pathway	Karyopherin	NLS or NES	Sequence
Classical	Importin α/β	SV40 NLS	PKKKRKVDPKKKRKVDPKKKRKVD
M9	Transportin 1	M9 domain hRNPA1 NLS	SYNDFGNYNNQSSNFGPMKGGNFGGRS SGPYGGGGQYFAKPRNQGGY
SR	Transportin 3	RS domain of SF2 NLS	RSPSYGRSRSRSRSRSRSRSRSNSRSRS YSPRRSRGSPRYSPRHSRSRSR
Crm1	Crm1	Leucine rich NES	NSNELALKLAGLDI

Table 4-1. Stable mCherry-NLS/NES HeLa cell lines.

Primary antibodies used in this study: mAb414 (mouse mAb,Covance) against Phe/Gly-containing Nups, αtubulin (mouse mAb, T4026, Sigma-Aldrich), αCAS (C-20) (goat pAb, sc-1708, Santa Cruz), αCrm1 (rabbit pAb, ab24189, abcam), αERK1/2 (rabbit pAb, 06-182, Millipore), αGST (mouse mAb, 71087, Novagen), αp38α (rabbit pAb, 9218, Cell Signalling), αMSK2 (D41A4) (rabbit mAb, 3679, Cell Signalling), αMEK2 (rabbit pAb, 9125, Cell Signalling), αP-MAPKAP2 (Thr334, 27B7) (rabbit mAb, 3007, Cell Signalling), αP-p38 (Thr180/Tyr182) (rabbit, pAb, 9211, Cell Signalling), αP-ERK1/2 (D13.14.4E) (rabbit mAb, 4370, Cell Signalling), αNup98 (2H10) (rat mAb, N1038, Sigma-Aldrich) and α-6xHis (mouse, mAb, 18184, Abcam).

Secondary antibodies used in this study: αmouse IgG (Fc specific) peroxidase (A2554, Sigmal-Aldrich), αgoat IgG (whole molecule) peroxidase conjugate (A5420, Sigma-Aldrich), αrat IgG (whole molecule) peroxidase (A5795, Sigma-Aldrich) and αrabbit IgG (H+L) HRP conjugate (W4011, Promega).

RESULTS AND DISCUSSION

Cardiovirus Ls disrupt classical, M9 and SR import. Previous work showed that EMCV (L_E) and TMEV L (L_T) proteins could disrupt the classical (NLS) import pathway (22, 75, 183, 257, 258), but it was unknown whether SafV L (L_S) could disrupt trafficking at all, or if the classical import pathway was the only one disrupted by cardioviruses. $L_{E,S,T}$-GSTs transfected into stable NLS-mCherry HeLa cell lines disrupt classical, M9 and SR import pathways, as indicated by fluorescent signal re-localizing to the cytoplasm (Fig 4-1). Both cap-dependent (pT1.1 L_E-GST) and IRES-driven (pIRES-GFP
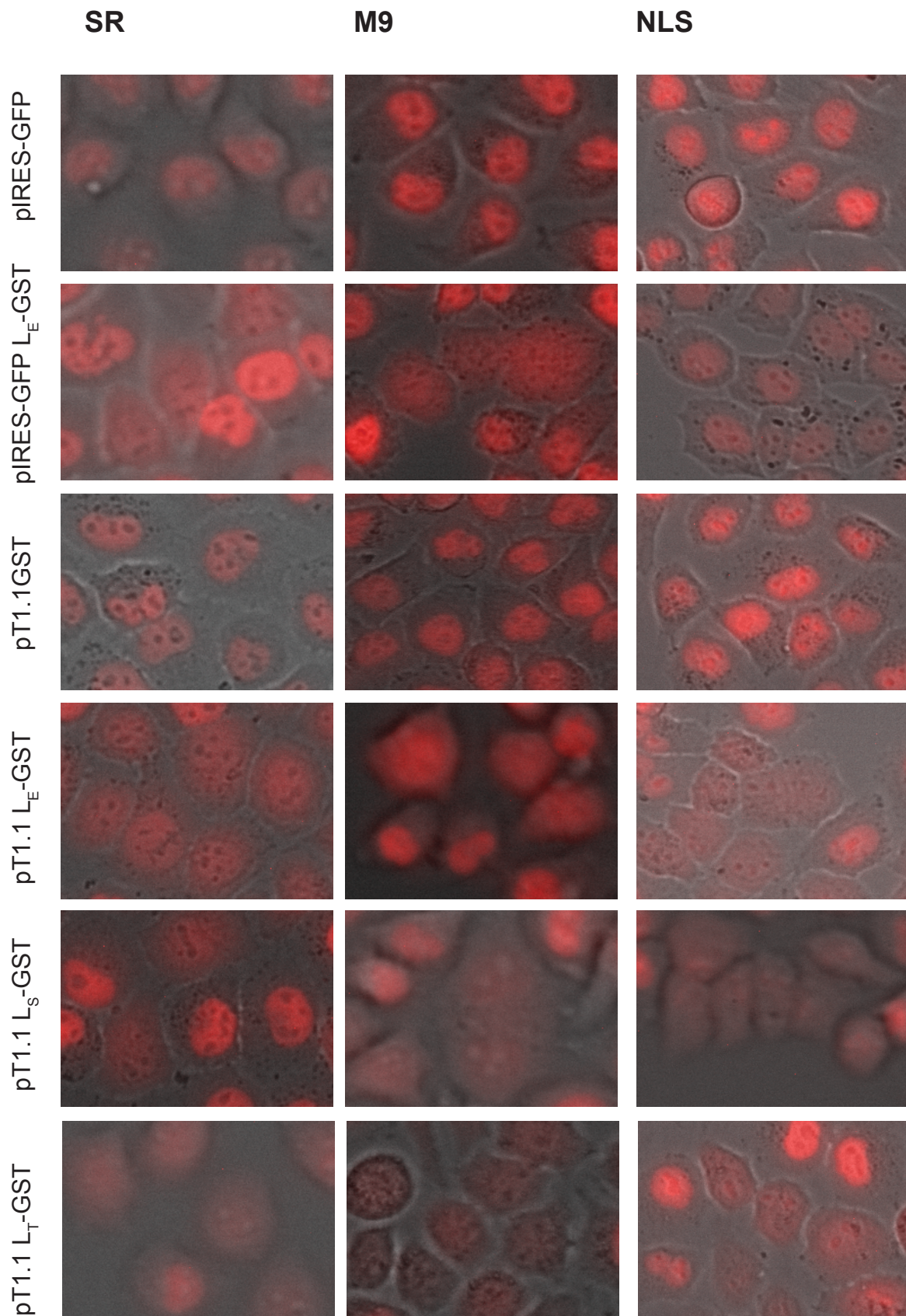
Figure 4-1. Nuclear import pathways disrupted by Cardiovirus Ls. HeLa cell lines stably expressing mCherry-NLS reporters for SR, M9 or clasical NLS tags (Table 4-1) were transfected with pIRES-GFP or pT1.1GST as controls, pIRES-GFP L_E-GST or $L_{E,S \text{ or } T}$-GST. Cells were imaged at 6 hours post-transfection.

L_E) EMCV L could disrupt all three import pathways (6 hr post transfection). Additionally, we show for the first time that SafV L can also disrupt all three pathways. We previously showed that EMCV, SafV and BeAn Ls alone, when transfected into HeLa cells, can induce the phosphorylation of Nup62 (Chapter 2). By targeting pivitol F/G repeat nups, cardiovirus Ls are able to disrupt the major import pathways; Nup62 is located in the central plug of the NPC and is essential for classical import (50). Furthermore, Nup98 is phosphorylated in the presence of all 3 Cardiovirus Ls (transfection into HeLa cells) (Fig 4-2), and is important for M9 import (89) and Crm1 export (225). We do not yet know whether this nup preference is conferred by L itself, its binding partners, or whether this is a consequence of kinase specificity (i.e. these are the only nups that contain the correct docking/phosphorylation sites).

Cardiovirus Ls cause activation of the MAPK pathway. We previously showed that L_E caused activation of p38 and ERK1/2 MAPKs and their downstream substrates (257). Here we show that L_S and L_T alone, when transfected into HeLa cells, can also activate MAPKs, specifically p38 and its substrate MAPKAP2. Transfection itself activated ERK1/2, making detection of ERK1/2 activation difficult (Fig 4-3). These findings suggest that the activation of MAPKs is a common mechanism undergone by Cardiovirus Ls to induce nup phosphorylation.

Cardiovirus Ls form complexes with members of the MAPK pathway. Although MAPKs have been implicated in L_E-driven nup phosphorylation (i.e. inhibitors to ERK1/2 and p38 prevented nup phosphorylation in the presence of EMCV L) (257), the mechanism by which L accomplished this was unknown. Activation of MAPKs alone does not induce nup phosphorylation, as okadaic acid (a broad-spectrum phosphatase

116
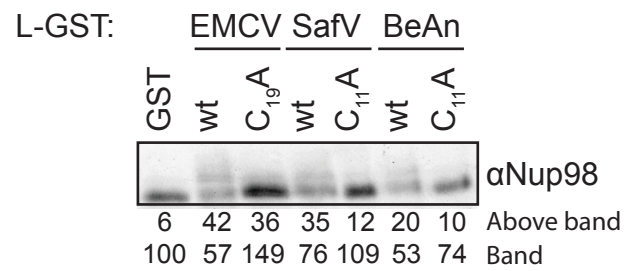
Figure 4-2. L-induced nup phosphorylation. HeLa cells were transfected with either pT1.1 L$_{wt}$GST or a zinc finger mutant (C$_{19}$A or C$_{11}$A) pT1.1LGST. Phosphorylation is by upwards mobility shift of Nup98 visualized via western blot. Quantification performed by TotalLabQuant software.
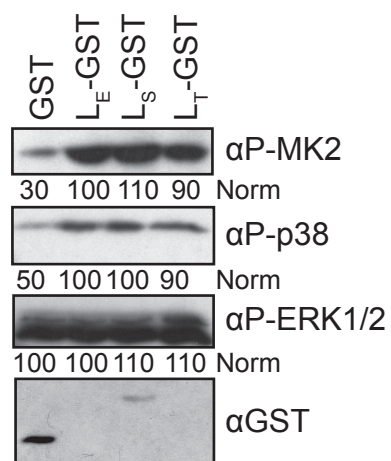
Figure 4-3. Activation of MAPKs by Cardiovirus L. HeLa cells were transfected with pT1.1L$_{wt}$GST and incubated for 18 hrs. Cells were lysed in Laemmli buffer and lysates analyzed via western blot for phosphorylated (active) MAPKAP-2, p38 and ERK1/2. GST blot indicates transfection of control pT1.1GST vector. Bands quantitated by densitometry (TotalLabQuant) relative to L$_E$.

inhibitor) has no effect on nups in the absence of L_E (though it enhances nup
phosphorylation when L_E is present) (J. Ciomperlik unpublished). Here we show that the
three cardiovirus Ls can complex with members of the MAPK pathway from HeLa
cytosol, specifically p38α, ERK1/2 and MSK2 (a substrate of both p38 and ERK) (Fig 4-
4). When recombinant ERK and L_E are reacted in the absense of cytosol, however, L
does not pulldown ERK, suggesting they interact through an intermediate (J. Ciomperlik
unpublished). Additionally, we do not yet know whether L is binding a complex of
MAPKs or a number of individual kinases.

Cardiovirus Ls bind RanGTPase. EMCV L can bind Ran with a very tight K_d (~3nM)
and the L:Ran interaction is necessary for L-dependent induction of nup
phosphorylation (16, 249, 256). We show here that in recombinant protein assays, all 3
Cardiovirus L-GST proteins can bind His-Ran protein (Fig 4-5). Despite cardioviruses
harboring significant sequence variability in the "hinge domain" between the zinc finger
and the acidic domain where Ran binds (16), two of the three residues found to be most
important for binding (16) are conserved in all Cardioviruses (D_{37} and W_{40}) (Fig 3-1).

Cardiovirus Ls bind exportins Crm1 and CAS. In a mass spectrometry analysis of
EMCV L binding partners in HeLa cytosol, two major exportins were identified: Crm1
and CAS (J. Ciomperlik unpublished). We show here that in L pulldowns from HeLa
cytosol, all three cardiovirus Ls are able to bind exportins Crm1 and CAS (Fig 4-6). The
binding of Crm1 and L_E was found to be direct, and not dependent on Ran *in vitro* (J.
Ciomperlik unpublished). ERK1/2 is exported in a Crm1-dependent manner (151),
suggesting that perhaps L interacts with MAPKs through exportin adaptors. It is not yet
clear whether L can selectively bind MAPK-bound importins, but a modeled protein

119
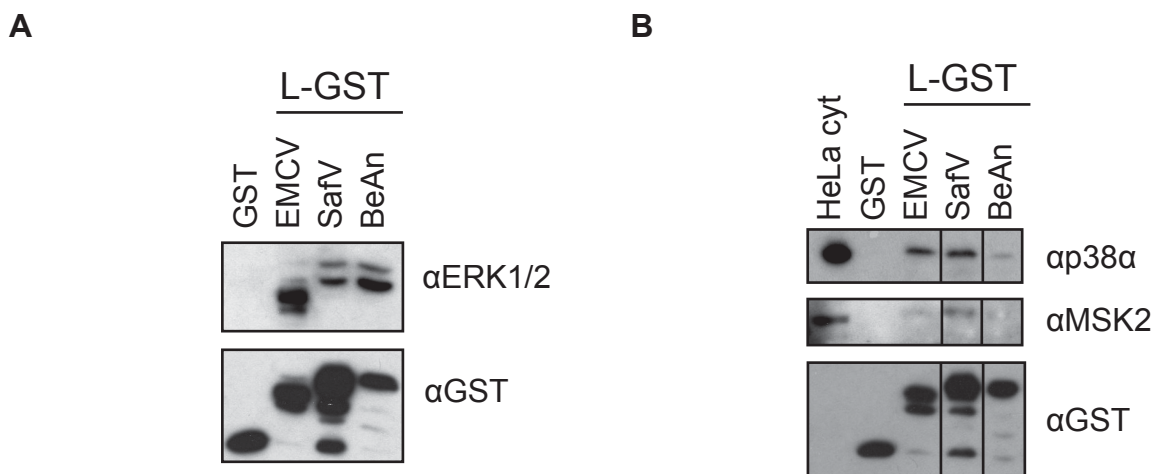
Figure 4-4. MAPKs pulled down by Cardiovirus Ls. Recombinant L-GST proteins bound to GST beads were reacted with HeLa cytosol at 4ºC overnight. Beads were washed then boiled in Laemmli buffer and analyzed via western blot for **A**. ERK1/2 and GST or **B**. p38, MSK2 and GST. HeLa cytosol (1µl) serves as a control. Note ERK1/2 antibody cross-reacts with EMCV-L.
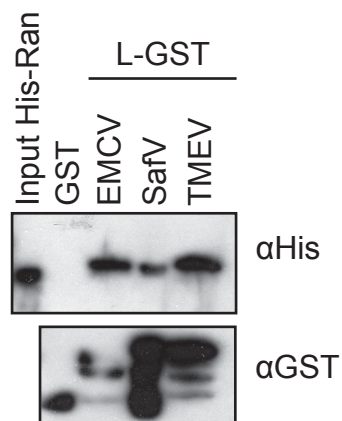
Figure 4-5. L:Ran binding. Recombinant His-Ran was reacted with cardiovirus LE,S, and T wt GST proteins, which were pulled down with glutathoine beads, eluted in Laemmli buffer and analyzed via western blot for His-Ran binding. GST was probed as a loading control.
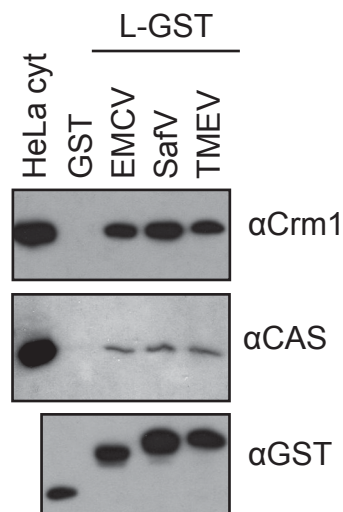
Figure 4-6. Exportins pulled down by cardiovirus Ls. L$_{E,S, and T}$ wt GST proteins were reacted with HeLa cytosol, pulled down with glutathoine beads, eluted in Laemmli buffer and analyzed via western blot for exportin (CAS and Crm1) binding. GST was probed as a loading control and 1μl of HeLa cytosol indicates endogenous levels of each protein.

complex of L, Crm1, Ran and cargo predicts that L_E's C-terminus could potentially interact with Crm1's cargo-binding site (Fig 1-8). Interestingly, the C-terminus is where cardioviruses differ the most, and were SafV and BeAn possess additional domains (Fig 1-4).

Cardiovirus Ls have unique binding partners. To test whether L_S and L_T do indeed bind a unique cohort of proteins, we performed pulldown reactions of the 3 L-GSTs in HeLa cytosol. Silver total protein stain of the 3 L's binding partners showed that, particularly in the higher molecular weight range (Fig 4-7B), the 3 Ls bound a distinct array of proteins. Many of these bands fall into the size range of karyopherins (~100kDa), suggesting perhaps the 3 Ls prefer a different subset of karyopherins/cargoes. Mass spectrometry will reveal the identity of these novel binding partners.

Phosphorylation state affects complex formation. We previously shownied that L_E phosphorylation has major effects on its activity, preventing nup phosphorylation (Chapter 2) and nucleocytoplasmic trafficking disruption (Chapter 3). However, we had yet to identify the step of L's function at which phosphorylation played a role. We therefore tested whether phosphorylation state affects exportin binding, as modulation of karyopherin binding by phosphorylation is common in the cell (48, 254)(117, 132, 195)(218) (171, 172). Using L proteins with mutated phosphorylation sites, we performed pulldown assays from HeLa cytosol and found that these phosphorylation site-mutated L proteins had reduced affinity for exportins and thereby ERK1/2 (Fig 4-8). Furthermore, pre-phosphorylation of EMCV L by CK2 increased its affinity for recombinant Crm1 (J. Ciomperlik unpublished).
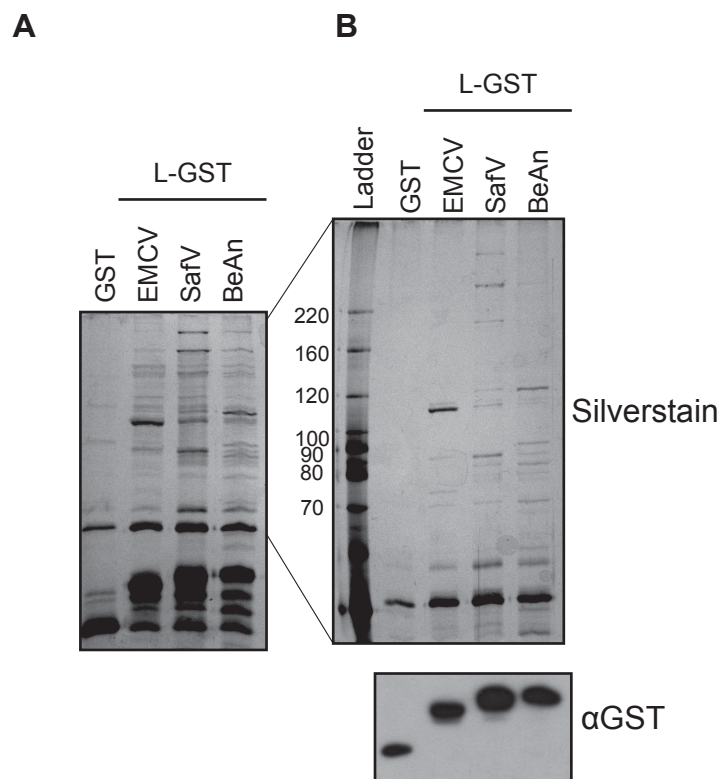
Figure 4-7. Cardiovirus L binding parters from HeLa cytosol. $L_{E,S, and T}$ wt GST proteins were reacted with HeLa cytosol, pulled down with glutathoine beads, eluted in Laemmli buffer, run on either a 10% SDS-PAGE gel (**A.**) or an 8% gel (**B.**) and analyzed via silver total protein stain for binding partners. A GST western blot was performed to indicated input L-GST protein levels.

A

L$_E$-GST

L-GST

B
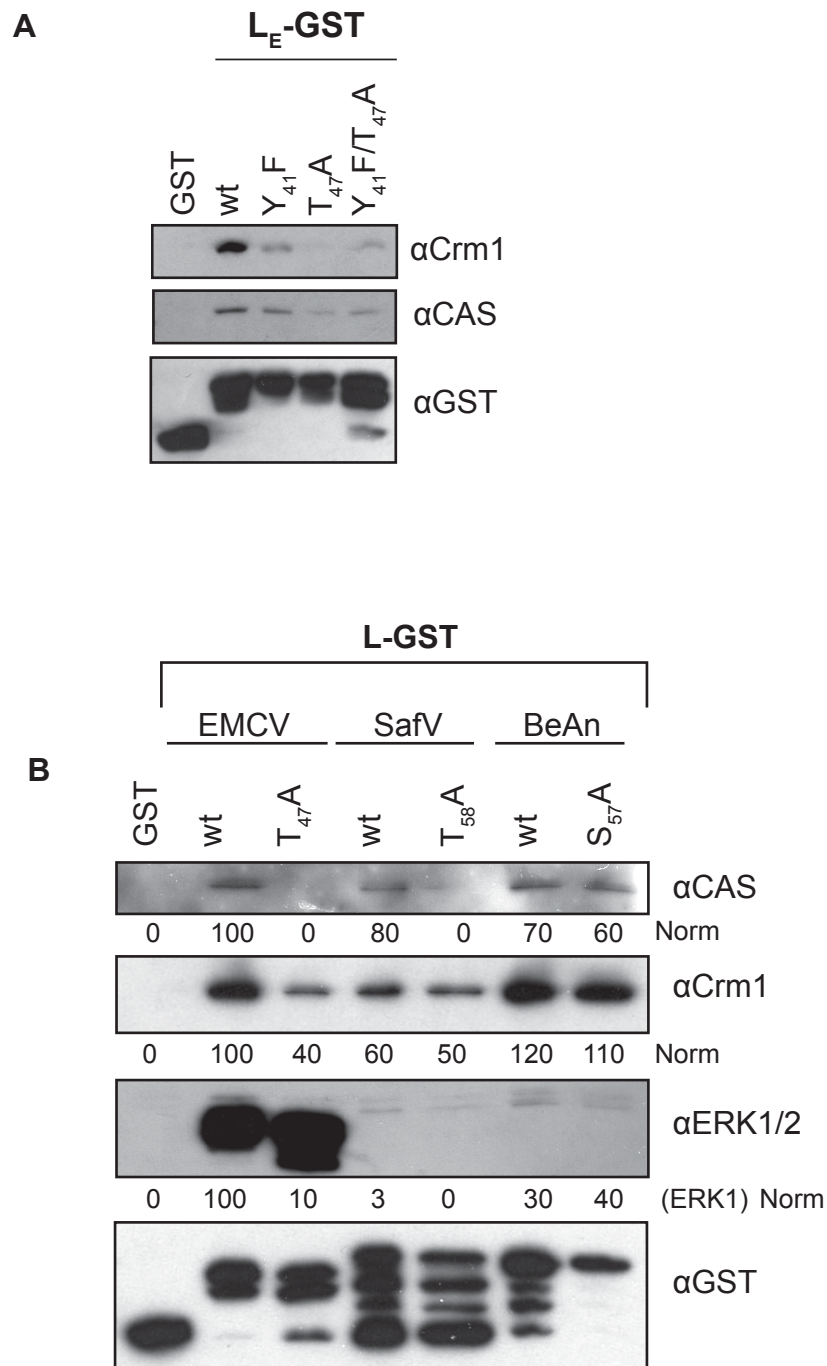
Figure 4-8. Cardiovirus L phosphorylation site mutations pulldowns of HeLa cytosol. **A**. L$_E$-GST single (Y$_{41}$F and T$_{47}$A) and double phosphorylation site mutations (Y$_{41}$F/T$_{47}$A) were reacted with HeLa cytosol and then pulled down with glutathoine beads. Samples were washed and then boiled in Laemmli buffer and analyzed via western blot for exportins (Crm1 and CAS). GST western blot serves as a loading control. **B**. L$_{E,S, and T}$ wt and single phosphorylation site mutations (T$_{47}$A, T$_{58}$A and S$_{57}$A) were reacted with HeLa cytosol, pulled down and analyzed as in A. for exportins (CAS and Crm1), ERK1/2 and GST.

Interestingly, L_S did not pull down either karyopherins or ERK1/2 to the levels seen in L_E or L_T. This finding could be explained by the incomplete phosphorylation of L_S in HeLa cytosol (Chapter 2, 3). Additionally, L_S-GST was the only L protein detectable in transfections when expressed cap-dependently (Fig 4-3), suggesting it incompletely shut down mRNA trafficking. Future work will clarify whether incomplete phosphorylation can account for the attenuation of L_S, and whether this attenuation can account for reduced viral pathogenicity.

Taken together, these findings provide a model wherein L binds 2A, which partially masks L phosphorylation sites (Appendix 3), and is released at the nuclear rim where it binds Ran. Phosphorylation can occur when L is bound to Ran (Chapter 2), and phosphorylated L and Ran bind an exportin loaded with MAPK. This complex localizes to the NPC, where the MAPK phosphorylates F/G-repeat nups. These phosphorylated nups lose affinity for importins and exportins, thereby disrupting nucleocytoplasmic trafficking by multiple pathways (classical, M9, S9 and Crm1).

CHAPTER 5.

Conclusions and Future Directions

Chapter Highlights and Summary

Chapter 1: Introduction

Chapter 2: Encephalomyocarditis Virus Leader is Sequentially Phosphorylated by CK2 and Syk as a Requirement for Subsequent Phosphorylation of Cellular Nucleoporins

- EMCV L is phosphorylated at two sites: Tyr_{41} and Thr_{47}.
- Syk and CK2 are responsible for phosphorylation of Tyr_{41} and Thr_{47}, respectively.
- Phosphorylation is sequential: Syk depends on CK2 to add a phosphate first.
- Inhibition of CK2 decreases EMCV L phosphorylation *in vitro.*
- Inhibition of CK2 decreases L-directed nup phosphorylation *in vivo.*
- Mutation of both EMCV L phosphorylation sites decreases nup phosphorylation induction.
- Ran binding does not inhibit EMCV L phosphorylation.
- SafV and TMEV (BeAn) Ls are phosphorylated (in multiple cytosol types), at different levels.
- SafV and TMEV (BeAn) Ls are NOT phosphorylated by CK2.

Chapter 3: Cardiovirus Leaders are phosphorylated by AMPK

- SafV L phosphorylation sites in HeLa cytosol: Thr_{36}, Thr_{40}, Tyr_{49} and Thr_{58}.
- TMEV (BeAn) L phosphorylation sites in HeLa cytosol: Tyr_{34} and Ser_{57}.
- Mutation of certain sites to phosphomimetic Asp residues in BeAn L increased phosphorylation signal.
- AMPK can phosphorylate all three Ls.
- AMPK phosphorylates EMCV L at Thr_{47}, SafV L at Thr_{58} and BeAn L at Ser_{57}.
- SafV L does not become fully phosphorylated in HeLa cytosol.
- CK2 is highly expressed in all cytosol types tested, while AMPK is only highly expressed in BHK-21 cytosol.
- vEC_9 infection causes activation of MAPKs and AMPK, but not CK2.
- Mutation to phosphorylation site $T_{47}A$ decreases vEC_9 activation of MAPKs and AMPK.
- Ser/Thr and Theilo domains are predicted to form a helix.

Chapter 4: Cardiovirus Leaders activate and complex with mitogen-activating kinases (MAPKs) and exportins to inhibit nucleocytoplasmic trafficking

- Cardiovirus Ls disrupt classical, M9 and SR import.
- Cardiovirus Ls cause activation of the MAPK pathway.
- Cardiovirus Ls form complexes with members of the MAPK pathway.
- Cardiovirus Ls bind Ran.
- Cardiovirus Ls bind exportins Crm1 and CAS.
- Cardiovirus Ls have unique binding partners.
- Phosphorylation site mutations in Ls decrease exportin and MAPK binding.

To prevent immune response activation, picornaviruses disrupt active trafficking through the nuclear pore complex (NPC). The cardioviruses accomplish this through the actions of the small, insidious protein, Leader (L). Although L proteins vary in sequence and domain architecture, they conserve a general list of responsibilites. In this thesis, we illustrate that representative cardioviruses (EMCV, SafV-2 and TMEV BeAn strain) all bind the viral 2A protein (Appendix 3), bind RanGTPase (Chapter 4), are phosphorylated (Chapter 2, 3), bind karyopherins (CAS and Crm1) (Chapter 4), complex with and activate members of the MAPK family (Chapter 4), induce phosphorylation of nucleoporins (nups) (Chapter 2, 4), and inhibit nuclear import (Chapter 4). Although this work has filled in many gaps in our knowledge of cardiovirus L function (Table 5-1), there are places that require clarification in our model (Figure 5-1).

Cardiovirus Ls bind 2A. EMCV L (pI=3.8) and 2A (pI=9.7) bind *in vitro* with a K_d of ~1.5µM (Appendix 3). 2A has an nuclear localization signal (NLS) and an eIF4e binding site, and it localizes to the nucleolus and binds RNA (104)(B. Brown unpublished). We hypothesize that L binds 2A and utilizes its NLS to hitch a ride to the nuclear rim (256). Once there, we believe Ran can displace 2A, as it does *in vitro* (Appendix 3), binding EMCV L with a much tighter K_d (3nM) (249). For the other cardiovirus Ls (SafV and BeAn), we've shown that they can bind their own 2A proteins *in vitro*, but actually prefer EMCV's 2A, which has a more basic pI (Appendix 3). Future directions include investigating whether this decreased affinity for their own 2A proteins associates with

any attenuation of the viral replication cycle. Additionally, the spacial and temporal

interactions of 2A and L have yet to be observed *in vivo*. Does L:2A binding occur pre-

L function or feature	EMCV	TMEV	Saffold
Required for viral persistence	NA	+	ND
Dispensable for viral genome replication	+	+	ND
Inhibition of type I IFN production	+	+	ND
Inhibition of IRF3 dimerization	+	+	ND
Inhibition of chemokine gene transcription	+	+	ND
Disruption of stress granules	+	+	+
Perturbation of nucleocytoplasmic trafficking	+	+	+
Alteration of nuclear pore architecture	+	ND	ND
Hyperphosphorylation of nucleoporins	+	+	+
Interaction with RanGTPase	+	+	+
Is phosphorylated	+	+	+
Binds Exportins	+	+	+
Binds MAPKs	+	+	+
Activates MAPKs	+	+	+

Table 5-1. Summary of cardiovirus L functional data. Modified from "Picornaviruses" 2013 Chapter 26 pg 412. NA=not applicable. ND=not determined. Red plus signs indicate data included in this thesis.

or post-polyprotein processing? Can this binding facilitate polyprotein processing? These early steps in L activity have yet to be elucidated.

Cardiovirus Ls cause activation MAPKs. Previous work showed that EMCV caused activation of mitogen activating kinases (MAPKs); specifically p38 and ERK1/2 and their downstream kinases RSK and MK2, respectively (257). MAPK activation was attributed to the L protein alone, and found to be indispensable to L's nup phosphorylation ability (using chemical inhibitors) (257). We show here that, like EMCV L, SafV and BeAn Ls can also cause the activation of MAPKs (Chapter 4). However, the exact step at which the MAPK pathway is activated has not been elucidated for any cardioviruses L, so it is not yet known if they target this pathway at the same junction, at the same speed or to the same levels.

Cardioviruses Ls complex with Ran, exportins and MAPKs. Next we hypothesize L, Ran, a karyopherin (CAS or Crm1) and one or more MAPKs form a complex that can phosphorylate nups. We know that the 3 cardiovirus Ls can bind Ran and Crm1 individually (Chapter 4), but ERK MAPK must be bound through an adaptor (likely Crm1) (J. Ciomperlik unpublished). We show here that, in addition to ERK, the cardiovirus Ls also pulldown MAPK family members p38α and MSK2. Though all 3 cardiovirus Ls cause activation of MAPK pathway members, the activation of these kinases in the absence of L does not cause nup phosphorylation or trafficking inhibition (J. Ciomperlik unpublished). We therefore hypothesize that L localizes these activated kinases to the nuclear pore, diverting them to phosphorylate specific nups. We have not yet shown a redistribution of MAPKs, nor do we know if L has any selectivity for Crm1 cargoes once it's bound. We don't currently know whether L:Ran and L:Crm1 complex

separately, or whether L:Ran:Crm1 bind together, with L lying at the interface (as modeled in Fig 5-1B). The structural model predicts the C-terminal tail (where the cardiovirus Ls differ the most) can loop over to Crm1's cargo binding site (Fig 5-1B), perhaps providing selectivity for cargoes. Indeed, each L has a unique cohort of binding partners (Chapter 4) to go with their unique C-termini, and mass spectrometry analysis will reveal their identity.

Cardiovirus Ls induce nup phosphorylation and inhibit nucleocytoplasmic trafficking. EMCV L was previously shown to be the sole protein required to induce phosphorylation of specific nucleoporins (nups) (62, 153, 214 and 358) and inhibit nucleocytoplasmic trafficking by the classical import pathway (258). Here we show that EMCV L can also induce the phosphorylation of Nup98, as well as abolish active import via the M9 and SR import pathways (Chapter 4). The other Cardiovirus, SafV and BeAn, Ls can also cause phosphorylation of nups 62 and 98, and shut down the M9, SR and classical import pathways (Chapter 4). Additional nups (ex. 153, 214 and 358) have not yet been tested for the two Theiloviruses, nor have any export pathways. Future work includes live cell imaging to compare the rates of trafficking inhibition by the 3 cardioviruses; perhaps their L proteins target different pathways with different kinetics, as observed with the rhinovirus 2A^{pro} (324)(Watters in preparation).

Cardiovirus Ls are phosphorylated. Phosphorylation of EMCV L itself plays an important role in its functionality, as mutations to phosphorylation sites delay L's nucleocytoplasmic shutdown ability (183), allow increased IFN-β production during infection (351) and attenuate L-directed nup phosphorylation (Chapter 2). EMCV L is phosphorylated sequentially by casein kinase 2 (CK2) and spleen tyrosine kinase (Syk)

on Thr_{47} and Tyr_{41}, respectively (Chapter 2). EMCV L can also be phosphorylated by AMP-activated protein kinase (AMPK) on Thr_{47}, as can SafV L (on Thr_{58}) and TMEV (BeAn) L (on Ser_{57}). We find that mutations to these phosphorylation sites diminish the 3 Ls' abilities to bind karyopherins CAS and Crm1, and thereby binding to MAPKs (specifically ERK) (Chapter 4). Furthermore, pre-phosphorylation of EMCV L increases its affinity for recombinant Crm1 (J. Ciomperlik unpublished). We therefore propose that phosphorylation serves to enhance L:karyopherin binding, in turn localizing more MAPK to the nuclear pore, increasing nup phosphorylation.

There are still many unanswered questions about L phosphorylation. Data suggests that EMCV L can be phosphorylated by either CK2 or AMPK, as CK2 inhibitors with off-target effects on AMPK abolish nup phosphorylation ability more effectively (Chapter 2). We therefore suspect that EMCV L can become phosphorylated more efficiently than either SafV or TMEV Ls, but this has not yet been tested. Furthermore, most comparison of the 3 cardiovirus Ls has been undergone in HeLa cells; the next step is to characterize kinase expression and L phosphorylation in more biologically relevant cell types (L929 or BHK-21 cells for TMEV). Knockdown of AMPK (by siRNA) will divulge whether this kinase is the most biologically relevant for SafV and TMEV Ls. While CK2 is constitutively active, AMPK is not, so it will be of interest to investigate whether viral infection activates AMPK, and whether activation changes during persistent infection of TMEV.

Immediate next steps include confirming L phosphorylation sites and their relevance in viral infection. Viral cDNAs have been created for EMCV and TMEV (BeAn) and their primary phosphorylation sites ($Thr_{47}Ala$ and $Ser_{57}Ala$, respectively).

These viruses will be tested for nup phosphorylation ability, MAPK activation, and nucleocytoplasmic trafficking inhibition (via mCherry-NLS/NES cell lines, see Chapter 4). We suspect that, like EMCV L $Thr_{47}Ala$, the BeAn phosphorylation site will have decreased nup phosphorylation ability leading to abolished or delayed nucleocytoplasmic trafficking inhibition. Furthermore, mutation of EMCV L phosphorylation site Thr_{47} decreases L-directed MAPK activation, however, this has not been tested for the other cardio L phosphorylation sites.

This work can also be extended to other Cardiovirus Ls. TMEV (GDVII, neurovirulent strain) L has a Pro at the position of TMEV (BeAn/DA, persistent demyelinating strains) L's primary phosphorylation site. This position (57) is seminal in strain specific phenotypes; when DA Ser is mutated to a Pro, DA acquires a GDVII phenotype (high titer, big plaques) in BHK-21 cells (305). This position is also thought to be important for differences in DA vs GDVII L apoptotic abilities (300). It will be interesting to investigate if GDVII has an alternate phosphorylation site and/or kinase that accounts for the observed differences in viral phenotype.

Summary. The data presented here support of model of L function whereby L binds 2A (Appendix 3) and traffics to nuclear rim where it is displaced by Ran and phosphorylated by multiple kinases. These phosphorylation events increase L's affinity to karyopherins (CAS or Crm1), which are bound to MAPKs (likely p38 and/or ERK). This L:Ran:Crm1:MAPK complex targets nups with phosphates, which decrease trafficking karyopherins' affinity for these nups, thereby inhibiting active transport. This inhibition of active trafficking prevents interferon signaling, allowing a productive viral infection.
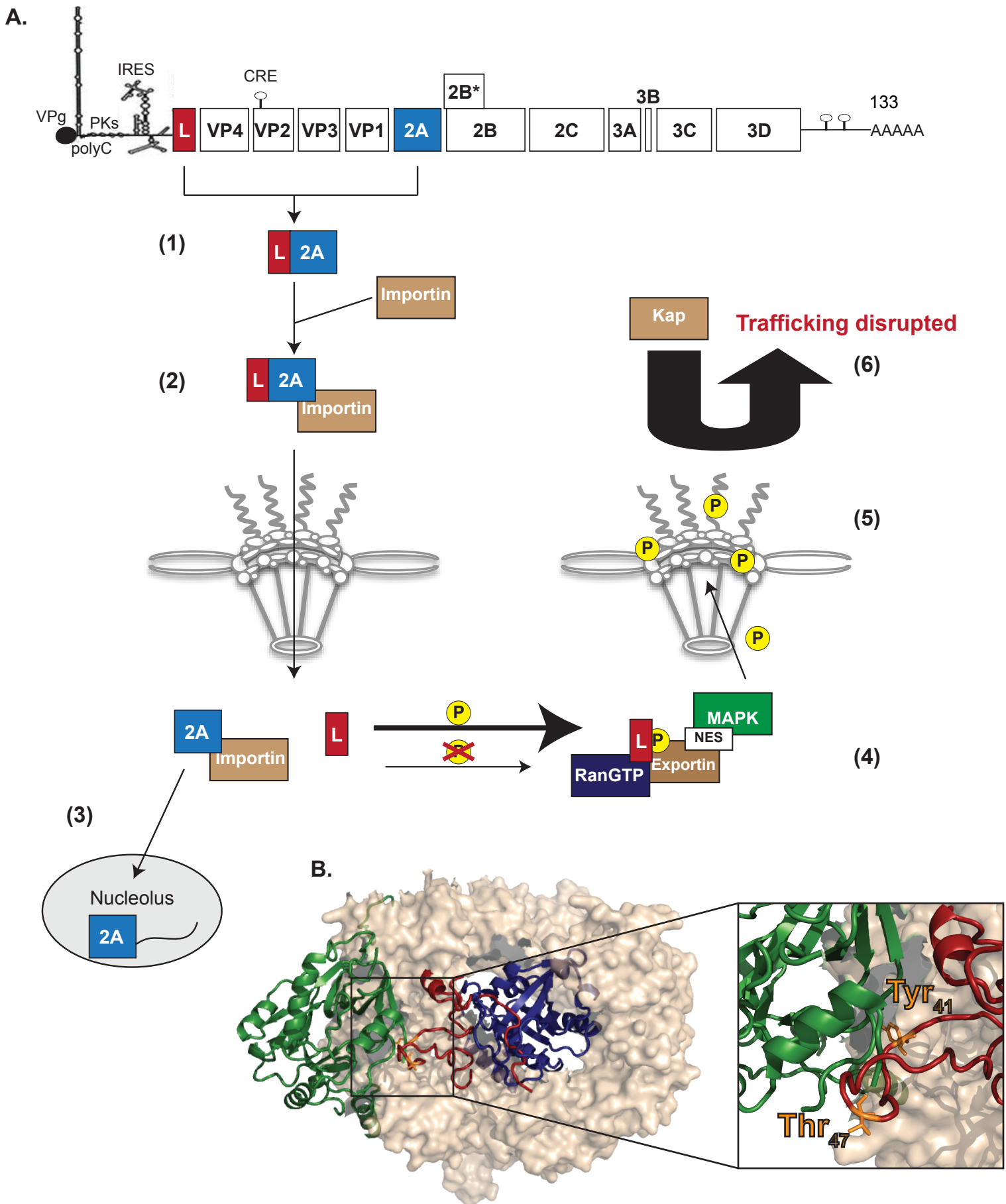
Figure 5-1. Model of Cardiovirus L function. A. (1) L binds 2A, which contains an NLS (Appendix 3). (2) L-2A trafficks to the nucleus. (3) L and 2A disocciate and 2A trafficks to the nucleolus, where it binds RNA. (4) L becomes phosphorylated, which increases its affinity for a complex containing RanGTPase (Chapter 3), an exportin (ex. Crm1), and MAP kinases, localizing ERK1/2 and/or p38 to the nuclear pore (Chapter 4), where it (5) phosphorylates nups (Chapter 2). Nup phosphorylation impedes association of karyopherins, (6) disrupting active nucleocytoplasmic trafficking (Chapter 4). B. Model of complex of EMCV L NMR structure (red) (Palmenberg unpublished) with Ran (blue), Crm1 (tan) and cargo (snurpoprtin) (green) (PDB:3GJX). L phosphorylation sites shown as orange sticks.

Appendix 1.

Modeling of the Human Rhinovirus C Capsid Suggests a Novel Topography with Insights on Receptor Preference and Immunogenicity

Holly A. Basta, Jean-Yves Sgro and Ann C. Palmenberg

Author contributions: JYS created the MODELLER RV-C15 model, Fig A1-4 capsid rendering, roadmaps and 5-fold axis representations, Fig A1-5 roadmap projections, and Fig A1-6 NIm representations. ACP curated the alignments and calculated NIm values in Table A1-3.

Justification: Human rhinovirus (RV)-C is a recently discovered RV species that is associated with up to half of infections in young children. RV-C eluded discovery because it does not grow in common cell culture lines. The RV-Cs use a receptor unique to those used by RV-A and –B species (ICAM-1 and LDLR), but this receptor has yet to be discovered. Some success has been made using primary human donor samples and air-liquid interface cultures, but these techniques cannot yield the mg amounts of virus needed for crystallographic studies. To circumvent these issues we used the robust alignment data set coupled with the multitude of solved RV-A and –B capsid structures to model the RV-C15 capsid structure.

Abstract

Features of human rhinovirus (RV)-C virions that allow them to use novel cell receptors and evade immune responses are unknown. Unlike the RV-A+B, these isolates cannot be propagated in typical culture systems or grown for structure studies. Comparative sequencing, I-TASSER, MODELLER, ROBETTA, and refined alignment techniques led to a structural approximation for C15 virions, based on the extensive, resolved RV-A+B datasets. The model predicts all RV-C VP1 proteins are shorter by 21 residues relative to the RV-A, and 35 residues relative to the RV-B, effectively shaving the RV 5-fold plateau from the particle. There are major alterations in VP1 neutralizing epitopes and the structural determinants for ICAM-1 and LDLR receptors. The VP2 and VP3 elements are similar among all RV, but the loss of sequence "words" contributing Nim1ab has increased the apparent selective pressure among the RV-C to fix mutations elsewhere in the VP1, creating a possible compensatory epitope.

Introduction

The human rhinoviruses (RV) comprise 3 species, RV-A, RV-B and RV-C, in the *enterovirus* genus of the *Picornaviridae* (232). Collectively, these positive sense RNA viruses are the most frequent cause of the common cold. Between 50-85% of asthma exacerbations are due to RV infections (78, 93, 114) and RV-induced wheezing illness in infants corresponds with a high risk of developing childhood asthma (139). Many infectious properties of the RV link directly to their virion structures. Like all picornaviruses, the capsids are icosahedral (pseudo T=3), composed of 60 copies each of four structural proteins, VP1, VP2, VP3 and VP4. The three largest proteins, VP1-3, assume similar 8-stranded, anti-parallel b-barrel motifs, despite being formed from very

different sequences (Fig A1-1). Protomer units of VP1-4 are derived from a common polyprotein precursor. Assembly is nucleated around the RNA during infection into particles with 5-fold, 3-fold and 2-fold axes of symmetry. The shapes and surface extensions inherent to individual VP1-3 confer strain-specific properties of immunogenicity, receptor binding and drug susceptibility to each RV isolate. The short VP4 proteins, cleaved from intermediate precursor VP0, become myristoylated (N-terminus) as an assembly prerequisite, and ultimately localize with protomer symmetry, inside the capsid, adjacent to the packaged RNA.

The 99 original serotypes of RV-A+B were defined by immunogenic cross-reactivity (147). But now more routinely, related isolates from all 3 species are binned as "genotypes" if their VP1 nucleotide relationships exceed 87% identity (205, 291). The RV-A (79 types) and RV-B (30 types) are well studied at the structural and clinical levels. All these utilize either ICAM-1 (98 "major" types) or LDLR (11 "minor" types) as their cellular receptors. The molecular nuances of these interactions have been described by co-crystallization and EM studies. The RV-A+B that make up the major and minor groups conserve surface footprints that explain how and why particular isolates use their respective receptors to interact with cells (39).

In 2006 the discovery a new RV species surprised the molecular and clinical communities. The RV-C are clearly rhinoviruses, but unlike RV-A+B, they are not readily propagated in typical cell culture systems, including WI-38, WisL, BEAS-2B, A549 and HeLa lines (39). The 51 recognized RV-C types (as binned by sequence analysis) were identified by PCR while fishing through patient samples for other RV. The new isolates have special clinical relevance since it is now recognized the RV-C are associated with
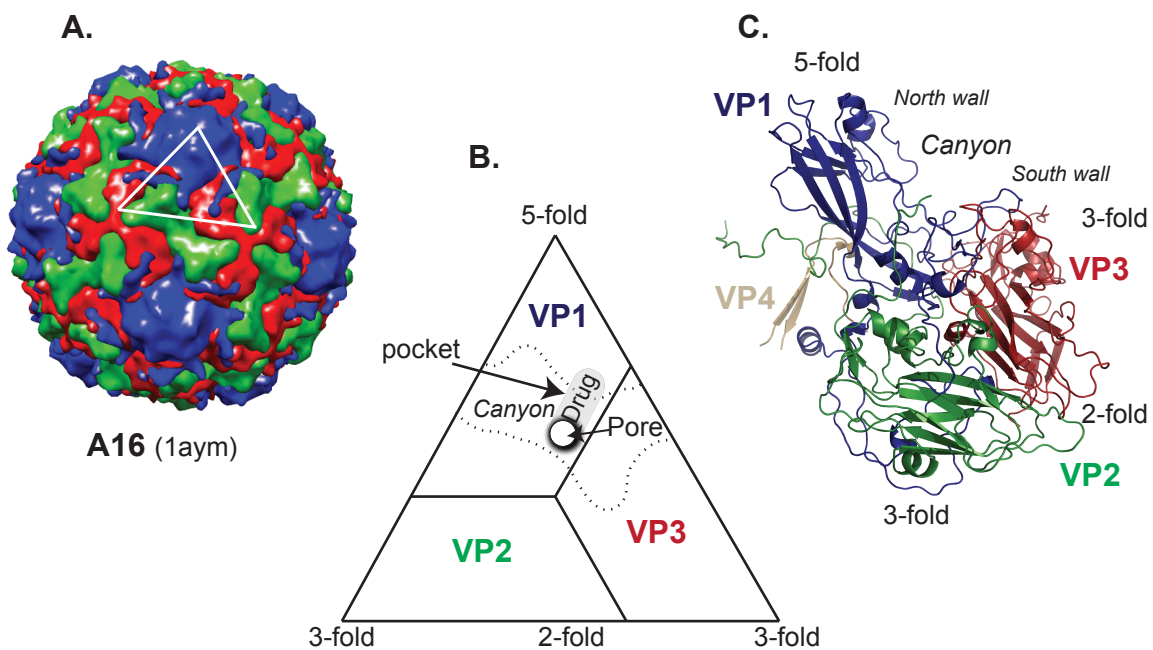
Figure A1-1. RV capsid arrangement. (A) Particles have 60 crystallographic subunits with VP1 (blue), VP2 (green) and VP3 (red) and VP4 (internal) proteins arranged in icosahedral symmetry. (B) A canyon-like depression circles each 5-fold axis from which a hydrophobic drug-binding pocket extends into the interior of each VP1. (C) Subunit ribbon diagram of A16 shows protein contributions to the north and south walls of the canyon. A biological assembly protomer would include this VP1, a VP2+4 precursor (VP0), and the VP3 from the adjacent (clockwise) crystallographic subunit. Figure modeled after Hadfield et al 1995 (104).

up to half of infections in young children (39, 178). They grow readily in both the lower and upper airways, tolerate higher growth temperatures (13), and use cell receptors not common to the RV-A+B (39). Complicated procedures have amplified some RV-C in mucosal organ cultures, but this technique is difficult and requires primary human donor samples (39). Parallel work with air-liquid interface (ALI) cultures is promising (13, 108), but neither technique has yet to produce enough virus for extensive biological or structural studies. Instead, RV-C information is projected by comparative sequencing. There are now full or nearly full genome datasets from ~68 isolates, with deeper information for the VP1 protein (~300 additional seqs). The genome of rhinovirus C15 (strain W10), an early isolate, was cloned into cDNA, and the resulting transcripts proved infectious to HeLa cells (39). Consequent inhibition assays with this (albeit low titer) virus showed that ICAM-1 and LDLR antibodies failed to prevent C15 from attaching to cells. This confirmed the RV-C use unique receptor(s) (39), although their basic biology is similar to other RV. Identification of this new receptor(s) is hampered by the lack of primary organ cultures and inconsistencies among donor samples. The same problems make antiviral tests difficult.

To gain more insight into the RV-C, we turned to computational structure prediction methods. Homology, protein threading and *ab initio* modeling are three kinds of these applications. Homology modeling uses sequence identity from robust alignments to search determined structures for likely homologs. Threading does not require outside sequences, but best-fits a protein to a database of known structure templates. *Ab initio* relies neither on homologs or existing structures and instead computes the lowest energy conformation(s) inherent to given protein. Multiple isolate

determinations of full-length RNA genomes, representing 141 RV types, have been

sequenced and aligned (232). There are atomic resolution structures for A1, A2, B3,

B14 and A16 protomers, along with numerous derivatives embodying capsid mutations

and drug-bound complexes. The extensive data cohort was ideal for homology

(MODELLER, ROBETTA) and threading methods (I-TASSER) when applied to

predictions of the C15 capsid. As reported here, the strength of these techniques,

backed by deep, refined alignments of all known rhinovirus isolates, allowed

construction of a highly predictive model that can guide antiviral drug targeting as well

as receptor discovery until an actual RV-C structure is resolved experimentally. The

data converge on the finding that all RV-C have major, conserved deletions in the VP1

protein, shaving significant mass from the 5-fold virion plateau, altering the canyon and

immunogenic profiles, and presenting novel receptor interfaces and chimeric

hydrophobic pockets for drug binding.

Results and Discussion

C15 Model Development. I-TASSER implements multiple threading algorithms and

iterative structure assembly simulations to find optimal sub-fragments within a database

of structures or within a user-specified structure (275, 338). Full-length models are

assembled by excising fragments using replica-exchange Monte Carlo simulations. The

functions and ligands are inferred with a final structure-structure alignment program.

Outputs consistently score well in CASP competitions (26, 64, 339, 340).

C15 was chosen to represent this species because an isolate (W10) was cloned

into infectious cDNA and was available as virus to test predictions (39). The C15 VP1-4

share 77% amino acid identity and equivalent indels among all known RV-C (consensus sequence). The respective proteins of 278, 265, 235, and 67 amino acids were assessed independently against the full I-TASSER database, including the known set of all determined picornavirus structures. The program picked A16 as the statistically best model for all VP1-3 sub-fragments (not shown). To refine this assessment, A16 and B14 files, with and without bound pleconaril as part of the structures, were resubmitted as specified templates. Each output (VP1-3) was evaluated according to I-TASSER metrics (275, 338). Again, native A16 (1aym) had the highest scoring confidence levels (C-score), and TM-scores, with RMSD relative to C15, in the 2-3 Å range (Table A1-1). Given that C15 and A16 share only 44-59% amino acid identity throughout their capsids (discounting indels) these are exceptionally good structure fits. All PDB depositions for the RV, especially for A16 and B14, register large portions of the VP4 sequence as disordered. I-TASSER was able to extrapolate a complete C15 VP4 only by using other enterovirus templates. Therefore, this portion of the model is clearly of lower quality (Table A1-1).

To evaluate whether similar results would be obtained by other prediction methods, the VP1-4 of C15 was submitted to MODELLER (278). This homology modeling program begins with a pairwise input alignment and calculates *an initio* model containing all likely non-hydrogen atoms that satisfy a spatial restraints methodology. Then, estimates of loops are calculated *de novo*, or relative to the input template if there is reasonable similarity. Regardless of the selected template (A16 and B14, with or without pleconaril) the resultant C15 models looked similar to each other and each scored well according to internal benchmarks (not shown). The VP1 C15 sequence was

Table A1-1

C15 I-TASSER Confidence Scores

	% identity[1]	% aligned[2]	RMSD[3]	E-value[3]	Z-score[3]	-ln(E)[3]
VP1	44	95.34	1.4	2.65E-14	35.53	31.26
VP2	59	94.34	1.84	7.28E-14	31.86	30.25
VP3	45	99.57	0.79	1.92E-13	30.82	29.28
VP4	62	43.94	3.09	6.15E-02	2.49	2.79

[1]Percent pairwise amino acid identity between A16 and C15.

[2] MAMMOTH (229) evaluated C15 output PDB files from I-TASSER and MODELLER as in Methods. "aligned" is the % of residues with common C-a backbone coordinates ($\leq$ 4 Å) in both models.

[3] Comparative output values for each protein are indicated. "RMSD" is root-mean-square deviation (in angstroms).

also submitted to ROBETTA (155), another online suite that combines "template-based" homology modeling with *ab initio* methods. Again, from among all possible homologs, the program selected A16 (1aym) as the preferred template. The I-TASSER, MODELLER and ROBETTA results were aligned to each other using MAMMOTH (229) or the MAMMOTH-multi suit (190). Among all outputs, there was 94-96% agreement for the C15 VP1 (Table A1-2) indicating strong similarity regardless of algorithm. However, since I-TASSER predicted the entire capsid length, albeit with tentative veracity for VP4, subsequent analyses were based on those predictions. That is, an I-TASSER model of C15 relative to A16 for VP1-3, and relative to the whole I-TASSER database for VP4.

The preferred model was then evaluated by ProQ, a structure quality predictor (316). It scored in the "extremely good" range (5.287) for the LGscore, and in the "fairly good" range for the MaxSub (0.361). As benchmarks for these values, parallel submission of the A16 parent (1aym) as resolved to 2.15 Å resolution, also scored "extremely good" for LGscore (5.998) and "fairly good" (0.44) for MaxSub. The projected C15 stereochemistry was checked for feasibility with PROCHECK, part of the PDBSum program suite (173). Calculations for the main-chains of the model showed key parameters (bad non-bonded interactions, C-α tetrahedral distortion, hydrogen bond energy and overall G-factor) to be within the normal range for a typical 2 Å resolution structure. Ramachandran plot quality assessment reflects a structure with between 2.5-3.0 Å resolution and the peptide bond planarity was above the normal range (~3-8 degrees standard deviation) at around 11 degrees. The side chain properties were all "normal" (or "better") relative to a typical 2 Å resolution structure. The tested parameters included standard deviation of the chi-1 gauche minus torsion angles, standard

Table A1-2

I-TASSER, MODELLER and ROBETTA Comparison

MAMMOTH[1]	VP	% aligned[1]	RMSD[2]	E-value[2]	Z-score[2]	-ln(E)[2]
ITAS vs MOD	1	95.34	1.4	2.65E-14	35.53	31.26
ITAS vs MOD	2	94.34	1.84	7.28E-14	31.86	30.25
ITAS vs MOD	3	99.57	0.79	1.92E-13	30.82	29.28
ITAS vs MOD	4	43.94	3.09	6.15E-02	2.49	2.79
MAMMOTH-mult[3]	**VP**	**% aligned[1]**	**RMSD[2]**	**E-value[2]**	**Z-score[2]**	**-ln(P)[2]**
A16 vs ITAS	1	92.09	1.91	0.6E-13	32.15	30.52
A16 vs MOD	1	92.09	1.90	0.6E-13	32.15	30.52
A16 vs Rob	1	91.01	3.10	0.8E-13	31.73	30.13
ITAS vs MOD	1	95.68	1.40	0.2E-13	33.53	33.53
ITAS vs Rob	1	93.53	2.84	0.3E-13	32.70	31.04
MOD vs Rob	1	94.96	2.69	0.2E-13	33.25	33.25

[1] MAMMOTH (229) evaluated C15 output PDB files from I-TASSER (ITAS) and MODELLER (MOD) as in Methods. "aligned" is the % of residues with common C-a backbone coordinates ($\leq$ 4 Å) in paired structures.

[2] Comparative output values for each protein are indicated. "RMSD" is root-mean-square deviation (Å).

[3] MAMMOTH-mult (190) evaluated VP1 PDB files from A16 (1aym) and C15 VP1 models generated by ITAS, MOD and Robetta (Rob).

deviation of the chi-1 trans torsion angles, standard deviation of the chi-1 gauche plus

torsion angles, pooled standard deviation of all chi-1 torsion angles and standard

deviation of the chi-2 trans torsion angles. Therefore, the selected model is strong and

feasible. Apart from VP4, which remains unresolved in most datasets, it is highly

consistent with measurable parameters of experimentally determined RV. Proteins for

A16   and C15 (model) are shown in Fig A1-2. The orientation and shapes of the b-

barrels are almost indistinguishable.

Topography of the C15 Model. Genome alignments are available for many

enteroviruses, and are especially deep for isolates in the RV species (232). The

alignments were founded on superimposition of known structures, particularly for the

capsid regions and therefore, analogy (same function) and homology (same lineage)

are clearly predicted. Indeed, within every viral protein, including VP1-4, there are

benchmark residues that unambiguously delineate every internal b or a element. Among

the RV, large relative indels are rare. Outside of VP1 and a few discontinuities that are

potential sequencing errors (*e.g.* C19 EU840728), the only serious length variance is at

the N-terminus of the 3A protein, where the RV-B are longer than the RV-A (2-3 aa) and

the RV-C (9 aa).

Given this conservation, the VP1 indels are striking. The b-barrel cores

superimpose, but the collective bB-bC, bD-bE and bH-bI loops of all RV-C are shorter

by ~22 aa relative to the RV-A, and ~28 aa relative to the RV-B. For C15 specifically,

the bB-bC loop is 10 aa shorter than A16 and 13 aa shorter than B14 (Fig A1-3). The

corresponding bD-bE loops are 8 and 10 amino acids shorter. The bH-bI loops are 4 aa

shorter. As these elements supply virtually all of the mass to the 5-fold virion plateau,
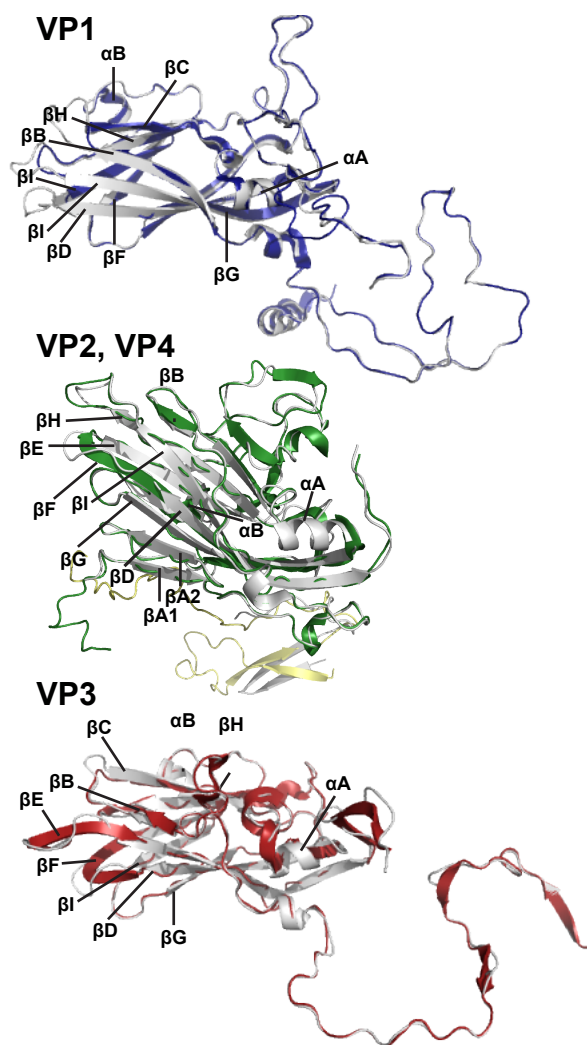
Figure A1-2. Structure comparison. Ribbon diagrams for A16 (gray) and C15 (blue, green, yellow, red; models) are labeled with features, using the nomenclature of Rossmann et al 1985 (272). The structures were formatted, oriented and rendered in MacPyMOL (1).
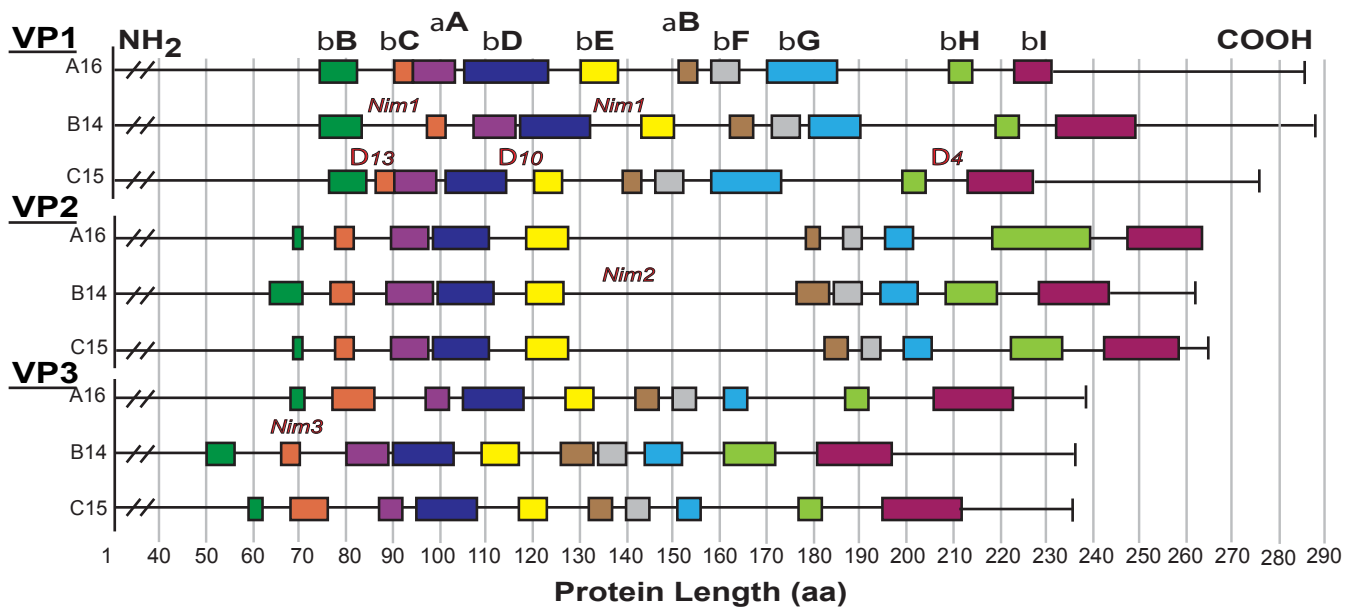
Figure A1-3. Core structure elements. The VP1-3 sequences for A16, B14 and C15 are illustrated to scale showing the color-coded locations of α and β segments using the nomenclature of Rossmann et al 1985 (272). The A16 and B14 elements are according to determined structures. The C15 elements are inferred by analogy in sequence alignments. B14 loops encoding neutralization escape mutations (Nim) are highlighted as are key, relative C15 deletions in VP1 (e.g. D13).

the C15 model predicts the capsid surface must change radically. Full reconstructions (Fig A1-4A, Fig A1-6E) and "roadmap" topographic projections (Fig A1-4B) highlight the impact. Relative to A16, B14 and every other resolved enterovirus structure (61 in the PDB) the 5-fold plateau of C15 is effectively gone. In its place, the missing mass is so severe as to cause a depression rather than a projection at the 5-fold. Depth-cued cross-sections measure the loss at up to 20 Å in plateau height (Fig A1-4C). Because of poorly resolved VP4 in existing structures it cannot be anticipated whether this "shaving" creates an overall thinner protein shell at the 5 fold, but most certainly it creates a different physical surface over at least 1/3 of the particle, including all territory "north" of the canyon.

The "south wall" of the C15 canyon, in contrast, and including the 2-fold and 3-fold regions, is more similar to A16 and B14. Side-by-side (Fig A1-2), it is hard to identify VP2-3 differences that overtly affect the mass or orientation of a b, a or loop element. Among all RV (N= 349), the longest VP2-3 indels are just 1-2 aa, and these tend to be type-, rather than species-specific (Fig A1-3). The canyon itself is maintained, as evidenced by the depression (blue) in the center of each roadmap icosahedral unit (crystallographic subunit). Additional shallow residues extend north-west and north-east of the central depression, ringing around the 5-fold and completing the canyon (Fig A1-4B). All 3 viruses have secondary depressions in the 2-fold region. This interface is formed by VP1 and VP3 interactions with contributions from the N-terminus of VP2 (259). As there are no indels covering any interface residues, and strong conservation at the sequence level, the C15 model preserves all relevant contacts at both the 2-fold and 3-fold. It should be noted though, that the structure files for A16 and B14 are
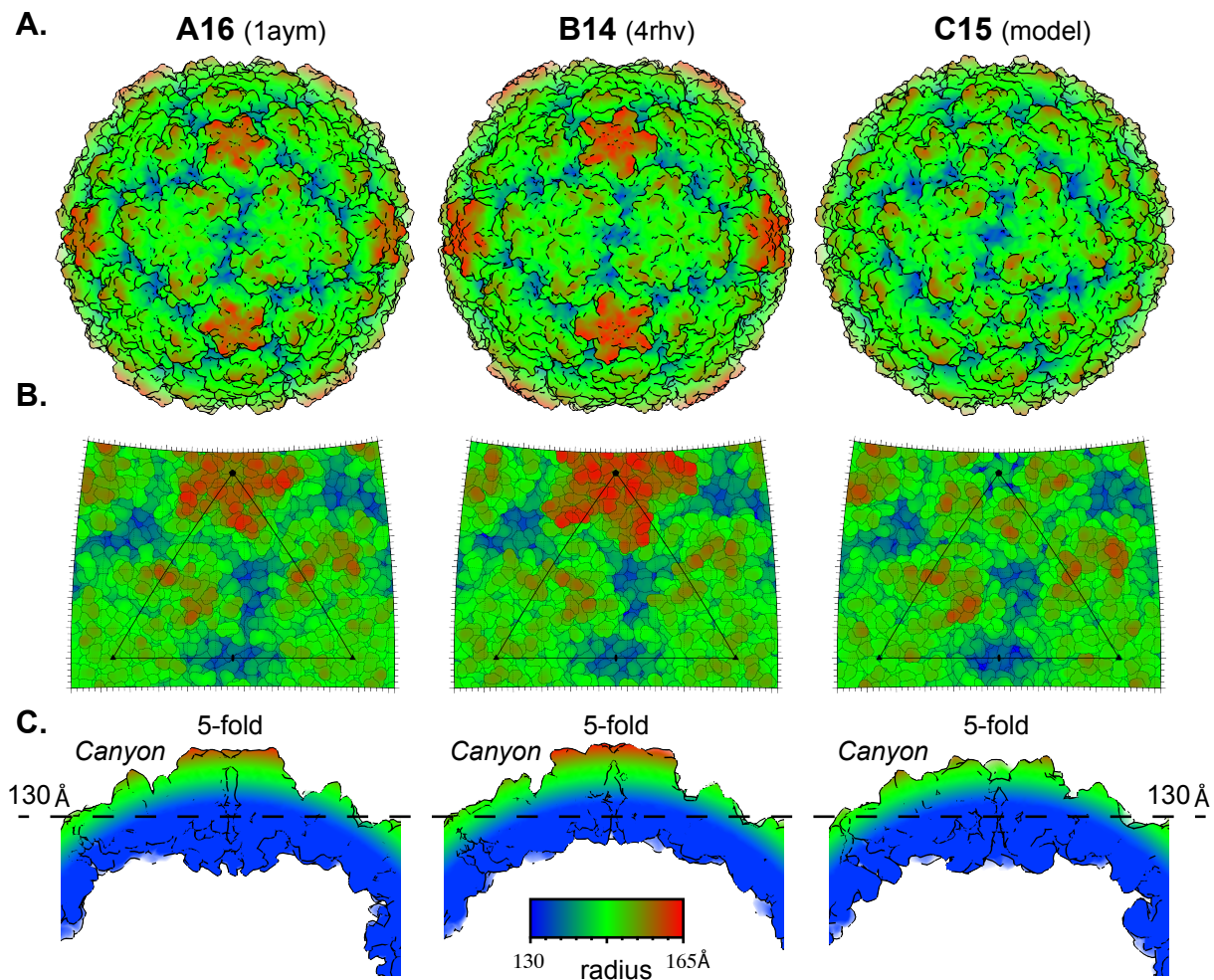
Figure A1-4. Surface topography. (A) Protomer PDB files for A14, B14 and C15 (model) were extrapolated to full icosahedral capsids using UCSF Chimera (245). The color scale illustrates the particle radius, spanning 130 Å (blue) to 165 Å (orange). (B) In parallel, radially depth-cued "road-maps" show the surface topographies for respective crystallographic subunits as calculated by RIVEM (328). The applied color scale is the same as A. (C). Cross sections of the particles in A, through equivalent 5-fold axes, compare the protein depths of the canyon region and 5-fold plateau. The structures were aligned, displayed and rendered using UCSF Chimera (245).

missing the N-terminus of VP2 (8-9 aa) and up to half of VP4 (29-40 aa). If the respective surfaces were to be influenced by inclusion of these full proteins, it isn't apparent from roadmaps.

C15 Surface Residues. Virion surfaces are under evolutionary pressure for immunological diversity and receptor binding. The charge distributions for A16 or B14 are typical of their species (Fig A1-5A,C). Uncharged or mildly polar (yellow: Asn, Gln, Ser and Thr) residues cluster around the 3-fold region, while the 2–fold conserves acid (red: Asp, Glu) and basic (blue: Arg, Lys, His) patches. The north wall of the canyon, edging the plateau, is strongly charged, contributing contacts for ICAM-1 and LDLR. Receptor footprint conservation within the RV-A+B is well described (122, 160), as is the lack of conservation of these same residues in an alignment of RV-C (39). The C15 model not only emphasizes the truncation of the required receptor binding sites (i.e. VP1 bB-bC loop), it shows that the residual VP1 sequence(s) display a very different charge pattern in addition to new topography (Fig A1-5E). The depression at the 5-fold for all RV-C is anchored with a basic His or Lys (VP1-161) then rimmed with uncharged amino acids in a pattern dissimilar to RV-A+B. Many of these newly exposed VP1 residues are conserved in every RV-C (Fig A1-5F, black), or present in >90% of the known sequences (dark gray). The model and the alignments converge on the idea of a unique receptor footprint, similar among all RV-C, and likely to map around the unusual shaved VP1 configuration at the 5-fold.

RV-C Immunogenicity. Neutralizing immunogenic sites (Nims) for B14 were originally identified in an historic study correlating the structure of the particle with monoclonal antibody escape mutations (289). Continuous and discontinuous epitopes take their
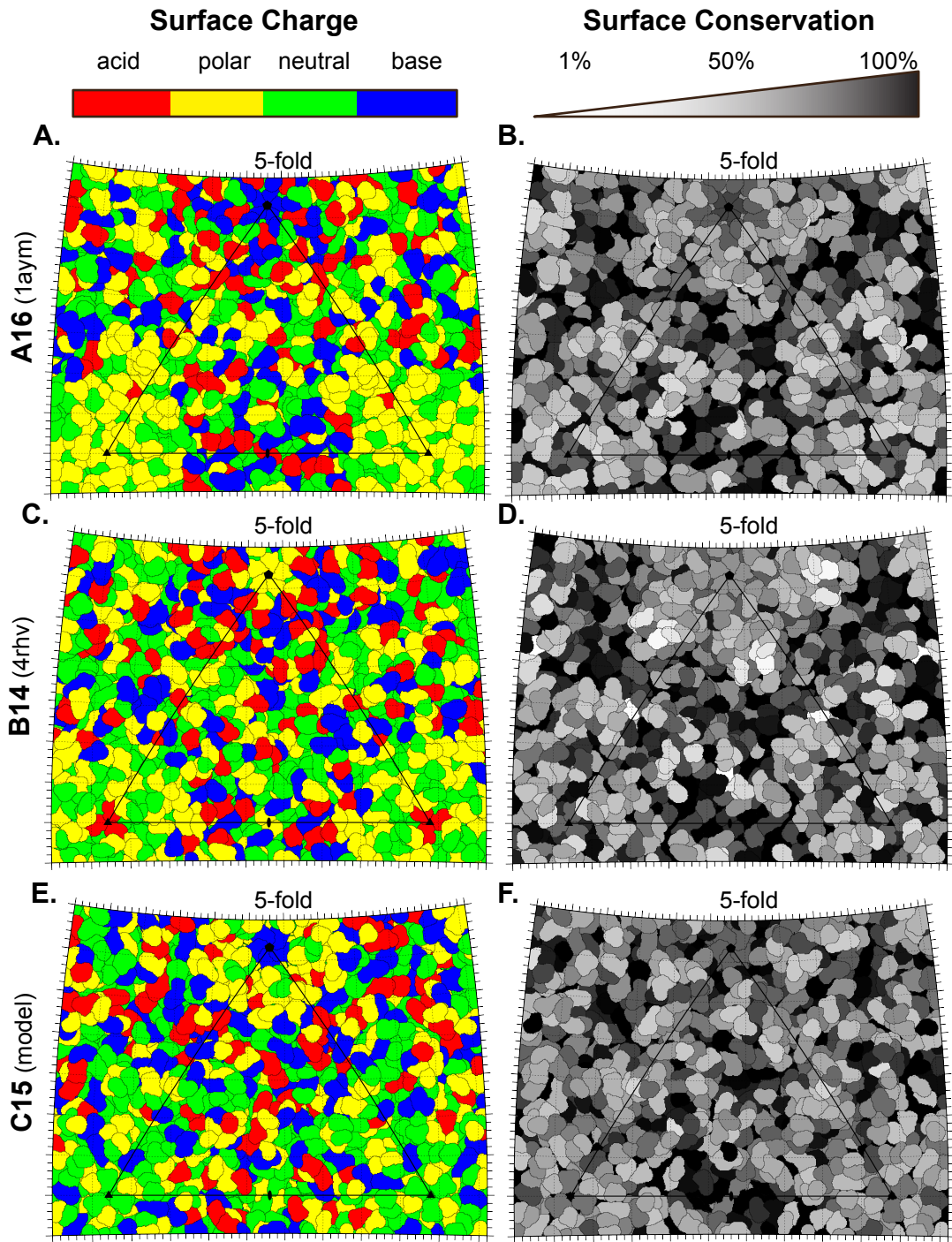
Figure A1-5. Surface character. (A,C,E) Roadmap (328) surface depictions for A16, B14 and C15 are color-coded by amino acid types. The color bins includ, acidic (Asp, Glu), polar (Asn, Gln, Ser and Thr), neutral (Ala, Cys, Ile, Gly, Leu, Met, Phe, Pro, Trp, Tyr and Val) and basic (Arg, His and Lys) residues. (B,D,F) Similar roadmaps depict species surface residue conservation. Capsid alignment positions were queried for conservation (% amino acid identity) relative to each species' consensus sequence. The observed identity, encoded in continuous grayscale (black = 100% conserved, white = 0% conserved), is superimposed on the A16, B14 and C15 residue positions.

names from the VP contributing the dominant surface loop (Fig A1-6A,B). Nim1a and Nim1b include fragments of the VP1 bB-bC and bH-bI loops. Nim2 pairs the bE-aB "puff" loops of VP2 with the bG-bH "FMDV" segment of VP1. Nim3 is formed by an insertion in the bB of VP3, with contributions from the bB-bC loop and the nearby VP1 COOH tail (272). Not surprisingly, in all resolved RV structures these regions display as raised features (Fig A1-6CD), allowing antibody contact without compromising the underlying core, the canyon, or receptor binding motifs. In C15, the physical loops for putative Nim2 and Nim3 analogs are similar to A16 and B14 (*e.g*. Fig A1-3). But the VP1 loops that would present Nim1a and Nim1b are removed by the species-wide deletions (Fig A1-6C).

Experimentally, the immunogenicity for any RV-C is unknown and the typing of current isolates is based solely on full-length VP1 pairwise identities. However, as the alignments contain multiple representatives of each RV-A+B; it is possible to record how loop sequences vary for known serotypes, and by inference, to extrapolate potential epitopes for the RV-C. Statistical screening depends on the concept that immunogenic sites fix mutations more readily than the genome as a whole. But given that 141 RV types are already defined, the formative selective pressures cannot be subtle. The alignment segments encoding VP1-3 surface elements were queried for the number of unique sequence "words" observed among the isolates (Table A1-3). For the RV-A+B in the mapped Nim sites, the sequence variability (observed words) was frequently greater than the number of types within the species. For example, the Nim2(b) loop residues 2155-2167 in VP2 record116 sequence variants among 79 types of RV-A. In the RV-B, there are 37 variants within 30 types. Many of these added sequences, however, co-

A.

5-fold

3-fold   2-fold   3-fold

B.

VP1   VP2   VP3

NImIb

NImIa

NImII

NImIII

B14 (4rhv)

C. A16 (1aym) **D. B14** (4rhv) **E. C15** (model)

transparent spheres at 155 Å radii
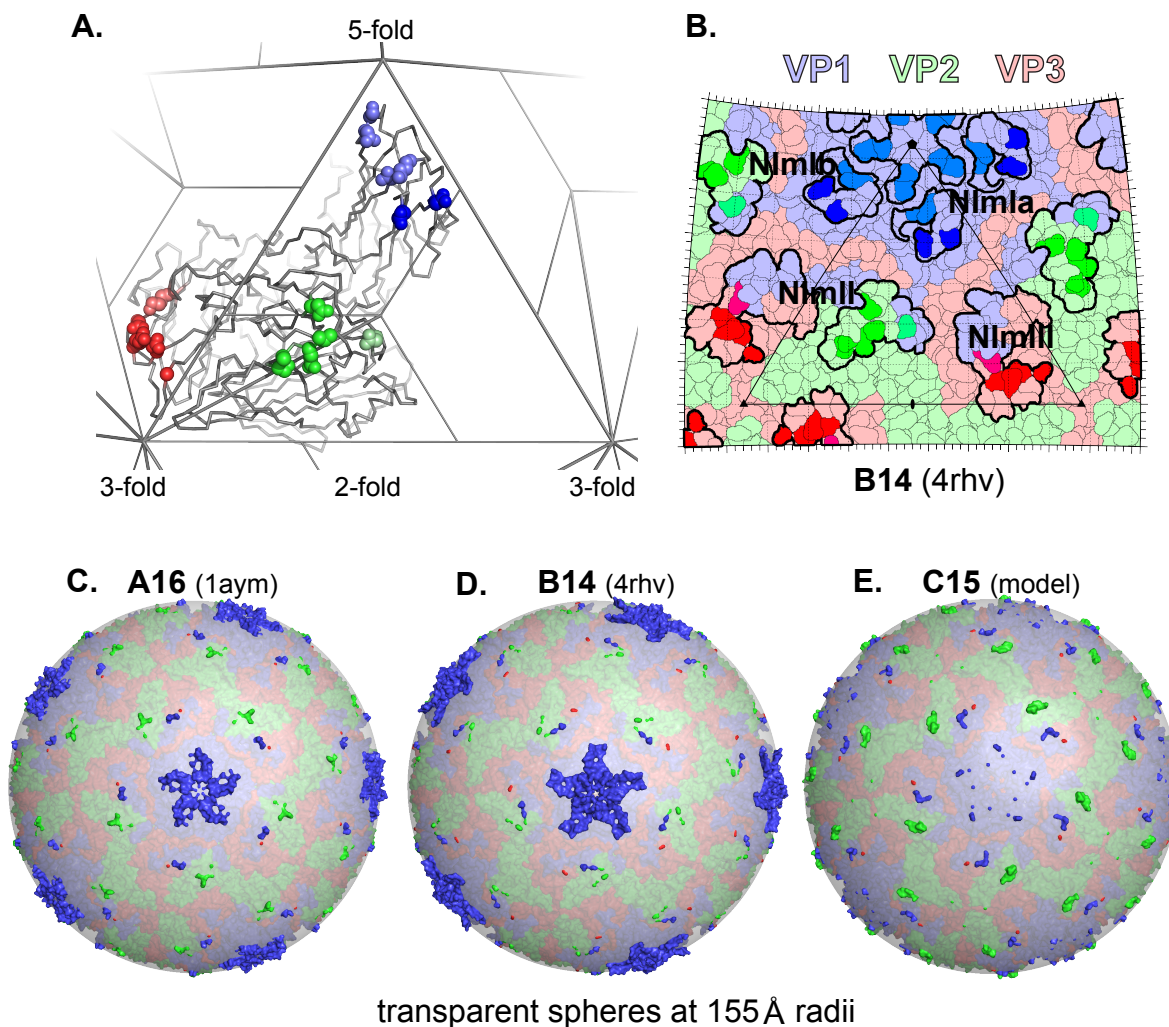
Figure A1-6. Immunogenic sites. (A) A B14 (4rhv) biological protomer highlights residues mapped with escape mutations to a panel of neutralizing monoclonal antibodies, as defined by Sherry et al 1986 (289). (B) The neutralizing immunogenic sites (Nims) cluster on the virion surface (intense colored residues) as part of continuous surface loops (strong outlines). The Nim2 and Nim3 epitopes are partially discontinuous with contributions from VP1 (blue) and non-adjacent segments of VP2 (green) and VP3 (red). These loops define the sequence fragments queried for Nim conservation in Table 3. (C,D,E) A16, B14 and C15 particles were rendered as in Fig 4 except that color was assigned by protein type (as in B) and a semi-transparent sphere was added, masking the topography below a cutoff of 155 Å. The remaining brightly colored features mark residues above this height, and for B14, include all mapped Nim escape mutation sites.

Table A1-3

Surface Sequence Variation versus Isolate Type

Segment	B14 residues	Observed sequence "Words" [1]			"Words" Predict RV Type [2]		
		RV-A[3]	RV-B[4]	RV-C[5]	RV-A[3]	RV-B[4]	RV-C[5]
VP2 Nim2(a)	2135-2143	115	21	32	85 %	80 %	94 %
VP2 Nim2(b)	2155-2167	116	38	38	96 %	93 %	97 %
VP3 Nim3(a)	3055-3064	106	36	36	92 %	96 %	97 %
VP3 Nim3(b)	3071-3079	103	31	35	98 %	95 %	95 %
VP3 COOH	3227-3236	68	15	36	95 %	82 %	94 %
VP1 Nim1ab	1083-1095	115	43	0	90 %	83 %	(deletion)
VP1 Nim1a	1135-1144	76	33	6[6]	85 %	95 %	61 %[6]
VP1 bG	1186-1198	12	10	7	66 %	68 %	62 %
VP1 bG-bH	1205-1212	77	22	36	90 %	77 %	98 %
VP1 COOH	1279-1289	113	39	38	86 %	93 %	95 %
3D-pol	318-331	10	12	21	64 %	72 %	76 %

[1] Unique sequences (words) in same alignment segment

[2] Words conserved within, but not between types (percent)

[3] 208 isolates, 79 types

[4] 74 isolates, 30 types

[5] 67 isolates, 32 types

[6] 7 of 10 residues deleted

vary within a single type, so that overall, about 93-96% of the measured words are unique to a given type, and predictive of it. The Nim-type predictions showed consistent values of 85-98% among the measured RV-A+B surface loop segments regardless of which Nim was queried. As expected, regions that are not under immune selection, fix mutations at lower frequencies. Fewer words (10-12) and lower type-correlations (64-77%) were observed in words from a core b segment (e.g. VP1 bG) or from a non-capsid region of the 3D pol. Here, multiple types frequently share the same sequence words. For perspective, 61% of all RV-A alignment positions and 66% of all RV-B alignment positions share >90% aa identity within their species, regardless of whether the residues are averaged from the P1 (capsid) or P23 (non-structural) regions.

The RV-C are less well conserved. Only 48% and 51% of the alignment positions share >90% identity among the P1 and P23 proteins as a whole, respectively. But in the putative Nim2 and Nim3 sites, including the VP1 and VP2 COOH ends (also on the C15 surface), the correlation with type was 94-97%. These high values suggest the compared words are legacies of strong evolutionary lineages, presumably immunologic, among all RV-C isolates. If true, it means the raised VP2 and VP3 surface topographies (Fig A1-4, Fig A1-6E) are likely to be authentic Nims for the RV-C. Moreover, recombination in the P1 region must be an infrequent means of epitope swapping because the diverse RV-C surface segments seem to hold true to type, as assigned through the VP1 as a whole. Surprisingly though, the type-specific word conservation also held true for the RV-C VP1 bG-bH loop, a surface segment contributing to the south wall of the canyon (Fig A1-2). In aphthoviruses and cardioviruses, which do not have canyon features, this "FMDV loop" is a dominant, continuous, immunogen (40,

306). In the RV-A+B, it is much less so. Relative to the other Nims, there are fewer words observed here among the RV-A+B isolates and lower covariance with type (Table A1-3). Only a single bG-bH residue (B14 1210) has been identified with antibody escape mutations (289). For these species, immunogenic access to this segment is limited by the steep north wall of the canyon (273). The RV-C however, vary this region equivalently to other surface loops, and for 98% of the isolates, the specific sequence is predictive of type. In contrast to the RV-A+B structures, the C15 model anticipates the shaved 5-fold region should expose more of this surface (Fig A1-6E), thereby strengthening selective pressure to fix mutations as a variable immunogen. The enhanced RV-C epitope potential is recorded in the bG-bH words and may reflect a degree of compensation for the structural loss of Nim1a and Nim1b. If this is a continuous, exposed surface epitope, as predicted by the model, antibodies to the segment should neutralize RV-C, perhaps more potently than for the equivalent RV-A+B segments.

Insights into RV disease. Isolates in RV-C species are clearly linked to more childhood illnesses involving lower airways than the other RV (32, 178). As a rule, the RV-B tend to limit their replication to sinus tissues and the upper airways, and the majority of RV-A+B are sensitive to culture temperatures above 33-35°C (299). The RV-C readily infect upper and lower airways and are stable to growth at 37°C (13), a property that is capsid-dependent. The lower airway infections by these viruses can be severe, accounting for the majority of asthma attacks resulting in children's hospitalization (32). The profound structure changes in the 5-fold region, predicted by the C15 model necessitate a receptor preference that is not shared by the RV-A+B and

preferred growth locale could be part of this. But these same changes could easily make the capsid more stable and less flexible, allowing replication at higher temperatures.

Materials and Methods

Sequences and Alignments. Refined alignments (349 seqs) of complete genome RV RNA sequences are based on foundation superimposition of determined structures as described (232). Clustal and profile fits added to this base all recent genome length (i.e. >6000 base) RV isolates available from GenBank. Placement required every indel to maximize identity within RV types and species. A translated polyprotein alignment with species, type and accession numbers is available in *.meg and *.fasta formats from *http://virology.wisc.edu/acp/aligns/*. The set includes RV-A (79 types, 208 seqs), RV-B (30 types, 74 seqs), RV-C (32 types, 67 seqs), and EV outgroups (4 species, 10 seqs). A subset alignment with just VP1 proteins was extracted then augmented with an additional ~500 RV-A+B+C datasets, ensuring representation for the 51 known types of RV-C, and adding depth to the RV-A+B within this gene. Current RV nomenclature (205) designates the species letter (A, B or C), and type number (e.g. A16). Strain designations are unique to each accession number.

I-TASSER. The I-TASSER threading method and online web site (*http://http://zhanglab.ccmb.med.umich.edu/I-TASSER/*) have been published (275, 338). The VP1-4 protein sequences of C15 strain W10 (GQ323774) were extracted into separate files. The VP1 was threaded in runs against: the entire I-TASSER template database (a subset of Protein Databank); A16 (PDB ID:1aym); A16 with pleconaril

(1ncr); B14 (4rhv); and B14 with pleconaril (1ncq). The VP2 and VP3 sequences were threaded against A16. The VP4 was threaded against the full template database. C-score, TM-score and RMSD were recorded for each model (Table A1-1). A biological protomer was constructed by superimposing the selected C15 models on their A16 (1aym) homologs using the alignment function of MacPyMOL (1). The orientations were exported then concatenated manually into a single PDB file. Helix and sheet lengths (Fig A1-3) were predicted relative to known elements in the refined alignments.

MODELLER. Independent C15 protomer models (VP1-4) were calculated (locally on a MacBookPro) using MODELLER version 9v8 (278), according to templates, 1aym (A16), 1ncr (A16 plus pleconaril) and 1ncq (B14 plus pleconaril). For each run, the complete protomer sequence was aligned against C15 with the "align2d" and heteroatoms (*e.g.* pleconaril) were accounted for. Each output included five different iterations, which were then compared to the source template with the "discrete optimized protein energy" algorithm "DOPE" (288).

ROBETTA. The C15 VP1 sequence was submitted to the Robetta server (*http://robetta.bakerlab.org/*) for Ginzu domain prediction using default settings (155). A full 3D prediction was requested.

Model Evaluation. The PDB file for the preferred I-TASSER C15 protomer model was submitted relative to the MODELLER protomer to MAMMOTH (MAtching Molecular Models Obtained from THeory) (229), for plausibility analyses as implemented with the online web site (*http://predictioncenter.org*). Using standard parameters, the suite aligns input structures, calculates the optimal local similarity of the protein backbone, and then

fills in the residues. The outputs are scored based on this alignment (percent of residues aligned, RMSD, E-value, Z-score and –ln(E)). ProQ (316) was also run online (*http://www.sbc.su.se/~bjornw/ProQ/ProQ.cgi*). It is a neural-network-based program that predicts the quality of a model or determined structure by extracting features (i.e. atom-atom contacts), evaluating their plausibility, and assigning scoring functions LGscore and MaxSub. The C15 VP1 PDB files from I-TASSER, MODELLER and ROBETTA were also compared to each other and to native A16 (1aym) using MAMMOTH-multi (190), in similar procedures (*http://ub.cbm.uam.es/servers/mammoth/mammothmult.php*). The sterochemical quality of C15 (I-TASSER) was also gaged with PROCHECK, part of the PDBSum suite as available online (*http://www.ebi.ac.uk/pdbsum/*) (173). The coordinates were refined for steric clashes (between and within putative protomers) with CHIRON (257). Protomer and virion coordinates for the full, preferred C15 model are available from VIPERdb (*http://viperdb.scripps.edu/*) using the accession code: *hrvc.*

Molecular Graphics. Protomer illustrations were oriented and rendered in MacPyMOL (1). UCSF Chimera (245) created full capsid structures and pentameric assemblies from protomer PDB files. Virion surface "roadmaps" displaying 3D topographies used the Radial Interpretation of Viral Electron Density Maps (RIVEM) program. RIVEM illustrates residues occupying the surface of a virus by reading standard PDB coordinates and plotting them onto stereographic spheres (328). For comparative roadmaps, A16 (1aym), B14 (4rhv) and C15 (model), protomer files were aligned to "standard Rossmann" (272) orientation. The HOH ATOM lines were removed in MacPyMOL. The amino acids were renumbered into standard "picornavirus format"

identifying the protein chain and sequence position (e.g. residue 1 of VP1 becomes

1001, residue 1 of VP2 is 2001, etc.). RIVEM (run locally in LINUX CENTOS 5, 32 bit)

then created radial coordinate surface maps with matching color scales according to

virion radii (Fig A1-4B). User specified properties such as residue charge,

hydrophobicity, chain identity (*e.g.* Fig A1-5A,C,E) can be selected within the program.

Roadmaps showing sequence conservation used PDB files with % identity embedded in

the B-factor column, according to the residue-specific values calculated from the full,

refined alignments.

Appendix 2.

Modeling of the Human Rhinovirus C Capsid Suggests Possible Causes for Antiviral Drug Resistance

Holly A. Basta, Shamaila Ashraf, Jean-Yves Sgro, Yury A. Bochkov, James E. Gern, and Ann C. Palmenberg

Author contributions: SA performed antiviral drug testing in Fig A2-2 and supplemental Fig A2-1B. JYS rendered images in A2-3B,C,D. YAB performed antiviral drug testing in supplemental Fig A2-1A. ACP curated sequence dataset and performed comparative sequence alignment.

Justification: As the human rhinovirus (RV)-C15 model capsid structure was of high quality, we used it to model the drug susceptibility of the RV-C species. These predictions were used to drive targeted experiments in air-liquid interface cultures, which are precious and time consuming. The combined strength of the model structure and the sequence dataset, we define the hydrophobic (drug-binding) pocket of RV-Cs as a novel "type 3" pocket. Drug susceptibility experiments show that drugs designed for type 1 and/or 2 pockets are ineffective on RV-C15.

Abstract

Human rhinoviruses of the RV-C species are recently discovered pathogens with greater clinical significance than isolates in the RV-A+B species. The RV-C cannot be propagated in typical culture systems; so much of the virology is necessarily derivative, relying on comparative genomics, relative to the better studied RV-A+B. We developed a bioinformatics-based structural model for a C15 isolate. The model showed the VP1-3 capsid proteins retain their fundamental cores relative to the RV-A+B, but conserved, internal RV-C residues affect the shape and charge of the VP1 hydrophobic pocket that confers antiviral drug susceptibility. When predictions of the model were tested in organ cultures or ALI systems with recombinant C15 virus, there was a resistance to capsid-binding drugs, including pleconaril, BTA-188, WIN56291, WIN52035 and WIN52084. Unique to all RV-C, the model predicts conserved amino acids within the pocket and capsid surface pore leading to the pocket may correlate with this activity.

Introduction

The human rhinoviruses (RV) are positive sense RNA viruses in the *enterovirus* genus of the *Picornaviridae* family (232). They are the most frequent causative agents of the "common cold" and responsible for millions of lost personnel hours in the workplace each year. The best studied isolates belong to the RV-A and RV-B species, where they are binned together if they share greater than 75% nucleotide identity (88% amino acid identity) in the VP1 region of their polyproteins. Each species further divides its isolates into multiple numbered genotypes. Originally, ~100 types from clinical panels archived by the American Type Culture Collection were indexed after assessment of antigenic

crossreactivity or serotyping in rabbits. RV-A87 was subsequently reassigned to the

Enterovirus D (EV-D68) after reevaluation of genetic, immunogenic and receptor

properties (282). Common to the original RV-A (74 serotypes) and RV-B (25 serotypes)

is the use of ICAM-1 or LDLR for cell attachment and entry (314). They are labile at low

pH (<5), and grow predominantly in sinus and upper airway tissues (for reviews, see

(13, 38)).

Because of their medical and economic importance, considerable resources

have been expended developing therapeutics against the RV-A+B. The ubiquitous

nature of these viruses and the many serotypes, preclude the practical use of vaccines.

Directed drugs that target protein elements in the RV replication cycle (e.g. rupintrivir),

can be effective (31). But the preferred strategy is to target the virus before infection,

usually by exploiting unique "pocket" features characteristic of all enterovirus virions.

The RV capsids are icosahedral (pseudo T=3), composed of 60 copies each of four

structural proteins, VP1, VP2, VP3 and VP4. The three largest proteins, VP1-3, assume

similar 8-stranded, anti-parallel b-barrel motifs, despite being formed from very different

sequences (Fig A2-1). Protomer subunits containing mature copies of VP1-4

spontaneously self-assemble into pentamers with the VP1 proteins assuming symmetry

around the 5-fold axes. When the pentamers coalesce into particles, encapsidating the

genome RNA, the VP2-3 proteins alternate around the 3-fold and 2-fold axes (Fig A2-

1A). A deep groove within each protomer, formed where VP1-3 abut, creates a

contiguous "canyon" circling each pentamer (Fig A2-1B). The canyon topography is

characteristic of all enteroviruses, and marks the thinnest portion of the capsid shell.
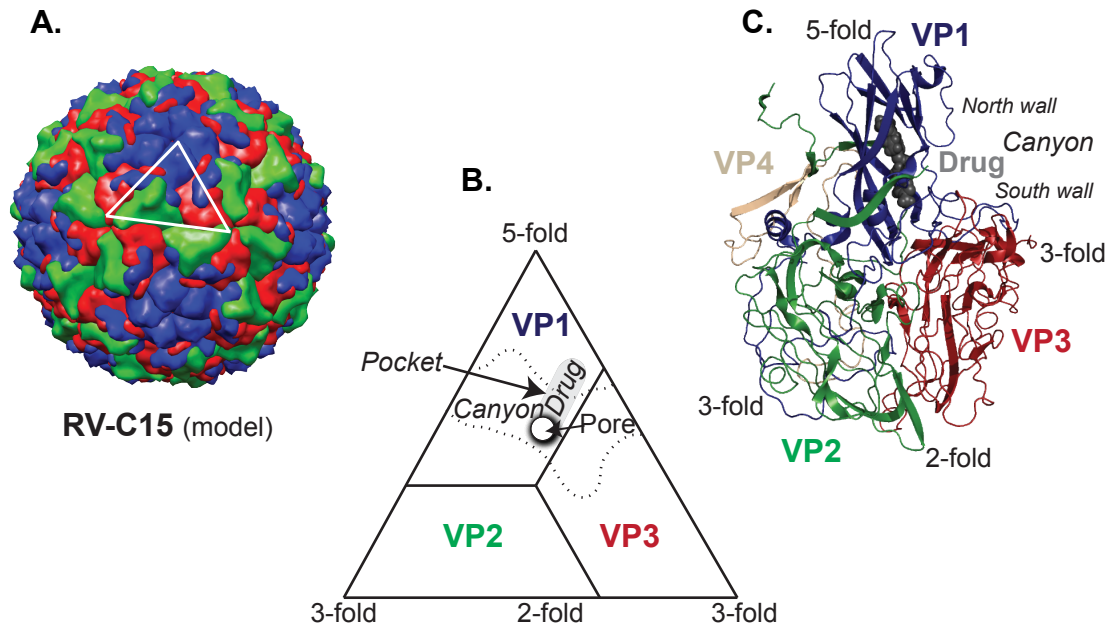
Figure A2-1: RV-C15 capsid model. (A) The C15 model with VP1 (blue), VP2 (green) and VP3 (red) proteins, around 5-fold, 2-fold and 3-fold axes of symmetry (25). The short VP4 protein (yellow) is internal. (B) A triangular crystallographic (PDB) subunit orients the VP1+VP2 from one biological subunit, with VP3 from the adjacent, counterclockwise unit. The hydrophobic drug binding pocket extends from a pore at the base of the canyon into the VP1 central core. (C) The VP1-3 proteins have similar 8-stranded b-barrels with extended connecting loops. The canyon is a depression in the surface topography, ringing the 5-fold. The north and south walls are landmark features. Pleconaril (gray spheres) is modeled into the VP1 pocket. Figure is after Hadfield et al 1995 (104).

The "north" (5-fold) and "south" (2-fold) walls of the canyon (Fig A2-1C) are lined with residues that confer receptor recognition and type-specific immunogenicity (10).

When the 99 historical RV-A+B types were tested for sensitivity against a panel of antiviral capsid-binding therapeutics they were found to subdivide, roughly along species lines, into two experimental groups (9). The structures of 28 virus-drug complexes have been determined to atomic resolution (Sup Table A2-1). The Group-1 viruses (predominantly RV-B) have long, narrow pockets interior to their VP1 proteins, which accommodate matching long chain hydrophobic drugs like WIN52084 (W84). The Group-2 viruses (most RV-A) have shorter, wider VP1 hydrophobic pockets, and therefore accept an alternate cohort of drugs, like R61837 (JEN). Each determined drug-virus structure shows a pore-like opening connecting each VP1 pocket to the deepest portions of the canyon, providing an entry port for the relevant drug (Fig A2-1B). Native RV-A+B in the absence of drugs, have "pocket factors", commonly modeled as sphingosine, in same interior VP1 locations. The intrinsic occupancy of these factors contributes to capsid stability (228). Displacement of the native factors with efficacious drugs prevents a required VP1 transition during the uncoating process, making such drugs inhibitory to infection. Compounds that exploit this mechanism and bind both Group pockets have shown clinical promise on a range of RV. For example, during Phase 3 evaluations, pleconaril (WIN63843) shortened the duration of the common cold and reduced the window of virus shedding. Despite this efficacy, the FDA disapproved pleconaril for over-the-counter use, citing concerns about interference with the metabolic pathways of other drugs (115). A newer analog, BTA-188, is reportedly more effective in reducing RV infections for many laboratory and clinical strains (23).

While a "cure" for the common cold might have seemed in the offing from this work, the discovery in 2006 of a completely new RV species, put optimism on hold. The RV-C are clearly rhinoviruses, but unlike RV-A+B, they are not readily propagated in typical cell culture systems (39). The currently recognized 51 types of RV-C were detected and characterized by direct sequencing from patient effluents. As with the RV-A+B, each RV-C type includes those isolates whose VP1 sequences exceed 87% pairwise identity at the nucleotide level (205, 291). The RV-C have special clinical relevance since it is now recognized these strains are associated with up to half of infections in young children (39). They grow readily in both the lower and upper airways and tolerate higher growth temperatures in culture (13). Moreover, the RV-C use cell receptors that are not common to the RV-A+B (39). Unfortunately, these receptors are apparently lost, whenever primary tissue snippets are transitioned to undifferentiated monolayers. RV-C can be grown in mucosal organ cultures, but this technique requires the availability of primary human donor samples (39). Parallel work with differentiated sinus or bronchial epithelial cells at air-liquid interface (ALI) is promising (13, 108), but neither technique has yet produced enough virus for extensive biological studies. Instead, RV-C information relies heavily on comparative sequence analysis to maximize data from limited experimental samples.

Current computational tools include a deep alignment of full-genome datasets for >350 RV-A+B+C isolates. It was nucleated by superimposition of determined capsid structures for multiple RV-A+B, then extended to the RV-C with Markov-based profile fits (232). Combined with the RV-A+B structures, the alignment helped to develop a high resolution 3D model for C15 (25), an isolate which has been cloned into cDNA, and

tested for biological activity in mucosal and ALI cultures (13, 39). The new model displays an altered surface topography for all RV-C, accounting for differential receptor use and diverse immunogenicity (25). It also shows the essential Ca backbone of the RV-C VP1 b-core that marks the capsid drug-binding pocket is superimposable on the RV-A+B, regardless of whether the model was tweaked by Group 1 (e.g. B14) or Group-2 (e.g. A16) structures. While this was reassuring in terms of model veracity, the outcome was puzzling in terms of biology, because in preliminary studies (below), recombinant C15 virus was known to behave somewhat differently from Group-1 or Group-2 RV.

The lack of primary organ cultures and inconsistencies among donor samples make tests against the RV-C difficult. We reported that WIN56291 (W91), a short chain (Group-2) compound, was efficacious against C15 when tested in sinus organ cultures (39), but it wasn't clear whether those results would be common to the more reliable ALI systems (13). Another study reported that the usually-more-potent pleconaril was only weakly effective against C15 when tested in ALI cultures (108), although it readily inhibited A16 controls. Therefore, it is indeterminate whether the RV-C are indeed susceptible to those capsid-binding drugs categorized by existing Groups, or if they represent a new category with a different pocket efficacy. To gain more insight, the C15 capsid model was re-probed against all known RV PDB datasets, looking for structural inconsistencies and/or conserved sequences that might explain observed drug reactivity. Parallel experiments in mucosal organ culture and ALI cultures re-tested the efficacy of W91, as well as W84, WIN52035 (W35), pleconaril and BTA-188, added or preloaded into C15 and A16 virions. The model, sequences and mutagenesis

experiments suggest there are multiple residues, including those at the entrance to the VP1 pore, that co-vary among all RV-C and contribute to a novel pocket environment. These "Group-3" pockets could explain why all RV-C are probably refractive to strategies with the current antiviral drugs.

Results and Discussion

C15 Drug Susceptibility. Pleconaril and BTA-188 are effective against many RV-A+B types. One study reported that BTA-188 inhibited 75% (of 56) tested strains, including A16 with an MIC_{50} of ~8 nM and B14 with MIC_{50} of ~68 nM (23). Pleconaril was reported effective on 93% (of 101) RV-A+B, with an EC_{50} of 0.59 μM for A16, and 0.16 μM for B14 (176). Drug testing for the RV-C is more difficult. Studies have described recombinant C15 as resistant to pleconaril (108), but susceptible to a related compound, W91 (39). Neither report did extensive testing because the RV-C can only be titered by qRT-PCR, and the yield in organ cultures (39) or ALI (13, 108) is relatively low. For organ cultures particularly, variability among donors creates significant reproducibility issues (39) as well as a paucity of viable samples for proper controls. In new attempts with this technique, W84 and W35 were tried in sinus organ culture against A1, A16 and C15. Both drugs seemed partially effective against A1 (n=1), and the yield of A16 also showed some reduction with W84. But neither reduced the replication of C15 (Sup Fig A2-1A).

The inherent inconsistencies with organ cultures warranted a change to human bronchial (HBE) or sinus (HSE) epithelial ALI cultures derived from primary tissue snippets. While again, cell expansion is limited, with successful cultures, the method

has less variability and more samples can be tested simultaneously. Pre-experiments

with WisL cells and A16 determined the lowest concentration of drugs that prevented

cytopathatic effect (CPE) and virus replication without overt toxicity (e.g. rounding or

lifting from the plate). For pleconaril and BTA-188, those were 10 mg/ml and 2 mg/ml,

respectively (Sup Fig A2-1B). When A16 and C15 were incubated with these drugs,

then titered in HSE-ALI cultures (Fig A2-2A), the controls showed typical virus

replication as evidenced by the 1-2 Log increase in genome signal (RNA Copies)

between 4 h (gray bars) and 24 h (blue/red bars) relative to a 0-time binding control

(white bar). Pleconaril or BTA-188 significantly reduced A16 amplification (blue bars),

but neither drug had the same effect on C15 (red bars). The same result was obtained

with a subsequent, independent ALI culture (Fig A2-2B). Whether the drugs were

present or not, C15 bound equivalently to the cultured cells, established productive

infections and amplified normal progeny numbers. In parallel experiments, C15 was

also resistant to W91 at a concentration (2 mg/ml) that reduced A16 growth by 1.3 Log

(Fig A2-2C). The previous partial susceptibility to this compound in organ culture could

not be repeated in ALI culture. It is possible the reported phenomenon was unique to

virus growth in that particular donor organ sample. In short, throughout multiple

attempts, none of the 5 tested capsid-binding drugs had efficacy against C15.

Capsid-Drugs Fit C15 Models. The activities of enterovirus capsid-binding drugs have

been reviewed extensively (e.g. (271, 290)). When such drugs intercalate into the VP1

hydrophobic pocket, they can deform the floor of the canyon to an extent that receptor

binding and attachment is inhibited (*e.g.* B14 and pleconaril) (247). Alternatively, they

may enter the pocket with minimum canyon deformation, but prevent required VP1
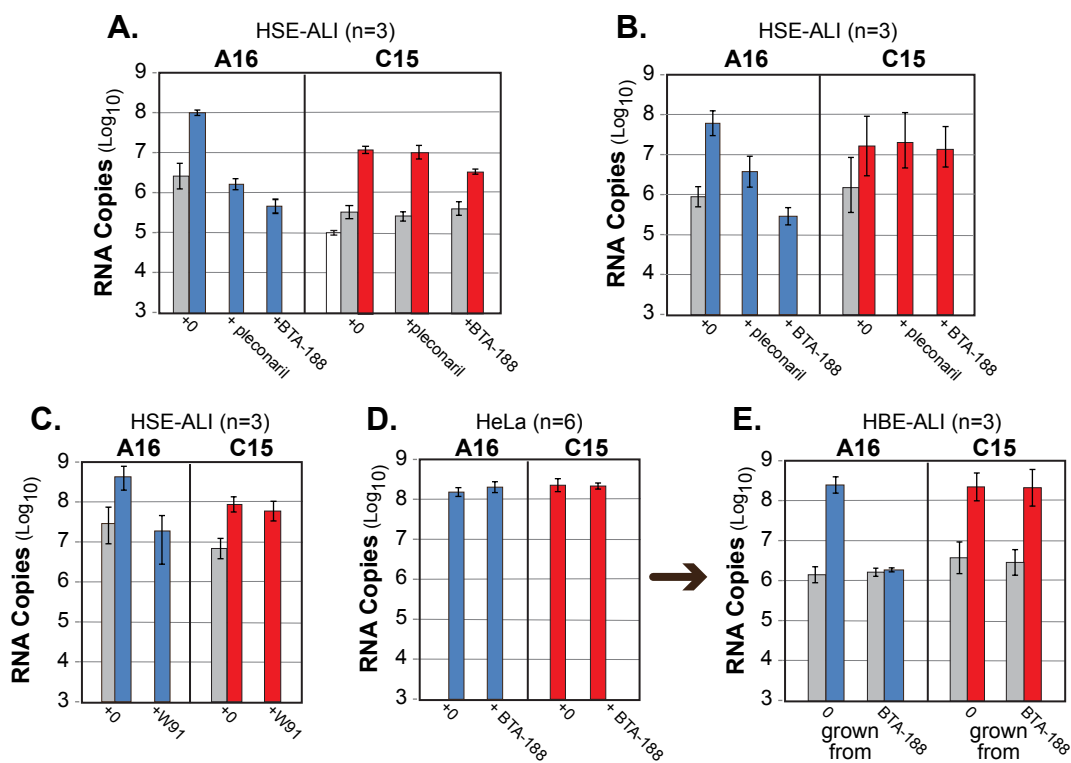
Figure A2-2. Drug Tests. (A) Recombinant A16 and C15 were titered for growth in HSE-ALI cultures in the presence of pleconaril or BTA-188. Colored bars (blue, red) are from samples harvested after 24 h PI. Gray bars were harvested after 4 h PI. White bars are 0-time binding controls. (B) Similar to A, this series used an independent HSE-ALI culture. (C) Similar to A, virus samples incubated with W91 were titrated for growth in HSE-ALI cultures. (D) Recombinant A16 and C15 transcripts were transfected into HeLa cells with (or without) BTA-188. After 24 h, virus was harvested and titered by qRT-PCR. (E) Output virus from D was infected into HBE- ALI culture as in A, except no additional drug was added during this phase. In all panels, qRT-PCR values (RNA Copies) were determined in duplicate. Experimental repeats are indicated (n). Bars indicate average error from n exps.

transitions for entry and uncoating (*e.g.* A1 and W56) (271). Assuming biostability is not

an issue, drug failure comes down to one of three mechanisms. The selected drug

might be a poor steric fit for a given pocket, and rejected. The drug might fit the pocket

but fail to prevent required VP1 changes. Or, the drug might be excluded from the

pocket altogether, either because it cannot enter, or cannot displace putative resident

pocket factors.

By definition, none of the determined RV-A+B structures exhibit steric clashes

between the VP1 proteins and their ligands. These would have been resolved at

coordinate deposition. Steric considerations that might explain C15 drug resistance

were explored with bioinformatics and the new capsid models. Since output coordinates

can adjust slightly, dependent on precise template selection, four C15 VP1 models were

created by I-TASSER (25), using independent A16 and B14 determined structures that

did or did not include bound plenonaril. An additional model was computed on the full I-

TASSER database, containing 31 RV files and 29 EV files. Each model was asked to

extract from these structures, the subset of 10 best ligand fits for that C15 VP1

conformation. Collectively they identified 12 synthetic compounds covering both Group-

1 and Group-2 capsid-binding drugs, and three natural compounds, myristate, succinate

and lauric acid, which were co-crystalized as natural ligands (Sup Table A2-2). For each

C15 dataset, the identified ligands were superimposed into chimeric PDB files then

assessed in MacPyMOL for steric clashes. A negative "C15 Fit" was defined as any

single VP1 atom lying closer than 0.35 Å to a ligand atom. W35 and W91 were included

for completeness although they were not directly selected by I-TASSER. The BTA-188

structure (in RV-A2) was a personal communication (Biota). As summarized in Table

A2-1, many of these drugs (or natural ligands) were excellent fits for the C15 pocket. Pleconaril and BTA-188 in particular, usually matched the cavity with ease (e.g. Fig A2-3B). Indeed, all 5 C15 models selected pleconaril as a preferred ligand, sometimes choosing multiple related structures (*e.g.* 1c8m and 1nd3) from the database.

"Fit" was assessed negatively if even a single atom overlapped, but in fact, every determined compound in the RV database was identified at least once by an I-TASSER model, as a potential ligand for C15. Of the 41 observed clashes, most involved a limited subset of residues (Fig A2-3A, Table A2-1). Only 1 of these (pleconaril and Met$_{204}$) originated from a ligand resolved as part of an RV-A structure (1nd3). Invariably, the conflicting atoms were contributed by a B14-bound drug, a suboptimal template for C15 modeling (25). All conflict locations were peripheral to the core of the C15 b-barrel, and scattered throughout its length (Fig A2-3A). W84, W56, W8R, were selected several times among the highest ranking ligands, even though they showed the most frequent (2-3) steric clashes. Perhaps not surprising, these same (Group-1) drugs have the longest chain lengths (Sup Table A2-1). They can be made to fit perfectly into C15, if allowed only slightly less rigid superimposition parameters (not shown). Indeed, any of the observed conflicts could probably be resolved easily by minor bond rotations (if permitted). Basically, the full modeling exercise was unable to identify any single, overt steric impediment that might prevent the well-studied cohort of capsid drugs from intercalating into the C15 VP1 pocket. In terms of physical constraint alone, the C15 model(s) do not immediately predict resistance, either to Group-1 or Group-2 drugs.

Drug Pocket Environment. The pocket residues important for A16 and B14 drug binding, especially for pleconaril, are well described (175, 341). An inclusive contact list
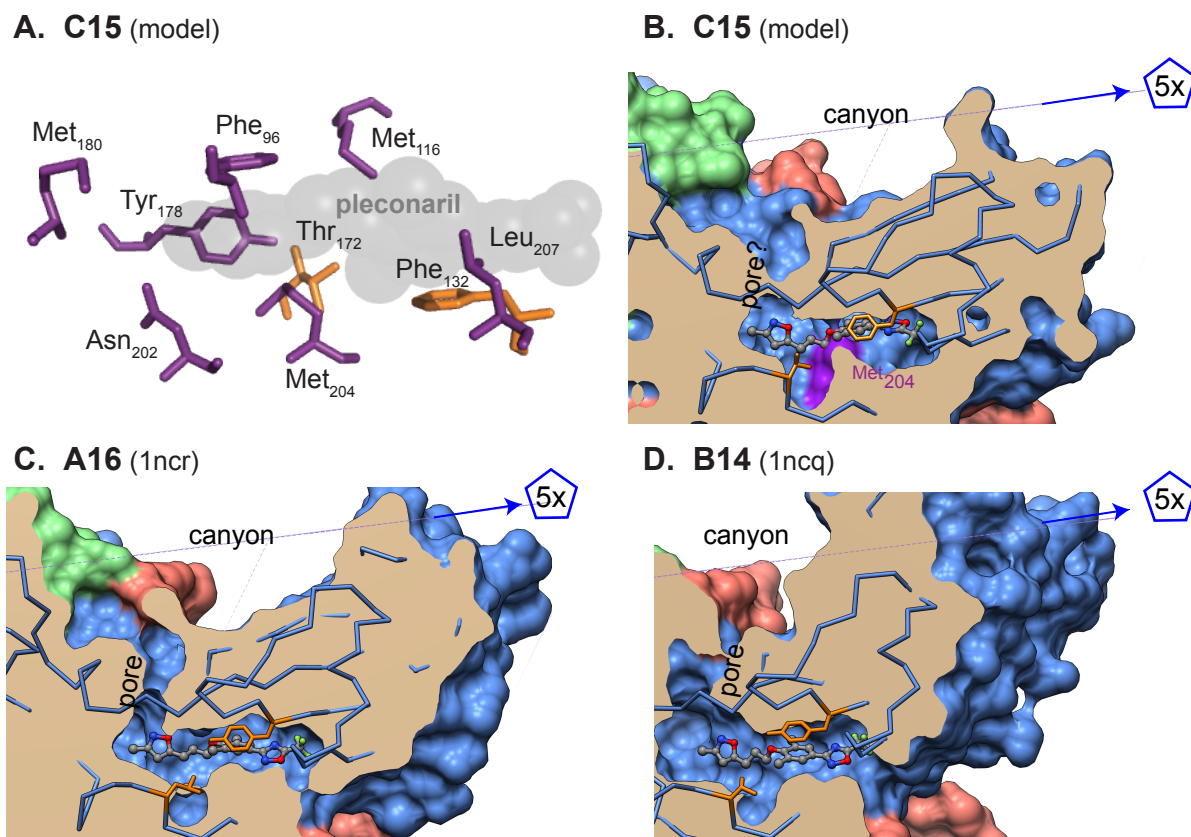
Figure A2-3. Key RV Residues and Pleconaril. (A) Pleconaril (spheres) modeled in the drug pocket of C15 highlights the distribution of any potential residue that could cause a steric clash with any modeled drug as per Table 1 (purple). Location of Phe132 and Thr172, the Ledford et al (175) residues that confer resistance to B14 are highlighted in orange (all panels). (B) C15 model, (C) A16 (1ncr) and (D) B15 (1ncq) with pleconaril are shown as cutaways through the drug pocket. The 5-fold is to the right. The 2-fold, canyon and entry pore (not always visible here) are at the upper left of the pockets.

Table A2-1: Summary of C15 Drug/Model Conflicts

Drug/Ligand[1]	Returned C15 models without steric clashes[2]	Returned C15 models with steric clashes[3]	Conflicting C15 VP1 residues[4]
BTA-188	1	0	none
Pleconaril	8	2	Phe132(1), Met204(1)
W91	1	0	none
W54	1	0	none
W84	0	6	Phe96(6), Asn202(5), Met204(6)
S57	1	1	Phe132(1)
W01	2	0	none
W03	3	0	none
W35	1	0	none
W71	2	0	none
J77	1	0	none
W56	1	4	Phe132(3), Met204(4)
W8R	0	2	Phe96(2), Met180(2), Met204(2)
SD8	1	0	None
JEN	1	4	Met116(1), Tyr178(3), Met204(3), Leu207(2)
Myristate	5	0	none
Lauric Acid	3	0	none
Succinate	2	0	none

Footnotes for Table A2-1

[1] Ligands selected by I-TASSER for any C15 model (Sup Table A2-1).

[2] Number of models returned by I-TASSER with no steric clashes (Sup Table A2-1, "C15 Fit" is "Yes").

[3] Number of models returned by I-TASSER with 1 or more clashes

[4] C15 VP1 residues with clashes (observations).

within the VP1 b-core was generated with Endscript (98), by evaluating the 28 RV-A+B

structures co-crystalized with drugs and returning every residue within 4 Å of any drug,

in any virus. The 43 C15-drug models were scored in parallel. The tabulation,

summarized by WebLogo (Fig A2-4), shows species variation and frequency according

to the deep RV alignments, for every putatively-involved amino acid. The C15 positions

identified by PyMOL as possible steric clashes are designated in purple. Below each

position, a stacked graph records the number of structures (RV-A, blue, N_{max}=7; RV-B,

red N_{max}=22) or models (RV-C, light green, N_{max}=43), placing that residue within 4 Å of

any drug. Defined, pleconaril-reactive residues (341) are bold-faced. The RV isolates

with Group-1 and Group-2 drug reactivity correlate roughly with the B and A species,

respectively (see Methods).

How do these pockets differ? The 36 profiled sites divide into obvious categories.

The first (Category-1) includes about half the residues, marking the positions least

frequently identified by the 4 Å proximity criterion. If only 1-10 models or structures

returned these sites (N_{max}=72), they are probably not key drug resistance determinants,

even though all of them must certainly contribute to the overall RV-C pocket

environment. The remainder had proximity thresholds that were returned by at least 11

models or structures. These include, among others, all site analogs previously

associated with pleconaril interactions (bold numbers). This cohort itself subdivides into

those where the residues are conserved among all RV-A+B+C (Category-2), or where

conservation is between the RV-C and either the RV-A or RV-B (Category-3), or where

the dominant RV-C sequence(s) is unique (Category-4). The RV common sites

(Category-2) include Ile_{94}, Phe_{114}, Met_{131}, Ser_{155}, Phe_{167}, Tyr_{178}, Asn_{202} and Met_{204}.

C15	80	94	95	96	97	102	105	106	112	114	116	118	120	130	131	132	154	155	156
B14	77	**104**	105	**106**	107	112	115	116	122	124	126	**128**	**130**	**150**	**151**	**152**	**174**	**175**	**176**
A16	77	**98**	99	**100**	101	106	109	110	116	118	120	**122**	**124**	**142**	**143**	**144**	**166**	**167**	**168**
Category	1	2	1	4	3	1	1	1	1	2	4	2	1	4	2	3	3	2	3

C15	167	169	172	173	174	178	179	180	198	201	202	203	204	207	222	224	246
B14	**186**	**188**	**191**	192	193	**197**	198	199	215	218	**219**	220	**221**	**224**	243	245	267
A16	**179**	**181**	**184**	185	186	**190**	191	192	208	211	**212**	213	**214**	**217**	236	238	260
Category	2	4	4	1	1	2	1	3	1	1	2	1	2	3	1	1	1

Figure A2-4. Drug pocket residues. WebLogo depictions {Crooks, 2004 #3056} for the RV-A+B+C were tabulated for all VP1 residues measured within 4 Å of any determined or modeled ligand as defined by Endscript (Methods). The sequence set was the refined genome alignment. The graphs show the number of determined structures (RV-B in blue, RV-A in red) and RV-C models (green) that placed that residue near a ligand. Position numbers are those for native A16, B14 and C15 VP1 sequences. Published interactions with pleconaril (341) are shown in bold. Residues identified in Table 1 with potential steric clashes are in purple. The 2 pleconaril-resistant locations, identified by Ledford et al 2005 (175) are highlighted in orange. The Category value assigned to each position is described in Results and Discussion.

Category-3 includes Gln_{97}, Val/Ile_{118}, Phe/Tyr_{132}, Pro_{154}, Val_{156}, Met_{180}, and Leu_{207}.

Collectively, Categories 2+3 contain 5 of the 7 residues with incidents of (putative) steric

clashes (Tyr_{178}, Met_{180}, Asn_{202}, Met_{204}, Leu_{207}). Again, these modeled clashes are

unlikely to be critical determinants of RV-C drug resistance, because the same residues

are frequently displayed equivalently in the pockets of many susceptible RV-A+B. The

same could be said for virtually all of the Category-2+3 residues, in that these

sequences, shared freely among at least 2 species, do not interfere with the defined

Group-1 or Group-2 drugs.

Residue Phe/Tyr_{132} is an exception, however. In 2005, as part of a pleconaril

study, Ledford *et al* (175) noted that not all RV-A+B were susceptible to this drug. B4,

B5, B42, B84, B93, B97 and B99 are resistant. When they compared the relative

sequences of 25 key B14 VP1 residues, it was noticed that susceptible viruses

invariably displayed Tyr_{152} and Val_{191} in their drug pockets, while the resistant viruses

had Phe and Leu at the same positions (orange). Between B14 (susceptible), and B5 or

B42 (resistant), these were the only sequence changes in the pocket (or the pore).

Recombinant exchange of these residues in a B14 context, reversed pleconaril

susceptibility. The study concluded that Leu_{191} was the "major driver" of reduced

susceptibility, but the effect was most profound if both sites were changed

simultaneously.

Among the RV-C, none, including C15, has the B14 susceptible profile for these

2 residues. The B14 Tyr_{152} is equivalent to C15 Phe_{132}. The B14 Val_{191} is equivalent to

C15 Thr_{172}, a Category-4 position, marking it as unique to the RV-C. Unfortunately, the

Ledford study never defined why these particular residues conferred apparent

resistance. The A16 analog, Tyr_{144}, undergoes the largest displacement in the pocket when pleconaril binds this virus (341). The Leu_{184} (in A16) or Val_{191} (in B14) localize nearby to the same Ring B segment of the drug (341) (Fig A2-3CD). Not only do the RV-C lack a susceptibility profile at these sites, they have 4 additional drug-proximal residues in Category-4 that again, mark them as unique. The C15 Phe_{96}, Met/Leu_{116}, Ile_{130} and Ile_{169} positions are rarely (or never) shared with the other species. The RV-C conserve these selections at 93%, 57/43%, 93% and 100%, respectively. In the various C15 models, the pocket floor (Fig A2-3AB), displaying Phe_{96} and Met_{116} caused occasional steric clashes with the longest (W56, W8R, W84) or fattest (JEN) drugs (Table A2-1), although as mentioned above, only a few of the drugs and a few of the models recorded such conflicts.

Drug Pocket Pores. For capsid drugs to be effective, they must traverse a narrow pore at the base of the canyon into the VP1 core. The opening is a clear, resolved feature in all B14 structures (Fig A2-5B). Sited in the very deepest portion of the canyon, the pore is immediately adjacent to the COOH end of VP3 (in red, Fig A2-5ABC). Several participating B14 residues, including Asn_{105}, Asn_{219} and His_{220} have been described with natural mutations conferring drug resistance or drug selectivity (104, 160). The observed mutations did not prohibit drug entry, but instead, partially compensated for drug-induced VP1 changes by providing tighter receptor interactions in the overlapping ICAM-1 footprint (104). The pore contributions are not as well studied for A16, but again, every resolved structure shows a distinct opening in the same location (Fig A2-5A). From the proper angle, the tails of VP1-embedded drugs, pleconaril in these illustrations (dark blue) can be glimpsed through the A16 and B14 holes. To better

A. A16 (1ncr)

B. B14 (1ncq)

C. C15 (model)

D.

C15	93	94	95	99	202	203	245	**246**	247
B14	103	104	**105**	216	**219**	**220**	266	**267**	268
A16	97	98	99	209	212	213	259	**260**	261
Category	4	2	2	4	2	3	4	4	4
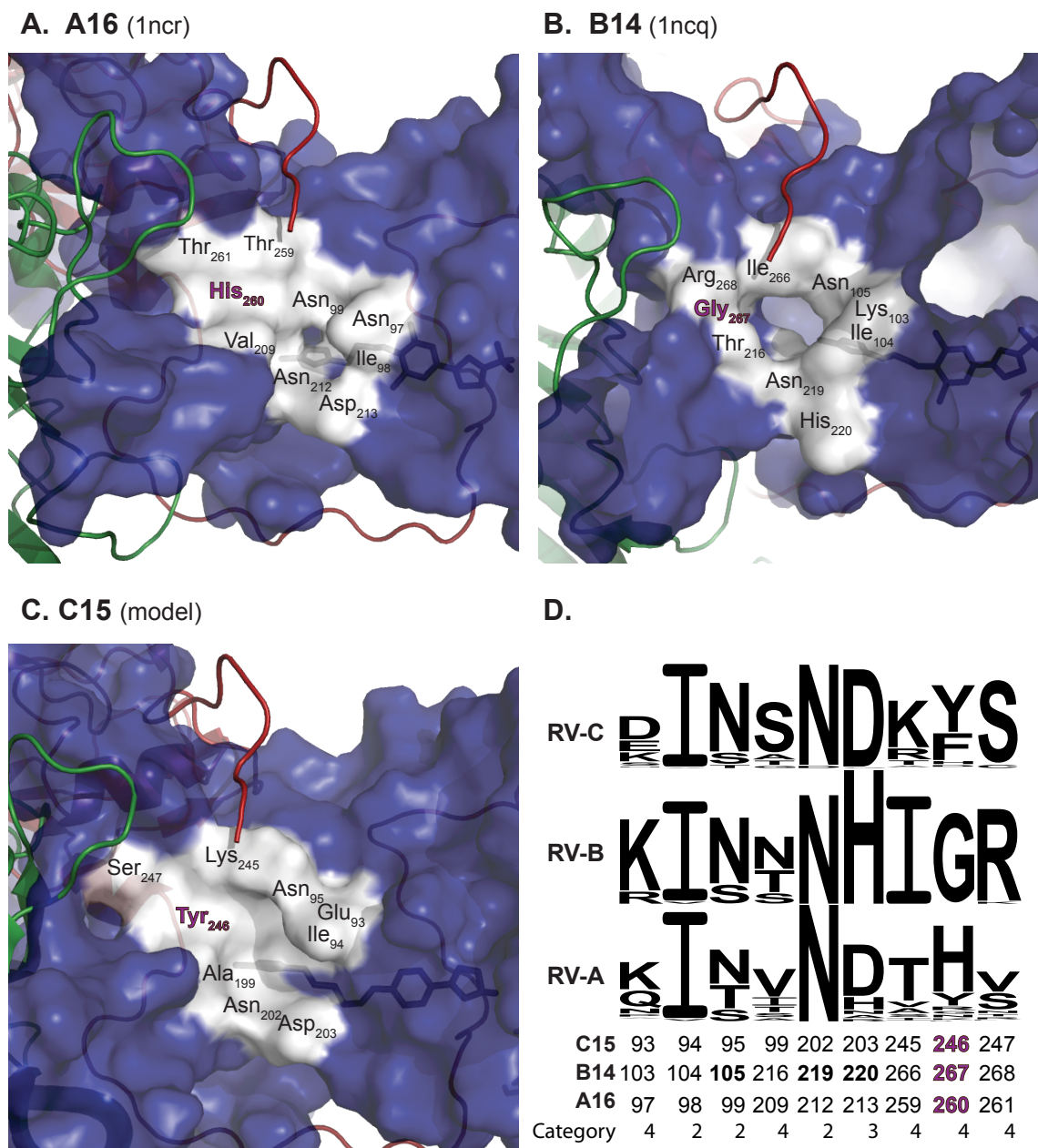
Figure A2-5. Drug Pocket Pores. (A) A16 (1aym), (B) B14 (4rhv), and (C) C15 (model) space-filling surfaces show VP1 residues at the base of the canyon, guarding the entrance to the drug-binding pockets. The COOH tail of VP3 (red) and pleconaril (dark blue) orient these figures clockwise, 90° relative to Fig A2-1, with the 5-fold to the right, and 2-fold to the left. (D) WebLogo depictions (66) for the RV-A+B+C were tabulated for these residues. The putatively obstructive C15 Tyr246 and its analogs are highlighted in purple.

describe these pores, all canyon residues within 7-9 Å of these tails, were compiled (MacPyMOL), then queried within the sequence alignment for analogues among the species. In the RV-C, 5 of the 9 residues showed Category-2 or Category-3 conservation, including the 3 mutant-defined B14 locations (C15) Asn_{95}, Asn_{202}, Asp_{203}, as well as Ile_{94} and Ser_{99} (Fig A2-4D). The other residues, Glu_{93}, Lys_{245}, Tyr_{246} and Ser_{247} were Category-4, and showed higher diversity within and between species. The RV-C do not use the same ICAM-1 footprint as the RV-A+B (39), so some diversity was expected here. What was not expected, was the visible absence of any discernible opening that even resembled a pore in the C15 model. In fact, none of the models, no matter which PDB templates refined them, showed an opening into the VP1 core at this locale (e.g. Fig A2-4C). The change in mass, blocking the opening was contributed by several residues, but primarily by Tyr_{246} (purple), conserved as Tyr or Phe in 88% of the RV-C. Every RV-B encodes Gly here (B14 267, 100%), while the RV-A have His (A16 260, 68%). Sterically, C15 Tyr_{246} is reasonably confined to this orientation as are its surrounding neighbors. If this model's predictions were true for real virions, drug entry might be slowed or even precluded by the tighter passageway. Conceivably though, an appropriately effective drug (pleconaril is modeled here) might find an alternate route elsewhere in the canyon into the VP1 core, or even persevere here by wiggling through tenaciously, despite the altered sequences.

C15 Grown with Drug. During sample preparation for crystallography, it is common to diffuse capsid-binding drugs into preformed virus arrays or to co-crystalize the materials. Should this not achieve sufficient occupancy for diffraction, the virus can be grown in the presence of the drug and then crystallized (341). If capsid drugs were

prevented from entering C15 when mixed with virus, it seemed reasonable that the impediment(s) might be resolved through co-culture conditions. Recombinant transcripts for A16 and C15 were transfected into HeLa cells in the presence or absence of BTA-188 then incubated for 24 h. After cell lysis and treatment with RNAse, qRT-PCR showed both preparations had produced stable virions. The progeny outputs (n=6) were similar whether or not the drug was present (Fig A2-2D). But when the derived lysates were tested for infectivity to ALI cultures, only the pre-treated A16 samples were unable to replicate (Fig A2-2E). Exposure to BT-188, even during the packaging of C15 progeny, did not inhibit their subsequent growth potential.

Predictions for RV-C Drug Reactivity. All of the Category-4 analogues in pockets and pores of the RV-A+B, as well as C15 Phe_{132}, are defined, important players in drug selection or binding, especially for pleconaril. The collective sequence changes, notably those involving polar residues (e.g. C15 Met_{118} vs B14 Ser_{128}, or C15 Thr_{172} vs B14 Val_{191}), and size changes (e.g. C14 Phe_{96} for B14 Leu_{106}, or C15 Ile_{169} for B14 Val_{188}, C15 Tyr_{256} for B14 Gly_{267}) must surely change the underlying character of the RV-C VP1, let alone its structural flexibility. Short of an experimental C15 structure with an active drug, it is impossible to anticipate the relative contributions of these residues to the broader question of drug resistance. The observed Category-2+3 residues are not wholly common or predictive of Group-1 or Group-2 isolates either. Instead, the sequence modeling, residue comparisons, and obviously the drug tests themselves, suggest the RV-C should be generalized with novel "Group-3" reactivity. Without labeled drug tracers, which are beyond the scope of this study, it cannot even be determined whether BTA-188 (and presumably pleconaril) actually intercalates into the C15

pockets. Possibly these drugs are indeed bound, but their inclusion is simply irrelevant to this virus life cycle. The RV-C do not use ICAM-1 or LDLR receptors which probe deeply to the canyon floor and are therefore sensitive to VP1 deformations (271). Alternatively, the Group-3 pockets may just be more strongly dependent on the presence of the native pocket factor(s) than the RV-A+B. If the RV-C preferentially incorporated and retained these factors, the essential, capsid-stabilizing properties would be relinquished only reluctantly and infrequently, to any drug replacement, even during protomer assembly. A putatively narrower or absent pore and the lack of reactivity even when C15 was grown in the presence of BTA-188 are consistent with this interpretation.

Materials and Methods

Sequences and Alignment. Refined alignments (337 seqs) of complete RV genome sequences are based on foundation superimposition of determined protein structures as described (25, 232). A translated polyprotein alignment with species, type and accession numbers are available in *.fasta and *.meg formats from http://virology.wisc.edu/acp/aligns/. The set includes RV-A (77 types, 203 seqs), RV-B (25 types, 69 seqs), RV-C (30 types, 65 seqs), and EV outgroups (4 species, 10 seqs). Current RV nomenclature designates the species letter (A, B or C), and type number (e.g. A16). Strain designations are unique to each accession number. Group-1 and Group-2 drug specificities are as defined (9). Briefly, Group-1 includes all RV-B plus A8, A13, A32, A43, A45, A54, and A95. Group-2 includes all remaining RV-A except A100-103, which like the RV-C were not tested in the original study. The amino acid numbering system is for C15 protein VP1 (GU219984), unless otherwise specified.

Analogous residues for A16 (L24917) and B14 (L05355) in the same alignment column

are referred to with their native (ungapped) sequence designations.

Molecular Modeling. An I-TASSER model, with output PDB file, was predicted for the

capsid of C15. It is primarily based on the structure of A16 (1aym) as has been

described (25). Refined, protomer and virion coordinates (hrvc) are available from

VIPERdb (http://viperdb.scripps.edu/). Subunit illustrations were rendered in

MacPyMOL (1). UCSF Chimera (245) created full capsid structures and pentameric

assemblies from protomer files. The PDB entries for enteroviruses (CB3, PV3) and RV-

A+B with antiviral drugs or identified pocket factors resolved within their VP1 pockets,

are summarized in Sup Table A2-1. Drug names, abbreviations, references and

published MIC_{50} are indicated. Each listed set of C15 coordinates was generated by I-

TASSER then submitted online (*http://endscript.ibcp.fr/*) to Endscript (98). The

Crystallography and NMR System (CNS) module within this program identified lists of

residues within 4 Å of any bound compounds for the RV-A+B (Fig A2-5), including (53x)

at least one iteration of every crystallized drug or pocket factor ligand. Additional

evaluations extracted list(s) of C15 residues within 4 Å of any (putative) ligands, should

the chimeric model(s) be representative of analogous interactions (see Sup Table A2-

2).

Viruses. Recombinant A16 was produced in WisL cells (179). When required, titration

was by plaque assay on HeLa cells. C15 virus was prepared by reverse genetics,

transfecting full-length RNA transcripts into HeLa or WisL cells, then purifying and

concentrating the progeny as described (39).

Drugs. WIN56291, WIN52035 and WIN52084 were provided by Dr. Wai-Ming Lee.

Pleconaril and BTA-188 were provided by BIOTA (Australia). Working concentrations

were prepared fresh for each experiment.

Drug Standardization. Pleconaril, BTA-188 and W91 were evaluated for minimum

inhibitory concentrations and toxicity using A16 in WisL cells grown in Medium A

(Eagle's Minimum essential medium with 1% non-essential amino acids, 5% fetal calf

serum and pen/strep) in 12-well plates. The drugs were diluted to 1, 2, 5 or 10 mg/ml,

and then incubated with virus ($2x10^7$ RNA copies, 15 min, room temperature). Aliquots

(200 ml) were added to cell-containing wells. After 15 min at room temperature, then 45

min at 34°C, the cells were washed (3x) with PBS then Medium A, containing the

respective concentrations of drug. Incubation continued at 34°C for 24 h. Control wells

without virus assessed potential effects of DMSO or the drugs alone. At 24 h PI, CPE

was recorded, if evident. The cells were frozen and thawed three times to release

particles. They were treated with RNase A (Qiagen) then assayed by qRT-PCR for RNA

content as described (39).

Drug Testing. Capsid-binding drug tests for C15 in human organ cultures have been

described (39). For ALI-based tests, cultures of differentiated human sinus epithelium

(HSE) or human bronchial epithelium (HBE) were grown in 12-well plates for 30 days in

ALI medium (1:1 BEGM (Lonza) and DMEM (Mediatech) with additives, then screened

for C15 growth before use (13). Successful cultures were gently washed (3x) with PBS

to remove mucus. Virus samples ($2x10^{7-8}$ RNA copies of A16 or C15) were incubated

with pleconaril (10 mg/ml, 26.24 μM), BTA-188 (2 mg/ml, 5.43μM) or W91 (2 mg/ml,

5.63μM) or DMSO (controls) in ALI medium (15 minutes at room temperature) then

inoculated into culture wells at the apical ALI surface. 15 min later (room temperature) the plates were transferred to 34°C for 3 hr 45 min. For samples harvested at this time, the cells were washed with PBS (3x), then lysed in RLT buffer (350 ml, Qiagen). The remaining cultures were fed basally with ALI medium (1 ml with drug) and incubation continued (to 24 h at 34°C). At harvest, the medium was aspirated from the outer wells and cells were lysed by RLT buffer. RNA extraction and qRT-PCR were as described (39). Virus titer is expressed as RNA copies ($\log_{10}$) averaged from duplicate qRT-PCR values and n=2-6. Average error is indicated for each sample type.
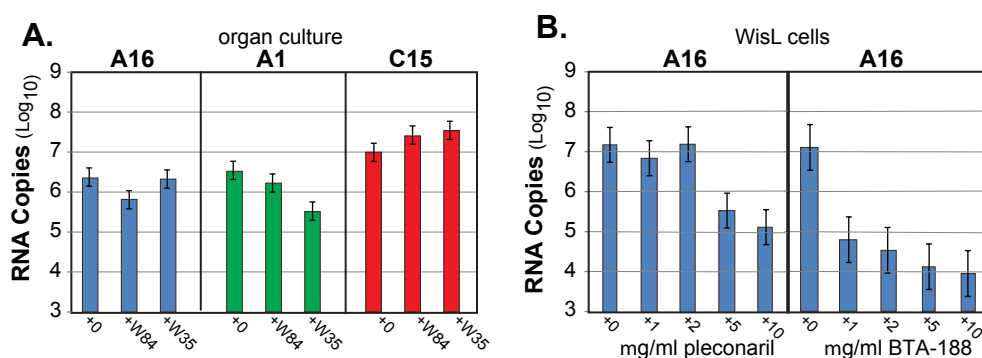
Supplemental Figure A2-1. Drug Tests. (A) A16, A1 and C15 virus samples were incubated with buffer (+0 control), W84 or W35 then tested for infectivity to organ culture (same donor, at 24 h PI) as described in Methods. (B) A16 virus was incubated with the indicated concentrations of pleconaril or BTA-188 then titered for growth (at 24 h) in WisL cells. Growth media contained the respective concentrations of drugs. All qRT-PCR values were determined in duplicate (n=1). (A) standard error; (B) average error.

Supplemental Table A2-1. Antiviral Drugs Described in this Study

A. Capsid Binding Drugs Tested Against C15										
Capsid Binding Compound Identifier	Full Name	Common name	PDB	Virus[a]	Chain Len Å[b]	# CH_2 chain	Gp[c]	MIC_{50} A16	MIC_{50} B14	ref[d]
Benzaldehyde 4-[2-[1-(6 methal-3-pyridazinyl)-4-piperidinyl]ethoxy]-O-ethyloxime	BTA-188	BTA-188	-	A2	19.8	2	1*	8 ± 2 nM	68 ± 33 nM	(23)
3-[3,5-dimethyl-4-[3-(3-methyl- 1,2-oxazol-5-yl)propoxyl]phenyl]-5-(trifluromethyl)- 1,2,4-oxadiazol	Win63843	Pleconaril or W11	1ncr 1c8m 1nd3 1na1 1ncq	A16 A16 A16 B14 B14	17.7	3	1	0.216 mg/ml	30 ng/ml	(341)
5-{3-[2,6-dichloro-4-(4,5-dihydro-1,3-oxazol-2-yl)phenoxy]propyl}-3-methylisoxazole	Win56291	W91	2hwb	B14	15.8	3	1	0.15 mg/ml	>8.7 mg/ml	(103)
5-{5-[2,6-dichloro-4-(4,5-dihydro-1,3-oxazol-2-yl)phenoxy]pentyl}-3-methylisoxazole	Win54954	W54	2hwc	A1	17.9	5	1	-	2.32 mM	(49)
3-methyl-5-(7-{4-[(4S)-4-methyl-4,5-dihydro-1,3-oxazol-2-yl]phenoxy}heptyl)isoxazole	Win52084	W84	1rud 1ruh 1rui 2rs1	B14-m B14-m B14-m B14	20.9	7	1	-	0.4 mg/ml	(16)
B. Additional Capsid Binding Drugs Modeled Against C15										
1-[6-(2-chloro-4-methoxyphenoxy)hexyl]-1H-imidazole	SCH38057	S57	1hri	B14	15.5	6	1	-	27.6 mM	(276)
5-{3,5-dimethyl-4-[3-(3-methylisoxazol-5-yl)propoxy]phenyl}-2-methyl-2H-tetrazole	Win61209	W01	1qju	A16	16.6	3	1	0.37 mg/ml	0.336 mg/ml	(103)
5-{3-[2,6-dimethyl-4-(2-methyl-1,3-oxazol-4-yl)phenoxy]propyl}-3-methylisoxazole	Win65099	W03	1qjy	A16	17.1	3	1	0.954 mg/ml	0.221 mg/ml	(103)
5-{5-[4-(4,5-dihydro-1,3-oxazol-2-yl)phenoxy]pentyl}-3-methylisoxazole	Win52035	W35	1ruc 1rue 1rug 2ro6	B14-m B14-m B14-m B14	17.6	5	1	-	0.92 mg/ml	(104)
5-{7-[4-(4,5-dihydro-1,3-oxazol-2-yl)phenoxy]heptyl}-3-methylisoxazole	Compound IV	W71	2r04 1d4m	B14 CA9	18.1	7	1	-	0.5 mM	(116)
ethyl 4-{2-[1-(6-methylpyridazin-3-yl)piperidin-4-yl]ethoxy}benzoate	R77975	Pirodavir or J77	1vbc	PV3	18.6	2	1	0.051 mg/ml	0.044 mg/ml	(290)
3-methyl-5-(5-{4-[(4S)-4-	Compound	W56	2rs5	B14	19.8	5	1	-	0.6	(16)

methyl-4,5-dihydro-1,3-oxazol-2-yl]phenoxy}pentyl)isoxazole	V(S)								mM	
3-methyl-5-(7-{4-[(4R)-4-methyl-4,5-dihydro-1,3-oxazol-2-yl]phenoxy}heptyl)isoxazole	Compound I(S)	W8R	2rr1	B14	21.2	7	1	-	0.03 mM	(16)
(2S)-1-(4-cyclohexylphenoxy)-3-(4-pyridin-2-ylpiperazin-1-yl)propan-2-ol	SDZ88061	SD8	1hrv	B14	15.5	0	2	<3.0	-	(290)
3-methoxy-6-[4-(3-methylphenyl)piperazin-1-yl]pyridazine	R61837	JEN	2hwf 1r09	B14 B14	13.4	0	2	-	42 mM	(49)
C. RV 3Cpro Protease Inhibitor										
Ethyl (E,4S)-4-[[(2R,5S)-2-[(4-flurophenyl)methyl]-6-methyl-5-[(5-methyl-1,2-oxazole-3-carbonyl)amino]-4-oxoheptanoyl]amino]-5-[(3S)-2-oxppyrrolidin-3-yl}pent-2-enoate	Rupintrivir									

Supplemental Table A2-1. **Antiviral Drugs Described in this Study**. The capsid binding compounds tested in C15 experiments or modeled into C15 structures are identified, along with their PDB structure designations, chain lengths, and reported MIC_{50}.

[a] The virus in structure(s) determined with this drug; "-m" designates mutated virus

[b] Maximum ligand length determined with the Measurement Wizard of MacPyMOL

[c] Supplemental Reference (9). *BTA-188 was not tested in that study but is presumed to be Group 1.

[d] Supplemental references specific to this table.

Supplemental Table A2-2. Fit of C15 Drug-Pocket Ligands Selected by I-TASSER

Template[1]	Model Rank[2]	PDB[3]	Virus[4]	Ligand[5]	Drug Gp[6]	C15 Fit[7] in VP1
1aym	1	2rs5	B14	W56	1	Phe132, Met204
1aym	2	2r04	B14	W71	1	Yes
1aym	3	1hri	B14	S57	1	Phe132
1aym	4	1na1	B14	pleconaril	1	Phe132
1aym	5	1nd2	A16	myristate	Natural	-
1aym	6	1qjy	A16	W03	1	Yes
1aym	7	1qju	A16	W01	1	Yes
1aym	8	2hwf	B14	JEN	2	Yes
1aym	9	1r1a	A1	succinate	Natural	-
1aym	10	1d4m	CA9	W71	1	Yes
1ncr	1	2rr1	B14	W8R	1	Phe96, Met180, Met204
1ncr	2	2rs5	B14	W56	1	Phe132, Met204
1ncr	3	1rui	B14	W84	1	Phe96, Asn202, Met204
1ncr	4	2rs1	B14	W84	1	Phe96, Asn202, Met204
1ncr	5	1nd2	A16	myristate	Natural	-
1ncr	6	1aym	A16	lauric acid	1	-
1ncr	7	1c8m	A16	pleconaril	1	Yes
1ncr	8	1nd3	A16	pleconaril	1	Met204
1ncr	9	1r1a	A1	succinate	Natural	-
1ncr	10	1qjy	A16	W03	1	Yes
4rhv	1	2rs5	B14	W56	1	Yes
4rhv	2	2hwc	A1	W54	1	Yes
4rhv	3	1hri	B14	S57	1	Yes
4rhv	4	1na1	B14	pleconaril	1	Yes
4rhv	5	1nd2	A16	myristate	Natural	-
4rhv	6	2hwf	B14	JEN	2	Tyr178, Met204
4rhv	7	1qjy	A16	W03	1	Yes
4rhv	8	1qju	A16	W01	1	Yes
4rhv	9	1vbc	PV3	J77	1	Yes
4rhv	10	1vrh	B14	SD8	1	Yes
1ncq	1	1na1	B14	pleconaril	1	Yes
1ncq	2	1rui	B14	W84	1	Phe96, Met204
1ncq	3	2rs1	B14	W84	1	Phe96, Asn202, Met204
1ncq	4	1ncq	B14	pleconaril	1	Yes
1ncq	5	1aym	A16	lauric acid	Natural	-
1ncq	6	2rs5	B14	W56	1	M204
1ncq	7	1nd2	A16	myristate	Natural	-
1ncq	8	1ncr	A16	pleconaril	1	Yes
1ncq	9	1r09	B14	JEN	2	Phe96, Met204, Leu207
1ncq	10	2hwf	B14	JEN	2	Phe96, Met204
database	1	1na1	B14	pleconaril	1	Yes
database	2	2rr1	B14	W8R	1	Phe96, Met180, Met204
database	3	1rui	B14	W84	1	Phe96, Asn202, Met204
database	4	2rs1	B14	W84	1	Phe96, Asn202, Met204

database	5	2rs5	B14	W56	1	Phe132, Met204
database	6	1aym	A16	lauric acid	Natural	-
database	7	1nd2	A16	myristate	Natural	-
database	8	1ncr	A16	pleconaril	1	Yes
database	9	1ncq	B14	pleconaril	1	Yes
database	10	2hwf	B14	JEN	2	Met116, Leu207
1aym	Fit	2r06	B14	W35	1	Yes
1aym	Fit	2hwb	B14	W91	1	Yes
1aym	Fit	Biota	A2	BTA-188	1*	Yes

Supplemental Table A2-2. Fit of C15 Drug-Pocket Ligands Selected by I-TASSER. Table lists the full dataset for template, model rank, returned PBD (drug and virus), drug group and all putative steric clashes observed between these drugs and any C15 modeled residue(s). These data were used to provide the summary in Table A2-1.

[1] C15 VP1 models based on these templates were used to query the I-TASSER database for ligand fits as described in Methods.

[2] Rank order of ligand fits as returned by I-TASSER

[3] PDB file returned by I-TASSER

[4] Virus in that PDB file

[5] Ligand in that PDB file

[6] Drug Group of ligand according to (9). * Not part of that study, but most similar to Group-1.

[7] "Yes" indicates no steric clashes between C15 VP1 residues and ligand; "-" were not evaluated for conflicts; or C15 VP1 residues in conflict.

Appendix 3.

Mapping and Biochemical Analyses of EMCV Leader and 2A Binding.

Petty RV, Basta HA, Bacot-Davis VR, Brown BA, Palmenberg AC.

To be submitted to J Virol (in preparation).

Author contributions: RVP contributed L:2A binding experiments (including 2A truncation products) (Fig A2-1), Ran/2A competition assay for L binding (Fig A3-3), and surface plasmon resonance K_d determination of L:2A binding (Fig A3-4). VRBD contributed experiments on L:2A binding effects on L phosphorylation (Fig A3-2). BAB cloned, expressed and purified 2A constructs, and performed 2A sequence analysis (Fig A3-6).

Justification: Previous yeast two-hybrid experiments suggested that EMCV L and 2A bound (unpublished). This study shows that L and 2A indeed bind *in vitro*. L localizes to the nuclear rim, presumably bound to Ran, but before this study we did not have a potential mechanism by L traverses to the nuclear rim in the first place. We now believe L and 2A bind either in the context of the polyprotein or shortly after release (judging by their high K_d), and traffick to the nucleus via 2A's nuclear localization signal. Ran then displaces 2A, and L remains at the nuclear rim while 2A continues on to the nucleolus. This study also reveals that representative cardioviruses Ls all bind their own 2As, and 2As can be swapped inter- and intraspecies and still bind.

ABSTRACT

The Leader (L) and 2A proteins of encephalomyocarditis virus (EMCV) are the primary anti-host proteins produced during infection. These proteins interact with several key cellular partners to shut down host defenses, including inhibition of nucleocytoplasmic trafficking and cap-dependent translation. Here we show for the first time that L and 2A bind one another *in vitro*. Between EMCV L and 2A, the binding displays a 1:1 stoichiometry with a K_D of 1.5 mM. The first 100 amino acids of 2A and several key residues in the hinge domain of L contribute to a binding that may partially overlap with the binding site on L for RanGTPase. L and 2A proteins from different cardiovirus species and serotypes, specifically TMEV(BeAn) and Saffold virus, can bind one another in a seemingly ionic-dependent fashion. Taken together, these data may explain how L is able to reach the nucleus early during infection, namely by binding and utilizing 2A's nuclear localization signal, and may also explain polyprotein processing defects observed with certain 2A mutant viruses.

INTRODUCTION

Cardioviruses are a genus within the *Picornaviridae* family that consists of three primary members, encephalomyocarditis virus (EMCV), Theiler's murine encephalomyelitis virus (TMEV) and the newly discovered Saffold virus (144, 219, 277). These viruses are all positive sense, single-stranded RNA viruses that possess a single open reading frame, which is cleaved co- and post-translationally by viral proteases (198). Cardioviruses possess several unique anti-host proteins, chief among them are Leader (L) and 2A (6, 37, 102, 111, 312, 344, 347). The L protein of EMCV, the prototypical cardiovirus,

induces rapid shutdown nucleocytoplasmic trafficking (NCT) during infection, in part by binding to Ran GTPase and inducing hyperphosphorylation of nuclear pore proteins (Nups) by host kinases (253-255). Furthermore, the 2A protein of EMCV has been shown to induce a shutdown of cap-dependent translation (6, 102). 2A can also bind the host translation initiation factor eIF4E and is associated with the 40S, but not the 60S or full 80S, ribosomal subunit during infection (101, 102).

L is the first protein translated in the cardioviral polyprotein. In EMCV, it is 67 amino acids long and possesses three distinct regions. The first region is an N-terminal CHCC zinc-finger with a novel fold (83). The second region is a short hydrophobic linker that connects the zinc-finger to the C-terminal acidic region. The acidic region is a long, flexible chain that imparts L with an overall pI of 3.8 (61). Both TMEV (76 amino acids) and Saffold (71 amino acids) share the zinc-finger, hinge, and acidic tail; however they also have an additional "Theilo" region, while TMEV possesses an additional Serine/Threonine-rich region. Precise functions for these additional sequences are currently unknown, but the Theilo region may be functionally related to the zinc-finger (261).

L is necessary and sufficient for inducing the shut-down of host NCT observed during EMCV infection (253). NCT shut-down occurs with the hyperphosphorylation of Nups, which is thought to inhibit the ability of transport proteins (karyopherins) to interact with their respective Nups (255). While the exact kinase, or kinases, responsible for these phosphorylation events is unknown, previous data implicates members of the MAPK family; p38 and ERK1/2 (254).

The functions of the 2A protein have been far less characterized than those of L. All picornaviruses possess a "2A" protein that induces self-cleavage of the P1 and P2 regions through a ribosome-skipping mechanism (77) or proteolytic self-cleavage (217). The 2A protein of EMCV, however, is larger than L (143 amino acids) and has been show to localize to nucleoli and induce a general shut-down of cap-dependent translation (6). Recently, we have identified several regions of EMCV 2A that include a nuclear localization signal and a C-terminal eIF4E binding site (101).

The interaction of these viral proteins with several of their known cellular partners has been the subject of much study (101, 102, 246, 253); however, little is known about their interaction with other viral proteins, including one another. Previous studies in our lab using yeast two-hybrid assays of EMCV proteins revealed a potential interaction between L and 2A (unpublished). Here, we present a detailed biochemical analysis that demonstrates the L and 2A proteins can bind one another *in vitro* not only within, but also across cardioviral species and map the respective sites on L and 2A that are critical to this binding.

MATERIALS AND METHODS

Recombinant Constructions. Plasmid pT-GB1 was engineered by amplification of the GB1 gene by PCR from the pET30-GBFusion1 vector (a kind gift from John Markley) with primers 1186 and 1187. The amplicon was digested with Nco I and Hind III, gel purified, then ligated into pTri-Ex 1.1 (Novagen) at the same restriction sites. The plasmid pGB12A was constructed by amplification of the 2A gene by PCR from pEC9 (3) with primers 1188 and 1189. The 2A amplicon was gel purified and digested with

Hind III and Xho I, then ligated into the corresponding restriction sites in pT-GB1.

pGB12A 1-50, 51-100, 101-143 where generated using the same strategy with different

primers (Table A3-1). GB12A constructs from Saffold and TMEV were amplified from

viral cDNAs SafV-2 and TMEV(BeAn) (a kind gift from Howard Lipton) similar to EMCV,

using different primers (Table A3-1). All clones were verified by Sanger sequencing.

pGST-L was previously described (4) which contains an N-terminal GST fused to EMCV

L. L_E-GST (EMCV), L_S-GST (Saffold), and L_B-GST (TMEV) are described in Chapter 2

and contain a C-terminal GST tagged to their respective L proteins.

Protein Purification. For expression, pGB1, pGB12A, pGB12A truncations, and

alternate species plasmids were transformed into Rosetta BL21(DE3) pLac I cells

(Novagen). A single colony was picked and grown overnight in 2XYT with 1% glucose,

34μg/mL Chloramphenicol, 50μg/mL ampicillin at 30ºC. The next day a larger volume of

2XYT with 1% glucose and 50μg/mL of ampicillin was inoculated with the overnight

culture. At an OD_{600} of 0.6, protein expression was induced by the addition of 1mM

Isopropyl ß-D-1-thiogalactopyranoside (IPTG). The cultures were incubated with

shaking at 30ºC until they reached an OD_{600} of 2.4-3.2. The cells were then pelleted

(6,000 x g, 15 min, 4ºC) and frozen overnight at -80ºC.

After thawing, the cell pellet was resuspended in His-2A buffer (50 mM NaH_2PO_4,

300 mM NaCl, 10 mM imidazole and 25% v/v glycerol) with 1mM fresh

phenylmethanesulfonylfluoride (PMSF). The resuspended cells were incubated with

lysozyme (1mg/mL) for 30 minutes at 4ºC and DNA sheared by sonication. The

insoluble fraction was removed by centrifugation (20,000 x g, 45 minutes, 4ºC). The

soluble lysate was filtered through a 0.2μM filter (GE Healthcare) to remove any

Table A3-1. Primer sequences.

Plasmid	Primer Number	Direction	Sequence
pT-GB1	1186	Forward	TTGCCATGGCTCACCATCATCATCATCATATGCAGTACAAACTGATCCTGAAC
	1187	Reverse	GTGAAGCTTTTCGGTAACGGTGAAGGTTTTGGTAGC
pGB12A	1188	Forward	ATTAAGCTTAGTCCAAATGCCCTAGACATTTCAA
	1189	Reverse	CTCGAGTTACCCTGGATTTGTCTCAATGTCATGAAT
pGB12A$_{1-50}$	1217	Forward	GTTACCGAAAAGCTTAGTCCAAAT
	1218	Reverse	CAGGAACTCGAGTTATTTGGTCTTTGATCT
pGB12A$_{51-100}$	1219	Forward	TCAAAGAAGCTTCAGGTCTCTTTCCTGAGC
	1220	Reverse	CTGAACCTCGAGTTATCTAAAAGGCCTGACTCTCTT
pGB12A$_{101-143}$	1221	Forward	AAGCCTAAGCTTCTGCCCCTGGTTCAGAAGGAA
	1189	Reverse	CTCGAGTTACCCTGGATTTGTCTCAATGTCATGAAT
pGB12A$_{TMEV}$	1366	Forward	AACCGACTCGAGCTAGCCTGGATTTGTTTCCA
	1367	Reverse	CTTGAAAAGCTTAATCCCGCTCTCTACCG
pGB12A$_{Saffold}$	1233	Forward	GTTTGGAAGCTTCCAAACCCCATTTCAATGTAT
	1235	Reverse	CGACTGCTCGAGTTAGCCAGGGTTTGCTTCAATGTC

particulates. Lysate was loaded onto a HisTrap HP column (GE Healthcare). Proteins

bound to the column were eluted by a step gradient of 20, 60, 120, 250 and 500 mM

imidazole. The fractions containing the protein of interest were pooled and

concentrated. Purified protein was then applied to a Sephacryl S-100 column (GE

Healthcare) and separated by size exclusion using His-2A dialysis buffer (50 mM

NaH_2PO_4, 300 mM NaCl, and 25% v/v glycerol). Fractions from a single peak were

collected and dialyzed against His-2A dialysis buffer. The proteins were then

concentrated, aliquoted, and stored at -80ºC.

GST-tagged proteins from EMCV, Saffold, and TMEV or GST alone were

expressed and purified as in (Chapter 2, (253)). Briefly, plasmids were transformed and

expressed (by IPTG induction) in Rosetta cells and lysates were reacted with a GSTrap

HP column. Eluted (10 mM reduced glutathione) fractions were reacted with a Hi-Q

cartridge (Bio-Rad) for anion exchange and eluted over a gradient of 50 mM to 2 M

NaCl. The fractions of interest were then dialyzed into HEPES buffer (pH 7.4),

concentrated, aliquoted, and stored at -80ºC.

His-Ran and GST-RCC1 were both expressed and purified as described

previously (246).

GST-L interaction with His-GB12A and truncations. Glutathione-sepharose beads

(GE Life Sciences, 10 uL/reaction) were washed two times in binding buffer (50 mM

HEPES, 150 mM NaCl, 0.5% NP40, pH 7.4) then incubated with GST-L or GST at 4^0C

overnight with agitation. The beads were washed and spun a 500xg two times in

binding buffer to remove any unbound GST-L or GST. His-GB12A, His-GB12A$_{1-50}$, His-

197

GB12A$_{51-100}$, and His-GB12A$_{101-143}$ (50 nM) were added and the incubation continued (1

hr, 25° C). The samples were pelleted (500 x g, 5 min) and the supernatant transferred

to separate tubes. These proteins were precipitated with 30% trichloroacetic acid (TCA)

on ice (1 hr), washed with acetone (3x), and resuspended in alkaline SDS buffer.

Beads were washed (3x) with binding buffer followed by addition of 30 uL 1x SDS

buffer. Protein/SDS solutions were boiled for 10 minutes prior to 12% SDS-PAGE

fractionation. Gel bands were transferred to PVDF membranes and analyzed by

Western blot using anti-His (Abcam, Product ab18184) or anti-GST (Novagen, Product

#71097) primary antibodies and anti-mouse secondary antibody (Sigma-Aldrich,

Product A2554).

Binding of L:2A via Surface Plasmon Resonance. Equilibrium binding studies were

performed on a BIAcore 2000 instrument (BIAcore AB, Uppsala, Sweden) loaded with

CM5 research grade sensor chips (GE Healthcare). Monoclonal antibodies specific to

GST (Novagen, Product #71097) were covalently attached to the chips with amine-

coupling chemistry. Purified recombinant GST-L (5 µg/mL, 120 nM) diluted in SPR

buffer (10 mM bis-tris propane, 100 mM NaCl, 0.005% Tween-20, pH 7.4) was flowed

over individual chip cells at a rate of 10 uL/min (75 µg total, 25^{0}C). His-GB12A was

then flowed over the same cells in varying concentrations (10/20/50 µg/mL, 20 µL/min).

The total injection time was 450/600 seconds (120/150 µL total) with a dissociation time

of 120 seconds. Chip surfaces were regenerated using 20 mM piperazine (pH=9) with 2

M KCl. Automatic, parallel reference subtractions were performed with an antibody-only

lane to account for non-specific and bulk interactions. These values were recorded then

removed from the data (BIA evaluation software, version 4.1) to provide the normalized binding constants specific to L and 2A.

Association and dissociation rate values were determined independently from best-fit curves, using Langmuir calculations at steady-state levels. The K_D was determined computationally by plotting the concentration of analyte (His-GB12A) against the K_{obs} in Excel. The slope and y-intercept were used to determine the final K_D.

In vitro L phosphorylation, competition. Purified GST (2.2µg) and GST-L EMCV (3.2µg) fusion proteins were incubated for 1 hour at room temperature with glutathione sepharose 4B beads. His-GB1or His-GB12A were added at 1:1, 4:1, and 4:1 (competitor:pre-bound GST/GST-L) molar ratios for 1 hour at room temperature. Manufacturer reaction buffers containing 5.0 µCi [γ-^{32}P] ATP (3,000Ci/mmol, 10mCi/ml), 10.0 units of CK2 (New England Biolabs), 10.3 units of SYK (SignalChem), or 10.0 units of both CK2 and SYK, were added to protein-bead complexes and incubated at 37°C for 60 minutes. Protein complexes were washed three times with PBS buffer containing 500mM NaCl and 0.02% Triton X-100, then subjected to gel electrophoresis. The gels were either exposed to a phosphorscreen and visualized with a Typhoon scanner (GE Healthcare), or silver-stained for total protein analysis.

Interaction of GST-L point mutations with GB12A, Ran competition. Point mutations in L, GST-L$_{K35Q}$, GST-L$_{D37A}$, and GST-L$_{W40A}$, were expressed and purified (15). These mutations, along with wild-type L, were reacted with glutathione beads and His-GB12A as above, except that incubation was 2 hours. In addition, His-Ran (50 nM)

was also reacted with GST-L, along with the corresponding L mutations, in the presence

or absence of His-GB12A. All reactions containing Ran also contained GST-RCC1 (1

nM). Proteins were detected by western blot using antibodies described above in

addition to anti-Ran primary (Santa Cruz Biotechnologies, Product sc-1156) and anti-

goat secondary (Sigma, Product A5420).

Interspecies L-GST/His-GB12A binding. Pull-downs were performed similar to GST-

L/GB12A as above, except that the supernatant was not retained or precipitated by TCA

and 10% SDS-PAGE was performed prior to western blotting. As the GB1 tag is a

derivative of the IgG binding B1 domain of the streptococcal Protein G, the mouse

secondary antibody is able to detect GB12A in the absence of primary antibody.

2A sequence alignment from representative cardioviruses. Amino acid sequences

from the 2A region of the polyprotein of EMCV (Genbank ABC25550.1), TMEV BeAn

(Swiss-Prot P08544.1), and Saffold (Genbank AFP86294.1) were obtained. Sequences

were aligned with MegAlign software (Lasergene 9, DNASTAR) using the Jotun Hein

method.

<div align="center">

RESULTS

</div>

GST-L binds His-GB12A at amino acids 1-50 and 51-100. We first wanted to

determine if there is a direct interaction between recombinant L and 2A. After

incubation with GST-L, but not GST alone, full-length His-GB12A was pulled down to

saturation (Fig A3-1A). Addition of a 2x molar ratio of His-GB12A relative to GST-L

revealed that much of the additional 2A was present in the supernatant strongly

implying a 1:1 binding ratio (Fig A3-1A, further quantified in Fig A3-5). In order to

A

GST-L:2A
1:1

GST-L:2A
1:2

GST:2A
1:1

Input
GST-L

GST-L ▬

GST ═
GB1-2A ═

anti-GST

Supernatant
Pellet

B

GB1-2A Variant

1-50

51-100

101-143

anti-GST

anti-His

Supernatant
Pellet

C

10.6	10.0	5.5	pI
1-50	51-100	101-143	Amino Acids

Nuclear localization
signal

eIF4E-binding

Primary cleavage

Biological Properties
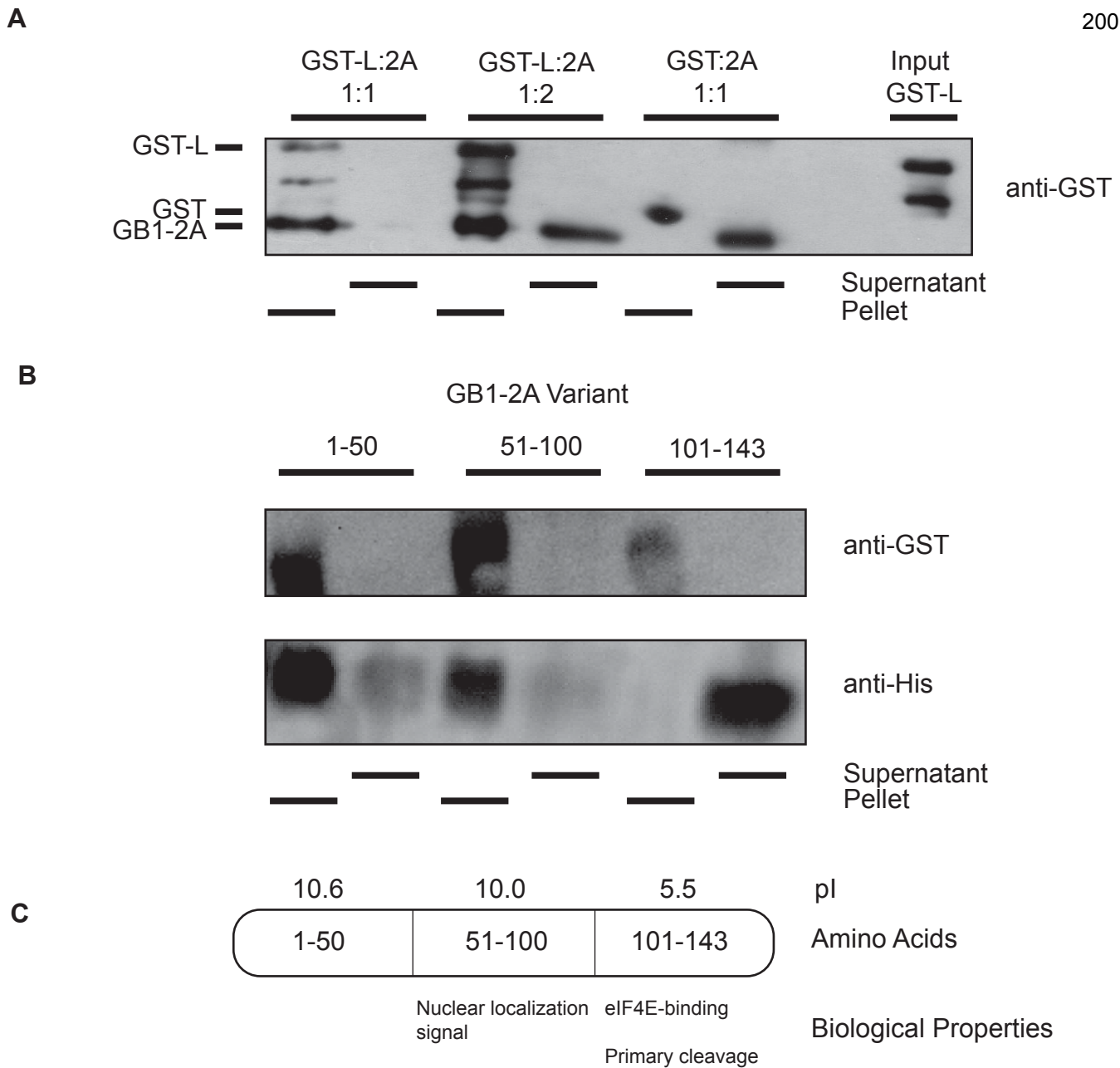
Figure A3-1. L:2A and 2A truncation binding A. Recombinant GST-L or GST alone pre-bound to gluta-thione sepharose beads were incubated with His-GB12A at 1:1 or 1:2 molar ratio (L:2A). After 1 hr incubation at 25°C, samples were spun (500 rcf, 5 min.), supernatant was removed and proteins were precipitated with TCA. Pellet and supernatant were analyzed by SDS-PAGE and western blot. B. Amino acids 1-50, 51-100, and 101-143 (tagged by His-GB1) were reacted with GST-L as above and analyzed by SDS-PAGE and western blot. C. Diagram of EMCV 2A segments used in pull downs. Computationally determined pI and verified biological properties (61,101) are listed for their respective fragments.

further identify regions of 2A that may be contributing to L:2A binding, we expressed

and purified 2A (also linked to His-GB1) in approximately 1/3 regions of the protein.

Both fragments His-GB12A$_{1-50}$ and His-GB12A$_{51-100}$ but not His-GB12A$_{101-143}$ could be

pulled down by GST-L. This is not surprising as the predicted pIs of these fragments

are 10.5 (1-50), 10.0 (51-100), and 5.4 (101-143) (Fig A3-1C and -6) while the predicted

pI of the Leader protein is 3.8.

2A binding blocks phosphorylation of L at Y$_{41}$ but not T$_{47}$. It is difficult to determine

precise regions of L that interact with other proteins, since deletions or even point

mutations can completely abrogate the structure of this small protein (15). Instead, we

tested to see if 2A-L binding could block specific phosphorylation events that are known

to occur on L. L can be phosphorylated *in vitro* by Casein Kinase II (CKII) at position

T$_{47}$, which has been shown to be a prerequisite to phosphorylation at position Y$_{41}$ by

Spleen Tyrosine Kinase (SYK) (Chapter 2) in the hinge domain of L (15). Pre-

incubation of His-GB12A, but not His-GB1 alone, with GST-L prevents the

phosphorylation of Y$_{41}$, even in the presence of the phosphomimetic T$_{47}$E mutant (Fig

A3-2) (Chapter 2). In the presence of 2A, T$_{47}$ can still be phosphorylated, indicating that

2A does not hinder access to this residue from the CKII. Previous experiments have

shown that pre-incubation with recombinant His-Ran, an important cellular binding

partner of L, did not block either Y$_{41}$ or T$_{47}$ phosphorylation (Chapter 2).

L$_{W40A}$ mutation inhibits 2A binding in the presence of Ran and RCC1. The

implication of Y$_{41}$ in the hinge domain led us to investigate several point mutations in L

that are known to misfold the protein (15). We have previously shown that Ran

guanine-nucleotide exchange factor RCC1 is required for efficient L-Ran binding *in vitro*
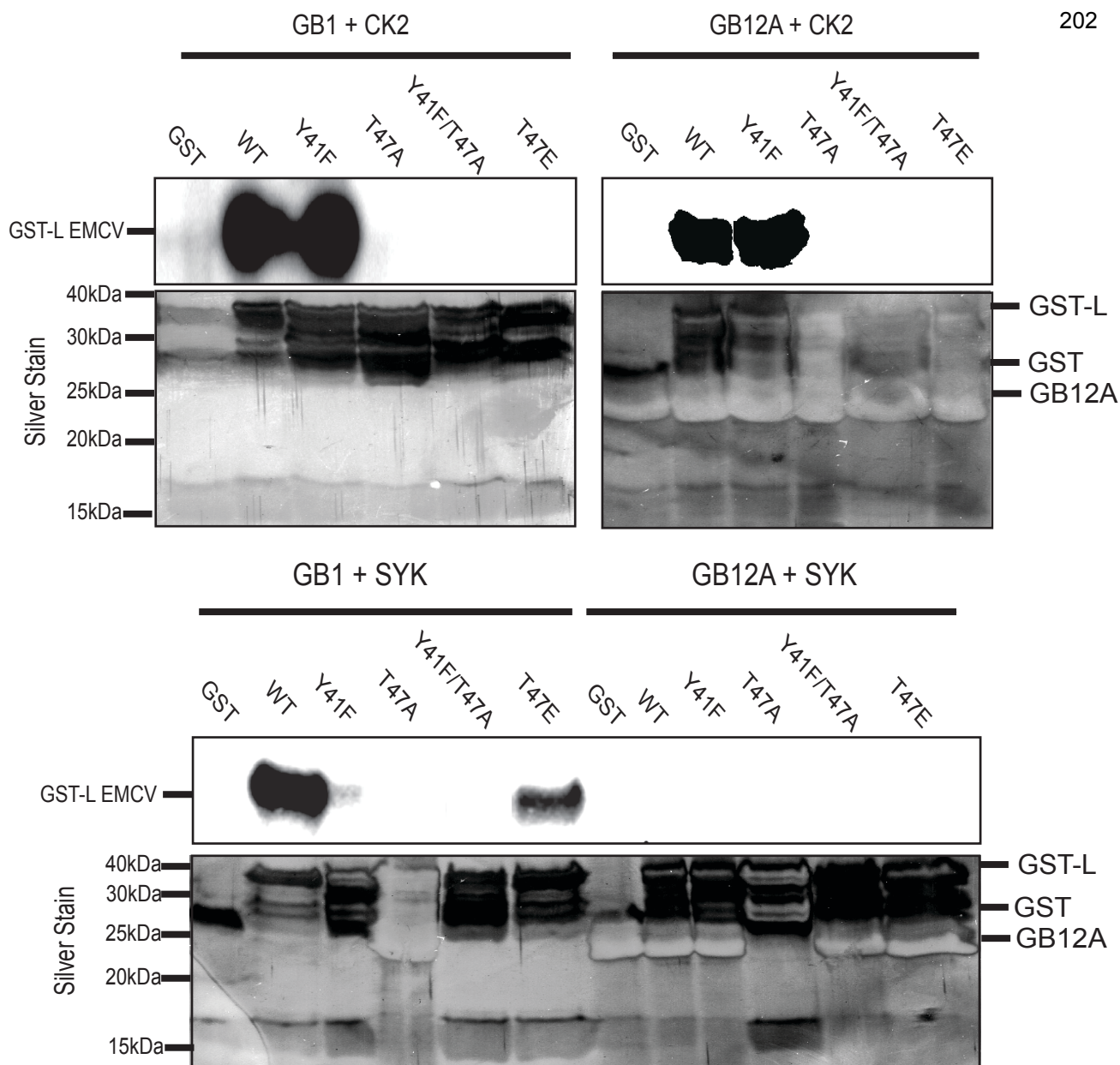
Figure A3-2. Effects of L:2A binding on phosphorylation of L. Recombinant GST-L phosphorylation site mutations were pre-bound with His-GB12A or His-GB1 alone for 1hr. Complexes were then incubated with recombinant Casein Kinase 2 (CK2) or Spleen Tyrosine Kinase (SYK) and [γ-^{32}P]-ATP for 1 hr at 37°C. Proteins bound to glutathione sepharose beads were washed analyzed by SDS-PAGE followed by silver staining and exposure to a phosphorscreen.

(246). In the absence of RCC1, we had identified several key residues on L which prevent Ran binding but do not alter the structure of L (15), namely $W_{40}A$, $K_{35}Q$, and $D_{37}A$. We tested if these mutations or binding of Ran impacted 2A-L interactions.

Using glutathione pull-downs as above, we compared 2A binding to L under three conditions, 2A alone, Ran (with catalytic amounts of RCC1 as (246)), and 2A and Ran together. With wild-type L, we found that the levels of Ran remained unchanged, indicating a saturation of the L in solution, whereas 2A binding dropped slightly when in the presence of Ran (Fig A3-3A, -3B). Differing effects were seen with point mutations in L ($W_{40}A$, $K_{35}Q$, $D_{37}A$). The most dramatic effect observed was with $W_{40}A$ in which the levels of 2A pulled-down by L dropped nearly 60% upon the addition of Ran. With mutations $K_{35}Q$ and $D_{37}A$, 2A binding dropped slightly in the presence of Ran, but these results were not statistically significant. Interestingly, in our experiments here with RCC1 added and incubation times extended (2 hours vs 1 hour) for solutions containing Ran-binding deficient point mutations studied previously (15), Ran binding was restored to wild-type levels (Fig A3-4A, see Ran-only lanes).

L:2A binding occurs at micromolar levels *in vitro*. To determine the binding constants of L:2A, we flowed increasing concentrations of His-GB12A (full length) over an antibody-fixed GST-L surface (Fig A3-3A). After reference subtraction and normalization of data, the K_D of the L:2A interaction was revealed to be 1.5 uM (Fig A3-3B). We also tested our various truncations of 2A, but we were not able to extract significant binding data for these protein pairs due to the poor signal to noise ratio (data not shown). This is likely due to the larger size of the His-GB1 tag relative to the individual fragments of 2A (i.e. His-GB1~11 kDa, $2A_{1-50}$~5 kDa etc).

A

B
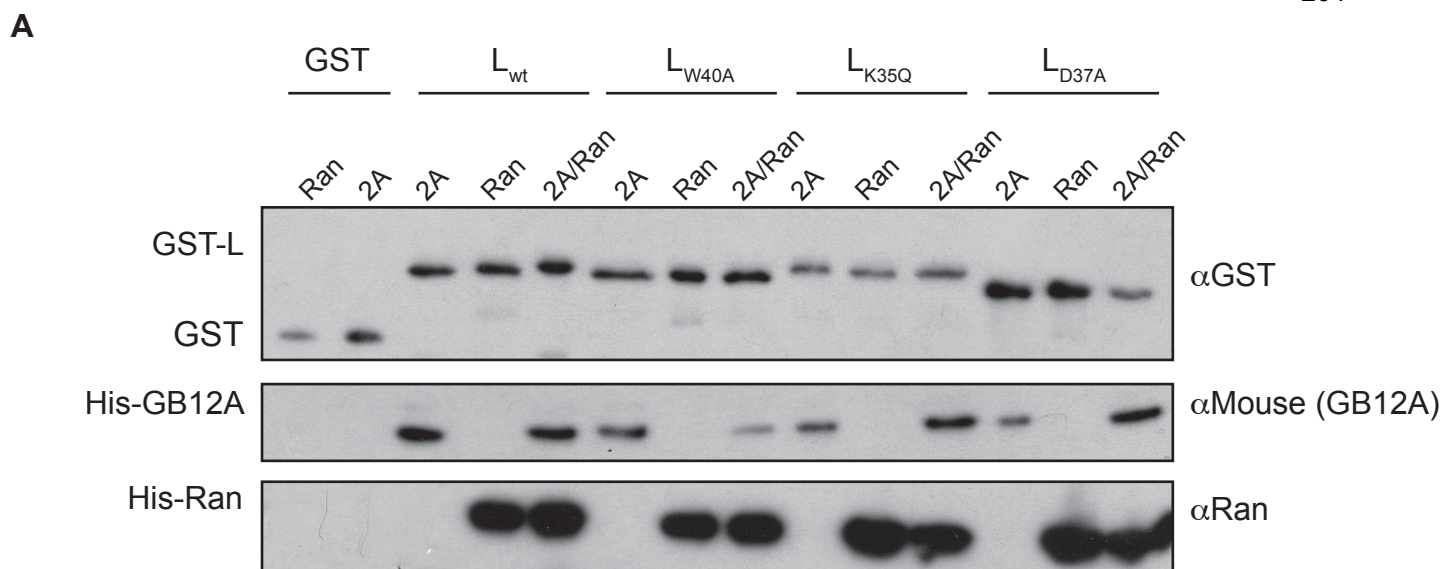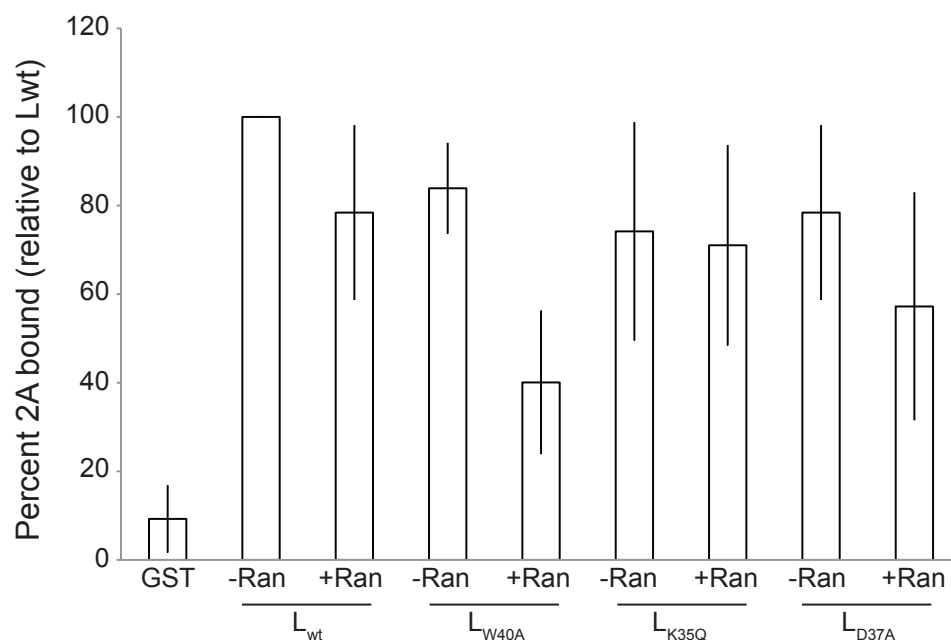
Figure A3-3. L point mutation and Ran impacts on L:2A binding. A. Recombinant GST alone or GST-L with mutations K35Q, D37A or W40A were pre-bound to glutathione sepharose was incubated with equimolar His-GB121, His-Ran (with 50 ng GST-RCC1), or His-GB12A and His-Ran together for 2 hours at 25°C. Beads were washed and subjected to SDS-PAGE followed by western blot. B. Amounts of His-GB12A pulled-down by GST-L were analyzed by ImageQuant software and values were normalized to levels of His-GB12A pulled down by wild-type L.
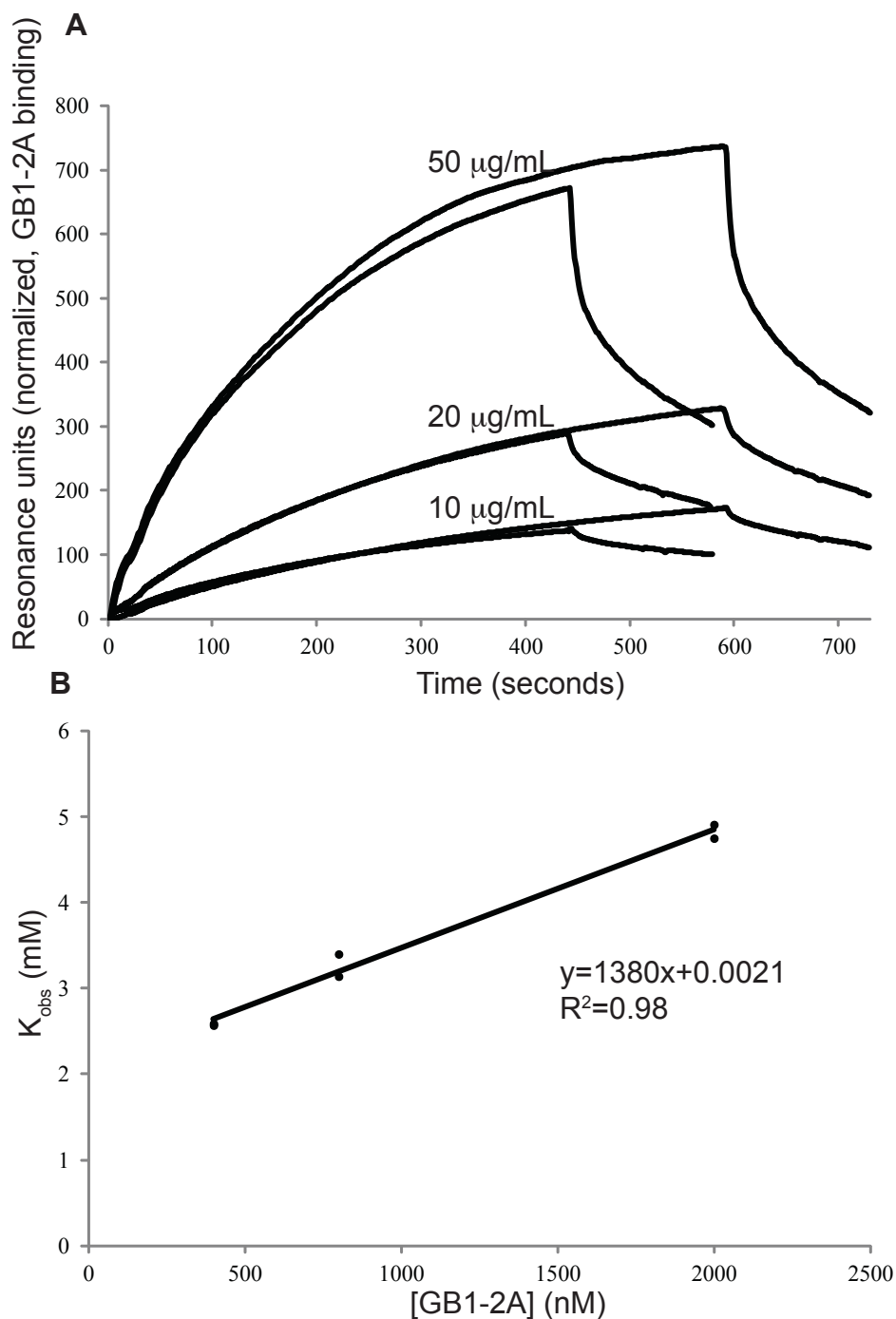
Figure A3-4. SPR of L:2A Binding. A. Varying concentrations of His-GB12A (10, 20, or 50 µg/mL) were flowed over a CM5 censor chip containing covalently attached anti-GST pre-bound with GST-L in a BIAcore 2000 instrument. Association phase was either 450 or 600 seconds with a dissociation phase of 120 seconds. Reference subtraction occurred using a lane containing only anti-GST (no GST-L). B. BIAevaluation software was used to extract association and dissociation rates based on sensorgram curves using Langmuir fitting. Observed dissociation constant was plotted against concentration of His-GB12A to extract the true K_d using a best-fit line in Excel.

Leader proteins bind 2A proteins of different cardiovirus species. 2A proteins from Saffold and TMEV share significant sequence identity; however, the 2A protein of EMCV shares little sequence identity with TMEV and Saffold except near the C-terminus of the protein, which contains the eIF4E binding site and primary cleavage cassette (101) (Fig A3-6). Despite this lack of sequence identity or even similarity, the first 100 amino acids of TMEV and Saffold all have alkaline pIs and conserve several positively charged amino acids. We therefore wanted to test if L proteins from different cardiovirus species could bind their own 2As. All species' L proteins could bind their respective 2A, we then mismatched to test interspecies binding (Fig A3-5).

All species of 2A and L could bind one another *in vitro*; however, the degree to which they could bind was revealing (Fig A3-5). As we had shown earlier, EMCV L and 2A could bind in an approximately 1:1 ratio, as could TMEV BeAn L and 2A. The interaction of Saffold L and 2A did not reach 1:1 stoichiometry in the pull-down assay. Furthermore, all species' L proteins preferred to bind EMCV 2A above their own respective 2A proteins (Fig A3-5).

DISCUSSION

At the initial stages of cardiovirus infection, viral proteins exist in very low abundance; therefore, the first few proteins translated from the viral genome must take swift action in order to combat host anti-viral defenses. The L protein of EMCV has been shown to rapidly shut down active transport of macromolecules across the nuclear pore (255). Due to the relatively low abundance of L at the time of NCT shutdown, it is unlikely that L can simply diffuse to the rim of the nuclear envelope and unleash such
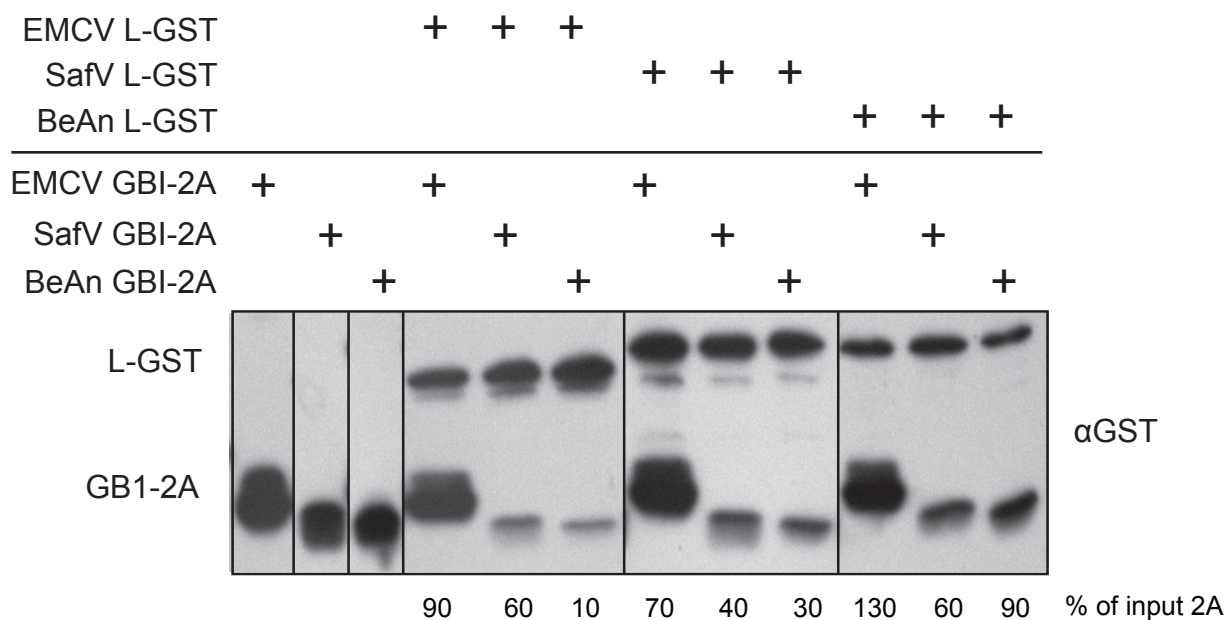
Figure A3-5. Intra- and interspecies L:2A binding. Recombinant GST-tagged L (pre-bound to gluta-thione beads) and His-GB12A from EMCV, Saffold-2, and TMEV BeAn strain were incubated with one another for 2 hrs at 25 °C. Beads were washed and bound-proteins were analyzed by SDS-PAGE followed by western blot. Quantification of His-GB12A was analyzed using ImageQuant against total input.

208

```
Majority        NPXALYRXDLFI TFXDXXI XFXYKVHGRXVXXFRI PGF- GLTRAGRXLVC          pI
                     10        20        30        40        50
2A EMCV         SPNAL- - - DI SRTYPTLHVLI QFNHRGLEVRLFRHGQFWAETRADVI LRS  47   10.57
2A TMEV BeAn    NPAALYRI DLFI TFTDEFI TFDYKVHGRPVLTFRI PGF- GLTPAGRMLVC  49   8.18
2A Saffold      NPVSI YRVDLFI NFSDTVI QFTYKVHGRTVCQYEI PGF- GLSRSGRLLVC  49   8.82

Majority        MGEQP- - - XXGPXXSX- - - - - - - - - KXXYHXVFTAXXXSFXXSI YKXRYR
                     60        70        80        90       100
2A EMCV         KTKQVSFLSNGNYPSMDSRAPWNPWKNTYQAVLRAEPCRVTMDI YYKRVR  97   10.01
2A TMEV BeAn    MGEQP- - - AHGPFTSS- - - - - - - - - RSLYHVI FTATCSSFSFSI YKGRYR  87   9.62
2A Saffold      MGEKP- - - CQLPI STP- - - - - - - - - KCFYHI VFTGSRNSFGVSI YKARYR  87   9.78

Majority        PWKXP- XHDELXDRGXXTFGXFFKAVRXYHAXYYXQRLI HDI ETNPG
                    110       120       130       140
2A EMCV         PFRLPLVQKEWPVREENVFG- LYRI FNAHYAGYFADLLI HDI ETNPG  143   5.45
2A TMEV BeAn    SWKKP- I HDELVDRGYTTFGEFFKAVRGYHADYYRQRLI HDVETNPG  133   6.79
2A Saffold      PWKQP- LHDELHDYGFSTFTDFFKAVRDYHASYYKQRLQHDI ETNPG  133   6.02
```

Figure A3-6. Cardioviral 2A sequence alignment. Sequences from the 2A proteins of EMCV, Saffold, and TMEV BeAn strain were aligned using MegAlign software and pIs of fragments were determined using Protean (Lasergene 9, DNASTAR).

catastrophic effects. We have earlier hypothesized that the viral 2A protein, which possesses an active nuclear localization signal, may shuttle L to the nuclear rim (246). This would, however, require a physical interaction between L and 2A either directly or indirectly.

We have demonstrated here that L and 2A can indeed directly bind *in vitro* (Fig A3-1A) and that this binding is stoichiometric in a 1:1 ratio (Fig A3-1A, A3-5). Furthermore, we have shown that the first 100 amino acids of 2A contribute to L-binding (Fig A3-1B). This is unsurprising as the pIs of the first and second 50 amino acids of EMCV 2A are highly basic at 10.6 and 10.0 (Fig A3-1C), respectively, while the pI of EMCV L is highly acidic at 3.8.

While the precise amino acid sequences of 2A proteins among cardioviruses are not well conserved (231) (Fig A3-6), the total alkaline pI and several positively charged amino acids are. We incubated the L and 2A proteins of the three main serotypes of cardioviruses (EMCV, TMEV (BeAn), and Saffold) with one another to examine if the observed L:2A binding is evolutionarily conserved. Not only did each respective L bind its own 2A, indeed all 2A proteins bound all L proteins from the 3 main cardioviruses. They all, however, bound with differing affinities. Both EMCV and TMEV Ls (BeAn strain) bound their respective 2As to a nearly saturated 1:1 stoichiometry (Fig A3-3). Interestingly, all Ls appeared to prefer to bind the 2A of EMCV above their own. One explanation is that EMCV 2A has the most alkaline pI of the 2A proteins tested at 9.67 while Saffold (8.83) and TMEV (9.17) are significantly less alkaline. This difference in pI may help to explain the differences in binding affinity observed between cardiovirus species and serotypes.

We have previously used biochemical methods to define the interactions of L with a cellular binding partner, RanGTPase (15, 246, 253). EMCV L is phosphorylated by Spleen Tyrosine Kinase (SYK) on Tyrosine 41 but only after Casein Kinase 2 (CK2) phosphorylation of Threonine 47 (Chapter 2). *In vitro* phosphorylation reactions using recombinant kinases revealed that pre-incubation of L and 2A blocks the phosphorylation of Y_{41}, but not T_{47} (Fig A3-2). In the solved NMR structure of EMCV L (15, 61), T_{47} is in a loop-like structure in the acidic domain of L, whereas Y_{41} sits of a surface of negatively charged amino acids that could serve as a binding surface for the positively charged N-terminus of 2A (Fig A3-7A, -7B). Given that 2A blocks phosphorylation of this site and that L need not be phosphorylated for L:2A binding (bacterially-expressed proteins lack post-translational modifications), whereas Ran does not block phsophorylation, it is likely that this phosphorylation event occurs after 2A has been released from L.

Using SPR, we demonstrated that L binds 2A with a K_D of 1.5 uM (Fig A3-4). This may seem like a rather high K_D for proteins produced in low quantities during the initial stages of infection; however, L and 2A are formed as a part of the L-P1-2A precursor polypeptide and can be considered a monomolecular reaction, which may overcome the apparently low binding affinity. More importantly, This K_D is also relatively low compared to the K_D of L-Ran, which suggests that Ran could simply displace 2A from an L:2A complex. Indeed, we found that incubation with Ran reduces but does not eliminate L:2A binding. The most dramatic effect observed was for the W40A L mutation. This is unsurprising as a proximal residue, Y_{41}, is also implicated in L:2A binding (Fig A3-2). An alternate hypothesis is that 2A binding is able to induce a
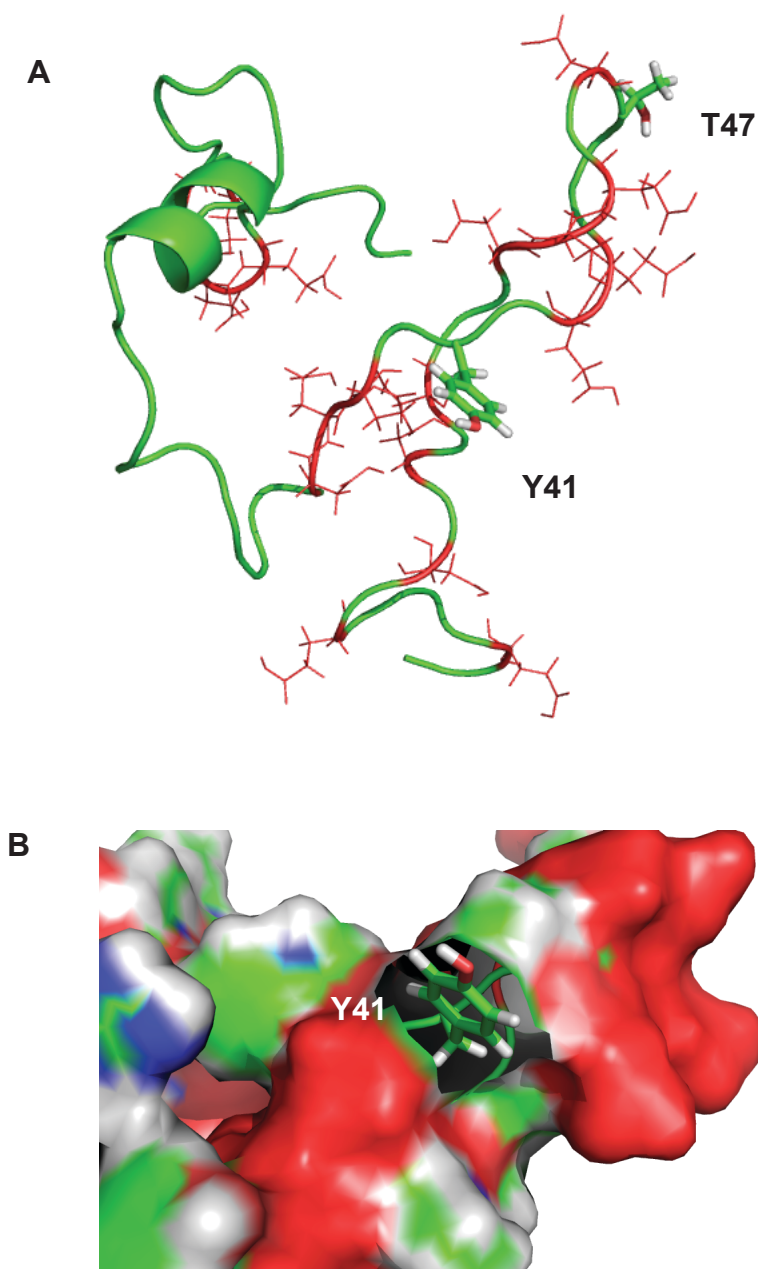
Figure A3-7. Mapping of L mutations which affect L:2A binding on L structure. A. The NMR structure of L (PDB: 2M7Y) was used to display the phosphorylation sites Y41 and T47. Negatively charged residues are displayed in red. B. The negatively charged surface, displayed in red, surrounding the phosphorylation site Y41, whose phosphorylation is blocked by 2A binding. Images were generated in PyMol (Version 1.4.1) (1).

conformational change in L that buries or otherwise blocks Y_{41} from being accessible to SYK. These data suggest that while Ran and 2A may both bind simultaneously L, their binding sites likely overlap to a degree. Ran binding may also induce a conformational change in L that is less amenable to subsequent 2A binding.

This differential binding suggests that the reactions are temporal in nature, which is to say that L:2A bind one another before the L-Ran complex is formed, as facilitated by RCC1 (246). This agrees with our current model that an L:2A heterodimer forms early in the viral lifecycle and that 2A may shuttle L to the nuclear rim until such a time that Ran, in the presence of RCC1, may displace 2A. Since Ran-binding still allowed substantial 2A to bind L, there may be additional L/Ran binding partners in the nucleus that can further displace 2A. Once 2A is freed, it may diffuse or be shuttled to the nucleolus where it accumulates during infection.

The 2A protein has important roles of its own in the viral lifecycle. 2A has been shown to bind the host eIF4E, the 40S ribosomal subunit, and localizes predominantly to the nucleolus, the site of ribosome biogenesis (6, 7, 101, 102). Through a poorly understood mechanism, 2A can also induce a shutdown of host cap-dependent translation, an important activity for a virus that translates its genome through a cap-independent mechanism (102). In addition, deletions in 2A can affect both primary and secondary cleavage of the P1 precursor by autocatalysis and the viral 3C protease, respectively (101, 105, 107)(unpublished data). One possibility is that these deletions affect the ability of L to bind 2A immediately after translation or release of the L-P1-2A precursor and that this binding facilitates proper folding of the polyprotein prior to 3C cleavage. Lending evidence to this hypothesis are several important facts. Firstly,

cleavage of the L-P1-2A precursor occurs in a stepwise manner, with L and 2A being the first and second respective proteins released from the polyprotein (42). Secondly, deletions of the 2A protein in regions not affecting primary cleavage can still affect cleavage of the P1 region as a whole (101).

A great deal of biochemical research has occurred recently to further reveal how cardioviruses induce a wide range of pathogenesis in their hosts. EMCV makes quick work of the cell through a variety of mechanisms involving the L and 2A proteins, whereas TMEV and Saffold can induce infections ranging from acute to persistent (44, 123, 332, 346). In this study, we have revealed that not only are viral-cellular protein interactions of significant interest, but also interactions between viral proteins themselves.

References

1. 2008. The PyMOL Molecular Graphics System, p. Open-source PyMol, 1.1r1 ed. DeLano Scientific LLC.
2. **Abed, Y., and G. Boivin.** 2008. New Saffold cardioviruses in 3 children, Canada. Emerg Infect Dis **14:**834-836.
3. **Agol, V. I., and A. P. Gmyl.** 2010. Viral security proteins: counteracting host defences. Nat Rev Microbiol **8:**867-878.
4. **Alessi, D. R., N. Gomez, G. Moorehead, T. Lewis, S. M. Keyse, and P. Cohen.** 1995. Inactivation of p42 MAP kinase by protein phosphatase 2A and a protein tyrosine phosphatase, but not CL100, in various cell lines. Current Biology **5:**283-295.
5. **Amanchy, R., B. Periaswamy, S. Mathivanan, R. Reddy, S. G. Tattikota, and A. Pandey.** 2007. A curated compendium of phosphorylation motifs. Nat Biotech **25:**285-286.
6. **Ambros, V., and D. Baltimore.** 1980. Purification and properties of a HeLa cell enzyme able to remove the 5' terminal protein from polioviral RNA. J.Biol.Chem. **255:**6739-6744.
7. **Aminev, A. G., S. P. Amineva, and A. C. Palmenberg.** 2003. Encephalomyocarditis viral protein 2A localizes to nucleoli and inhibits cap-dependent mRNA translation. Virus Research **95:**45-57.
8. **Aminev, A. G., S. P. Amineva, and A. C. Palmenberg.** 2003. Encephalomyocarditis virus (EMCV) proteins 2A and 3BCD localize to nuclei and inhibit cellular mRNA transcription but not rRNA transcription. Virus Research **95:**59-73.
9. **Anderson, P., and N. Kedersha.** 2009. RNA granules: post-transcriptional and epigenetic modulators of gene expression. Nat Rev Mol Cel Biol **10:**430-436.
10. **Andries, K., B. Dewindt, J. Snoeks, L. Wouters, H. Moereels, P. J. Lewi, and P. A. Janssen.** 1990. Two groups of rhinoviruses revealed by a panel of antiviral compounds present sequence divergence and differential pathogenicity. J. Virol. **64:**1117-1123.
11. **Arnold, E., and M. G. Rossmann.** 1990. Analysis of the structure of a common cold virus, human rhinovirus 14, refined at a resolution of 3.0 angstroms. J.Mol.Biol. **211:**763-801.
12. **Arnold, M.** 2006. Multiple Importins Function as Nuclear Transport Receptors for the Rev Protein of Human Immunodeficiency Virus Type 1. J Biol Chem **281:**20883-20890.
13. **Arslan, S. Y., K.-N. Son, and H. L. Lipton.** 2012. The antiapoptotic protein Mcl-1 controls the type of cell death in Theiler's virus-infected BHK-21 cells. J Virol **86:**1922-1929.
14. **Ashraf, S., R. Brockman-Schneider, Y. A. Bochkov, T. R. Pasic, and J. E. Gern.** 2013. Biological characteristics and propagation of human rhinovirus-C in differentiated sinus epithelial cells. Virology **436:**143-149.
15. **Aubert, C., M. Chamorro, and M. Brahic.** 1987. Identification of Theiler's virus infected cells in the central nervous system of the mouse during demyelinating disease. Microb Pathog **3:**319-326.
16. **Bacot-Davis, V. R., and A. C. Palmenberg.** 2013. Encephalomyocarditis virus Leader protein hinge domain is responsible for interactions with Ran GTPase. Virology **443:**177-185.
17. **Badger, J., I. Minor, M. A. Oliveira, T. J. Smith, and M. G. Rossmann.** 1989. Structural analysis of antiviral agents that interact with the capsid of human rhinoviruses. Proteins **6:**1-19.
18. **Baida, G., B. Popko, L. Wollmann, S. Stavrou, W. Lin, M. Tretiakova, T. N. Krausz, and R. P. Roos.** 2008. A Subgenomic Segment of Theiler's Murine Encephalomyelitis Virus RNA Causes Demyelination. J Virol **82:**5879-5886.
19. **Bain, J., L. Plater, M. Elliott, N. Shpiro, J. Hastie, H. McLauchlan, I. Klevernic, J. S. C. Arthur, D. R. Alessi, and P. Cohen.** 2007. The selectivity of protein kinase inhibitors: a further update. Biochem J **408:**297-315.
20. **Ball, J. R., and K. S. Ullman.** 2005. Versatility at the nuclear pore complex: lessons learned from the nucleoporin Nup153. Chromosoma **114:**319-30.
21. **Balvay, L., R. S. Rifo, E. P. Ricci, D. Decimo, and T. Ohlmann.** 2009. Structural and functional diversity of viral IRESes. BBA - Gene Reg Mech **1789:**542-557.

22.   **Bardina, M. V., P. Lidsky, E. V. Sheval, K. V. Fominykh, F. J. van Kuppeveld, V. Y. Polyakov, and V. Agol.** 2009. Mengovirus-induced rearrangements of the nuclear pore complex: Hijacking cellular phosphorylation machinery. J Virol **83:**3150-3161.

23.   **Barik, S., and A. K. Banerjee.** 1992. Phosphorylation by cellular casein kinase II is essential for transcriptional activity of vesicular stomatitis virus phosphoprotein P. PNAS **89:**6570-6574.

24.   **Barnard, D. L., V. D. Hubbard, D. F. Smee, R. W. Sidwell, K. G. Watson, S. P. Tucker, and P. A. Reece.** 2004. In vitro activity of expanded-spectrum pyridazinyl oxime ethers related to pirodavir: novel capsid-binding inhibitors with potent antipicornavirus activity. Antimicrobial agents and chemotherapy **48:**1766-72.

25.   **Barral, P. M., J. M. Morrison, J. Drahos, P. Gupta, D. Sarkar, P. B. Fisher, and V. R. Racaniello.** 2007. MDA-5 Is Cleaved in Poliovirus-Infected Cells. J Virol **81:**3677-3684.

26.   **Basta, H. A., V. R. Bacot-Davis, J. J. Ciomperlik, and A. C. Palmenberg.** 2014. Encephalomyocarditis virus leader is phosphorylated by CK2 and Syk as a requirement for subsequent phosphorylation of cellular nucleoporins. J. Virol. **88:**2219-2226.

27.   **Basta, H. A., J.-Y. Sgro, and A. C. Palmenberg.** 2013. Modeling of the human rhinovirus C capsid suggests a novel topography with insights on receptor preference and immunogenicity. Virology **448:**176-184.

28.   **Battey, J. N. D., J. Kopp, L. Bordoli, R. J. Read, N. D. Clarke, and T. Schwede.** 2007. Automated server predictions in CASP7. Proteins **69:**68-82.

29.   **Bayliss, R., T. Littlewood, and M. Stewart.** 2000. Structural basis for the interaction between FxFG nucleoporin repeats and importin-β in nuclear trafficking. Cell **102:**99-108.

30.   **Beckes, J. D., and J. Perrault.** 1992. Stepwise phosphorylation of vesicular stomatitis virus P protein by
virion-associated kinases and uncoupling of second step from in vitro
transcription. Virology **199:**606-617.

31.   **Ben-Levy, R., H. Hooper, R. Wilson, H. F. Paterson, and C. J. Marshall.** 1998. Nuclear export of the stress-activated protein kinase p38 mediated by its substrate MAPKAP kinase-2. Curr Biol **8:**1049-57.

32.   **Bernad, R.** 2006. Nup214-Nup88 Nucleoporin Subcomplex Is Required for CRM1-mediated 60 S Preribosomal Nuclear Export. J Biol Chem **281:**19378-19386.

33.   **Binford, S., P. Weady, F. Maldonado, M. Brothers, D. Matthews, and A. Patick.** 2007. In vitro resistance study of rupintrivir, a novel inhibitor of human rhinovirus 3C protease. Antimicrobial Agents and Chemotherapy **51:**4366-4373.

34.   **Bizzintino, J., W.-M. Lee, I. A. Laing, F. Vang, T. Pappas, G. Zhang, A. C. Martin, S.-K. Khoo, D. W. Cox, G. C. Geelhoed, P. C. McMinn, J. Goldblatt, J. E. Gern, and P. N. Le Souëf.** 2011. Association between human rhinovirus C and severity of acute asthma in children. Eur. Respir. J. **37:**1037-42.

35.   **Blinkova, O., A. Kapoor, J. Victoria, M. Jones, N. Wolfe, A. Naeem, S. Shaukat, S. Sharif, M. Masroor Alam, M. Angez, S. Zaidi, and E. Delwart.** 2009. Cardioviruses are genetically diverse and cause common enteric infections in South Asian children. J Virol **83:**4631-4641.

36.   **Blom, N., S. Gammeltoft, and S. Brunak.** 1999. Sequence and structure-based prediction of eukaryotic protein phosphorylation sites. J Mol Biol **294:**1351-1362.

37.   **Blom, N., J. Hansen, D. Blass, and S. Brunak.** 1996. Cleavage site analysis in picornaviral polyproteins: discovering cellular targets by neural networks. Protein Sci **5:**2203-2216.

38.   **Blom, N., T. Sicheritz-Ponten, R. Gupta, S. Gammeltoft, and S. Brunak.** 2004. Prediction of post-translational glycosylation and phosphorylation of proteins from the amino acid sequence. Proteomics **4:**1633-1649.

39.   **Bochkov, Y., and A. C. Palmenberg.** 2006. Translational efficiency of an EMCV IRES in bicistronic vectors is dependent upon IRES sequence and gene location. BioTechniques **41:**238-290.

40.   **Bochkov, Y. A., and J. E. Gern.** 2012. Clinical and molecular features of human rhinovirus C. Microbes and Infection **14:**485-94.

41. **Bochkov, Y. A., A. C. Palmenberg, W.-M. Lee, J. A. Rathe, S. P. Amineva, X. Sun, T. R. Pasic, N. N. Jarjour, S. B. Liggett, and J. E. Gern.** 2011. Molecular modeling, organ culture and reverse genetics for a newly identified human rhinovirus C. Nature Medicine **17:**627-32.

42. **Boege, U., D. Kobasa, S. Onodera, D. G. Scraba, G. D. Parks, and A. C. Palmenberg.** 1991. Characterization of Mengo virus neutralization epitopes. Virology **181:**1-13.

43. **Borghese, F., and T. Michiels.** 2011. The leader protein of cardioviruses inhibits stress granule assembly. J. Virol. **85:**9614-22.

44. **Butterworth, B. E., and R. R. Rueckert.** 1972. Kinetics of synthesis and cleavage of encephalomyocarditis virus-specific polypeptides. Virology **50:**535-549.

45. **Calado, A., U. Kutay, U. Kuhn, E. Wahle, and M. Carmo-Fonseca.** 2000. Deciphering the cellular pathway for transport of poly(A)-binding protein II. RNA **6:**245-56.

46. **Calenoff, M. A., C. S. Badshah, M. C. Dal Canto, H. L. Lipton, and M. K. Rundell.** 1995. The leader polypeptide of Theiler's virus is essential for neurovirulence but not for virus growth in BHK cells. J.Virol. **69:**5544-5549.

47. **Calenoff, M. A., K. S. Faaberg, and H. L. Lipton.** 1990. Genomic regions of neurovirulence and attenuation in Theiler murine encephalomyelitis virus. Proc.Nat.Acad.Sci.U.S.A. **87:**978-982.

48. **Calvert, M. E. K., K. M. Keck, C. Ptak, J. Shabanowitz, D. F. Hunt, and L. F. Pemberton.** 2008. Phosphorylation by Casein Kinase 2 Regulates Nap1 Localization and Function. Mol Cell Biol **28:**1313-1325.

49. **Carocci, M., and L. Bakkali-Kassimi.** 2012. The encephalomyocarditic virus. Virulence **3:**351-367.

50. **Carocci, M., and L. Bakkali-Kassimi.** 2012. The encephalomyocarditis virus. Virulence **3:**351-367.

51. **Carocci, M., N. Cordonnier, H. Huet, A. Romev, A. Relmy, K. Gorna, S. Blaise-Boisseau, S. Zientara, and L. B. Kassimi.** 2011. Encephalomyocarditis Virus 2A Protein Is Required for Viral Pathogenesis and Inhibition of Apoptosis. J Virol **85:**10741-10754.

52. **Chapman, M. S., I. Minor, M. G. Rossmann, G. D. Diana, and K. Andries.** 1991. Human rhinovirus 14 complexed with antiviral compound R61837. J Mol Biol **217:**455-63.

53. **Chatel, G., and B. Fahrenkrog.** 2012. Dynamics and diverse functions of nuclear pore complex proteins. Nucleus **3:**162-171.

54. **Chen, H.-H., W.-P. Kong, and R. P. Roos.** 1995. The leader peptide of Theiler's murine encephalomyelitis virus is a zinc-binding protein. J.Virol. **69:**8076-8078.

55. **Chen, H. H., W. P. Kong, L. Zhang, P. L. Ward, and R. P. Roos.** 1995. A picornaviral protein synthesized out of frame with the polyprotein plays a key role in a virus-induced immune-mediated demyelinating disease. Nat Med **1:**927-931.

56. **Chen, K., X. Xu, S. Kobayashi, D. Timm, T. Jepperson, and Q. Liang.** 2011. Caloric Restriction Mimetic 2-Deoxyglucose Antagonizes Doxorubicin-induced Cardiomyocyte Death by Multiple Mechanisms. J Biol Chem **286:**21993-22006.

57. **Chinsangaram, J., M. E. Piccone, and M. J. Grubman.** 1999. Ability of foot-and-mouth disease virus to form plaques in cell culture is associated with suppression of alpha/beta interferon. J Virol **73:**9891-9898.

58. **Chiu, C. Y., A. L. Greninger, E. C. Chen, T. D. Haggerty, J. Parsonnet, E. Delwart, J. L. Derisi, and D. Ganem.** 2010. Cultivation and serological characterization of a human Theiler's-like cardiovirus associated with diarrheal disease. J Virol **84:**4407-4414.

59. **Chiu, C. Y., A. L. Greninger, K. Kanada, T. Kwok, K. F. Fischer, C. Runckel, J. K. Louie, C. A. Glaser, S. Yagi, D. P. Schnurr, T. D. Haggerty, J. Parsonnet, D. Ganem, and J. L. DeRisi.** 2008. Identification of cardioviruses related to Theiler's murine encephalomyelitis virus in human infections. PNAS **105:**14124-14129.

60. **Cho, M. W., N. Teterina, D. Egger, K. Bienz, and E. Ehrenfeld.** 1994. Membrane rearrangement and vesicle induction by recombinant poliovirus 2C and 2BC in human cells. Virology **202:**129-145.

61. **Choe, S. S., D. A. Dodd, and K. Kirkegaard.** 2005. Inhibition of cellular protein secretion by picornaviral 3A proteins. Virology **337:**18-29.

62. **Chumakov, K. M., and A. S. Karavanov.** 1986. Preliminary characterization of an organism isolated from a case of Viluy encephalomyelitis indicates a protozoal, rather than viral, aetiology. J Gen Microbiol **132:**1127-1133.

63. **Conti, E., C. W. Muller, and M. Stewart.** 2006. Karyopherin flexibility in nucleocytoplasmic transport. Curr Opin Struct Biol **16:**237-244.

64. **Cornilescu, C. C., F. W. Porter, Q. Zhao, A. C. Palmenberg, and J. L. Markley.** 2008. NMR structure of the Mengovirus leader protein zinc-finger domain. FEBS Letters **582:**896-900.

65. **Corton, J. M., J. G. Gillespie, S. A. Hawley, and D. G. Hardie.** 1995. 5-aminoimidazole-4-carboxamide ribonucleoside. A specific method for activating AMP-activated protein kinase in intact cells? Eur J Biochem **229:**558-565.

66. **Coulombe, P., G. Rodier, S. Pelletier, J. Pellerin, and S. Meloche.** 2003. Rapid turnover of extracellular signal-regulated kinase 3 by the ubiquitin-proteasome pathway defines a novel paradigm of mitogen-activated protein kinase regulation during cellular differentiation. Mol Cell Biol **23:**4542-4558.

67. **Cozzetto, D., A. Kryshtafovych, K. Fidelis, J. Moult, B. Rost, and A. Tramontano.** 2009. Evaluation of template-based models in CASP8 with standard measures. Proteins **77:**18-28.

68. **Crampton, N., M. Kodiha, S. Shrivastava, R. Umar, and U. Stochaj.** 2009. Oxidative stress inhibits nuclear protein export by multiple mechanisms that target FG nucleoporins and Crm 1. Mol Biol Cell **20:**5106-16.

69. **Crooks, G. E., G. Hon, J.-M. Chandonia, and S. E. Brenner.** 2004. WebLogo: A Sequence Logo Generator. Genome Res **14:**1188-1190.

70. **Crute, B. E.** 1998. Functional Domains of the alpha 1 Catalytic Subunit of the AMP-activated Protein Kinase. J Biol Chem **273:**35347-35354.

71. **Czubryt, M. P., J. A. Austria, and G. N. Pierce.** 2000. Hydrogen peroxide inhibition of nuclear protein import is mediated by the mitogen-activated protein kinase, ERK2. J Cell Biol **148:**7-16.

72. **de Jong, A. S.** 2003. Determinants for Membrane Association and Permeabilization of the Coxsackievirus 2B Protein and the Identification of the Golgi Complex as the Target Organelle. J Biol Chem **278:**1012-1021.

73. **de Jong, A. S., F. de Mattia, M. M. Van Dommelen, K. Lanke, W. J. G. Melchers, P. H. G. M. Willems, and F. J. M. van Kuppeveld.** 2008. Functional analysis of picornavirus 2B proteins: Effects on calcium homeostasis and intracellular protein trafficking. J Virol **82:**3782-3790.

74. **de Jong, A. S., I. W. J. Schrama, P. H. G. M. Willems, J. M. D. Jochem, W. J. G. Melchers, and F. J. M. van Kuppeveld.** 2002. Multimerization reactions of coxsackievirus proteins 2B, 2C and 2BC: a mammalian two-hybrid analysis. J Gen Virol **83:**783-793.

75. **Delhaye, S., V. van Pesch, and T. Michiels.** 2004. The leader protein of Theiler's virus interferes with nucleocytoplasmic trafficking of cellular proteins. J Virol **78:**4357-62.

76. **Denis, P., H. D. Liebig, N. Nowotny, C. Billinis, O. Papadopoulos, R. S. O'Hara, N. S. Knowles, and F. Koenen.** 2006. Genetic variability of encephalomyocarditis virus (EMCV) isolates. Vet Microbiol **113:**1-12.

77. **Dever, T. E.** 2002. Gene-specific regulation by general translation factors. Cell **108**.

78. **Doedens, J. R., and K. Kirkegaard.** 1995. Inhibition of cellular protein secretion by poliovirus proteins 2B and 3A. EMBO J. **14:**894-907.

79. **Donnelly, M. L., L. E. Hughes, G. Luke, H. Mendoza, E. ten Dam, D. Gani, and M. D. Ryan.** 2001. The 'cleavage' activities of foot-and-mouth disease virus 2A site-directed mutants and naturally occurring '2A-like' sequences. J Gen Virol **82:**1027-1041.

80. **Donnelly, M. L., G. Luke, A. Mehrotra, X. Li, L. E. Hughes, D. Gani, and M. D. Ryan.** 2001. Analysis of the aphthovirus 2A/2B polyprotein 'cleavage' mechanism indicates not a proteolytic reaction, but a novel translational effect: a putative ribosomal 'skip'. J Gen Virol **82:**1013-1025.

81. **Dougherty, R. H., and J. V. Fahy.** 2009. Acute exacerbations of asthma: epidemiology, biology and the exacerbation-prone phenotype. Clin Exp Allergy **39:**193-202.

82. **Drexler, J. F., L. K. Luna, A. Stocker, P. S. Almeida, T. C. Ribeiro, N. Petersen, P. Herzog, C. Pedroso, H. I. Huppertz, H. C. J. Ribeiro, S. Baumgarte, and C. Drosten.** 2008. Circulation of 3 lineages of a novel Saffod cardiovirus in humans. Emerg Infect Dis **14:**1398-1405.

83. **Duke, G. M., J. E. Osorio, and A. C. Palmenberg.** 1990. Attenuation of Mengo virus through genetic engineering of the 5' noncoding poly(C) tract. Nature **343:**474-476.

84. **Duke, G. M., and A. C. Palmenberg.** 1989. Cloning and synthesis of infectious cardiovirus RNAs containing short, discrete poly(C) tracts. J.Virol. **63:**1822-1826.

85. **Duncan, J. S., and D. W. Litchfield.** 2008. Too much of a good thing: the role of protein kinase CK2 in tumorigenesis and prospects for therapeutic inhibition of CK2. Biochim Biophys Acta **1784:**33-47.

86. **Dvorak, C. M. T., D. J. Hall, M. Hill, M. Riddle, A. Pranter, J. Dillman, M. Deibel, and A. C. Palmenberg.** 2001. Leader protein of encephalomyocarditis virus binds zinc, is phosphorylated during viral infection and affects the efficiency of genome translation. Virology **290:**261-271.

87. **Emara, M. M., and M. A. Brinton.** 2007. Interaction of TIA-1/TIAR with West Nile and dengue virus products in infected cells interferes with stress granule formation and processing body assembly. PNAS **104:**9041-9046.

88. **Enslen, H., D. M. Brancho, and R. J. Davis.** 2000. Molecular determinants that mediate selective activation of p38 MAP kinase isoforms. EMBO J **19:**1301-11.

89. **Faria, P. A., P. Chakraborty, A. Levay, G. N. Barber, H. J. Ezelle, J. Enninga, C. Arana, J. van Deursen, and B. M. Fontoura.** 2005. VSV disrupts the Rae1/mrnp41 mRNA nuclear export pathway. Mol Cell **17:**93-102.

90. **Fiol, C. J., A. Wang, R. W. Roeske, and P. J. Roach.** 1990. Ordered multisite protein phosphorylation. Analysis of glycogen synthase kinase 3 action using model peptide substrates. J Biol Chem **265:**6061-5.

91. **Flotow, H., P. R. Graves, A. Q. Wang, C. J. Fiol, R. W. Roeske, and P. J. Roach.** 1990. Phosphate groups as substrate determinants for casein kinase I action. J Biol Chem **265:**14264-14269.

92. **Fontoura, B. M., G. Blobel, and N. R. Yaseen.** 2000. The nucleoporin Nup98 is a site for GDP/GTP exchange on ran and termination of karyopherin beta 2-mediated nuclear import. J Biol Chem **275:**31289-96.

93. **Forwood, J. K., A. Brooks, L. J. Briggs, C. Y. Xiao, D. A. Jans, and S. G. Vasudevan.** 1999. The 37-amino-acid interdomain of dengue virus NS5 protein contains a functional NLS and inhibitory CK2 site. Biochem Biophys Res Comm **257:**731-7.

94. **Fuller, K. G., J. K. Olson, L. M. Howard, J. L. Croxford, and S. D. Miller.** 2004. Mouse models of multiple sclerosis: experimental autoimmune encephalomyelitis and Theiler's virus-induced demyelinating disease. Methods Mol Med **102:**339-361.

95. **Gerety, S. J., W. J. Karpus, A. R. Cubbon, R. G. Goswami, M. K. Rundell, J. D. Peterson, and S. D. Miller.** 1994. Class II-restricted T cell responses in Theiler's murine encephalomyelitis virus-induced demyelinating disease. V. Mapping of a dominant immunopathologic VP2 T cell epitope in susceptible SJL/J mice. J Immunol **152:**908-918.

96. **Gern, J. E., and W. W. Busse.** 1999. Association of rhinovirus infections with asthma. Clin Microbiol Rev **12:**9-18.

97. **Ghadge, G. D., L. Ma, S. Sato, J. H. Kim, and R. P. Roos.** 1998. A protein critical for a Theiler's virus-induced immune system-mediated demyelinating disease has a cell type-specific antiapoptotic effect and a key role in virus persistence. J Virol **72:**8605-8612.

98. **Ghadge, G. D., R. Wollmann, G. Baida, M. Traka, and R. P. Roos.** 2011. The L-Coding Region of the DA Strain of Theiler's Murine Encephalomyelitis Virus Causes Dysfunction and Death of Myelin-Synthesizing Cells. J Virol **85:**9377-9384.

99. **Gilchrist, D.** 2002. Accelerating the Rate of Disassembly of Karyopherin-Cargo Complexes. J Biol Chem **277:**18161-18172.

100. **Gnad, F., J. Gunawardena, and M. Mann.** 2011. PHOSIDA 2011: the posttranslational modification database. Nucleic acids research **39:**D253-D260.

101. **Gouet, P., and E. Courcelle.** 2002. ENDscript: a workflow to display sequence and structure information. Bioinformatics **18:**767-8.

102. **Grankowski, N., B. Boldyreff, and O. G. Issinger.** 1991. Isolation and characterization of recombinant human casein kinase II subunits alpha and beta from bacteria. Eur J Biochem / FEBS **198:**25-30.

103. **Green, A. J., T. M. Sivtseva, A. P. Danilova, V. L. Osakovsky, V. A. Vladimirtsev, M. Zeidler, R. S. Knight, F. A. Platonov, A. Shatunov, V. P. Alekseev, V. G. Krivoshapkin, C. L. Masters, D. C. Gajdusek, and L. G. Goldfarb.** 2003. Viliuisk encephalomyelitis: intrathecal synthesis of oligoclonal IgG. J Neurol Sci **212:**69-73.

104. **Groppo, R., B. A. Brown, and A. C. Palmenberg.** 2011. Mutational analysis of EMCV 2A protein identifies a nuclear localization signal and an eIF4E binding site. Virology **410:**257-267.

105. **Groppo, R., and A. Palmenberg.** 2007. Cardiovirus 2A protein associates with 40S but not 80S ribosome subunits during infection. J. Virol. **81:**13067-13074.

106. **Hadfield, A. T., G. D. Diana, and M. G. Rossmann.** 1999. Analysis of three structurally related antiviral compounds in complex with human rhinovirus 16. PNAS **96:**14730-5.

107. **Hadfield, A. T., M. A. Oliveira, K. H. Kim, I. Minor, M. J. Kremer, B. A. Heinz, D. Shepard, D. C. Pevear, R. R. Rueckert, and M. G. Rossmann.** 1995. Structural studies on human rhinovirus 14 drug-resistant compensation mutants. J Mol Biol **253:**61-73.

108. **Hahn, H., and A. C. Palmenberg.** 2001. Deletion mapping of the encephalomyocarditis virus 2A protein and the adjacent primary cleavage site. J.Virol. **75:**7215-7218.

109. **Hahn, H., and A. C. Palmenberg.** 1995. Encephalomyocarditis viruses with short poly(C) tracts are more virulent than their Mengo virus counterparts. J.Virol. **69:**2697-2699.

110. **Hahn, H., and A. C. Palmenberg.** 1996. Mutational analysis of the encephalomyocarditis virus primary cleavage. J.Virol. **70:**6870-6875.

111. **Hao, W., K. Bernard, N. Patel, N. Ulbrandt, H. Feng, C. Svabek, S. Wilson, C. Stracener, K. Wang, J. Suzich, W. Blair, and Q. Zhu.** 2012. Infection and propagation of human rhinovirus C in human airway epilethial cells. J Virol **86:**24-32.

112. **Hardie, D. G.** 2007. AMP-activated/SNF1 protein kinases: conserved guardians of cellular energy. Nat Rev Mol Cel Biol **8:**774-785.

113. **Hardie, D. G., and D. Carling.** 1997. The AMP-activated protein kinase--fuel gauge of the mammalian cell?. Eur J Biochem **246:**259-273.

114. **Hato, S. V., C. Ricour, B. M. Schulte, K. H. Lanke, M. de Bruijni, J. Zoll, W. J. Melchers, T. Michiels, and F. J. van Kuppeveld.** 2007. The mengovirus leader protein blocks interferon-alpha/beta gene transcription and inhibits activation of interferon regulatory factor 3. Cell Microbiol **9:**2921-2930.

115. **Hawley, S. A., J. Boudeau, J. L. Reid, K. J. Mustard, L. Udd, T. P. Mäkelä, D. R. Alessi, and D. G. Hardie.** 2003. Complexes between the LKB1 tumor suppressor, STRAD alpha/beta and MO25 alpha/beta are upstream kinases in the AMP-activated protein kinase cascade. J Biol **2:**28.

116. **Hawley, S. A., D. A. Pan, K. J. Mustard, L. Ross, J. Bain, A. M. Edelman, B. G. Frenguelli, and D. G. Hardie.** 2005. Calmodulin-dependent protein kinase kinase-beta is an alternative upstream kinase for AMP-activated protein kinase. Cell Metab **2:**9-19.

117. **Hayden, F. G.** 2004. Rhinovirus and the lower respiratory tract. Rev Med Virol **14:**17-31.

118. **Hayden, F. G., D. T. Herrington, T. L. Coats, K. Kim, E. C. Cooper, S. A. Villano, S. Liu, S. Hudson, D. C. Pevear, M. Collett, and M. McKinlay.** 2003. Efficacy and safety of oral pleconaril for treatment of colds due to picornaviruses in adults: results of 2 double-blind, randomized, placebo-controlled trials. Clinical Infectious Diseases **36:**1523-32.

119. **Heinz, B. A., R. R. Rueckert, D. A. Shepard, F. J. Dutko, M. A. McKinlay, M. Fancher, M. G. Rossmann, J. Badger, and T. J. Smith.** 1989. Genetic and molecular analyses of spontaneous mutants of human rhinovirus 14 that are resistant to an antiviral compound. J Virol **63:**2476-2485.

120. **Heizmann, B., M. Reth, and S. Infantino.** 2010. Syk is a dual-specificity kinase that self-regulates the signal output from the B-cell antigen receptor. PNAS **107:**18563-18568.

121. **Hellen, C. U. Y., and E. Wimmer.** 1995. Enterovirus structure and assembly, p. 155-170. *In* H. A. Robart (ed.), Human Enterovirus Infections. ASM Press, Washington, D.C.

122. **Henderson, A. P. D., M. H. Barnett, J. D. E. Parratt, and J. W. Prineas.** 2009. Multiple sclerosis: Distribution of inflammatory cells in newly forming lesions. Ann Neurol **66:**739-753.

123. **Herold, J., and R. Andino.** 2000. Poliovirus requires a precise 5' end for efficient positive-strand RNA synthesis. J Virol **74:**6394-400.

124. **Hertzler, S., Z. Liang, B. Treso, and H. L. Lipton.** 2011. Adaptation of Saffold virus 2 for high-titer growth in mammalian cells. J Virol **85:**7411-8.

125. **Hewat, E. A., E. Neumann, J. F. Conway, R. Moser, B. Ronacher, T. C. Marlovits, and D. Blass.** 2000. The cellular receptor to human rhinovirus 2 binds around the 5-fold axis and not in the canyon: a structural view. EMBO J **19:**6317-6325.

126. **Himeda, T., T. Hosomi, T. Okuwa, Y. Muraki, and Y. Ohara.** 2013. Saffold Virus Type 3 (SAFV-3) Persists in HeLa Cells. PloS one **8:**e53194.

127. **Himeda, T., Y. Ohara, K. Asakura, Y. Kontani, M. Murakami, H. Suzuki, and M. Sawada.** 2005. A lentiviral expression system demonstrates that L* protein of Theiler's murine encephalomyelitis virus (TMEV) is essential for virus growth in a murine macrophage-like cell line. Virus Res **108:**23-28.

128. **Hindiyeh, M., Q. H. Li, R. Basavappa, J. M. Hogle, and M. Chow.** 1999. Poliovirus mutants at histidine 195 of VP2 do not cleave VP0 into VP2 and VP4. J. Virol. **73:**9072-9079.

129. **Ho, S. H., H. D. Hunt, R. M. Horton, J. K. Pullen, and L. R. Pease.** 1989. Site-directed mutagenesis by overlap extension using the polymerase chain reaction. Gene **77:**51-59.

130. **Hogle, J. M.** 2002. Poliovirus cell entry: common structural themes in viral cell entry pathways. Ann Rev Microbiol **56:**677-702.

131. **Hollinger, S., and J. R. Hepler.** 2004. Methods for measuring RGS protein phosphorylation by G protein-regulated kinases. Methods Mol Biol. **237:**205-19.

132. **Hornbeck, P., J. Kornhauser, S. Tkachev, B. Zhang, E. Skrzypek, B. Murray, V. Latham, and M. Sullivan.** 2012. PhosphoSitePlus: a comprehensive resource for investigating the structure and function of experimentally determined post-translational modifications in man and mouse. Nuc Acids Res **40:**D261-D270.

133. **Huber, S. A.** 1994. VCAM-1 is a receptor for encephalomyocarditis virus on a murine vascular endothelial cells. J.Virol. **68:**3453-3458.

134. **Hurley, R. L., L. K. Barre, S. D. Wood, K. A. Anderson, B. E. Kemp, A. R. Means, and L. A. Witters.** 2006. Regulation of AMP-activated Protein Kinase by Multisite Phosphorylation in Response to Agents That Elevate Cellular cAMP. J Biol Chem **281:**36662-36672.

135. **Hutten, S., and R. H. Kehlenbach.** 2007. CRM1-mediated nuclear export: to the pore and beyond. Trends Cell Biol **17:**193-201.

136. **Hutten, S., and R. H. Kehlenbach.** 2006. Nup214 is required for CRM1-dependent nuclear protein export in vivo. Mol Cell Biol **26:**6772-85.

137. **Hutten, S., S. Walde, C. Spillner, J. Hauber, and R. H. Kehlenbach.** 2009. The nuclear pore component Nup358 promotes transportin-dependent nuclear import. J Cell Sci **122:**1100-1110.

138. **Iakoucheva, L. M., P. Radivojac, C. J. Brown, T. R. O'Connor, J. G. Sikes, Z. Obradovic, and A. K. Dunker.** 2004. The importance of intrinsic disorder for protein phosphorylation. Nuc Acids Res **32:**1037-49.

139. **Iijima, M., M. Suzuki, A. Tanabe, A. Nishimura, and M. Yamada.** 2006. Two motifs essential for nuclear import of the hnRNP A1 nucleocytoplasmic shuttling sequence M9 core. FEBS Lett **580:**1365-70.

140. **Itagaki, I., C. Abiko, Y. Aoki, T. Ikeda, K. Mizuta, M. Noda, H. Kimura, and Y. Matsuzaki.** 2011. Saffold cardiovirus infection in children associated with respiratory disease and its similarity to coxsackievirus infection. Pediatr Infect Dis J. **8:**680-683.

141. **Itagaki, T., C. Abiko, T. Ikeda, Y. Aoki, J. Seto, K. Mizuta, T. Ahiko, H. Tsukagoshi, M. Nagano, M. Noda, T. Mizutani, and H. Kimura.** 2010. Sequence and phylogenetic analyses of Saffold cardiovirus from children with exudative tonsillitis in Yamagata, Japan. Scand J Infect Dis **42:**950-952.

142. **Jackson, D. J., R. E. Gangnon, M. D. Evans, K. A. Roberg, E. L. Anderson, T. Pappas, M. Printz, W. Lee, P. Shult, E. Reisdorf, K. Carlson-Dakes, L. Salazar, D. Dasilva, C. Tisler, J. Gern, and R. Lemanske.** 2008. Wheezing Rhinovirus Illnesses in Early Life Predict Asthma Development in High-Risk Children. Am J Respir Crit Care Med **178:**667-672.

143. **Jackson, R. J., and A. Kaminski.** 1995. Internal initiation of translation in eucaryotes: The picornavirus paradigm and beyond. RNA **1:**985-1000.

144. **Jang, S. K., M. V. Davies, R. J. Kaufman, and E. Wimmer.** 1989. Initiation of protein synthesis by the internal entry of ribosomes into the 5' nontranslated region of encephalomyocarditisvirus RNA in vivo. J.Virol. **63:**1651-1660.

145. **Jelachich, M. L., C. Bramlage, and H. L. Lipton.** 1999. Differentiation of M1 myeloid precursor cells into macrophages results in binding and infection by Theiler's murine encephalomyelitis virus and apoptosis. J Virol **73:**3227-3235.

146. **Ji, W. T., L. H. Lee, F. L. Lin, L. Wang, and H. J. Liu.** 2009. AMP-activated protein kinase facilitates avian reovirus to induce mitogen-activated protein kinase (MAPK) p38 and MAPK kinase 3/6 signalling that is beneficial for virus replication. J Gen Virol **90:**3002-3009.

147. **Jones, M. S., V. V. Lukashov, R. D. Ganac, and D. P. Schnurr.** 2007. Discovery of a novel human picornavirus in a stool sample from a pediatric patient presenting with fever of unknown origin. J Clin Microbiol **45:**2144-2150.

148. **Jones, M. S., V. V. Lukashov, R. D. Ganac, and D. P. Schnurr.** 2007. Discovery of a novel human picornavirus in a stool sample from a pediatric patient presenting with fever of unknown origin. J. Clin. Microbiol. **45:**2144-2150.

149. **Kaminski, A., S. L. Hunt, J. G. Patton, and R. J. Jackson.** 1995. Direct evidence that polypyrimidine tract binding protein (PTB) is essential for internal initiation of translation of encephalomyocarditis virus RNA. RNA **1:**924-938.

150. **Kapikian, A. Z.** 1967. Rhinoviruses: A numbering system. Nature **213:**761-762.

151. **Karlsson, M.** 2004. Both Nuclear-Cytoplasmic Shuttling of the Dual Specificity Phosphatase MKP-3 and Its Ability to Anchor MAP Kinase in the Cytoplasm Are Mediated by a Conserved Nuclear Export Signal. J Biol Chem **279:**41882-41891.

152. **Kataoka, N., J. L. Bachorik, and G. Dreyfuss.** 1999. Transportin-SR, a nuclear import receptor for SR proteins. The Journal of Cell Biology **145:**1145-1152.

153. **Katz, E.** 2005. MMTV Env encodes an ITAM responsible for transformation of mammary epithelial cells in three-dimensional culture. J Exp Med **201:**431-439.

154. **Kazgan, N., T. Williams, L. J. Forsberg, and J. E. Brenman.** 2010. Identification of a nuclear export signal in the catalytic subunit of AMP-activated protein kinase. Mol Cell Biol **21:**3433-3442.

155. **Keating, J., and R. Striker.** 2011. Phosphorylation events during viral infections provide potential therapeutic targets. Rev Med Virol **22:**166-181.

156. **Kehlenbach, R. H., R. Assheuer, A. Kehlenbach, J. Becker, and L. Gerace.** 2001. Stimulation of nuclear export and inhibition of nuclear import by a Ran mutant deficient in binding to Ran-binding protein 1. J Biol Chem **276:**14524-14531.

157. **Khetsuriani, N., D. R. Prevots, L. Quick, M. E. Elder, M. Pallanch, O. Kew, and R. W. Sutter.** 2003. Persistence of vaccine-derived polioviruses among immunodeficient persons with vaccine-associated paralytic poliomyelitis. J Infect Dis **188:**1845-1852.

158. **Kim, D., D. Chivian, and D. Baker.** 2004. Protein structure prediction and analysis using the Robetta server. Nucleic Acids Research **32:**526-531.

159. **Kirkegaard, K.** 2009. Current Topics in Microbiology and Immunology. **335:**323-333.

160. **Klebe, C., H. Prinz, A. Wittinghofer, and R. S. Goody.** 1995. The kinetic mechanism of Ran-nucleotide exchange catalyzed by RCC1. Biochemistry **34:**12543-12552.

161. **Kodiha, M., J. G. Rassi, C. M. Brown, and U. Stochai.** 2007. Localization of AMP kinase is regulated by stress, cell density, and signaling through the MEK->ERK1/2 pathway. Cell Phys **293:**C1427-C1436.

162. **Kodiha, M., D. Tran, A. Morogan, C. Qian, and U. Stochai.** 2009. Dissecting the Signaling Events That Impact Classical Nuclear Import and Target Nuclear Transport Factors. Plos One **4:**8420.

163. **Kolatkar, P. R., J. Bella, N. H. Olson, C. M. Bator, T. S. Baker, and M. G. Rossmann.** 1999. Structural studies of two rhinovirus serotypes complexed with fragments of their cellular receptor. EMBO J **18:**6249-59.

164. **Kong, W.-P., G. D. Ghadge, and R. P. Roos.** 1994. Involvement of cardiovirus leader in host-restricted virus expression. Proc.Natl.Acad.Sci.U.S.A. **91:**1796-1800.

165. **Kosako, H., and N. Imamoto.** 2010. Phosphorylation of nucleoporins. Signal transduction-mediated regulation of their interaction with nuclear transport receptors. Nucleus **1:**309-313.

166. **Kosako, H., N. Yamaguchi, C. Aranami, M. Ushiyama, S. Kose, N. Imamoto, H. Taniguchi, E. Nishida, and S. Hattori.** 2009. Phosphoproteomics reveals new ERK MAP kinase targets and links ERK to nucleoporin-mediated nuclear transport. Nat Struct Mol Biol **16:**1026-1035.

167.   **Kumar, A. S. M., P. Kallio, M. Luo, and H. L. Lipton.** 2003. Amino acid substitutions in VP2 residues contacting sialic acid in low-neurovirulence BeAn virus dramatically reduce viral binding and spread of infection. J Virol **77:**2709-16.

168.   **Kumar, S. H., and A. Rangarajan.** 2009. Simian Virus 40 Small T Antigen Activates AMPK and Triggers Autophagy To Protect Cancer Cells from Nutrient Deprivation. J Virol **83:**8565-8574.

169.   **La Cour, T.** 2003. NESbase version 1.0: a database of nuclear export signals. Nuc Acids Res **31:**393-396.

170.   **Lagunoff, M., L. D.M., and D. Ganem.** 2001. Immunoreceptor tyrosine-based activation motif-dependent signaling by Kaposi's sarcoma-associated herpesvirus K1 protein: effects on lytic viral replication. J Virol **75:**5891-5898.

171.   **Lai, M. C.** 2000. A Human Importin-beta Family Protein, Transportin-SR2, Interacts with the Phosphorylated RS Domain of SR Proteins. J Biol Chem **275:**7950-7957.

172.   **Lai, M. C., R. I. Lin, and W. Y. Tarn.** 2001. Transportin-SR2 mediates nuclear import of phosphorylated SR proteins. PNAS **98:**10154-10159.

173.   **Lama, J., A. K. Paul, K. S. Harris, and E. Wimmer.** 1994. Properties of purified recombinant poliovirus protein 3AB as substrate for viral proteinases and as co-factor for RNA polymerase 3D. . J. Biol. Chem. **269:**66-70.

174.   **Lange, A., R. E. Mills, C. J. Lange, M. Stewart, S. E. Devine, and A. H. Corbett.** 2006. Classical Nuclear Localization Signals: Definition, Function, and Interaction with Importin J Biol Chem **282:**5101-5105.

175.   **Larkin, M., G. Blackshields, N. Brown, R. Chenna, P. McGettigan, H. McWilliam, F. Valentin, I. Wallace, A. Wilm, R. Lopez, J. Thompson, T. Gibson, and D. Higgins.** 2007. Clustal W and Clustal X version 2.0. Bioinformatics (Oxford, England) **23:**2947-2948.

176.   **Laskowski, R. A., M. M.W., D. S. Moss, and J. M. Thornton.** 1993. PROCHECK: a program to check the stereochemical quality of protein structures. J Appl Cryst **26:**283-291.

177.   **Lawson, T. G., D. L. Gronros, J. A. Werner, A. C. Wey, A. M. DiGeorge, J. L. Lockhard, J. W. Wilson, and P. L. Wintrode.** 1994. The encephalomyocarditis virus 3C protease is a substrate for the ubiquitin-mediated proteolytic system. J Biol Chem **269:**28429-28435.

178.   **Ledford, R. M., M. S. Collett, and D. C. Pevear.** 2005. Insights into the genetic basis for natural phenotypic resistance of human rhinoviruses to pleconaril. Antiviral Research **68:**135-138.

179.   **Ledford, R. M., N. R. Patel, T. M. Demenczuk, A. Watanyar, T. Herbertz, M. S. Collett, and D. C. Pevear.** 2004. VP1 sequencing of all human rhinovirus serotypes: insights into genus phylogeny and susceptibility to antiviral capsid-binding compounds. J Virol **78:**3663-74.

180.   **Lee, B.-S., S.-H. Lee, P. Feng, J. R. Chang, N.-H. Cho, and J. U. Jung.** 2005. Characterization of the Kaposi's sarcoma-associated herpesvirus K1 signalosome. J Virol **79:**12173-12184.

181.   **Lee, W.-M., R. F. Lemanske, M. D. Evans, F. Vang, T. Pappas, R. Gangnon, D. J. Jackson, and J. E. Gern.** 2012. Human rhinovirus species and season of infection determine illness severity. Am. J. Respir. Crit. Care Med. **186:**886-891.

182.   **Lee, W. M., W. Wang, and R. R. Rueckert.** 1995. Complete sequence of the RNA genome of human rhinovirus 16, a clinically useful common cold virus belonging to the ICAM-1 receptor group. Virus Genes **9:**177-181.

183.   **Lidsky, P. L., S. Hato, M. V. Bardina, A. G. Aminev, A. C. Palmenberg, E. V. Sheval, V. Y. Polyakov, F. J. van Kuppeveld, and V. Agol.** 2006. Nucleo-cytoplasmic traffic disorder induced by cardioviruses. J. Virol. **80:**2705-2717.

184.   **Lindsay, M. E., J. M. Holaska, K. Welch, B. M. Paschal, and I. G. Macara.** 2001. Ran-binding protein 3 is a cofactor for Crm1-mediated nuclear protein export. J Cell Biol **153:**1391-1402.

185.   **Lipton, H. L.** 2008. Human Vilyuisk encephalitis. Rev Med Virol **18:**347-352.

186.   **Lipton, H. L.** 1980. Persistent Theiler's murine encephalomyelitis virus infection in mice depends on plaque size. J Gen Virol **46:**169-177.

187.   **Lipton, H. L., G. Twaddle, and M. L. Jelachich.** 1995. The predominant virus antigen burden is present in macrophages in Theiler's murine encephalomyelitis virus-induced demyelinating disease. J Virol **69:**2525-2533.

188.   **Litchfield, D. W.** 2003. Protein kinase CK2: structure, regulation and role in cellular decisions of life and death. Biochem J **369:**1-15.

189. **Lobert, P. E., N. Escriou, J. Ruelle, and T. Michiels.** 1999. A coding RNA sequence acts as a replication signal. Proc.Natl.Acad.Sci.U.S.A. **96:**11560-11565.

190. **Loughran, G., A. E. Flrth, and J. F. Atkins.** 2011. Ribosomal frameshifting into an overlapping gene in the 2B-encoding region of the cardiovirus genome. PNAS **108:**1111-1119.

191. **Lu, J.** 2006. Syk Tyrosine Kinase Mediates Epstein-Barr Virus Latent Membrane Protein 2A-induced Cell Migration in Epithelial Cells. J Biol Chem **281:**8806-8814.

192. **Luke, G. A., P. De Felipe, A. Lukashev, S. E. Kallioinen, E. A. Bruno, and M. D. Ryan.** 2008. Occurrence, function and evolutionary origins of '2A-like' sequences in virus genomes. J Gen Virol **89:**1036-1042.

193. **Lupyan, D., A. Leo-Macias, and A. Ortiz.** 2005. A new progressive-iterative algorithm for multiple structure alignment. Bioinformatics **21:**3255-3263.

194. **Luz, S., P. Kongsuphol, A. Mendes, F. Romeiras, M. Sousa, R. Schreiber, P. Matos, P. Jordan, A. Mehta, M. Amaral, K. Kunzelmann, and C. Farinha.** 2011. Contribution of Casein Kinase 2 and Spleen Tyrosine Kinase to CFTR Trafficking and Protein Kinase A-Induced Activity. Mol Cell Biol **31:**4392-4404.

195. **Macaulay, C., E. Meier, and D. J. Forbes.** 1995. Differential mitotic phosphorylation of proteins of the nuclear pore complex. J Biol Chem **270:**254-62.

196. **Madshus, I. H., S. Olsnes, and K. Sandvig.** 1984. Different pH requirements for entry of the two picornaviruses, human rhinovirus 2 and murine encephalomyocarditis virus. Virology **139:**346-357.

197. **Mankouri, J., and M. Harris.** 2011. Viruses and the fuel sensor: the emerging link between AMPK and virus replication. Rev Med Virol **21:**205-12.

198. **Mankouri, J., P. R. Tedbury, S. Gretton, M. E. Hughes, S. D. C. Griffin, M. L. Dallas, K. A. Green, D. G. Hardie, C. Peers, and M. Harris.** 2010. Enhanced hepatitis C virus genome replication and lipid accumulation mediated by inhibition of AMP-activated protein kinase. PNAS **107:**11549-11554.

199. **Martin, L. R., Z. C. Neal, M. S. McBride, and A. C. Palmenberg.** 2000. Mengovirus and encephalomyocarditis virus poly(C) tract lengths can affect virus growth in murine cell culture. J. Virol. **74:**3074-3081.

200. **Martin, L. R., and A. C. Palmenberg.** 1996. Tandem Mengovirus 5' pseudoknots are linked to viral RNA synthesis, not poly(C)-mediated virulence. J.Virol. **70:**8182-8186.

201. **Martinez-Salas, E., and M. D. Ryan.** 2010. Translation and protein processing, p. 141-161. *In* E. Ehrenfeld, E. Domingo, and R. P. Roos (ed.), The Picornaviruses. ASM Press, Washington D.C.

202. **Matreyek, K. A., and A. Engelman.** 2011. The Requirement for Nucleoporin NUP153 during Human Immunodeficiency Virus Type 1 Infection Is Determined by the Viral Capsid. J Virol **85:**7818-7827.

203. **Matsuura, Y., A. Lange, M. T. Harreman, A. H. Corbett, and M. Stewart.** 2003. Structural basis for Nup2p function in cargo release and karyopherin recycling in nuclear import. EMBO J **22:**5358-69.

204. **Matsuura, Y., and M. Stewart.** 2005. Nup50/Npap60 function in nuclear protein import complex disassembly and importin recycling. EMBO J **24:**3681-3689.

205. **Matthews, D. A., W. W. Smith, R. A. Ferre, B. Condon, G. Budahazi, W. Sisson, J. E. Villafranca, C. A. Janson, H. E. McElroy, C. L. Gribskov, and S. Worland.** 1994. Structure of human rhinovirus 3C protease reveals a trypsin-like polypeptide fold, RNA-binding site, and means for cleaving precursor polyprotein. Cell **77:**761-771.

206. **McArdle, J., N. J. Moorman, and J. Munger.** 2012. HCMV Targets the Metabolic Stress Response through Activation of AMPK Whose Activity Is Important for Viral Replication. PLoS Pathog **8:**1002502.

207. **McInerney, G. M., N. L. Kedersha, R. J. Kaufman, P. Anderson, and P. Liljeström.** 2005. Importance of eIF2alpha phosphorylation and stress granule assembly in alphavirus translation regulation. Mol Cell Biol **16:**3753-3763.

208. **McIntyre, C., L., N. J. Knowles, and P. Simmonds.** 2013. Proposals for the classification of human rhinovirus species A, B and C into genotypically assigned types. J Gen Virol **in press**.

209.   **Meggio, F., and L. A. Pinna.** 2003. One-thousand-and-one substrates of protein kinase CK2? FASEB **17:**349-368.

210.   **Mehla, R., S. B. Bivalkar-Mehla, S. Ruonan, I. Handy, H. Albrecht, S. Giri, P. Nagarkatti, M. Nagarkatti, and A. Chauhan.** 2010. Bryostatin Modulates Latent HIV-1 Infection via PKC and AMPK Signaling but Inhibits Acute Infection in a Receptor Independent Manner. Plos One **5:**e11160.

211.   **Meyer, R., M. N. Nalaskowski, P. Ehm, C. Schröder, X. Naj, M. A. Brehm, and G. W. Mayr.** 2012. Nucleocytoplasmic shuttling of human inositol phosphate multikinase is influenced by CK2 phosphorylation. Biol Chem **393:**1-12.

212.   **Mirzayan, C., and E. Wimmer.** 1994. Biochemical studies on poliovirus polypeptide 2C: evidence for ATPase activity. Virology **199:**176-187.

213.   **Mócsai, A., J. Ruland, and V. L. J. Tybulewicz.** 2010. The SYK tyrosine kinase: a crucial player in diverse biological functions. Nat Rev Immunol **10:**387-402.

214.   **Molla, A., K. S. Harris, A. K. Paul, S. H. Shin, J. Mugavero, and E. Wimmer.** 1994. Stimulation of poliovirus proteinase 3C-related proteolysis by the genome-linked protein VPg and its precursor 3AB. J.Biol.Chem. **269:**27015-27020.

215.   **Montagnier, L., and F. K. Sanders.** 1963. Replicative form of encephalomyocarditis virus ribonucleic acid. Nature **199:**664-667.

216.   **Moroianu, J.** 1999. Nuclear import and export pathways. J Cell Biochem **Suppl 32-33:**76-83.

217.   **Murray, K. E., and D. J. Barton.** 2003. Poliovirus CRE-dependent VPg uridylylation is required for positive-strand RNA synthesis but not for negative-strand RNA synthesis. J Virol **77:**4739-50.

218.   **Mylonis, I., G. Chachami, E. Paraskeva, and G. Simos.** 2008. Atypical CRM1-dependent Nuclear Export Signal Mediates Regulation of Hypoxia-inducible Factor-1 by MAPK. J Biol Chem **283:**27620-27627.

219.   **Neznanov, N., A. Kondratova, K. M. Chumakov, B. Angres, B. Zhumabayeva, V. I. Agol, and A. V. Gudkov.** 2001. Poliovirus protein 3A inhibits tumor necrosis factor (TNF)-induced apoptosis by eliminating the TNF receptor from the cell surface. J Virol **75:**10409-10420.

220.   **Nicklin, M. J. H., H. G. Krausslich, H. Toyoda, J. J. Dunn, and E. Wimmer.** 1987. Poliovirus polypeptide precursors: Expression in vitro and processing by exogeneous 3C and 2A proteinases. Proc.Natl.Acad.Sci.U.S.A. **84:**4002-4006.

221.   **Nielsen, A. C. Y., B. Bottiger, J. Banner, T. Hoffmann, and L. P. Nielsen.** 20120. Serious invasive Saffold virus infections in children, 2009. Emerging Infect Dis **18:**7-12.

222.   **Nitayaphan, S., D. R. Omilianowski, M. M. Toth, G. D. Parks, R. R. Rueckert, A. C. Palmenberg, and R. P. Roos.** 1986. Relationship of Theiler's murine encephalomyelitis viruses to the cardiovirus genus of picornaviruses. Intervirology **26:**140-148.

223.   **Nomoto, A., Y. F. Lee, and E. Wimmer.** 1976. The 5'-end of poliovirus mRNA is not capped with m^7G(5')pppG(5')Np. Proc.Natl.Acad.Sci.U.S.A. **73:**375-380.

224.   **Novak, J. E., and K. Kirkegaard.** 1991. Improved method for detection poliovirus negative strands, used to demonstrate specificity of positive-strand encapsidation and the ratio of positive to negative strands in infected cells. J.Virol. **65:**3384-3387.

225.   **Nugent, C. I., K. L. Johnson, P. Sarnow, and K. Kirkegaard.** 1999. Functional coupling between replication and packaging of poliovirus replicon RNA. J.Virol. **73:**427-435.

226.   **Oakhill, J. S., Z.-P. Chen, J. W. Scott, R. Steel, L. A. Castelli, N. Ling, S. L. Macaulay, and B. E. Kemp.** 2010. β-Subunit myristoylation is the gatekeeper for initiating metabolic stress sensing by AMP-activated protein kinase (AMPK). PNAS **107:**19237-19241.

227.   **Obenauer, J.** 2003. Scansite 2.0: proteome-wide prediction of cell signaling interactions using short sequence motifs. Nuc Acids Res **31:**3635-3641.

228.   **Oka, M., M. Asally, Y. Yasuda, Y. Ogawa, T. Tachibana, and Y. Yoneda.** 2010. The mobile FG nucleoporin Nup98 is a cofactor for Crm1-dependent protein export. Mol Cell Biol **21:**1885-96.

229.   **Okuwa, T., N. Taniura, M. Saito, T. Himeda, and Y. Ohara.** 2010. The opposite effects of two nonstructural proteins of Theiler's murine encephalomyelitis virus (TMEV) regulates apoptotic cell death in BHK-21 cells. Microb Immun **54:**639-643.

230.   **Oleszak, E. L., J. R. Chang, H. Friedman, C. D. Katsetos, and C. D. Platsoucas.** 2004. Theiler's virus infection: a model from multiple sclerosis. Clin Microbiol Rev **17:**174-207.

231. **Oliveira, M. A., R. Zhao, W. Lee, M. J. Kremer, I. Minor, R. R. Rueckert, G. D. Diana, D. C. Pevear, F. J. Dutko, and M. A. McKinlay.** 1993. The structure of human rhinovirus 16. Structure **1:**51-68.

232. **Ortiz, A. R., C. E. Strauss, and O. Olmea.** 2002. MAMMOTH (matching molecular models obtained from theory): an automated method for model comparison. Protein Sci **11:**2606-21.

233. **Pagano, M. A., G. Poletto, G. Di Maira, G. Cozza, M. Ruzzene, S. Sarno, J. Bain, M. Elliott, S. Moro, G. Zagotto, F. Meggio, and L. A. Pinna.** 2007. Tetrabromocinnamic acid (TBCA) and related compounds represent a new class of specific protein kinase CK2 inhibitors. Chembiochem **8:**129-139.

234. **Palmenberg, A. C.** 1987. Comparative organization and genome structure in picornaviruses, p. 25-34. *In* M. A. Brinton and R. R. Rueckert (ed.), Positive Strand RNA Viruses. Alan R. Liss Press, New York.

235. **Palmenberg, A. C., D. Spiro, R. Kuzmickas, S. Wang, A. Djikeng, J. A. Rathe, C. M. Fraser-Liggett, and S. B. Liggett.** 2009. Sequencing and analysis of all known human rhinovirus genomes reveals structure and evolution. Science **324:**55-59.

236. **Panasyuk, G., I. Nemazanyy, A. Zhyvoloup, M. Bretner, D. W. Litchfield, V. Filonenko, and I. T. Gout.** 2006. Nuclear Export of S6K1 II Is Regulated by Protein Kinase CK2 Phosphorylation at Ser-17. J Biol Chem **281:**31188-31201.

237. **Papon, L., A. Oteiza, T. Imaizumi, H. Kato, E. Brocchi, T. G. Lawson, S. Akira, and N. Mechti.** 2009. The viral RNA recognition sensor RIG-I is degraded during encephalomyocarditis virus (EMCV) infection. Virology **393:**311-318.

238. **Park, N., T. Skern, and K. E. Gustin.** 2010. Specific cleavge of the nuclear pore complex protein Nup62 by a viral protease. J. Biol. Chem. **285:**28796-28805.

239. **Parks, G. D., J. C. Baker, and A. C. Palmenberg.** 1989. Proteolytic cleavage of encephalomyocarditis viral capsid region substrates by precursors to the 3C enzyme. J.Virol. **63:**1054-1058.

240. **Patel, S. S., B. J. Belmont, J. M. Sante, and M. F. Rexach.** 2007. Natively unfolded nucleoporins gate protein diffusion across the nuclear pore complex. Cell **129**.

241. **Pathak, H. B., H. S. Oh, I. G. Goodfellow, J. J. Arnold, and C. E. Cameron.** 2008. Picornavirus genome replication: Roles of precursor proteins and rate-limiting steps in oriI-dependent VPg uridylyation. J Biol Chem **283:**30677-30688.

242. **Paul, A.** 2002. Possible unifying mechanism of picornavirus genome replication, p. 227-246. *In* B. L. Semler, Wimmer, E. (ed.), Molecular Biology of Picornaviruses. ASM Press, Washington D. C.

243. **Paul, A. V., E. Rieder, D. W. Kim, J. H. van Boom, and E. Wimmer.** 2000. Identification of an RNA hairpin in poliovirus RNA that serves as the primary template in the in vitro uridylylation of VPg. J.Virol. **74:**10359-10370.

244. **Paul, A. V., J. H. van Boom, D. Filippov, and E. Wimmer.** 1998. Protein-primed RNA synthesis by purified poliovirus RNA polymerase. Nature **393:**280-284.

245. **Paul, S., and T. Michiels.** 2006. Cardiovirus leader proteins are functionally interchangeable and have evolved to adapt to virus replication fitness. J. Gen. Virol **87:**1237-1246.

246. **Pearson, G., F. Robinson, T. Beers, B. E. Gibson, B. E. Xu, M. Karandikar, K. Berman, and M. H. Cobb.** 2001. Mitogen-activated protein (MAP) kinase pathways: regulation and physiological functions. Endocr Rev **22:**153-183.

247. **Percipalle, P., W. D. Clarkson, H. M. Kent, D. Rhodes, and M. Stewart.** 1997. Molecular interactions between the importin alpha/beta heterodimer and proteins involved in vertebrate nuclear protein import. J Mol Biol **266:**722-32.

248. **Pettersen, E. F., T. D. Goddard, C. C. Huang, G. S. Couch, D. M. Greenblatt, E. Meng, and T. Ferrin.** 2004. UCSF Chimera - A visualization system for exploratory research and analysis. J Comput Chem **25:**1605-1612.

249. **Petty, R. V., and A. C. Palmenberg.** 2013. Guanine-nucleotide exchange factor RCC1 facilitates a tight binding between EMCV Leader and cellular Ran GTPase. J Virol. **87:**6517-6520.

250. **Pevear, D. C., M. J. Fancher, P. J. Felock, M. G. Rossmann, M. S. Miller, G. D. Diana, A. M. Treasurywala, M. A. McKinlay, and F. J. Dutko.** 1989. Conformational change in the floor of the human rhinovirus canyon blocks adsorption to HeLa cell receptors. J.Virol. **63:**2002-2007.

251. **Pfister, T., K. W. Jones, and E. Wimmer.** 2000. A cysteine-rich motif in poliovirus protein 2C(ATPase) is involved in RNA replication and binds zinc in vitro. J.Virol. **74:**334-343.
252. **Pilipenko, E. V., E. G. Viktorova, S. T. Guest, V. I. Agol, and R. P. Roos.** 2001. Cell-specific proteins regulate viral RNA translation and virus-induced disease. EMBO J **20:**6988-6908.
253. **Piotrowska, J., S. J. Hansen, N. Park, K. Jamka, P. Sarnow, and K. E. Gustin.** 2010. Stable formation of compositionally unique stress granules in virus-infected cells. J Virol **84:**3653-3665.
254. **Plotnikov, A., D. Chuderland, Y. Karamansha, O. Liynah, and R. Seger.** 2011. Nuclear Extracellular Signal-Regulated Kinase 1 and 2 Translocation Is Mediated by Casein Kinase 2 and Accelerated by Autophosphorylation. Mol Cell Biol **31:**3515-3530.
255. **Polekhina, G., A. Gupta, B. Michell, B. van Denderen, S. Murthy, S. C. Feil, I. G. Jennings, D. J. Campbell, L. A. Witters, M. W. Parker, B. E. Kemp, and D. Stapleton.** 2003. AMPK beta subunit targets metabolic stress sensing to glycogen. Curr Biol **13:**867-871.
256. **Porter, F. W., Y. A. Bochkov, A. J. Albee, C. Wiese, and A. C. Palmenberg.** 2006. A picornavirus protein interacts with Ran-GTPase and disrupts nucleocytoplasmic transport. PNAS **103:**12417-12422
257. **Porter, F. W., B. Brown, and A. Palmenberg.** 2010. Nucleoporin phosphorylation triggered by the encephalomyocarditis virus leader protein is mediated by mitogen-activated protein kinases. J Virol **84:**12538-12548.
258. **Porter, F. W., and A. C. Palmenberg.** 2009. Leader-induced phosphorylation of nucleoporins correlates with nuclear trafficking inhibition of cardioviruses. J Virol **83:**1941-1951.
259. **Pritchard, A. E.** 1992. Nucleotide sequence identifies Vilyuisk virus as a divergent Theiler's virus. Virology **191:**469-472.
260. **Ramachandran, S., P. Kota, F. Ding, and N. V. Dokholyan.** 2011. Automated minimization of steric clashes in protein structure. Proteins: Str., Funct., Bioinf. **79:**261-270.
261. **Rebane, A., A. Aab, and J. A. Steitz.** 2004. Transportins 1 and 2 are redundant nuclear import factors for hnRNP A1 and HuR. RNA **10:**590-9.
262. **Reisdorph, N., J. J. Thomas, U. Katpally, E. Chase, K. Harris, G. Siuzdak, and T. J. Smith.** 2003. Human rhinovirus capsid dynamics is controlled by canyon flexibility. Virology **314:**34-44.
263. **Ren, L., R. Gonzalez, Z. Xie, Y. Xiao, Y. Li, C. Liu, L. Chen, Q. Yang, G. Vernet, G. Paranhos-Baccalà, Q. Jin, K. Shen, and J. Wang.** 2010. Saffold cardioviruses of 3 lineages in children with respiratory tract infections, Beijing, China. Emerging Infect Dis **16:**1158-1161.
264. **Ricour, C., F. Borghese, F. Sorgeloos, S. V. Hato, F. J. van Kuppeveld, and T. Michiels.** 2009. Random mutagenesis defines a domain of Theiler's virus leader protein that is essential for antagonism of nucleocytoplasmic trafficking and cytokine gene expression. J Virol **83:**11223-11232.
265. **Ricour, C., S. Delhaye, S. V. Hato, T. D. Olenyik, B. Michel, F. J. van Kuppeveld, K. E. Gustin, and T. Michiels.** 2009. Inhibition of mRNA export and dimerization of interferon regulatory factor 3 by Theiler's virus leader protein. J Gen Virol **90:**177-86.
266. **Riedl, S. J., and G. S. Salvesen.** 2007. The apoptosome: signalling platform of cell death. Nat Rev Mol Cel Biol **8:**405-413.
267. **Rodriguez, M.** 1985. Virus-Induced Demyelination in Mice: "Dying Back" of Oligodendrocytes. Mayo Clinic Proceedings **288:**495-498.
268. **Rodriguez, M., J. L. Leibowitz, and P. W. Lampert.** 1983. Persistent infection of oligodendrocytes in Theiler's virus-induced encephalomyelitis. Ann Neurol **13:**426-433.
269. **Rodriguez, P. L., and L. Carrasco.** 1995. Poliovirus protein 2C contains two regions involved in RNA binding activity. J Biol Chem **270:**10105-10112.
270. **Romanova, L., P. Lidsky, M. Kolesnikova, K. V. Fominykh, A. P. Gmyl, E. V. Sheval, S. V. Hato, F. J. van Kuppeveld, and V. Agol.** 2009. Antiapoptotic activity of the cardiovirus leader protein, a viral "security" protein. J Virol **83:**7273-7284.
271. **Roos, R. P., and R. Wollmann.** 1984. DA strain of Theiler's murine encephalomyelitis virus induces demyelination in nude mice. Ann Neurol **15:**494-499.

272.	**Ross, S. R., J. W. Schmidt, E. Katz, L. Cappeli, S. Hultine, P. Gimotty, and J. G. Monroe.** 2006. An Immunoreceptor Tyrosine Activation Motif in the Mouse Mammary Tumor Virus Envelope Protein Plays a Role in Virus-Induced Mammary Tumors. J Virol **80:**9000-9008.

273.	**Rossi, C. P., E. Cash, C. Aubert, and A. Coutinho.** 1991. Role of the humoral immune response in resistance to Theiler's virus infection. J Virol **65:**3895-3899.

274.	**Rossmann, M. G.** 1994. Viral cell recognition and entry. Protein Science **3:**1712-1725.

275.	**Rossmann, M. G., E. Arnold, J. W. Erickson, E. A. Frankenberger, J. P. Griffith, H.-J. Hecht, J. E. Johnson, G. Kamer, M. Luo, A. G. Mosser, R. R. Rueckert, B. Sherry, and G. Vriend.** 1985. The structure of a human common cold virus (Rhinovirus 14) and its functional relations to other picornaviruses. Nature **317:**145-153.

276.	**Rossmann, M. G., and A. C. Palmenberg.** 1988. Conservation of the putative receptor attachment site in picornaviruses. Virology **164:**373-382.

277.	**Roux, P. P., and J. Blenis.** 2004. ERK and p38 MAPK-activated protein kinases: a family of protein kinases with diverse biological functions. Microbiol Mol Biol Rev **68:**320-344.

278.	**Roy, A., A. Kucukural, and Y. Zhang.** 2010. I-TASSER: a unified platform for automated protein structure and function prediction. Nat Protoc **5:**725-738.

279.	**Rozhon, E., S. Cox, P. Buontempo, J. O'Connell, W. Slater, J. De Martino, J. Schwartz, G. Miller, E. Arnold, and A. Zhang.** 1993. SCH 38057: a picornavirus capsid-binding molecule with antiviral activity after the initial stage of viral uncoating. Antiviral research **21:**15-35.

280.	**Rozhon, E. J., H. L. Lipton, and F. Brown.** 1982. Characterization of Theiler's murine encephalomyelitis virus RNA. J.Gen.Virol. **61:**157-165.

281.	**Sali, A., and T. L. Blundell.** 1993. Comparative protein modelling by satisfaction of spatial restraints. J Mol Biol **234:**779-815.

282.	**Salvi, M., S. Sarno, L. Cesaro, H. Nakamura, and L. A. Pinna.** 2009. Extraordinary pleiotropy of protein kinase CK2 revealed by weblogo phosphoproteome analysis. Mol Cell Res **1793:**847-859.

283.	**Sanders, M. J., P. O. Grondin, B. D. Hegarty, M. A. Snowden, and D. Carling.** 2007. Investigating the mechanism for AMP activation of the AMP-activated protein kinase cascade. Biochem J **403:**139.

284.	**Sarmanova, E. S., and H. H. Chumachenko.** 1960. Study of the etiology of Viliuisk encephalomyelitis. I. Study of the biological characteristics of virus strains isolated from patients. Voprosy MeditsinskoiVirusologii (Moscow) **6:**211-214.

285.	**Savolainen, C., S. Blomqvist, M. N. Mulders, and T. Hovi.** 2002. Genetic clustering of all 102 human rhinovirus prototype strains: serotype 87 is close to human enterovirus 70. J. General Virology **83:**333-340.

286.	**Scheper, G. C., M. S. Van Der Knapp, and C. G. Proud.** 2007. Translation matters: protein synthesis defects in inherited disease. Nat Rev Genet **8:**771-723.

287.	**Schlax, P. E., J. Zhang, E. Lewis, A. Planchart, and T. G. Lawson.** 2007. Degradation of the encephalomyocarditis virus and hepatitis A virus 3C proteases by the ubiquitin/26S proteasome system in vivo. Virology **360:**350-363.

288.	**Schlegel, A., T. H. Giddings, M. s. Ladinsky, and K. Kirkegaard.** 1996. Cellular origin and ultrastructure of membranes induced during poliovirus infection. J.Virol. **70:**6576-6588.

289.	**Scraba, D. G.** 1990. Functional aspects of the capsid structure of Mengo virus. J.Struct.Biol. **104:**52-62.

290.	**Scraba, D. G., and A. C. Palmenberg.** 1999. Cardioviruses (Picornaviridae), p. 1-10, The Encyclopedia of Viruses. Academic Press.

291.	**Shen, M. Y., and A. Sali.** 2006. Statistical potential for assessment and prediction of protein structures. Protein Sci **15:**2507-24.

292.	**Sherry, B., A. G. Mosser, R. J. Colonno, and R. R. Rueckert.** 1986. Use of monoclonal antibodies to identify four neutralization immunogens on a common cold picornavirus, human rhinovirus 14. J. Virol. **57:**246-257.

293.	**Shih, S., S. Chen, G. Hakimelahi, H. Liu, C. Tseng, and K. Shia.** 2004. Selective human enterovirus and rhinovirus inhibitors: An overview of capsid-binding and protease-inhibiting molecules. Med Res Rev **24:**449-474.

294.   **Simmonds, P., C. McIntyre, C. Savolainen-Kopra, C. Tapparel, I. M. Mackay, and T. Hovi.** 2010. Proposals for the classification of human rhinovirus species C into genotypically assigned types. J. Gen. Virol. **91:**2409-2419.

295.   **Slee, E. A.** 2001. Executioner caspase-3, -6, and -7 perform distinct, non-redundant roles during the demolition phase of apoptosis. J Biol Chem **276:**7320-7326.

296.   **Son, K.-N., R. P. Becker, P. Kallio, and H. L. Lipton.** 2008. Theiler's virus-induced intrinsic apoptosis in M1-D macrophages is Bax mediated and restricts virus infectivity: a mechanism for persistence of a cytolytic virus. J Virol **82:**4502-4510.

297.   **Son, K.-N., S. Pugazhenthi, and H. L. Lipton.** 2009. Activation of tumor suppressor protein p53 is required for Theiler's murine encephalomyelitis virus-induced apoptosis in M1-D macrophages. J Virol **83:**10770-10777.

298.   **St-Denis, N. A., and D. W. Litchfield.** 2009. Protein Kinase CK2 in Health and Disease. Cell Mol Life Sci **66:**1817-1829.

299.   **Stavrou, S., G. Baida, E. Viktorova, G. D. Ghadge, V. I. Agol, and R. P. Roos.** 2010. Theiler's murine encephalomyelitis virus L* amino acid position 93 is important for virus persistence and virus-induced demyelination. J Virol **84:**1348-1354.

300.   **Stavrou, S., G. D. Ghadge, and R. P. Roos.** 2011. Apoptotic and antiapoptotic activity of L protein of Theiler's murine encephalomyelitis virus. J Virol **85:**7177-7185.

301.   **Steinberg, G. R., and B. E. Kemp.** 2009. AMPK in Health and Disease. Physiol Rev **89:**1025-1078.

302.   **Stott, E. J., and G. F. Heath.** 1970. Factors affecting the growth of rhinovirus 2 in suspension cultures of L132 cells. J Gen Virol **6:**15-24.

303.   **Sugden, P. H., S. J. Fuller, S. C. Weiss, and A. Clerk.** 2009. Glycogen synthase kinase 3 (GSK3) in the heart: a point of integration in hypertrophic signalling and a therapeutic target? A critical analysis. Brit J Pharm **153:**S137-S153.

304.   **Suter, M., U. Riek, R. Tuerk, U. Schlattner, T. Wallimann, and D. Neumann.** 2006. Dissecting the Role of 5'-AMP for Allosteric Stimulation, Activation, and Deactivation of AMP-activated Protein Kinase. J Biol Chem **281:**32207-32216.

305.   **Takano-Maruyama, M., Y. Ohara, K. Asakura, and T. Okuwa.** 2006. Theiler's murine encephalomyelitis virus leader protein amino acid residue 57 regulates subgroup-specific virus growth on BHK-21 cells. J. Virol. **80:**12025-12031.

306.   **Taniura, N., M. Saito, T. Okuwa, K. Saito, and Y. Ohara.** 2009. Different subcellular localization of Theiler's murine encephalomyelitis virus leader proteins of GDVII and DA strains in BHK-21 cells. J Virol **83:**6624-6630.

307.   **Theiler, M.** 1934. Spontaneous encephalomyelitis of mice - a new virus disease. Science **80:**112.

308.   **Theiler, M.** 1937. Spontaneous encephalomyelitis of mice, a new virus disease. J Exp Med **65:**705-719.

309.   **Thomas, A. A., R. J. Woortmeijer, W. Puijk, and S. J. Barteling.** 1988. Antigenic sites on foot-and-mouth disease virus type A10. J Virol **62:**2782-9.

310.   **Tourriere, H.** 2003. The RasGAP-associated endoribonuclease G3BP assembles stress granules. J Cell Biol **160:**823-831.

311.   **Towner, J. S., T. V. Ho, and B. L. Semler.** 1996. Determinants of membrane association for poliovirus protein 3AB. J.Biol.Chem. **271:**26810-26818.

312.   **Tsukagoshi, H., K. Mizuta, C. Abiko, T. Itagaki, M. Yoshizuma, S. Kobayashi, M. Kuroda, K. Kozawa, M. Noda, A. Ryo, and H. Kimura.** 2011. The impact of Saffold cardiovirus in patients with acute respiratory infections in Yamagata, Japan. Scand J Infect Dis **43:**669-671.

313.   **van Eyll, O., and T. Michiels.** 2000. Influence of the Theiler's virus L* protein on macrophage infection, viral persistence, and neurovirulence. J Virol **74:**9071-9077.

314.   **van Kuppeveld, F. J. M., J. G. J. Hoenderop, R. L. L. Smeets, P. H. G. M. Willems, B. P. M. Dijkman, J. M. D. Galama, and W. J. G. Melchers.** 1997. Coxsackievirus protein 2B modifies endoplasmic reticulum membrane and plasma membrane permeability and facilitates virus release. EMBO J. **16:**3519-3532.

315. **van Pesch, V., O. van Eyll, and T. Michiels.** 2001. The leader protein of Theiler's virus inhibits immediate-early alpha/beta interferon production J. Virol. **75:**7811-7817.

316. **Virgen-Slane, R., J. M. Rozovics, K. D. Fitzgerald, T. Ngo, W. Chou, G. J. van der Heden van Noort, D. V. Filippov, P. D. Gershon, and B. L. Semler.** 2012. An RNA virus hijacks an incognito function of a DNA repair enzyme. PNAS **109:**14634-14639.

317. **Vlasak, M., M. Roivainen, M. Reithmayer, I. Goesler, P. Laine, L. Snyers, T. Hovi, and D. Blaas.** 2005. The minor receptor group of human rhinovirus (HRV) includes HRV23 and HRV25, but the presence of a lysine in the VP1 H1 loop is not sufficient for receptor binding. J Virol **79:**7389-7395.

318. **von Knethen, A., N. Tzieply, C. Jennewein, and B. Brune.** 2010. Casein-kinase-II-dependent phosphorylation of PPAR provokes CRM1-mediated shuttling of PPAR from the nucleus to the cytosol. J Cell Sci **123:**192-201.

319. **Wallner, B., and A. Elofsson.** 2003. Can correct protein models be identified? Protein Sci **12:**1073-86.

320. **Wang, C. Y. T., R. M. Greer, E. Delwart, T. P. Sloots, and I. M. Mackay.** 2012. A newly designed real-time RT-PCR for SAFV detects SAFV-2 and SAFV-3 in the respiratory tracts of ill children during 2011. J Clin Virol **55:**173-176.

321. **Wang, S., P. Song, and M.-H. Zou.** 2012. AMP-activated protein kinase, stress responses and cardiovascular diseases. Clin Sci **122:**555-573.

322. **Wang, T., Q. Yu, J. Chen, B. Deng, L. Qian, and Y. Le.** 2010. PP2A Mediated AMPK Inhibition Promotes HSP70 Expression in Heat Shock Response. PloS One **5:**13096.

323. **Wang, Y., and P. J. Roach.** 1993. Inactivation of rabbit muscle glycogen synthase by glycogen synthase kinase-3. Dominant role of the phosphorylation of Ser-640 (site-3a). J Biol Chem **268:**23876-80.

324. **Watters, K., and A. Palmenberg.** 2011. Differential processing of nuclear pore complex proteins by rhinovirus 2A proteases from different species and serotypes. J Virol **85:**10874-10883.

325. **Wessels, E., D. Duijsings, K. H. Lanke, S. H. van Dooren, C. L. Jackson, W. J. Melchers, and F. J. van Kuppeveld.** 2006. Effects of picornavirus 3A proteins on protein transport and GBF1-dependent COP-I recruitment. J Virol **80:**11852-11860.

326. **White, J. P., A. M. Cardenas, W. Marissen, and R. E. Lloyd.** 2007. Inhibition of cytoplasmic mRNA stress granule formation by a viral proteinase. Cell Host Microbe **2:**295-305.

327. **Woods, A., P. C. Cheung, F. C. Smith, M. D. Davison, J. W. Scott, R. K. Beri, and D. Carling.** 1996. Characterization of AMP-activated protein kinase beta and gamma subunits. Assembly of the heterotrimeric complex in vitro. J Biol Chem **271:**10282-10290.

328. **Woods, A., S. R. Johnstone, K. Dickerson, F. C. Leiper, L. G. D. Fryer, D. Neumann, U. Schlattner, T. Wallimann, M. Carlson, and D. Carling.** 2003. LKB1 is the upstream kinase in the AMP-activated protein kinase cascade. Curr Biol **13:**2004-2008.

329. **Woods, A., D. Vertommen, D. Neumann, R. Turk, J. Bayliss, U. Schlattner, T. Wallimann, D. Carling, and M. H. Rider.** 2003. Identification of phosphorylation sites in AMP-activated protein kinase (AMPK) for upstream AMPK kinases and study of their roles by site-directed mutagenesis. J. Biol. Chem. **278:**28434-28442.

330. **Wu, Y., P. Song, J. Xu, M. Zhang, and M.-H. Zou.** 2007. Activation of Protein Phosphatase 2A by Palmitate Inhibits AMP-activated Protein Kinase. J Biol Chem **282:**9777-9788.

331. **Xiao, B., R. Heath, P. Saiu, F. C. Leiper, P. Leone, C. Jing, P. A. Walker, L. Haire, J. F. Eccleston, C. T. Davis, S. R. Martin, D. Carling, and S. J. Gamblin.** 2007. Structural basis for AMP binding to mammalian AMP-activated protein kinase. Nature **449:**496-500.

332. **Xiao, C., and M. G. Rossmann.** 2007. Interpretation of electron density with stereographic roadmap projections. J Struct Biol **158:**182-187.

333. **Xu, Z.-Q., W.-X. Cheng, H.-M. Qi, S.-X. Cui, Y. Jin, and Z.-J. Duan.** 2009. New Saffold cardiovirus in children, China. Emerging Infect Dis **15:**993-994.

334. **Xue, L., W.-H. Wang, A. Iliuk, L. Hu, J. Galan, S. Yu, M. Hans, R. L. Geahlen, and W. A. Tao.** 2012. Sensitive kinase assay linked with phosphoproteomics for identifying direct kinase substrates. PNAS **109:**5615-5620.

335. **Xue, Y., A. Li, L. Wang, H. Feng, and X. Yao.** 2006. PPSP: prediction of PK-specific phosphorylation site with Bayesian decision theory. BMC Bioinformatics **7:**163.

336. **Yamada, M., A. Zurbriggen, and R. S. Fujinami.** 1991. Pathogenesis of Theiler's murine encephalomyelitis virus. Advances in Virus Research **39:**291-320.

337. **Yanagi, S., R. Inatome, T. Takano, and H. Yamamura.** 2001. Syk Expression and Novel Function in a Wide Variety of Tissues. Biochem Biophys Res Comm **288:**495-498.

338. **Yang, Y., Y. Liang, Q. Lin, Z. Chen, M. Yi, K. Li, and S. M. Lemon.** 2007. Disruption of innate immunity due to mitochondrial targeting of a picornaviral protease precursor. PNAS **104:**7253-7258.

339. **Yoon, J. W., and H.-S. Jun.** 2006. Viruses Cause Type 1 Diabetes in Animals. Ann N Y Acad Sci **1079:**138-146.

340. **Yoon, J. W., T. Onodera, and A. L. Notkins.** 1977. Virus-induced diabetes mellitus. VIII. Passage of encephalomyocarditis virus and severity of diabetes in susceptible and resistant strains of mice. J.Gen.Virol. **37:**225-232.

341. **Zhang, H.-S., and M.-R. Wu.** 2009. SIRT1 regulates Tat-induced HIV-1 transactivation through activating AMP-activated protein kinase. Virus Res **146:**51-57.

342. **Zhang, Y.** 2008. I-TASSER server for protein 3D structure prediction. BMC Bioinformatics **9:**40.

343. **Zhang, Y.** 2009. I-TASSER: Fully automated protein structure prediction in CASP8. Proteins **77:**100-113.

344. **Zhang, Y.** 2007. Template-based modeling and free modeling by I-TASSER in CASP7. Proteins **69:**108-117.

345. **Zhang, Y., A. A. Simpson, R. M. Ledford, C. M. Bator, S. Chakravarty, G. A. Skochko, T. M. Demenczuk, A. Watanyar, D. C. Pevear, and M. G. Rossmann.** 2004. Structural and virological studies of the stages of virus replication that are affected by antirhinovirus compounds. J Virol **78:**11061-9.

346. **Zhou, G., R. Myers, Y. Li, Y. Chen, X. Shen, J. Fenyk-Melody, M. Wu, J. Ventre, T. Doebber, N. Fujii, N. Musi, M. F. Hirshman, L. J. Goodyear, and D. E. Moller.** 2001. Role of AMP-activated protein kinase in mechanism of metformin action. J Clin Invest **108:**1167-1174.

347. **Zhu, B., Y. Zhou, F. Xu, J. Shuai, X. Li, and W. Fang.** 2012. Porcine Circovirus Type 2 Induces Autophagy via the AMPK/ERK/TSC2/mTOR Signaling Pathway in PK-15 Cells. j Virol **86:**12003-12012.

348. **Zoll, J., J. M. D. Galama, F. J. M. van Kuppeveld, and W. J. G. Melchers.** 1996. Mengovirus leader is involved in the inhibition of host cell protein synthesis. J.Virol. **70:**4948-4958.

349. **Zoll, J., H. A. Heus, F. J. M. van Kupperveld, and W. J. G. Melchers.** 2009. The structure-function relationship of the enterovirus 3'-UTR. Virus Research **139:**209-216.

350. **Zoll, J., S. E. Hulshof, K. Lanke, F. V. Lunel, W. J. G. Melchers, E. S.-v. d. Ven, M. Roivainen, J. M. D. Galama, and F. J. M. v. Kuppeveld.** 2009. Saffold virus, a human Theiler's-like cardiovirus, is ubiquitous and causes infection early in life. PLoS Pathogens **5:**1-10.

351. **Zoll, J., W. J. Melchers, J. M. Galama, and F. J. van Kuppeveld.** 2002. The mengovirus leader protein suppresses alpha/beta interferon production by inhibition of the iron/ferritin-mediated activation of NF-kappa B. J Virol **76:**9664-72.

352. **Zuvich, R. L., J. L. Mccauley, J. R. Oksenberg, S. J. Sawcer, P. L. Jager, C. Aubin, A. H. Cross, L. Piccio, N. T. Aggarwal, D. Evans, D. A. Hafler, A. Compston, S. L. Hauser, M. A. Pericak-Vance, and J. L. Haines.** 2010. Genetic variation in the IL7RA/IL7 pathway increases multiple sclerosis susceptibility. Hum Genet **127:**525-535.